AMPA RECEPTORS:
ROLE IN BRAIN INJURY

© Jill H Fowler B.Sc (Hons)
June 2003

A Thesis submitted for the degree of Doctor of Philosophy to the Faculty of Medicine, University of Glasgow

Division of Clinical Neuroscience
Wellcome Surgical Institute and Hugh Fraser Laboratories
University of Glasgow
Garscube Estate, Bearsden Road
Glasgow, G61 1QH.

UNIVERSITY
of
GLASGOW

Acknowledgements

First and foremost, I wish to express my sincere gratitude to my PhD supervisors, Professor Jim McCulloch and Dr Debbie Dewar for their constant support, scientific advice and enthusiasm. I am greatly indebted to you both.

I also wish to extend my thanks and appreciation to Dr Mike O'Neill, my industrial supervisor at Eli Lilly, for welcoming me to his lab at Windlesham, and for all his support and good humour during the other countless times I have called on his assistance. Thanks also to Dr Tracy Murray, Mr Mark Ward, Dr Chris Casely, Christine Robinson and Julia Turnock for making me feel welcome and helping me out during my time at Eli Lilly.

A special acknowledgement must be made to Dr Eileen McCracken, Dr Karen Horsburgh and Dr Julia Edgar for their expert teaching and many pearls of wisdom. Further thanks to the excellent assistance provided by the technical staff at the Wellcome Surgical Institute, particularly Mrs Joan Stewart and Mrs Lindsay Gallagher. Thanks also to my fellow PhD students, Barry McColl, David McCaig, Dan Cuthill, Debs Bingham, Jetta McGill, Kirsty Wallace and Debbie Bentley for all their support and for sharing the many required drinking sessions.

I am greatly appreciative of the opportunity to collaborate with Professor Ian Griffiths, Dr Julia Edgar and Dr Mark McGlaughlin. Thank you for allowing me to share your bench space.

I must also thank Eli Lilly, the Medical Research Council and the British Neuroscience Association for providing financial assistance during my PhD and for enabling me to attend two international conferences.

Finally, I am indebted and truly grateful to my parents and Colin for their constant loving and financial support over the course of my PhD. I dedicate this thesis to you.

Contents

List of Tables

List of Figures

Abbreviations

AMPA	α-amino-3-hydroxy-5-methyl-4-isoxazole propionic acid
AIDS	Acquired Autoimmune deficiency syndrome
APP	Amyloid precursor protein
ATP	Adenosine triphosphate
BDNF	Brain-derived neurotrophic factor
BSA	Bovine serum albumin
Ca^{2+}	Calcium
CAM-IIK	Calcium/calmodulin dependent protein kinase II
CNQX	6-Cyano-7-nitroquinoxaline-2,3-dione
CNS	Central nervous system
DAI	Diffuse axonal injury
DNQX	6,7-dinitroquinoxaline-2,3-dione
EAA	Excitatory amino acid
EAAC	Excitatory amino acid carrier
EAAT	Excitatory amino acid transporter
ECL	Entorhinal cortex lesion
EM	Electron microscope
GFAP	Glial fibrillary acidic protein
GLAST	Glutamate-aspartate transporter
GLT	Glutamate transporter
H & E	Haematoxylin and eosin
LCGU	Local cerebral glucose utilisation
LTD	Long term depression
LTP	Long term potentiation
MAP 5	Microtubule associated protein-5
MAPK	Mitogen-activated protein kinase
MBP	Myelin basic protein
MK-801	Dizocilpine maleate
NBQX	6-nitro-7-sulfamoylbenzo(*f*)quinoxaline-2,3-dione
NF	Neurofilament
NF 200	Neurofilament 200 (Heavy chain component of neurofilament)
MCAO	Middle cerebral artery occlusion

Na^+	Sodium
NMDA	*N*-methyl-D-aspartate
NO	Nitric Oxide
3-NPA	3-Nitropropionic acid
PBS	Phosphate buffered saline
PKA	cAMP-dependent protein kinase
PKC	Protein kinase C
PLP	Proteolipid protein
ROD	Relative optical density
ROS	Reactive oxygen species
SDS-PAGE	Sodium dodecyl sulphate polyacrylamide gel electrophoresis
SEM	Standard error of the mean
SMI 32	Antibody raised against non-phoshphorylated neurofilament 200
SPD 502	8-methyl-5-(4-(*N*,*N*-dimethylsulfamoyl)phenyl)-6,7,8,9,-tetrahydro-1*H*-pyrrolo[3,2-*h*]-isoquinoline-2,3-dione-3-*O*-(4-hydroxybutyric acid-2-yl)oxime
TBI	Traumatic brain injury
TBS	Tris buffered saline
WT	Wild Type

Summary

Glutamate can be considered a 'Jekyll and Hyde' molecule that serves an essential role as neurotransmitter whilst having potentially damaging, neurotoxic effects. The neurotransmitter and neurotoxic properties of glutamate are partly mediated by AMPA receptors. Due to their ubiquitous distribution in the central nervous system (CNS), events occurring at the AMPA receptor can have profound consequences for CNS functioning. In this thesis, two AMPA receptor-mediated events were examined. Firstly, the neurotoxic potential of AMPA receptor-mediated excitotoxicity was examined in white matter. Secondly, AMPA receptor potentiators, which enhance glutamatergic neurotransmission, were investigated.

The role of AMPA receptors in mediating axonal damage *in vivo*

White matter is vulnerable to injury in a variety of neurological disorders, however, comparatively less is known about the mechanisms of white matter injury compared to grey matter injury. In addition to their presence on neuronal perikarya, AMPA receptors are present on the cellular components of white matter. To determine if axons were vulnerable to AMPA receptor-mediated excitotoxicity *in vivo*, AMPA (2.5 or 25 nmol) or vehicle was injected into the subcortical white matter of rats. AMPA induced a dose dependent increase in axonal damage assessed with MAP 5 immunohistochemistry. In addition, AMPA induced myelin, oligodendroglial and neuronal damage. The AMPA-induced damage was attenuated by pre-treatment with the AMPA receptor antagonist SPD 502 (16mg/kg), but not with co-administration of the NMDA receptor antagonist (MK 801, 5nmol); suggesting that it occurs through AMPA-receptor mediated mechanisms. The role of AMPA receptor-mediated excitotoxicity in mediating axonal damage following focal cerebral ischaemia was also examined. In addition to protecting grey matter damage, pre-treatment with the AMPA receptor antagonist SPD 502 (16mg/kg) significantly reduced axonal damage following middle cerebral artery occlusion. Collectively, these data suggest a role for AMPA receptors in mediating both grey and white matter damage, and suggest that AMPA receptor antagonists are capable of salvaging multiple cellular elements required for the functioning of the CNS.

Establishing a mouse model of AMPA-induced axonal damage

As transgenic mice were subsequently utilised in this thesis, an *in vivo* mouse model of AMPA-induced axonal damage was established by injecting AMPA in the caudate nucleus of mice. The effects of energy inhibition in mediating axonal damage were also examined by injecting the mitochondrial inhibitor, malonate, into the caudate nucleus of mice. AMPA-induced axonal swellings were evident in white matter tracts of the caudate nucleus in NF 200 immunostained sections, however axonal damage was not detected with APP immunohistochemistry. In contrast, malonate induced axonal swellings that were evident in both NF 200 and APP immunostained sections. To further examine the contrasting mechanisms by which AMPA and malonate act, the effects of either toxin of glucose metabolism were examined 1 hour following intrastriatal injection. AMPA induced a marked increase in glucose utilisation in the caudate nucleus, whereas malonate induced a marked decrease in glucose utilisation. Collectively, these studies highlight the divergent mechanisms by which these two pathogenic mediators of white matter pathology act.

AMPA-induced axonal damage is attenuated in PLP, but not MBP deficient mice

At present, there is no evidence to suggest that AMPA receptors are located on axons. Therefore, AMPA-induced axonal damage must be secondary to damage occurring at another cellular element. Transgenic mice deficient in PLP or MBP, the two major proteins expressed in oligodendroglia and myelin, contain axonal abnormalities and therefore provide a useful model for examining the role of glia-axonal relationships in mediating AMPA-induced axonal damage. In addition, it is possible that excitotoxic mechanisms may contribute to the pathology observed in these mice. To determine if PLP and MBP deficient mice exhibit altered sensitivity to excitotoxicity, AMPA was injected in the caudate nucleus of these mice. There was no difference in the amount of AMPA-induced axonal, or neuronal, damage in MBP deficient mice. However, AMPA-induced axonal damage was significantly attenuated ($P<0.05$), and neuronal damage was reduced ($P=0.06$) in PLP deficient mice. These data suggest that excitotoxic mechanisms do not contribute to the pathology exhibited by PLP or MBP deficient mice. However, PLP, but not MBP, mediated interactions with the axon may be important in mediating AMPA-induced axonal damage.

Mapping the functional effects of the AMPA receptor potentiator, LY404187, with ^{14}C-2-deoxyglucose autoradiography

AMPA receptor potentiators act as positive AMPA receptor modulators, which enhance AMPA receptor mediated glutamatergic neurotransmission. AMPA receptor potentiators have demonstrated efficacy in animal models of cognition and depression, however the anatomical basis of the action of AMPA receptor potentiators was not known. This was investigated using ^{14}C-2-deoxyglucose autoradiography following administration of the biarylpropylsulfonamide AMPA receptor potentiator, LY404187 (0.05, 0.5, or 5mg/kg). The AMPA receptor potentiator LY404187 (0.5mg/kg) produced statistically significant increases in glucose utilisation in 28 of the 52 anatomical areas examined, which included the cerebral cortex (layer IV), the hippocampus, the dorsal raphe nucleus, locus coeruleus and lateral habenula. These increases were blocked by pre-treatment with the AMPA receptor antagonist, LY293558 (25mg/kg), suggesting that the AMPA receptor potentiator LY404187 acts through AMPA receptor mediated mechanisms. Despite the ubiquitous distribution of AMPA receptors, the anatomically discrete actions of the AMPA receptor potentiator LY404187 suggests that it may enhance specific AMPA receptor mediated processes in the cerebral cortex and limbic system. These data provide an anatomical basis for the cognitive enhancing and anti-depressant effects of LY404187.

The effects of the AMPA receptor potentiator LY404187 on regeneration in the dentate gyrus following entorhinal cortex lesion

AMPA receptor potentiators can enhance brain derived neurotrophic factor (BDNF) in the hippocampus *in vitro* and *in vivo*. BDNF may participate in the reorganisation of anatomical circuitry that occurs in the dentate gyrus, following lesioning of its afferent input from the entorhinal cortex. In addition, the generation of new neurons (neurogenesis) occurs in the dentate gyrus following entorhinal cortex lesioning, whose survival may depend upon neurotrophic factors. To determine if an AMPA receptor potentiator could enhance regeneration in the dentate gyrus, LY404187 (0.5mg/kg), was administered twice daily, for 7 or 14 days, in animals that survived for 14 and 21 days respectively, following entorhinal cortex lesion (ECL). GAP 43 and synaptophysin immunoreactivity were used to determine fibre sprouting and synaptogenesis, respectively. The effects of LY404187 on the number of BrdU cells

labelled prior to drug treatment (day 6 post ECL) were also examined. Compared with vehicle treatment, there was no evidence that LY404187 altered the optical density of GAP 43 or synaptophysin immunostaining, at either time point. In addition, treatment with LY404187 did not significantly alter the number of BrdU cells in the dentate gyrus at either time point examined. These data suggest that, at the doses used in the current study, the AMPA receptor potentiator, LY404187 did not enhance regeneration in the dentate gyrus following entorhinal cortex lesioning.

Collectively, these data highlight the importance of AMPA-receptor mediated transmission for the normal functioning of the central nervous system. Based on their important role in neurotransmission, and their potentially damaging capacities, AMPA receptors represent an important therapeutic target in a number of clinical conditions. The data presented in this thesis highlight the role of AMPA receptors in mediating white matter damage, and the clinical potential of AMPA receptor potentiators in treating cognitive deficits and depression.

CHAPTER 1

INTRODUCTION

1.1 AMPA receptors

1.1.1 Glutamate neurotransmission and receptor classification

The amino acid glutamate is a ubiquitous biological molecule, serving roles as an intermediate in metabolism and as a structural component of proteins. It is now almost 50 years since the pioneering experiments of Hayashi, Curtis and colleagues that suggested glutamate might have a role as a neurotransmitter within the central nervous system (CNS) (Hayashi, 1952, 1954; Curtis *et al.*, 1959). During this era however, most scientists dismissed a putative role as a transmitter based on its other cellular functions. Numerous experiments have since established that glutamate meets the criteria for a CNS neurotransmitter.

Johnston and colleagues (1974) were first to suggest that analogues of glutamate might act at different glutamate receptor subtypes. Since then, the development and use of synthetic and natural agonists and antagonists of glutamate receptors; pharmacological, electrophysiological and ligand binding studies; and subsequent molecular cloning techniques have led to an evolution in the classification of glutamate receptor subtypes, which has culminated in the currently accepted classification, presented in figure 1.1 and figure 1.2.

Physiological and pharmacological studies in the 1970s inspired the early classification of glutamate receptor subtypes. *N*-methyl-D-aspartate (NMDA), quisqualic, kainic and ibotenic acids were among the first glutamate analogues to be developed and it was found that the potency of these compounds varied between cells (Curtis and Watkins, 1963; Shinozaki and Shibuya, 1970; Biscoe *et al.*, 1976). Watkins and Evans (1981) reviewed the evidence and suggested three distinct glutamate receptor subtypes: kainate, quisqualate and NMDA. However, it was later discovered that quisqualate could activate a receptor coupled to the generation of 2^{nd} messenger systems (Sladeczek *et al.*, 1985; Nicoletti *et al.*, 1986). In 1980, Krogsgaard-Larsen and co-workers synthesised the compound α-amino-3-hydroxy-5-methyl-4-isoxazole propionic acid (AMPA), which was a more selective, potent, quisqualate like agonist. This lead to a further revision of the nomenclature of glutamate receptor subtypes (Collingridge and Lester, 1989; Lodge and Collingridge, 1990). It is currently accepted that glutamate receptors are subdivided into

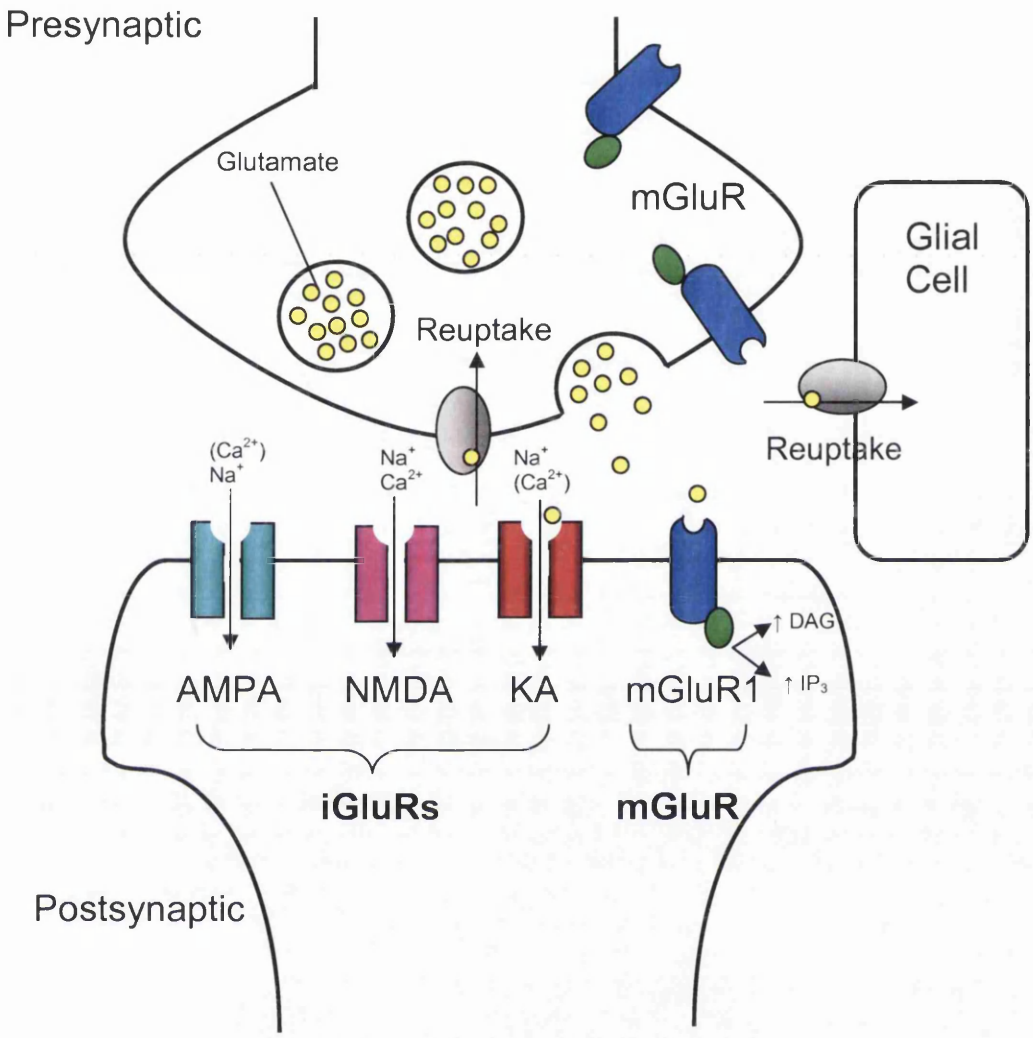

Figure 1.1 Diagrammatic representation of the major subtypes of glutamate receptors at the glutamate synapse

Glutamate is synthesised and stored in vesicles at the presynaptic terminal. Excitation of the presynaptic terminal causes the release of glutamate into the synapse, where it acts on glutamate receptors. There are three subtypes of **ionotropic** glutamate receptor, NMDA, AMPA and kainate (KA). NMDA receptors are permeable to Ca^{2+} and Na^+; whereas AMPA and kainate receptors primarily gate Na^+. K^+ efflux occurs through all ionotropic receptors. **Metabotropic** glutamate receptors (mGluR) are coupled to G proteins that can activate second messenger systems. Reuptake of glutamate occurs at high affinity glutamate transporters located on astrocytes and presynaptic terminals.

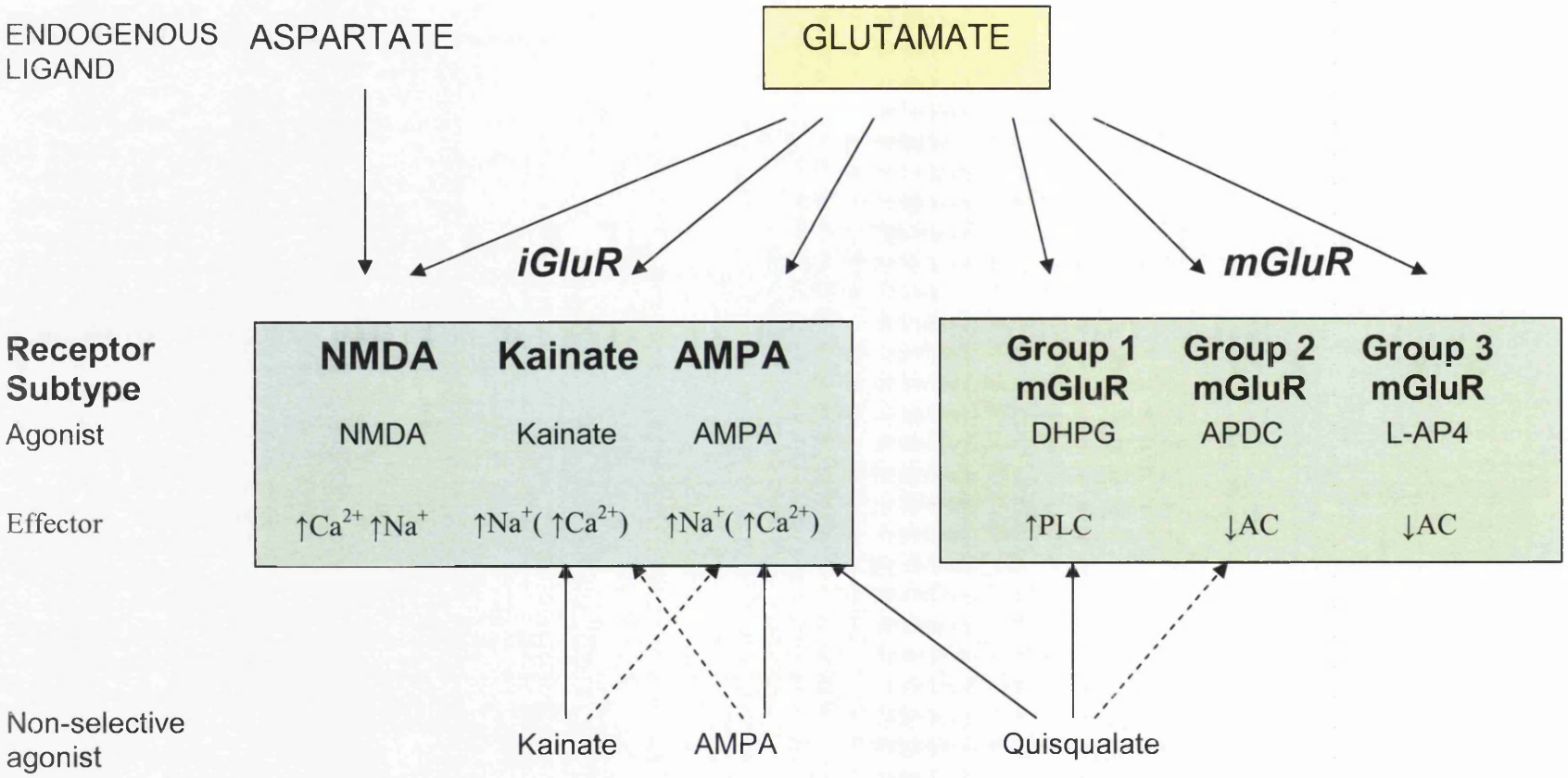

Figure 1.2 Pharmacology of glutamate receptor subtypes

The ionotropic (iGluR) and metabotropic (mGluR) glutamate receptors, their subtypes, agonists and the intracellular event associated with their activation. Adapted from Harris (1995).

ionotropic glutamate receptors (iGluRs) and **metabotropic** glutamate receptors (mGluRs; see Fig. 1.1 and 1.2). Ionotropic receptors contain integral cationic ion channels that are associated with a ligand binding site. iGluRs primarily gate Na^+, and in some cases Ca^{2+} influx, and K^+ efflux. mGluRs receptors are coupled to G proteins that modulate the production of intracellular second messenger systems. A number of subtypes of mGluRs exist, which cause changes in intracellular Ca^{2+} or cAMP levels.

iGluRs were subdivided into three major glutamate receptor subtypes, NMDA, AMPA and kainate on the basis of agonist specificities (Fig. 1.2 and 1.3). However, the iGluRs were commonly referred to as the NMDA and non-NMDA receptors because historically, no agonists or antagonists could clearly distinguish between AMPA or kainate receptors. Radioligand and electrophysiological studies revealed that there was an overlap between the actions of AMPA and kainate (reviewed in Fletcher and Lodge, 1996).

Using a variety of approaches, it was eventually proven that AMPA and kainate receptors are separate entities. Radioligand binding studies showed that separate *high* affinity [^{3}H]AMPA and [^{3}H]kainate binding sites are present in the rat brain (Young and Fagg, 1990). Secondly, the desensitising responses of the two receptors can differ upon application of agonists or modulators. At AMPA receptors, AMPA evokes rapidly desensitising responses, whereas kainate evokes comparatively nondesensitising responses. In contrast, at kainate receptors, kainate causes rapid desensitisation, whilst AMPA evokes weak, non-desensitising currents (Fletcher and Lodge, 1996, Wilding and Heuttner, 1997). The plant lectin concanavalin A (conA) selectively blocks desensitisation of only kainate receptors, whereas the benzothiazide cyclothiazide selectively blocks desensitisation of AMPA receptors, whilst remaining inactive at kainate receptors (Partin *et al.*,1993; Yamada and Tang, 1993). These drugs have become extremely useful for distinguishing between AMPA and kainate receptors. Thirdly, crucial evidence for a distinction between AMPA and kainate receptors came from the synthesis of antagonists that are selective only for the AMPA or kainate receptor. For example the AMPA antagonists GYKI 52466 and GKYI 53655 (LY300168), which are a 2,3 benzodiazepines, have a blocking effect on AMPA receptors, but have little effect on kainate receptors (Donevan and Rogawaski, 1993; Donevan *et al.*, 1994; Wilding

and Huettner, 1995). However, the ultimate, compelling evidence for distinct AMPA and kainate receptors came from revolutionary advances in molecular biology techniques. The molecular cloning of glutamate receptor subunits has identified the genetic basis for GluRs, and finally confirmed that there are distinct genes for AMPA and kainate receptors (Hollmann *et al.*, 1989; Bettler *et al.*, 1990; Keinanen *et al.*, 1990).

1.1.2 Molecular Biology of AMPA receptors

One of the most important advancements in the study of glutamate receptors was the discovery and cloning of the genes that encode the glutamate receptor subtypes. Several distinct but related genes have been identified; this diversity accounts for the pharmacological and functional heterogeneity of glutamate receptors throughout the brain (Hollmann and Heinemann, 1994). Hollmann and colleagues cloned the first glutamate receptor in 1989, which was later discovered to be an AMPA receptor subunit (GluR1). Using the sequence of GluR1 enabled homology cloning of the other subunits of the AMPA receptor, which are named GluR2, GluR3 and GluR4 (Bettler *et al.*, 1990; Keinanen *et al.*, 1990). Other ionotropic and metabotropic glutamate family member genes have been identified, as figure 1.3 shows. There are currently 6 families of iontropic glutamate receptors which have been identified by sequence homology: a single AMPA family, two for kainate and three for NMDA (see figure 1.3A, reviewed in Dingledine *et al.*, 1999). Within a family, there is considerable homology, but between families a lesser degree of similarity exists, roughly 40-50%. This suggests a common evolutionary origin for all ionotropic glutamate receptor subtypes (Dingledine *et al.*, 1999; Dingledine and McBain, 1999; see Fig. 1.3B).

AMPA Receptor Subunit Topology

The currently proposed topology for the glutamate receptor subunit is presented in figure 1.4. It is comprised of three transmembrane segments (M1, M3, M4), a loop segment in the membrane which does not transverse the membrane (M2), and an intracellular C terminus (figure 1.4; Bennett and Dingledine, 1995). The M3 to M4 domain is extracellular, this loop is important for the desensitising properties of the receptor (Fletcher and Lodge, 1996). Regions in both the amino terminal (NH_2) and in the loop between M3 and M4 (referred to as S1 and S2) form glutamate binding domains, thought to exist as two lobes separated by a cleft (Armstrong *et al.*, 1998).

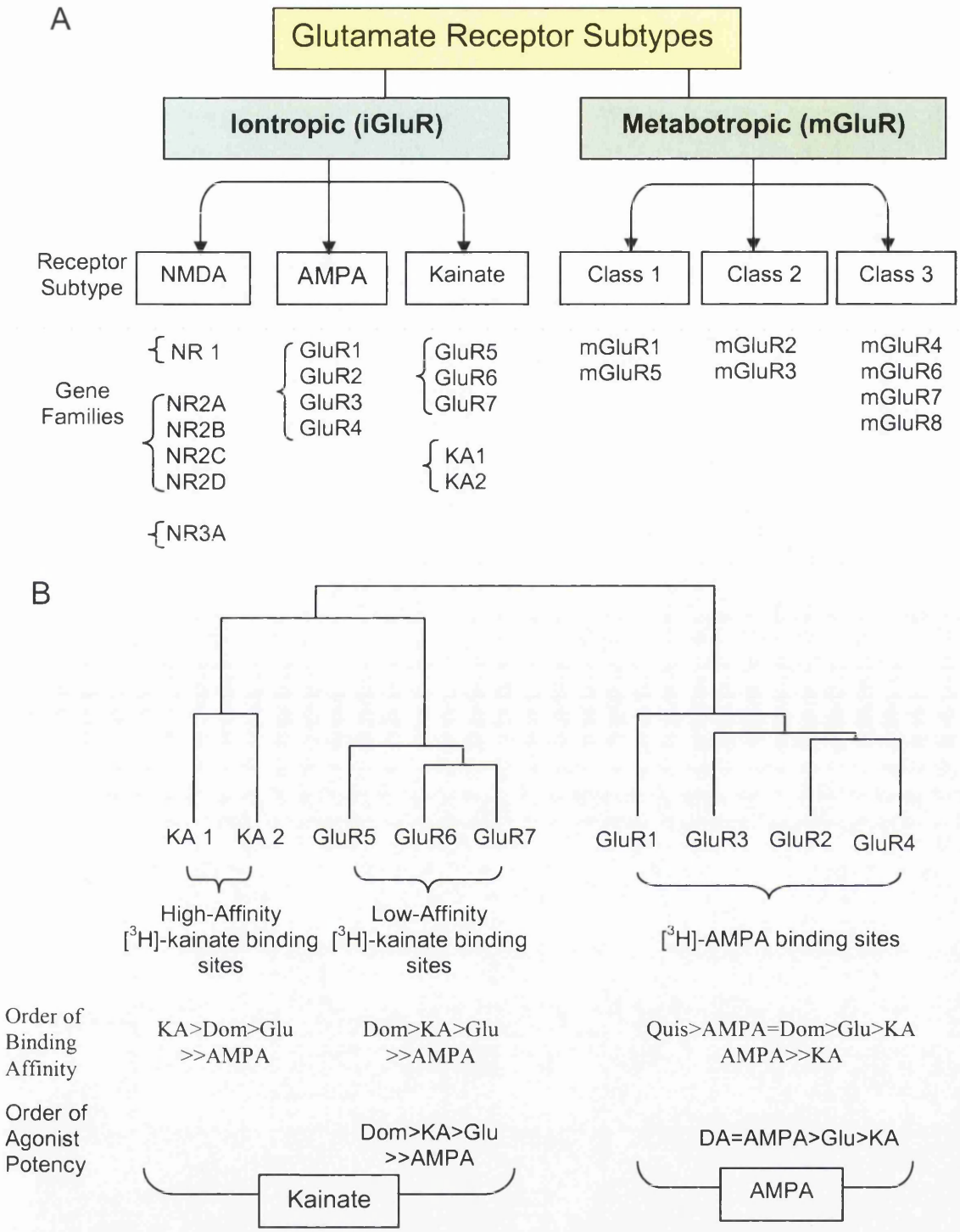

Figure 1.3 Molecular families of glutamate receptors

A. The receptor subtypes of iGluRs and mGluRs, which each have three defined groups of receptors, which are comprised of individual subunits, each encoded by a different gene (from Dingledine and McBain, 1999).

B. Evolutionary relationship among cloned AMPA and kainate receptor subunits. The length of line separating the subunits is proportional to their evolutionary distance (adapted from Bettler and Mulle, 1995 and Fletcher and Lodge, 1996). KA=kainate; Dom= domoate; Glu=glutamate; Quis=quisqualate.

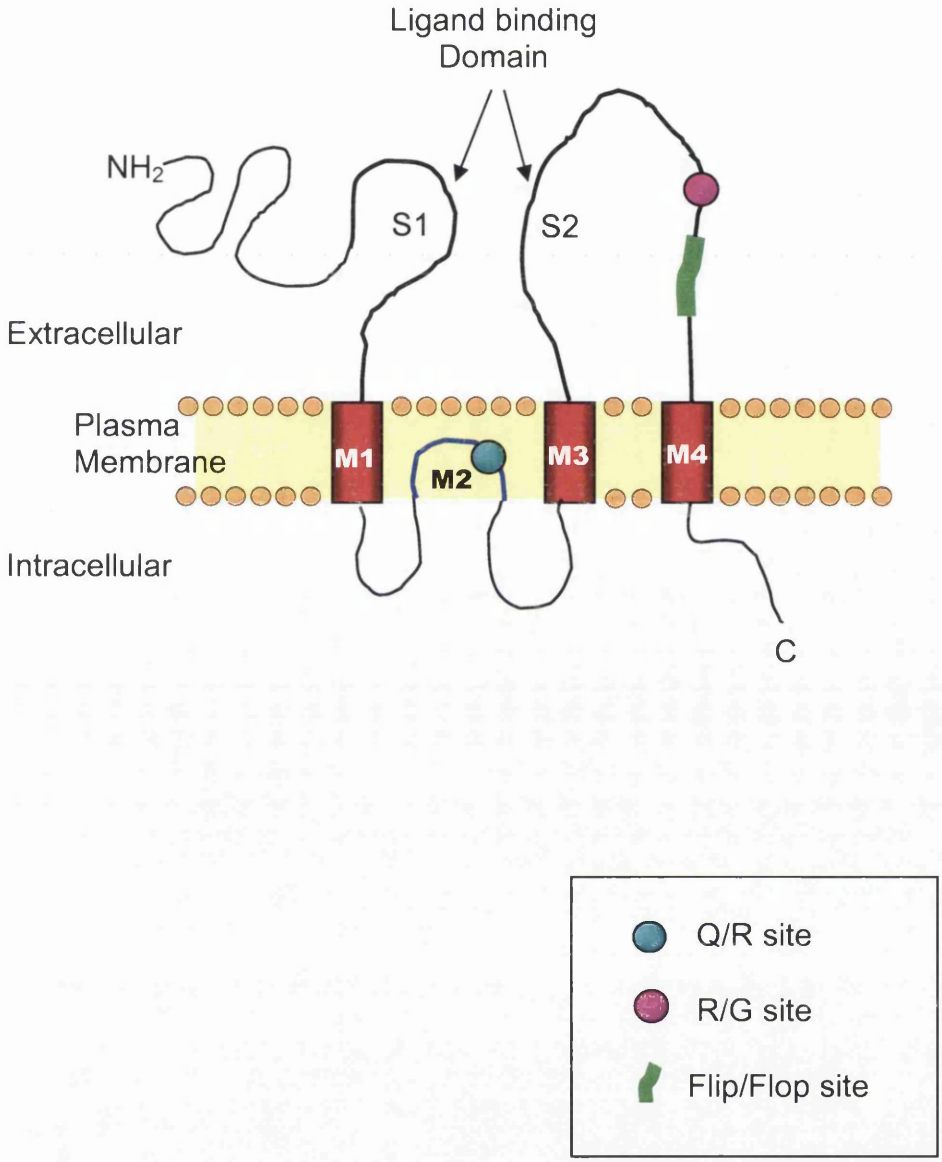

Figure 1.4 Structure of the AMPA receptor subunit

There are three transmembrane domains (M1, M3, M4). Two portions of the extracellular domains (S1 and S2) are thought to form the ligand binding domain. The intracellular loop portion (M2) contains the Q/R site, editing here governs the Ca^{2+} permeability of the receptor subunit. Adapted from Bennett and Dingledine (1995).

The re-entrant membrane loop M2, is thought to be responsible for the ion pore lining region of the receptor; editing of this domain at a 'Q/R' site can affect the ion permeability of the receptor (see later).

AMPA receptor stoichiometry

In vivo, AMPA receptors are thought to be multimeric assemblies of individual subunits. Recent data favours a tetrameric complex (Dingledine *et al.*, 1999; Egebjerg and Jensen, 2002). Considerable functional diversity arises from the conformation of the subunits, as AMPA receptor subunits can generate receptors in homomeric (i.e. composed of one receptor subtype) or heteromeric (i.e. composed of combinations of GluR1-4) combinations (Wenthold *et al.*, 1996). *In situ* hybridisation and immunocytochemical studies have revealed a varied distribution of the subunits GluR1-4 in the CNS (Keinanen *et al.*, 1990; Petralia and Wenthold, 1992). However, little information is available regarding the exact subunit conformation of native AMPA receptors. Evidence suggests that AMPA receptor subunit stoichiometry is not fixed but can vary, and furthermore, different AMPA receptor combinations can co-exist within the same neuron (Dingledine *et al.*, 1999).

Alternative Splicing and RNA editing of AMPA receptor subunits

The presence or absence of the GluR2 subunit in AMPA receptors has important implications for the ion permeability of the receptor. If GluR2 is present, the receptor has low permeability to Ca^{2+} and exhibits a linear relationship between voltage applied to the membrane and current passing through the ion channel. However, receptors that do not possess the GluR2 subunit have high Ca^{2+} permeability and current-voltage relationships that double rectify (Hollman *et al.*,1991; Burnashev *et al.*, 1992; Jonas and Burnashev, 1995). A single amino acid in the M2 channel pore is responsible for impermeability of GluR2 to Ca^{2+} (Hume *et al.*, 1991; Verdoorn *et al.*,1991). At position 586 in the protein, GluR2 has an arginine residue, whereas GluR1, -3 and –4 have a glutamine residue in the same location. Glutamine is a neutral amino acid that will confer Ca^{2+} permeability, whereas arginine is positively charged, and repels Ca^{2+}. Based on the shorthand for arginine (R) and glutamine (Q), this site has been named the Q/R site, (see figure 1.4). The conversion of glutamine (Q) to arginine (R) on GluR2 subunits is not

encoded by the GluR2 gene, but instead arises as a result of post-transcriptional editing of the mRNA (Sommer *et al.,* 1991; Higuchi *et al.,* 1993). In health, the majority of GluR2 subunits have undergone this editing in the adult rat brain, and are therefore impermeable to Ca^{2+}. However, in some neurodegenerative conditions, there is a down regulation of GluR2 gene expression, resulting in an increase of Ca^{2+} permeable AMPA receptors, which may enhance the toxicity of glutamate (Pellegrini-Giampietro *et al.,* 1997; Weiss and Sensi, 2000).

Further heterogeneity in the physiological characteristics of AMPA receptors arises from the 'flip' and 'flop' exon splice variants of the AMPA receptor subunits. The mRNA encoding GluR1-4 can exist in two forms that differ by 9-11 amino acids contained within a 38 amino acid sequence in the M3-M4 extracellular loop (Figure 1.4; Sommer *et al.,* 1990). This flip/flop region comprises only ~4% of the subunit protein, yet it can alter the electrophysiological and drug binding properties of the receptor. This is because 'flip' isoforms desensitise less rapidly than 'flop' isoforms, thus altering the sensitivity of the receptor to allosteric modulators (see section 1.1.4; Sommer *et al.,* 1990). Greater levels of the flip isoform are expressed in the neonate, whereas the mature CNS contains predominately flop isoforms, although there are regional variances (Sommer *et al.,* 1990; Monyer *et al.,* 1991; Fletcher and Lodge, 1996). Further diversity arises from editing at an exon preceding the flip/flop site. At this site, editing of an arginine (R) to a glycine (G) results in currents that recover more rapidly from agonist-induced desensitisation. Editing at this R/G site occurs in GluR-2, -3 and –4 but not GluR1 (Lomeli *et al.,* 1994). Again, the extent of editing at the R/G site varies during development, but in adults, most R/G sites are edited to glycine. Taken together, these findings suggest that an array of functionally distinct AMPA receptors could exist in the brain depending on the subunit composition and degree of post-transcriptional editing. This heterogeneity could account for the diversity of excitatory neurotransmission within the CNS.

Post-translational modification of AMPA receptors

Following synthesis of the AMPA receptor subunit, it can undergo enzymatic post-translational modifications that can affect the function of the receptor. For example, glutamate receptors are under tight control by various phosphokinases (Wenthold and Roche, 1998; Dingledine *et al.,*1999). Substantial evidence suggests that

phosphorylation of AMPA receptors by cAMP-dependent protein kinase (PKA), protein kinase C (PKC) and calcium/calmodulin dependent protein kinase II (CAM-KII) potentiates current flow in AMPA receptors (reviewed in Wenthold and Roche, 1998; Dingledine *et al.*, 1999). Conversely, dephoshorylation of glutamate receptor subunit protein has the opposite effect, diminishing the response of the receptor to agonists, where as inhibiting phosphatases (enzymes that remove phosphate groups) enhances the currents stimulated by agonists (Raymond *et al.*, 1993; Wang *et al.*, 1996). Phosphorylation and subsequent modulation of AMPA receptors is an important mechanism of synaptic plasticity. This will be discussed in more detail in section 1.1.6.

1.1.3 Neurotransmission at AMPA receptors

Within glutamatergic synapses, glutamate is stored in synaptic vesicles at relatively high concentrations (~20mM). Following depolarisation of the terminal, glutamate is released into the synaptic cleft in a Ca^{2+} dependent, quantal manner (roughly 1mM/vesicle), where it can activate AMPA receptors located at the postsynaptic membrane (Nicholls, 1998). AMPA receptors are permeable to Na^+, and depending on the receptor subunit composition, can be permeable to Ca^{2+} (see section 1.1.2). Glutamate evokes fast depolarising currents and rapid desensitisation at AMPA receptors. This contrasts with the slow, prolonged depolarisation that occurs following glutamate activation of NMDA receptors (Trussel, 1998). Glutamate must be removed from the synaptic cleft rapidly, so that postsynaptic stimulation reflects release, and to avoid the toxic effects of high concentrations of glutamate (see section 1.2). Glutamate is unable to diffuse across plasma membranes, and no extracellular enzymes are capable of metabolising it. Instead, high affinity, Na^+ dependent glutamate transporters present on neurons and glial cells remove the extracellular glutamate. Five different Na^+ dependent glutamate receptors have cloned so far: GLAST (EAAT1); GLT (EAAT2); EAAC (EAAT3); EAAT4 and EAAT5. These different subtypes of glutamate receptor are expressed differentially throughout the CNS. The transporters utilise the electrochemical gradients of Na^+, K^+ and H^+ to drive glutamate into cells (Levy, 2002).

In addition to their function as ion channels, AMPA receptors can act as signal transducers, which can transmit signals to the nucleus to influence gene expression.

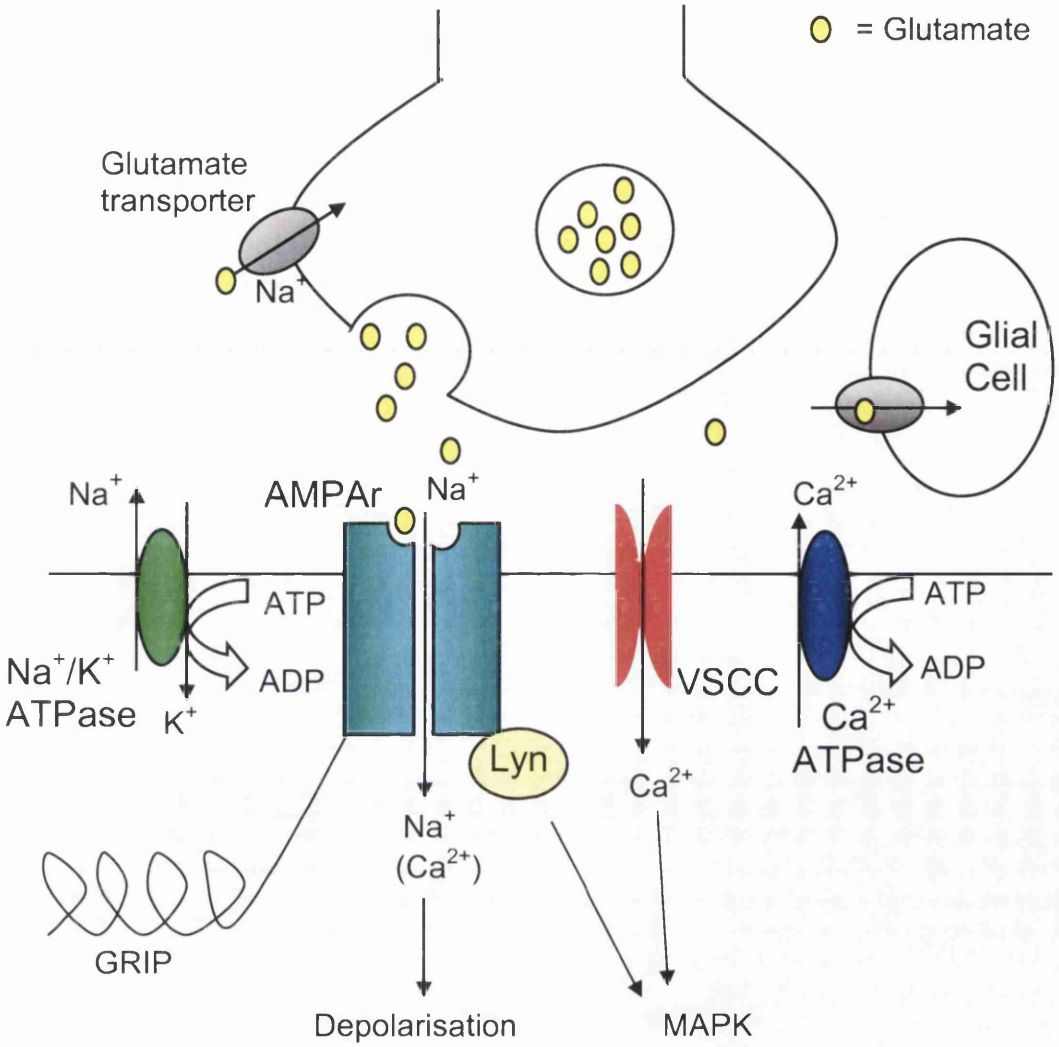

Figure 1.5 Glutamatergic neurotransmission at AMPA receptors

Glutamate is contained within synaptic vesicles, where it can reside at high concentrations (~20mM). Glutamate is released from synapses in a Ca^{+} dependent manner following depolarisation of the presynaptic neuron. Activation of the AMPA receptor results in Na^{+} influx; Ca^{2+} influx can also occur if GluR2 is absent from the receptor. High affinity glutamate transporters situated in the presynaptic neuron and adjacent glial cells rapidly take up glutamate from the synapse. Depolarisation of the postsynaptic membrane can cause Ca^{2+} influx through voltage sensitive Ca^{2+} channels (VSCC). Ion channels in the postsynaptic membrane actively pump ions to maintain the membrane potential (Na^{+}/K^{+} ATPase; Ca^{2+} ATPase; Ca^{2+}/Na^{+}anti-porter (not shown)). Activation of AMPA receptors can trigger mitogen-activated protein kinase pathways (MAPK) via activation of Lyn, with which it interacts. AMPA receptors are anchored in the postsynaptic density through interactions with GRIP.

This occurs via mitogen-activated protein kinase (MAPK) signalling pathways (Wang and Durkin, 1995; Wang *et al.*, 1997; Hayashi *et al.*,1999; Perkinton *et al.*,1999). For example, AMPA receptors have been shown to interact with the Src-family protein tyrosine Lyn, which can activate MAPK pathways that can induce synthesis of brain derived neurotrophic factor (Hayashi *et al.*, 1999).

1.1.4 Pharmacology of AMPA receptors

Agonists

AMPA receptors were originally termed quisqualate receptors based on the potency of quisqualate at these receptors, however the synthesis of AMPA, and the discovery that it was more selective than quisqualate at AMPA receptors, led to the revised nomenclature that is accepted today (figure 1.2; Krogsgaard-Larsen *et al.*, 1980; Collingridge and Lester, 1989; Lodge and Collingridge, 1990). Recombinant AMPA receptors (GluR1-4) have affinities for AMPA at least two fold higher than for kainate. However whilst AMPA, quisqualate, and glutamate evoke rapidly desensitising responses at AMPA receptors, kainate and domoate evoke non-desensitising responses (Keinanen *et al.*, 1990; Fletcher and Lodge, 1996). The rank order of agonist potency and order of binding affinity of these compounds is illustrated in figure 1.3B.

Competitive AMPA receptor antagonists

The development of a group of compounds called the quinoxalinediones, by Honore and colleagues (1988), revolutionised the study of selective AMPA antagonists, because until that point few non-NMDA antagonists were available. 6,7-dinitroquinoxaline-2,3-dione (DNQX) and 6-cyano-7-nitroquinoxaline-2,3-dione (CNQX) were the first reported compounds of this class. These are competitive antagonists at AMPA receptors; however, they also have antagonist effects at KA receptors, and can interact with the NMDA receptor glycine site (Birch *et al.*,1988). The quinoxalinediones 2,3-dihydroxy-6-nitro-7-sulfamoylbenzo(*F*)quinoxaline (NBQX) and 6-(1J-imidazol-1-yl)-7-nitro-2,3(1H,4H)-quinoxalinedione hydrochloride (YM90K) were developed by further substitution and modification of this class of antagonist (Sheadown *et al.*, 1990; Ohmori *et al.*, 1994). These AMPA receptor antagonists are considerably more potent and selective for AMPA compared to kainate receptors than CNQX or DNQX (Sheardown *et al.*, 1990). NBQX and other quinoxalinediones have been extremely useful compounds, used in a variety of

studies for manipulating AMPA/kainate receptors, however the low solubility and toxic effects in the kidney precludes their development as clinical compounds.

In the last ten years, numerous other competitive AMPA receptor antagonists have been developed with improved solubility and brain penetration (reviewed in Lees, 2000). For example the modified quinoxalinedione fanapanel (ZK-200775) has increased solubility and similar affinities and selectivity to NBQX (Turski *et al.*, 1998). An isatine oxime modification of the quinoxalinedione structure has resulted in the synthesis of SPD 502 (NS 1209) that exhibits similar potency to NBQX but is soluble, devoid of kidney toxicity and has longer lasting duration (Nielson *et al.*, 1999). YM872 is a further competitive AMPA receptor antagonist that has been developed which is soluble and potent, with low affinity for other glutamate receptors (Takahashi *et al.*, 2002).

A further class of potent, soluble competitive antagonists called the decahydroisoquinolines have been engineered, of which LY293558 is a representative compound (O'Neill *et al.*, 1998). These compounds were initially reported to be potent, selective AMPA antagonists based on their action at cerebellar purkinje neurons thought to comprise the AMPA receptor subunits GluR1-4. However, it was later shown that they have antagonist activity at iGluR5 receptors (Bleakman *et al.*, 1996).

Non-competitive AMPA receptor antagonists

The antagonists described in the previous section compete with agonists at the ligand-binding site. Non-competitive antagonists act at a different site on the receptor. One of the important and extensively studied groups of non-competitive AMPA antagonists are the 2,3 benzodiazepines, which are negative allosteric modulators (Vizi *et al.*, 1996). They can act on either open or closed channels, and hence do not show voltage- or use- dependency (Donevan and Rogawski, 1993). Two examples of this group are GYKI 52466 and GYKI 53655 (LY300164). These compounds appear to show a high degree of selectivity for AMPA compared to kainate receptor mediated events, and have therefore become important tools for the pharmacological separation of these two receptor subtypes (Wilding and Heuttner, 1995; Fletcher and Lodge, 1996). The potencies of 2,3 benzodiazepines

are affected by cyclothiazide, a desensitisation blocker that acts as a positive allosteric modulator (Palmer and Lodge, 1993). It was once thought that cyclothiazide and the 2,3 benzodiazepines may act at a common site. However, mutating the site on the AMPA receptor subunit at which cyclothiaziade acts does not alter the sensitivity of the receptor to 2,3 benzodiazepine (Partin and Mayer, 1996), confirming that these compounds act a different sites on the AMPA receptor. Further non-competitive AMPA receptor antagonists which have recently been developed are CP-465,022 and YM928 (Lazzaro *et al.,* 2002; Menniti *et al.,* 2003; Ohno *et al.,* 2003).

AMPA receptor potentiators

AMPA receptor potentiators are positive allosteric modulators that increase current flux through the ion channel in the presence of agonist, by reducing desensitisation and/or deactivation of the receptor (Yamada and Tang, 1993; Partin *et al.,* 1994, 1995, 1996; Arai *et al.,* 1996; Sekiguchi *et al.,* 1997; Miu *et al.,* 2001). Fifteen years ago, relatively little was known about AMPA receptor potentiators, however since then a number of different classes of AMPA receptor potentiators have been synthesised, and a wealth of experiments has contributed to an increased understanding of their mechanism of action and effects. Experiments utilising these compounds have also contributed to the understanding of the kinetics of glutamate receptor desensitisation; furthermore, they represent a novel therapeutic strategy in a number of neurological conditions. Three major classes of AMPA receptor potentiators have been developed, the pyrrolidinones and related compounds, thiazide derivatives and the biarylpropylsulfonamides.

The plant lectin concanavalinA, was amongst the first non-NMDA receptor potentiator to be utilised (Mayer and Vycklicky, 1989; Huettner, 1990). Ito and colleagues (1990) then performed a crucial experiment that advanced the understanding and development of AMPA receptor potentiators. A group of 'nootropic' drugs, called pyrrolidinones, of which aniracetam and piracetam are examples, had been known to possess positive effects in treating cognitive deficits (reviewed in Lee and Benfield, 1994). However, little was understood about the mechanism of action of pyrrolidinones. On the basis that non-NMDA receptors contributed to the cellular mechanisms of long term potentiation (LTP), a neural substrate that contributes to the formation of memory, Ito and colleagues (1990)

hypothesised that aniracetam may act by potentiating activity at non-NMDA receptors. They reported that aniracetam could selectively enhance quisqualate or AMPA receptor-mediated responses in *Xenopus* oocytes injected with rat brain mRNA, or in hippocampal pyramidal cells. It was subsequently revealed that aniracetam enhanced AMPA receptor mediated responses by reducing receptor desensitisation and slowing the decay of fast excitatory synaptic currents upon removal of agonist (deactivation) (Icaason and Nicoll, 1991; Tang *et al.,* 1991).

Pyrrolidones such as aniracetam are metabolised rapidly, have poor brain penetrability and low potencies. A group of structurally related benzoylpiperidines and benzoylpyrollidines that have AMPA receptor potentiating properties have been developed, which are commonly referred to as 'Ampakines' (Arai *et al.,* 1994; Staubli *et al.,* 1994a, b; Davies *et al.,*1997; Hamspson *et al.,* 1998). These include 1-(1,3-benzodioxol-5-ylcarbonyl) piperidine (1-BCP, BDP, BA-14), BDP-12 (BA-74 or CX-516) and its analogue BDP-20, and CX-546. These compounds have greater potency and blood brain barrier permeability than aniracetam and piracetam.

Another class of AMPA receptor potentiators are thiazide derivatives, of which diazoxide is the prototype. Yamada and Rothman (1992) initially used diazoxide to activate ATP-sensitive K^+ channels, however unexpectedly discovered that it caused potentiation of glutamatergic synaptic responses. Structural similarities of diazoxide with a group of clinically utilised diuretics called benzothiazides prompted Yamada and Tang (1993) to evaluate the effects of these compounds on quisqualate evoked currents. This led to the discovery that cyclothiazide was a potent and efficacious AMPA receptor potentiator (Yamada and Tang, 1993). Since then, cyclothiazide has been one of the most extensively utilised AMPA receptor potentiators. Partin and colleagues (1993) used recombinant AMPA and kainate subunits to determine that cyclothiazide was a highly selective modulator of AMPA receptors; whereas ConA was a highly selective modulator of kainate receptors. In addition, cyclothiazide appears to have preferential activity at flip isoforms of AMPA receptors (Partin *et al.,* 1995). Another thiazide derivative is IDRA 21, which acts selectively at AMPA receptors to reduce receptor desensitisation (Bertolino *et al.,* 1993; Impagnatiello *et al.,* 1997).

A third class of AMPA receptor potentiators has recently been developed, the biarylpropylsulfonamide compounds, of which LY404187 and LY392098 are representative compounds (Ornstein *et al.*, 2000). LY392098 and LY404187 enhance AMPA- or glutamate-induced currents *in vitro* and *in vivo*, with greater potency than previously described AMPA receptor potentiators such as CX-516 (Baumbarger *et al.*, 2001a and b; Gates *et al.*, 2001; Vandergriff *et al.*, 2001). LY392098 can enhance the action potential discharge rate in response to stimulation of glutamatergic afferents *in vivo* (Baumarger *et al.*, 2001a, b, Vandergriff *et al.*, 2001). Furthermore, LY404187 or LY392098 have minimal effects on NMDA or GluR5 mediated-kainate induced currents *in vitro*, and AMPA receptor antagonism attenuates the effects of LY329098 *in vitro*, suggesting the these compounds are selective for AMPA receptors (Baumbarger *et al.*, 2001a, b;Gates *et al.*, 2001). Studies with recombinant homomeric AMPA receptor subunits have suggested that LY392098 and LY404187 have different potencies at receptors composed of GluR1-4, for example, LY404187 is most potent at GluR2 and least potent at GluR4 receptor subunits (Miu *et al.*, 2001). Furthermore, LY404187 is more potent at flip versus flop AMPA receptors (Miu *et al.*, 2001).

Other compounds also possess modulatory influences on AMPA receptors. PEPA is a sulfonylamino compound that can potentiate glutamate-evoked currents in recombinant AMPA but not kainate or NMDA receptors. In contrast to cyclothiazide and LY404187, PEPA preferentially modulates AMPA receptor flop isoforms, with a selectivity profile for the AMPA receptor subunits of GluR3>GluR4>GluR1 (Sekiguchi *et al.*, 1997). Thiocyanate is a chaotropic modulator, previously shown to enhance high affinity AMPA binding, which decreases the desensitisation of recombinant GluR1 flop, but increases the desensitisation of GluR1 flip receptors (Partin *et al.*, 1996).

Site directed mutagenesis studies have revealed that a single serine amino acid within the flip/flop domain ($S^{750}Q$) of GluR1 is responsible for determining the cyclothiazide sensitivity of the AMPA receptor subunit, (Partin *et al.*, 1994). Replacing the serine with a variety of different amino acids differentially modulates the effects of aniracetam or cyclothiazide on desensitisation and deactivation, suggesting that these two AMPA receptor potentiators may act at different sites or by different mechanisms (Partin *et al.*, 1996). A mutation on the equivalent domain of

GluR4 ($S^{776}Q$) reduces, but does not eliminate the sensitivity of the subunit to potentiation by LY404187 (Quirk *et al.,* 2002).

The different classes of AMPA receptor potentiator described above vary in potency and selectivity in a subunit and splice variant specific manner. In addition, AMPA receptor potentiators can have varying effects on AMPA receptors *in situ.* For example, cyclothiazide can potentiate synaptic responses to AMPA in brainstem slices, yet it has minimal effects in hippocampal slices (Yamada *et al.,* 1998a), whilst LY404187 is more efficacious at purkinje cells compared to neurons from the prefrontal cortex (Quirk and Nisenbaum, 2002). This diversity is likely to reflect the heterogeneity of receptor subunit combinations and splice variants in the brain, which in turn suggests that there is physiological diversity of excitatory neurotransmission.

1.1.5 Distribution of AMPA receptors in the CNS

A variety of techniques have examined the distribution of AMPA receptors in the rodent CNS, which are abundant and widespread. The distribution of AMPA receptors within the CNS was initially investigated using [^{3}H] AMPA ligand-binding studies. The brain regions that contain the highest levels of [^{3}H] AMPA binding were the hippocampus, cerebral cortex, septum and striatum (Monaghan *et al.,* 1984; Rainbow *et al.,* 1984; Olsen et al; 1987; Insel *et al.,* 1990). In particular, within the hippocampus, higher receptor densities were found in CA1 and dentate gyrus compared with CA2/3, and in the pyramidal cell layer compared to the stratum radiatum and stratum oriens (Olsen *et al.,*1987; Insel *et al.,*1990). In the cortex, similar levels of [^{3}H] AMPA binding were reported in the frontal, parietal and temporal cortices; however, a laminar appearance was evident, with higher binding levels in the outer layers (I-III) compared with the middle (V) and deep (VI) layers. The entorhinal and pyriform cortices contained a more uniform pattern of [^{3}H] AMPA binding, with particularly low and high levels of binding, respectively (Monaghan *et al.,* 1984). In the striatum, the caudate nucleus contained intermediate levels of receptor binding, whereas the globus pallidus contains lower levels of ^{3}H-AMPA binding. Lower levels of [^{3}H]AMPA binding are reported in the midbrain and brainstem.

The discovery of the genes encoding the four subunits of the AMPA receptor, GluR1-4, initiated further investigation into the distribution of the particular subunits within the CNS, using *in situ* hybridisation to detect mRNA, and immunohistochemistry to detect proteins (Keinanen *et al.,* 1990; Sommer *et al.,* 1990; Petralia and Wenthold *et al.,* 1992; Martin *et al.,* 1993). Immunolabelling of the GluR1-4 subunits was consistent with the distribution of mRNA and with the overall pattern of [^{3}H]AMPA binding, however there were regional differences in the pattern of the individual subunits (Petralia and Wenthold, 1992). For example, the pattern of GluR1 immunostaining was heterogeneous, with marked contrast between densely and lightly stained structures. GluR2/3 exhibited the most widespread and densely immunostained pattern, and there were moderate levels of GluR4 immunostaining. In the cortex, GluR2 is expressed uniformly throughout all layers, whereas GluR1 and 4 are more abundant in layers I, V and VI; in the hippocampus, GluR1 and 2/3 are abundant, but there is less GluR4. This differential pattern of immunostaining suggests that a large number of subunit combinations can be expressed by neurons, and single cell PCR studies confirm this (Lambolez *et al.,* 1992; Mackler and Eberwine, 1993). In the adult, the flop isoforms of AMPA receptors predominate, although there are regional variances, for example, hippocampal CA3 pyramidal cells express only flip subunits (Sommer *et* al., 1990; Monyer *et al.,* 1991). In addition, within the mature nervous system, the majority of GluR2 subunits have undergone editing at the Q/R site, whilst virtually all GluR2-4 subunits have undergone R/G editing (Sommer *et al.,* 1991; Lomeli *et al.,* 1994).

At the cellular level, AMPA receptor subunits are located at the plasma membrane of cell bodies and dendrites of neurons, where they are localised predominantly at postsynaptic densities (Petralia and Wenthold, 1992). AMPA receptors with different subunit stoichiometry can co-exist on an individual neuron. They can also-coexist with kainate or NMDA receptors on individual neurons (Dingledine *et al.,* 1999). In addition to their presence on neurons, AMPA receptors have also been localised to glial cells such as astrocytes, microglia and oligodendrocytes (Noda *et al.,* 2000; Gallo and Ghiani, 2000); this will be discussed in greater detail in section 1.3.3.

1.1.6 Function of AMPA receptors – fast excitatory transmission and plasticity

Activation of AMPA receptors by glutamate is thought to be responsible for the majority of fast excitatory transmission with the brain. Given their ubiquitous distribution, AMPA receptors are involved in many of the functions of the CNS. The physiological relevance of AMPA receptor-mediated transmission can often be inferred by examining clinical disorders where glutamatergic transmission is disturbed, or where AMPA receptor ligands are therapeutically beneficial. Thus, the involvement of AMPA receptors in ischaemia, trauma, epilepsy, pain, schizophrenia, and potential roles in neurodegenerative diseases highlights the importance and ubiquitous nature of fast glutamatergic transmission at AMPA receptors.

AMPA receptors are also involved in long-lasting alterations in neuronal structure and function, known as synaptic plasticity. One example of this is long-term potentiation (LTP), a proposed cellular mechanism of memory formation. LTP describes the long lasting enhancement of synaptic transmission at a synapse following a short burst of presynaptic stimulation (Bliss and Lomo, 1973; Bliss and Collingridge, 1993). LTP depends on simultaneous electrical activity in both the pre- and post-synaptic neurons. The enhancement of synaptic transmission appears to involve both increased glutamate release and an enhanced post-synaptic response. Ca^{2+} entry through NMDA receptors, and the subsequent activation of protein kinases, calpains, phospholipases, and phosphatases are thought to contribute to the mechanism of LTP. Activity at AMPA receptors contributes to the induction of LTP by depolarising the postsynaptic membrane and relieving the Mg^{+} block of NMDA receptors to enable their activation. The contribution of AMPA receptors to LTP is inferred from the ability of AMPA receptor potentiators to augment LTP and enhance performance in rodent and human tests of cognition (Stuabli *et al.,* 1994a, b; Ingvar *et al.,* 1997); conversely, AMPA receptor antagonism results in cognitive deficits (Riedel *et al.,* 1999). Aside from their role as a fast acting neurotransmitter that can relieve the Mg^{+} block of NMDA receptors, events at the AMPA receptor can also induce long lasting plastic changes that may contribute to LTP. Phosphorylation of AMPA receptors (see section 1.1.2), which can potentiate ion flux through the receptor, is thought to be one of the underlying mechanisms of LTP. Thus, electrical stimulation of neurons resulting in LTP causes phosphorylation of AMPA receptors mediated by CAM-KII (Barria, 1997). In addition to modulation of AMPA

receptors, it has been hypothesised that phosphorylation of the AMPA receptor may increase the number of functional AMPA receptors in the postsynaptic membrane (Wenthold and Roche, 1998). Irrespective of the role of phosphorylation, it has been speculated that the induction of LTP may involve a switch from synapses containing only NMDA receptors ('silent synapses') to synapses containing both functional AMPA and NMDA receptors, via the insertion of new AMPA receptors into the membrane from intracellular stores (Luscher and Frerking, 2001; Henley, 2003).

Stimulation of AMPA receptors can trigger signal transduction cascades through the interaction of the AMPA receptor with the Src-family tyrosine kinase Lyn (Hayashi *et al.*, 1999). Na^+ and Ca^{2+} independent Lyn activation following AMPA receptor activity triggers mitogen-activated protein kinase (MAPK) signalling pathways which influence gene expression at the nucleus. For example, AMPA-receptor mediated MAPK pathways can cause the induction of brain-derived neurotrophic factor (BDNF) gene expression (Hayashi *et al.*, 1999). BDNF expression may also be activated following AMPA receptor activation via Ca^{2+} influx through voltage activated Ca^{2+} channels. BDNF is thought to play a crucial role in synaptic plasticity, including the induction, expression and maintenance of LTP (McAllister *et al.*, 1999; Poo, 2001).

1.2 Mechanisms of Brain Injury - Excitotoxicity

Glutamate can be considered a 'Jekyll and Hyde' molecule that serves essential roles as a neurotransmitter and metabolic intermediate whilst having potentially damaging, neurotoxic effects (Olney, 1990). Based on its role in metabolism, it was initially hypothesised that application of glutamate to the eye may alleviate retinal neurodegeneration. Instead however, it was unexpectedly discovered that it induced rapid neurodegeneration (Lucas and Newhouse, 1957). This neurotoxic property was later confirmed in the brain, and was subsequently named 'excitotoxicity' by John Olney (Olney, 1969; Olney and Sharp, 1969; Olney, 1971). These initial experiments focused on peripheral administration of high concentrations of glutamate, which was only toxic to neurons in certain brain areas of immature animals. However subsequent studies showed that intracerebral injection of glutamate or analogues of glutamate caused neuronal damage (Olney *et al.*, 1975;

Coyle and Schwarz, 1976; Simson *et al.,* 1977). In addition, exposure of neuronal cell cultures to glutamate induces toxic effects (Choi *et al.,* 1987).

1.2.1 Mechanisms of glutamate-induced excitotoxicity

High concentrations of glutamate or glutamate analogues are thought to kill neurons by over-activation of glutamate receptors. Thus, blockade of glutamate receptors prevents excitotoxicity *in vivo* and *in vitro* (Olney *et al.,* 1979, 1981; Foster *et al.,* 1984; Rothman *et al.,* 1984). Olney initially based his 'excitotoxic' theory on the correlation that existed between the excitatory actions of various glutamate agonists with their toxicity, suggesting that sustained depolarisation of the neuron by glutamate resulted in a lethal exhaustion of cellular energy reserves. Subsequent evidence suggested an important role for ionic imbalances and Ca^{2+} -mediated mechanisms, and suggested that there may be two phases in glutamate receptor-mediated toxicity. Initially, the sustained depolarisation associated with over activation of glutamate receptors results in Na^+ and Cl^- influx through monovalent ion channels. Because the vast Na^+ and Cl^- influx is larger than the K^+ efflux, water enters neurons passively, causing cell swelling and oedema. Removal of Na^+ or Cl^- from the media of cultured neurons prevented the initial cell swelling caused by toxic levels of glutamate (Rothman 1985; Olney *et al.,* 1986). Rapid Na^+ entry is thought to be responsible for early glutamate-induced necrosis. Whilst removal of Na^+ and Cl^- prevented initial cell swelling following glutamate exposure, neurons still degenerated at a later time point which was dependent on the presence of Ca^{2+} in the medium, suggesting that a secondary, delayed Ca^{2+}-dependent excitotoxic death occurred (Choi, 1987). Pre-treatment with Ca^{2+} chelators can attenuate excitotoxic neuronal cell death *in vivo* and *in vitro* (Tymianski *et al.,* 1993). Elevated levels of intracellular Ca^{2+} initiate a complex cascade of inter-related intracellular events that ultimately result in cell death. For example, the activation of nucleases can result in DNA fragmentation; cytosolic proteases such as calpain can attack the cytoskeleton; kinases such as PKC can modify the phosphorylation states of proteins and disrupt cell function; whilst lipases can attack the cell membrane and intracellular organelles. In addition, Ca^{2+} can also activate enzymes involved in the production of reactive oxygen species (ROS) and nitric oxide (NO) (Kristian and Siesjo, 1997).

There are a number of hypothesised routes by which intracellular Ca^{2+} can become elevated following glutamate receptor activation (Choi, 1988). Glutamate receptor

activation could cause a Ca^{2+} influx directly through NMDA or Ca^{2+} permeable AMPA receptors. Activation of glutamate receptors causes depolarisation in the postsynaptic cell, which activates voltage sensitive Ca^{2+} channels, causing further influx of Ca^{2+}. The disruption of ionic homeostasis caused by sustained depolarisation may disturb the ion pumps that act to keep intracellular Ca^{2+} levels low; thus reversal of the Na^{+}/Ca^{2+} exchanger and inactivation of the Ca^{2+}-ATPase will result in elevated $[Ca^{2+}]_i$. Disrupted ionic homeostasis may also result in the release of Ca^{2+} from intracellular stores.

1.2.2 Excitotoxicity and acute neuronal degeneration

The potential role of excitotoxicity as a pathogenic mediator of CNS disorders was investigated when the neurotoxic potential of glutamate was established. A compelling role for excitotoxic mechanisms in the pathogenesis of cerebral ischaemia was recognized. Rothman (1984) was amongst the first to suggest a role for excitotoxicity in ischaemia when he showed that a glutamate receptor antagonist could attenuate anoxic neuronal death *in vitro*. Microdialysis techniques subsequently demonstrated that there was a massive increase in the extracellular concentration of glutamate following experimental focal or global cerebral ischaemia and CNS trauma (Benveniste *et al.*, 1984; Butcher *et al.*, 1990). Following focal cerebral ischaemia, the rise in extracellular glutamate positively correlated with the size of lesion that subsequently developed (Butcher *et al.*, 1990). Microdialysis monitoring of patients with ischaemic stroke or head injury has extended these observations to humans, demonstrating elevated levels of glutamate in CSF (Persson *et al.*, 1992; Castillo *et al.*, 1997). However, perhaps the most compelling role for excitotoxicity in cerebral ischaemia is the significant attenuation of ischaemia cell damage following administration of glutamate receptor antagonists in experimental models of focal and global cerebral ischaemia. Due to the direct permeability of NMDA receptors to Ca^{2+} and the evidence suggesting the importance of Ca^{2+}-mediated damage in excitotoxicity, NMDA receptors were thought to be the main mediators of excitotoxic damage and hence NMDA receptor antagonists were examined initially. NMDA receptor antagonists confer robust neuroprotection in animal models of focal cerebral ischemia (Ozyurt *et al.*, 1988; Park *et al.*, 1988a, b; Bullock *et al.*, 1990). Initial, promising neuroprotective effects with NMDA receptor antagonism in models of global ischaemia may have been due to hypothermic

affects, and the general consensus now is that they are less effective in global ischaemia models (Gill *et al.,* 1987; Buchan and Pulsinelli, 1990). In contrast, AMPA receptor antagonism confers potent, neuroprotective effects in both focal and global models of cerebral ischaemia, confirming the fundamental role for this receptor in excitotoxicity (Gill *et al.,* 1992; Buchan *et al.,* 1993; Sheardown *et al.,* 1990, 1993; Bullock *et al.,* 1994; Xue *et al.,* 1994). The superior neuroprotection conferred by AMPA receptor antagonists, combined with a longer therapeutic time window than NMDA receptor antagonists suggested they may be more efficacious in the clinic, however glycine site NMDA receptor antagonists may also have these attributes (Gotti *et al.,* 1988).

Taken collectively, there is convincing evidence that excitotoxicity contributes to pathology underlying cerebral ischaemia. It is the metabolic inhibition and impaired ATP production that particularly predisposes ischaemic tissue to excitotoxic damage (see Fig. 1.6). Ionic membrane pumps such as the Ca^{2+} ATPase and the Na^{+}/K^{+} ATPase cease functioning with lack of ATP. Consequently ionic gradients are disrupted, membrane potential is lost, and neurons depolarise. Glutamate transporters, which normally utilise ionic gradients to remove glutamate from the extracellular cleft, cease functioning and may reverse, leading to a build up of glutamate in the extracellular cleft, which in turn causes continued depolarisation. Thus, a vicious circle ensues, and once neurons become damaged, they release further glutamate by cell lysis, resulting in massive increases in extracellular glutamate, which affects increasing numbers of surrounding cells.

Excitotoxic mechanisms have also been implicated in the acute brain pathology resulting from seizures. For example, the infusion of glutamate or more potent glutamate analogues into the brain can cause convulsions, neuronal pathology and epileptiform activity measured electrophysiologically (Hayashi *et al.,* 1952, Ben-Ari *et al.,* 1980). The epileptogenic potential of glutamate analogues in humans was highlighted following an outbreak of poisoning that occurred in Canada in 1987. This was caused by the contamination of mussels with domoic acid, a potent agonist of kainate receptors. In some cases, seizures were reported, and one patient developed chronic temporal epilepsy. Neuropathological examination of three patients that died revealed pathology in limbic structures such as the hippocampus and amygdala, which is similar to the pattern of pathology following kainate administration in

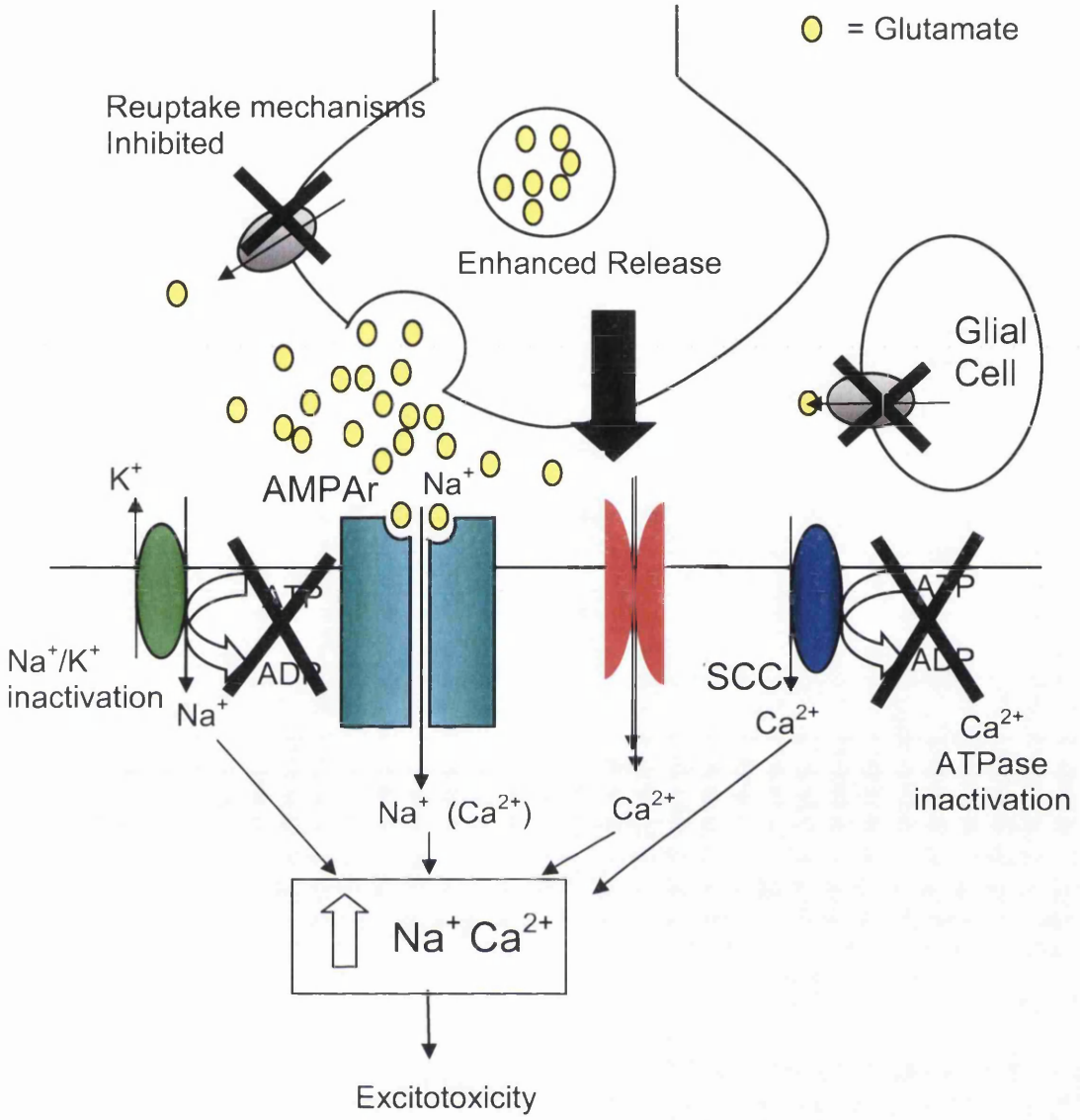

Figure 1.6 Excitotoxicity at AMPA receptors during ischaemia

When energy required to maintain ionic gradients is lost, cells depolarise, release more glutamate, which in turn causes further depolarisation, and hence a viscous circle ensues. This leads to vast influx of Na^+ through AMPA receptors, which leads to cell swelling and necrosis. Ca^{2+} also enters cells via voltage sensitive calcium channels (VSCC), or through Ca^{2+} permeable AMPA receptors. Ca^{2+} mediated mechanisms can cause cellular damage via a variety of mechanisms.

rodents (Ben-Ari *et al.*, 1980; Perl *et al.*, 1990; Teitelbaum *et al.*, 1990; Cendes *et al.*, 1995). Elevated levels of glutamate are also reported in patients with epilepsy (During and Spencer, 1993). Accordingly, glutamate receptor antagonism has anticonvulsant properties (Yamaguchi *et al.*, 1993; Chapman, 1998).

1.2.3 Excitotoxicity and chronic neurodegenerative disorders

Two chronic neurodegenerative diseases thought to be directly associated with excitotoxic mechanisms are neurolathyrism and amyotrophic lateral sclerosis on the Pacific island of Guam (Spencer *et al.*, 1986, 1987). Neurolathyrism and Guam disease are associated with dietary intake β-oxylylamino-L-alanine (BOAA) and β-methylamino-L-alanine (BMAA), both agonists of AMPA receptors (Bridges *et al.*, 1989; Smith and Meldrum, 1992; Willis *et al.*, 1993;). Whilst the associations made between these two disorders and chronic consumption of glutamate analogues are by no means conclusive, they suggest that an excitotoxic mechanism may be the primary cause of neurodegeneration.

Evidence linking excitotoxicity with other chronic neurodegenerative diseases such as Parkinson's or Alzheimer's disease is less convincing than for acute neurological disorders such as cerebral ischaemia. For instance, there is no compelling, consistent data to suggest that EAA levels are elevated in the extracellular space in these disorders. However, it has been hypothesised that in situations of chronic degeneration, disruptions in normal cellular metabolism can predispose neurons to excitotoxic demise in the absence of elevations of extracellular glutamate. Therefore normal levels of glutamate can become toxic if the cell is unable to maintain ionic gradients and membrane potential. This hypothesis, known as 'slow', 'weak' or 'secondary' excitotoxicity, was formed on the basis of *in vitro* experiments demonstrating that impaired energy metabolism increases the vulnerability of neurons to excitotoxic challenges (Novelli *et al.*, 1988; Zeevalk and Nicklas, 1990). Flint Beal and colleagues have demonstrated this concept *in vivo*, showing that neuronal damage induced by 'metabolic toxins' such as malonate or 3-nitropropionic acid can be attenuated with glutamate receptor antagonists (Beal *et al.*, 1993a, b; Henshaw *et al.*, 1994). Secondary excitotoxicity may act as a common mechanism contributing to pathology in a number of neurological disorders (Lipton and Rosenberg, (1994).

1.3 Effect of brain injury to white matter

1.3.1 Composition of white matter

Coronal sectioning of the human cerebral cortex reveals a convoluted outer rim of grey matter that overlies areas of white matter (see Fig. 1.7). Grey matter contains neuronal cell bodies, dendrites, local ramifications of axons and glial cells; whereas white matter is composed of myelinated axons and glial cells. White matter is coloured white due to the high lipid content of the myelin sheath. During the evolution of mammalian brains, the neocortex has expanded in size considerably. However, as brain size increases, the volume of white matter beneath the cortex increases disproportionately faster than the volume of cortical grey matter (Zhang and Sejnowski, 2000). Thus, white matter comprises 5% of the cortical mantle of rats, 35% in non-human primates, and nearly half in humans (Frahm *et al.*, 1982). Myelinated axons contained within white matter are the conducting units of neurons, conveying signals to other cells via the action potential. Therefore the normal functioning of the CNS is critically dependent upon the components of white matter.

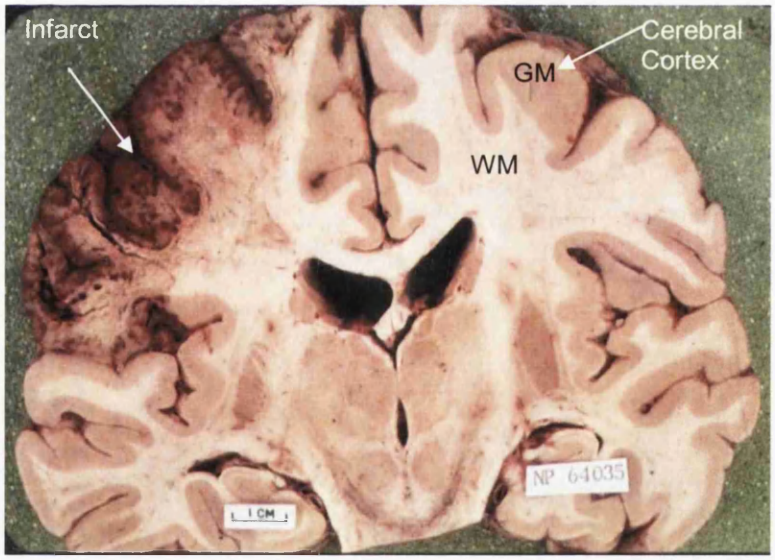

Figure 1.7 White matter in the human brain

Coronal section through a human brain revealing convoluted grey matter in the cortex overlying white matter areas. This patient has suffered from a stroke affecting the middle cerebral artery that has resulted in tissue damage (discoloured area on left hand side) that has affected both grey and white matter. Image courtesy of Professor D. I. Graham, department of Neuropathology, University of Glasgow.

Axonal structure

Axons emerge from the neuron cell body as slender threads that remain uniform in diameter and generally do not branch until they reach their target. Axons consist of a gelatinous core of neuronal cytoplasm known the axoplasm, which is surrounded by the neuronal membrane, referred to as the axolemma. CNS axons are generally myelinated by oligodendrocytes as a means of improving salutatory conduction. The myelin is laid down in segments, known as internodes, with unmyelinated areas called Nodes of Ranvier between the internodes. The axon contains a specialised architecture of ion channels and transporters that facilitate saltatory conduction. For example, voltage gated Na^+ channels are clustered at high densities at the nodal membrane, whilst Na^+/K^+ ATPase and Ca^{2+}ATPase transporters and Na^+/Ca^{2+} exchangers are present on the axolemma to maintain ionic gradients (Ritchie and Rogart, 1977; Waxman and Ritchie, 1993). The shape and integrity of the axoplasm is maintained by the cytoskeleton, a form of cellular scaffolding, which also forms the tracks required for axonal transport of mitochondria, vesicles and proteins (see Fig. 1.8). The cytoskeleton of axons is composed of distinct and interacting components; microtubules (MTs), neurofilaments (NFs) and actin microfilaments (MFs). NFs can be considered as the characteristic organelle of the axon; they comprise the bulk of axonal volume and outnumber microtubules. They are 10nm tubular structures that are arranged parallel to the long axis of the axon. Axonal NFs contain side arms that project from their surface and ensure that they are widely spaced within the axolemma. Axonal NFs are usually phosphorylated, unlike those in the neuronal perikarya (Sternberger and Sternberger, 1983). In the axon, NFs are composed of three subunit proteins; NF high molecular weight subunit (NF-H or NF 200; ~200kDa); NF medium molecular weight subunit (NF-M or NF 150; ~150kDa) and NF light molecular weight subunit (NF-L or NF 68 ~68kDa). MTs are also arranged parallel to the long axis of the axon; they are 25nm hollow rod polymers composed of α- and β-tubulin. Microtubule associated proteins (MAPS) stabilise MTs against disassembly and mediate their interaction with other cellular components. There are several categories of MAPS: MAP1a, MAP1b (MAP 5); MAP2 and the tau proteins. These have different cellular distributions; tau is enriched in axons; MAP 2 is found mainly in neuronal perikarya and dendrites; MAP1a and MAP 1b (MAP 5) occur in somato-dendrite regions and axons, however MAP 1b (MAP 5) is expressed preferentially in axons (Sato-Yoshitake *et al.*, 1989).

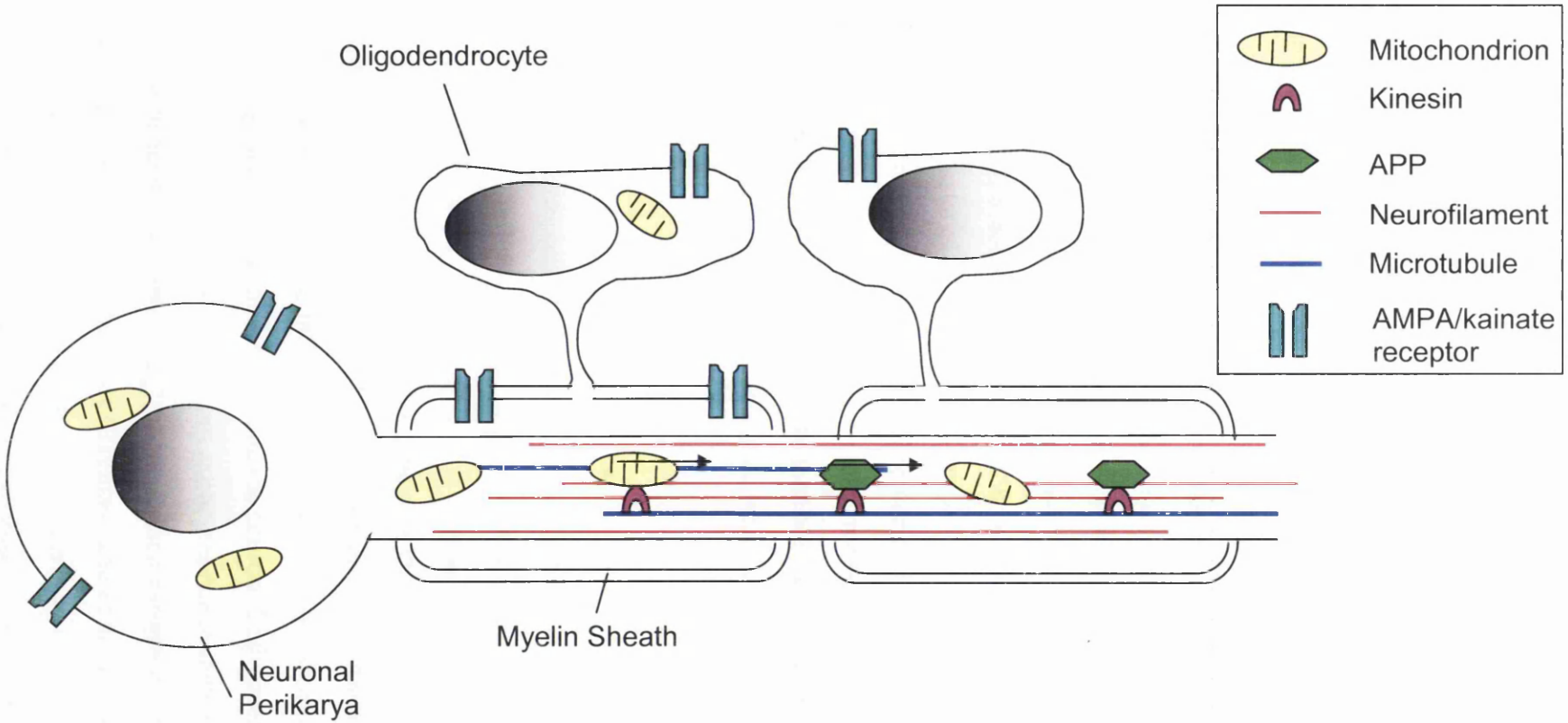

Figure 1.8 Structure of the axon cylinder

The axon is ensheathed by oligodendrocytes which form the myelin sheath to enable fast saltatory conduction and to provide support for the axon. The axoplasm contains cytoskeletal elements such as neurofilaments and microtubules to maintain shape. In addition, microtubules form the tracks required for axonal transport. Anterograde transport is depicted here, where mitochondria and proteins such as amyloid precursor protein are transported down the axon with the aid of the motor protein, kinesin. Mitochondria are present in the axoplasm to provide energy. AMPA receptors are present on the oligodendrocyte soma and myelin sheath, as well as the neuronal perikarya.

MFs are 3-5nm polymers composed of actin; they are commonly anchored at the axolemma by the protein spectrin.

As genetic material and protein synthesis machinery is located in the neuronal perikarya, the axon has a supply line that can deliver constituents essential for axonal function to the axon and the axon terminal. The delivery of proteins and organelles towards the nerve terminal is called anterograde transport, whereas the transport of constituents back to the neuronal perikarya is referred to as retrograde transport. Synaptic vesicles, mitochondria, enzymes, neuropeptides and membrane lipids move along the axon at the rate of 50 - 400mm a day (fast anterograde transport; Brady, 1991; Steonien and Brady, 1999); whereas cytoskeletal components such as MTs and NFs are transported anterogradely at the slower rate of 0.2 - 8mm per day (slow anterograde transport; Steonien and Brady, 1999). Retrograde transport of trophic factors, exogenous material and old membrane constituents occurs at the rate of 200-300 mm per day (fast retrograde transport; Steonien and Brady, 1999). Axonal transport of constituents is thought to occur along microtubules, which serve as the 'tracks', whilst motor proteins are thought to mediate the movement. Kinesin is the motor protein utilised for anterograde transport, whilst dynein is thought to mediate retrograde axonal transport.

Oligodendrocyte structure

Oligodendrocytes are responsible for production and maintenance of CNS myelin; they may also serve to influence axonal maintenance (Ludwin *et al.,* 1997). They reside in white matter, where they are aligned in rows and are known as interfasicular oligodendrocytes; and in grey matter, where they are known as perineuronal oligodendrocytes (Peters *et al.,* 1991). Another class of perineuronal oligodendrocyte that are not associated with myelin formation are satellite oligodendrocytes, which may serve to regulate the environment around the neuron (Ludwin *et al.,* 1997). Oligodendrocytes can be distinguished from astrocytes due to their smaller size, absence of intermediate filaments and glycogen in their cytoplasm, and their enormously high content of microtubules (Baumann and Pham-Dinh, 2001). Oligodendrocytes are a heterogeneous cell type; numerous attempts have been made to classify these types based on the number of processes they possess, the thickness of myelin sheath they produce, or the density of their cytoplasm (Baumann and Pham-Dinh, 2001). On the same axon, adjacent myelin segments (internodes) are

ensheathed by different oligodendrocytes, therefore individual oligodendrocytes are capable of myelinating numerous axons (see Fig.1.9).

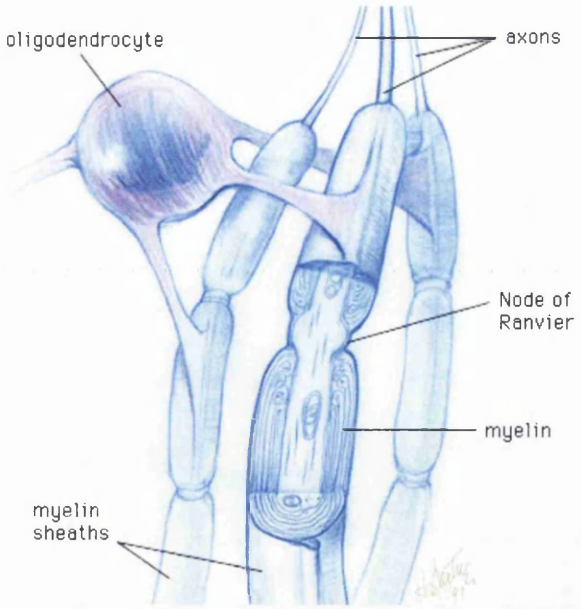

Figure 1.9 Myelinated axon fibres

Each oligodendrocyte extends processes to separate axons and repeatedly envelopes each axon with a myelin sheath. Image taken from www.science-education.nih.gov.

Myelin Sheath Structure

Multispiral myelin sheaths are formed from membranous processes of oligodendrocytes that repeatedly envelope the axon and subsequently compact together. At the electron microscope level, cross sectioning of the myelin sheath reveals concentric electron dense and light layers. The electron dense areas, known as the major dense lines, are formed from the cytoplasmic or intracellular surfaces of the oligodendrocyte processes that are in close apposition with each other (see figure 1.10). The electron light areas, known as intraperiod lines are formed by the fused extracellular membrane surfaces (Fig. 1.10). The myelin sheath is a phospholipid bilayer interspersed with proteins that are integral to its function (Fig. 1.10) Proteolipid protein (PLP) is a 30kDa integral membrane protein of CNS myelin, accounting for approximately 50% of all CNS myelin protein. Based on the phenotype of PLP-deficient mice, PLP is thought to be important for stabilising intraperiod lines and for the maintenance of axonal function (Boison and Stoffel, 1994; Griffiths *et al.,* 1998; Edgar *et al.,* 2001). Myelin basic protein (MBP) is the second most abundant myelin protein, constituting up to 40% of myelin proteins. MBP represents a family of proteins of which 6 isoforms exist, ranging from 14 – 21kDa. Unlike PLP, MBP proteins are cytoplasmic, and are localised in the major dense line of myelin (Monuki and Lemke, 1995). The lack of compact myelin, devoid of the major dense line in MBP deficient mice (*shiverer* mice) suggests that

MBP is essential for the formation of compact CNS myelin (Roach et al, 1983; Readhead *et al.,* 1987). Other, minor protein components of the myelin sheath include myelin associated glycogen protein (MAG), which comprises ~1% of myelin protein and is thought to mediate axon-glial adhesion events that precede myelination (Trapp, 1990); and 2',3'-cyclic nucleotide 3'-phosphodiestarase (CNP), which comprises 4% of total myelin proteins and may play a role in anchoring cytoskeletal elements to cytoplasmic surface of the plasma membrane (Laezza *et al.,* 1997).

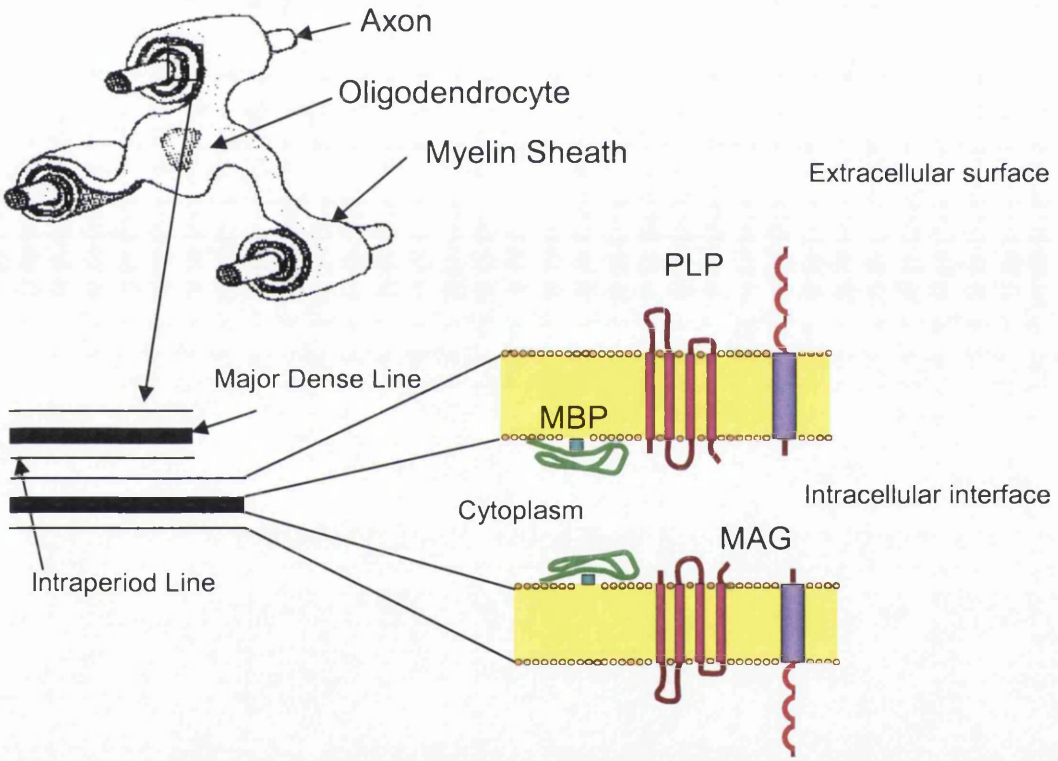

Figure 1.10 Composition of the myelin sheath

The myelin sheath is formed by a phospholipid bilayer interspersed by several proteins. MBP is a cytoplasmic protein; PLP transverses the membrane with intra- and extra-cellular portions and MAG has a membrane spanning domain with an extracellular region. Cross sectioning the myelin sheath at EM level reveals concentric electron dense (major dense line) and electron light layers (intraperiod line), which are formed by apposition of the intracellular, cytoplasmic interface and the extracellular membrane, respectively.

1.3.2 White matter is vulnerable to injury

Acute Brain Injury

Histological stains used to evaluate volume of pallor or neuronal perikaryal damage traditionally dominated the study of CNS tissue changes following experimental ischaemia. Using such methodology, it was historically assumed that white matter components were less vulnerable than grey matter to ischaemic damage, and that white matter changes were secondary to neuronal cell body damage (Marcoux *et al.*, 1982). In the past ten years, the use of alternative methodology has highlighted that white matter is highly vulnerable to ischaemia.

Isolated white matter tract preparations provide a useful model, devoid of neuronal perikarya, to examine the responses of white matter components to ischaemic-like insults. Exposure of *in vitro* optic nerve preparations to anoxia results in a rapid abolition of action potential conduction (Stys *et al.*, 1990). The ultrastructural correlates of this white matter dysfunction are loss of axonal microtubules and neurofilaments, swollen mitochondria and the presence of intramyelinic spaces (Waxman *et al.*, 1992). Similarly, exposure of *in vitro* optic nerve preparations to anoxia combined with glucose deprivation (oxygen/glucose deprivation) results in axonal swelling, degeneration and swollen axonal mitochondria (Garthwaite *et al.*, 1999). Subjecting spinal cord dorsal columns to anoxia results in myelin and axonal swelling and disruption (Li *et al.*, 1999). Deprivation of oxygen and glucose results in cell death in oligodendrocyte cultures (Lyons and Kettenmann, 1998; McDonald *et al.*, 1998a; Yoshioka *et al.*, 2000). Collectively, these studies highlight that white matter is vulnerable to energy/oxygen deprivation *independently* of neuronal perikaryal changes.

White matter damage has also been demonstrated following experimental cerebral ischaemia *in vivo*. Pantoni and colleagues (1996) used ultrastuctrual studies to demonstrate that oligodendrocyte swelling and myelin vacuolation occurred 30 minutes following middle cerebral artery occlusion. The oligodendroglial changes were thought to occur independently from grey matter changes, as there was no evidence of neuronal perikaryal pathology until 3 hours following middle cerebral artery occlusion (MCAO; Pantoni *et al.*, 1996). Similarly, there is ultrastructural evidence that microtubule accumulation and swelling occurs rapidly in oligodendrocytes following transient global ischaemia. Furthermore,

oligodendrocytes are thought to be more sensitive to global ischaemia than neurons in certain brain areas (Petito *et al.,* 1986, 1998).

Whilst electron microscope studies provide useful information about the temporal evolution and ultrastructural changes occurring in white matter tissue, they can only provide information about relatively small sample areas, and therefore cannot impart quantitative information about the effects of drug intervention. However, the use of immunocytochemical methods to detect and quantify white matter changes has added impetus to the study of white matter pathology. Antibodies raised against components of the axonal cytoskeleton (neurofilaments and microtubules) are commonly used to assess axonal loss or disruption following experimental brain injury (Yaghmai and Povlishock, 1992; Dewar and Dawson, 1997; Saatman *et al.,* 1998; Yam *et al.,* 1998; McCracken *et al.,* 2002). Under normal physiological circumstances, proteins such as amyloid precursor protein (APP) are transported along the axon by fast anterograde transport (Koo *et al.,* 1990). However, if the axonal transport system becomes disrupted, for example by cytoskeletal disruption, then APP can accumulate proximal to the disrupted segment. APP immunohistochemistry is a sensitive, quantifiable marker of axonal pathology following a number of acute brain insults (Gentleman *et al.,* 1993; Sherriff *et al.,* 1994a; Yam *et al.,* 1997; Imai *et al.,* 2002; Medana and Esiri, 2003). One of the advantages of APP immunohistochemistry is that it detects low, diffuse amounts under normal circumstances, but following axonal injury, APP immunostained axons are strikingly visible (figure 1.11; Sherriff *et al.,* 1994a). Disruption of the cytoskeletal network of oligodendrocytes can also be assessed with immunohistochemistry. Increased immunoreactivity of the microtubule associated protein tau is a sensitive marker of oligodendrocyte damage following brain injury (figure 1.11; Dewar and Dawson, 1995; Irving *et al.,* 1996b, 1997; Valeriani *et al.,* 2000).

These methods have been utilised to confirm the vulnerability of white matter following cerebral ischemia *in vivo*. Dewar and Dawson (1997) demonstrated axonal damage in striatal white matter tracts following focal cerebral ischaemia, using MAP1a and MAP 5 immunohistochemistry. Similarly, Yam et al (1998) showed that there was a rapid disruption in the pattern of MAP 5 immunostaining in white matter tracts following MCAO, and that similar disruptions and axonal

swellings were evident using antibodies raised against the light chain component of neurofilaments (NF 68). In addition, they demonstrated impaired axonal transport following focal cerebral ischaemia, evident as accumulations of SNAP 25, another protein that undergoes fast anterograde transport (Yam *et al.,* 1998). Accumulation of APP in damaged axons, generally located at the boundary of infarction is also evident following focal cerebral ischaemia (Stephenson *et al.,* 1992; Kalaria *et al.,* 1993; Yam *et al.,* 1997; Dietrich *et al.,* 1998). Alterations in tau immunoreactivity within oligodendrocytes were observed, as early as 40 minutes, following focal cerebral ischaemia; confirming the sensitivity of oligodendrocytes to ischaemic injury *in vivo* (Dewar and Dawson, 1995; Irving *et al.,* 1997; Valeriani *et al.,* 2000). Tau-1 and APP immunohistochemistry can also be used to assess longer term changes in white matter pathology (Irving *et al.,* 2001) and to quantify changes in white matter pathology following intervention strategies (Yam *et al.,* 1997; Valeriani *et al.,* 2000; Yam *et al.,* 2000; Imai *et al.,* 2001; 2002).

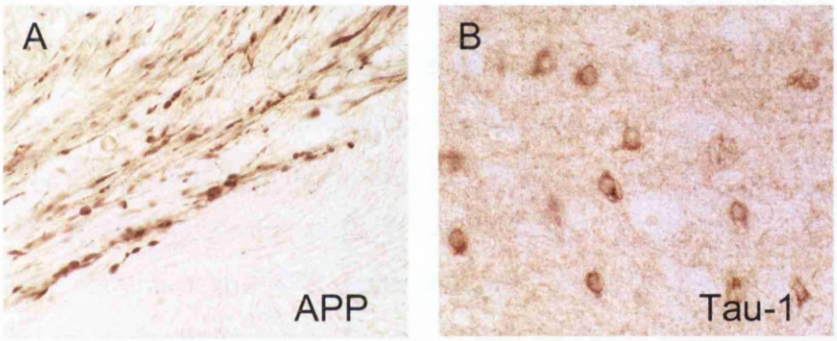

Figure 1.11 APP and Tau-1 immunohistochemistry following focal cerebral ischemia

A. Axonal swellings visualised in APP immunostained sections at the boundary of an ischaemic lesion. The increased immunostaining contrasts with the low level of diffuse staining in the uninjured tissue

B. Tau-positive oligodendrocytes in the cerebral cortex following focal cerebral ischaemia. This section was immunostained with the Tau-1 antibody.

Images taken by Dr D. Dewar.

Perhaps the most compelling evidence for the vulnerability of white matter to ischaemia is the high incidence of white matter damage following human stroke. A large number of strokes can affect both grey and white matter. For example, middle cerebral artery occlusion in man, a common cause of human stroke, can cause both white and grey matter infarction (see Fig. 1.7). A retrospective study of stroke

patients concluded that 44% of patients with strokes or transient ischaemic attacks had white matter changes, and that these were associated with a higher risk of mortality or dependency (Leys *et al.,* 1999). The presence of tau positive oligodendrocytes and APP immunoreactive axons in humans has been confirmed in post mortem material from stroke patients (Irving *et al.,* 1996b; Jendroska *et al.,* 1997).

White matter pathology resulting from head injury is perhaps the most comprehensively examined form of acute white matter injury. Diffuse axonal injury (DAI) can occur following non-missile (rapid acceleration and deceleration of the brain inside the skull) head injury (Adams *et al.,* 1982, 1989). The presence of damaged axons has been confirmed microscopically in post mortem tissue from patients that have died following head injury. Whilst antibodies to cytoskeletal components have been used to determine traumatically injured axons, APP immunohistochemistry is the most commonly deployed methodology (Gentleman *et al.,* 1993; Grady *et al.,* 1993; Blumbergs *et al.,* 1994; Sheriff *et al.,* 1994a, b; Geddes *et al.,* 2000). The presence of axonal swellings in APP immunostained sections can occur rapidly (within 2-3 hours) following head injury, and axonal swellings are thought to increase in size with increasing survival time following head injury (Sheriff *et al.,* 1994b; McKenzie *et al.,* 1996; Wilkinson *et al.,* 1999). The presence of cytoskeletal disruption and APP immunoreactive axons is also observed following experimental traumatic brain injury (Yaghmai and Povlishock, 1992; Bramlett *et al.,* 1997; Saatman *et al.,* 1998; Stone *et al.,* 2001), and has allowed the underlying mechanisms of traumatic axonal injury to be examined. These studies have suggested that most axons are not principally torn at the moment of injury, but that axotomy occurs some hours following the initial injury (reviewed in Graham and Genarelli, 1997; Maxwell *et al.,* 1997).

Other Neurological diseases and chronic neurodegenerative diseases

The use of immunohistochemical techniques such as APP immunostaining in conditions such as ischaemia and trauma has established that they are sensitive means of detecting axonal damage. These techniques have now been applied to a number of other CNS disorders, where they have been used to detect axonal damage

and to highlight the importance and functional consequences of axonal pathology. A recent post mortem study has demonstrated that axonal injury, detected with APP immunohistochemistry, was associated with the impaired consciousness and cerebral dysfuction caused by complications of malaria infection (Medana *et al.,* 2002). Widespread axonal damage has also been detected in the brains of HIV and AIDS patients (An *et al.,* 1997; Raja *et al.,* 1997; Gray *et al.,* 1998). In particular, APP immunoreactive axons were commonly correlated with areas of myelin pallor, a common autopsy finding in HIV patients (Raja *et al.,* 1997). Proximal axonal swellings detected with APP immunohistochemistry in post mortem tissue from Amyotrohpic lateral sclerosis (ALS) patients may be associated with early disease changes (Sasaki and Iwata, 1999).

The presence of axonal damage in the CNS of multiple sclerosis (MS) patients has been documented for over a century, however the development of new means to examine axonal pathology has expanded knowledge about this phenomenon. Using neurofilament and APP immunohistochemistry, it has been established that axonal damage occurs early in the disease progression, in acute plaques during demyelinating stages (Ferguson *et al.,* 1997; Trapp *et al.,* 1998; Kornek *et al.,* 2000). The presence of early axonal pathology has also been confirmed in animal models of MS (EAE models), and in living MS patients using magnetic resonance spectroscopy (MRS) imaging to measure N-acetylaspartate (NAA, an index of axonal integrity) (Kornek *et al.,* 2000; Stefano *et al.,* 2001; Bjartmar *et al.,* 2002; Filippi *et al.,* 2003). Axonal pathology is also documented in a number of other myelin disorders (Bjartmar *et al.,* 1999). Charcot-Marie-Tooth (CMT) disease is a peripheral neuropathy characterised by distal weakness, and decreased sensory and tendon reflexes. This disease encompasses a number of different forms, which are related to mutations in peripheral myelin proteins. Axonal loss and degeneration are characteristic of some forms of CMT (Dyck *et al.,* 1989; Hanemann *et al.,* 2001). Axonal loss, demonstrated by MRS imaging of NAA levels, has also been demonstrated in patients with Pelizaeus Merzbacher disease (PMD) caused specifically by PLP deficiency (Garbern *et al.,* 2002). In addition, post mortem material from PLP deficient patients reveals the presence of degenerating axons at EM level (Garbern *et al.,* 2002). Late onset axonal pathology has also been demonstrated in genetically engineered mice that lack MAG, CNP or PLP (Yin *et al.,* 1998; Griffiths *et al.,* 1998; Uschkureit *et al.,* 2000; Garbern *et al.,* 2002; Lappe-

Siefke *et al.,* 2003). Collectively, these studies suggest that axonal pathology is a common consequence of myelin disorders, and highlights the importance of normal glial-axonal relationships for maintaining normal axonal function.

1.3.3 AMPA receptors in white matter

In addition to their presence on neuronal perikarya and dendrites, AMPA/kainate receptors have been localised to white matter tracts (Petralia and Wenthold, 1992; Jensen and Chiu, 1993; Garcia-Barcina and Matute, 1998; Matute, 1998; reviewed in table 1.1). At a cellular level, functional AMPA/kainate receptors have been localised to astrocytes and microglia (Noda *et al.,* 2000; Seifert and Steinhauser, 2001). However, of direct relevance to this thesis is the expression of AMPA/kainate receptors in oligodendrocytes and myelin. Furthermore, a number of studies have determined that the oligodendrocyte lineage expresses functional AMPA receptors (reviewed in Verkhratsky and Steinhauser, 2000). AMPA and/or kainate receptors have been localised to oligodendrocytes from a variety of anatomical locations, in both developing and mature oligodendrocytes. This is reviewed in table 1.2. AMPA receptors have also been localised to the myelin sheath. GluR4 has been detected in the myelin sheath of rat spinal cord dorsal columns (Li and Stys, 2000); whilst KA-2 has been localised at myelin sheaths in the mouse spinal cord, in close proximity to nodes of Ranvier (Brand-Schieber and Werner, 2003).

Anatomical location / origin	Developmental Stage	AMPA/kainate receptor subunit	Reference
Corpus Callosum Optic Nerve Fornix	Adult bovine	Abundant GluR1-3 Trace GluR4	Garcia-Barcina and Matute, 1998
Optic Nerve	Adult rat	Abundant GluR1,3,4, GluR5, 6, 7 KA1, 2	Matute, 1998
Optic Nerve	Post natal day 15 and adult rat	Abundant GluR1 Trace GluR3	Jensen and Chiu, 1994

Table 1.1 Expression of AMPA / kainate receptor subunits in white matter homogenates

AMPA or kainate receptor subunits were detected in white matter homogenates from various anatomical areas using reverse-transcription – polymerase chain reaction (RT-PCR).

Anatomical location / origin	Developmental Stage	AMPA/kainate receptor subunit	Reference
In vitro			
Cerebral Cortex	O-2A progenitors E20-P1 rats	Abundant GluR2, 3, 4, GluR6, 7, KA-1, KA-2 Trace GluR1	Patneau *et al.*, 1994
Glial cell line	CG-4 OL's	Abundant GluR2, 3, 4, Abundant GluR 6, KA-2 Trace GluR7, KA1	Patneau *et al.*, 1994
Glial cell line	CG-4 OL's	GluR2, 3, 4 GluR5, 6, 7, KA-1, KA2	Yoshioka *et al.*, 1995
Corpus callosum	P6 rats OPCs	GluR1, 2, 3 GluR5, 6, 7, KA-1, KA-2	Yoshioka *et al.*, 1995
Corpus callosum	P6 rats Mature OL's	GluR1, 2, 3 GluR5, 6, 7, KA-1, KA-2	Yoshioka *et al.*, 1995
Optic nerve	P12 rats Mature OL's - Gal C / MBP expressing)	GluR3, 4, GluR6, 7, KA-1, KA-2	Sanchez-Gomez and Matute, 1999
Optic Nerve	P7-12 rats Mature OL's - Gal C	GluR3, 4 GluR6, 7, KA1, KA-2	Matute *et al.*, 1997
Forebrain	Mouse P1-3 Mature OL's CNP, Gal C expressing	GluR2/3	McDonald *et al.*, 1998a
In situ / In vivo			
Subcortical white matter	Adult rat RIP expressing OL's	GluR2/3	McDonald *et al.*, 1998a
Corpus callosum, int & external capsule	P7 rat Immature OL's O1 expressing	GluR4	Follett *et al.*, 2000
Corpus Callosum	Adult bovine Immature OL's	GluR4	Garcia-Barcina and Matute, 1998
Spinal cord dorsal columns	Adult rats Mature OL's	GluR3, 4	Li and Stys, 2000
Spinal Cord	Mouse CNP+ MBP- OL's	KA2	Brand-Schieber and Werner, 2003

Table 1.2 Expression of AMPA / kainate receptor subunits in immature and mature oligodendrocytes

Detected by RT-PCR, southern blotting or Immunocytochemistry. OL's = oligodendrocytes, OPC's = oligodendrocyte progenitor cells

1.4 Regeneration following brain injury

Historically, the CNS was viewed on as having only a limited capacity for regeneration. This idea has been challenged in recent years, in part by the studies described in the following sections.

1.4.1 Regeneration following entorhinal cortex lesioning

A well characterised *in vivo* model for examining degeneration and regeneration of the CNS is the entorhinal cortex lesion model (Deller and Frotscher, 1997; Savaskan and Nitsch, 2001, see figure 1.12). Glutamatergic neurons from the entorhinal cortex project via the perforant pathway to the dentate gyrus of the hippocampus. Neurons in the granule cell layer of the dentate gyrus extend their dendrites into the molecular layer of the dentate gyrus; entorhinal fibres project to the outer two thirds of this layer (Fig 1.12), where they form 80-90% of all synapses (Steward and Vinsant, 1983). Commissural and associational fibres from the hippocampus project to the inner third of the molecular layer. The molecular layer of the dentate gyrus has a laminated appearance because of the segregation of these projections from different fibre systems, (Fig. 7.6) which enables changes in neuronal connectivity to be readily quantified. Lesioning the entorhinal cortex induces reorganisation of hippocampal circuitry (reviewed in Deller and Frotscher *et al.,* 1997; Savaskan and Nitsch, 2001; Ramirez, 2001).

The temporal evolution of degeneration and regeneration in the dentate gyrus following entorhinal cortex lesioning has been extensively examined with electron microscopy. Lesioning the entorhinal cortex results in degeneration of entorhinal neurons and their axons, and a loss of synapses in the outer molecular layer of the dentate gyrus (Matthews *et al.,* 1976; Savaskan and Nitsch, 2001). The degeneration appears to induce the sprouting of fibres, not from the lesioned entorhinal cortex, but from neighbouring, intact afferent fibre systems (Steward and Vinsant, 1983). Sprouting is thought to mainly occur between 4-12 days following lesioning, and the formation of new synapses, which has been named reactive synaptogenesis, proceeds slightly later (Lee *et al.,* 1977; Cotman and Nadler, 1978; Steward and Vinsant, 1983). The time course of degeneration and regeneration have also been examined using immunohistochemistry and light microscopy with molecular makers of sprouting and synatogenesis, GAP-43 and synaptophysin (Masliah *et al.,* 1991).

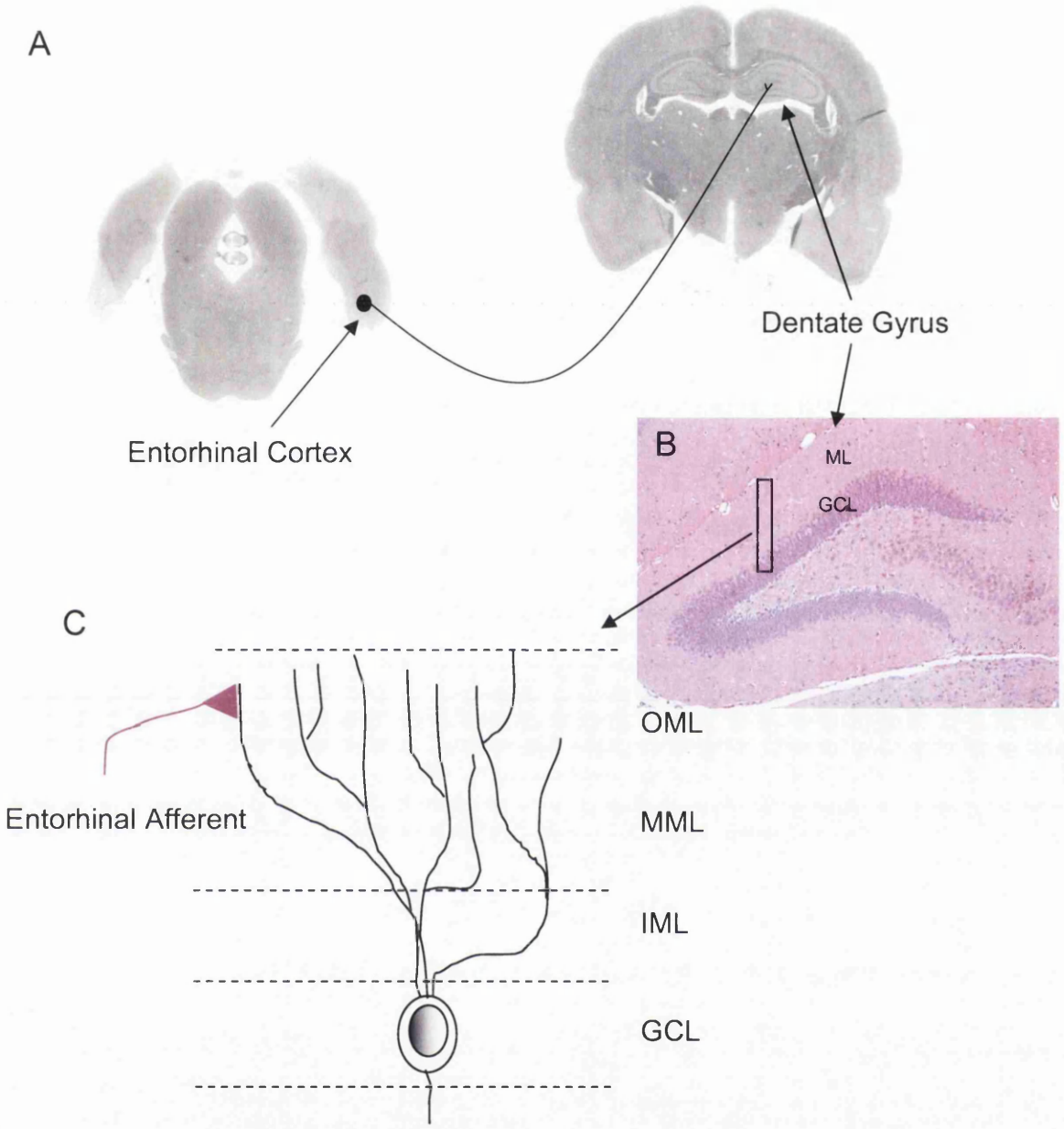

Figure 1.12 Afferent projections from the entorhinal cortex to the molecular layer of the dentate gyrus

A. Digitised H & E sections demonstrating the perforant pathway projection from the entorhinal cortex to the dentate gyrus

B. Higher magnification view of the dentate gyrus, illustrating the granule cell layer (GCL) and the molecular layer (ML).

C. Neurons in the granule cell layer (GCL) extend there dendrites into the molecular layer, which has a laminated apperance comprising of the inner molecular layer (IML), middle molecular layer (MML) and outer molecular layer (OML). Fibres from the entorhinal cortex project to the outer two thirds of the molecular layer where they form syapses with dendritic branches of the granule cell layers.

GAP-43 is a presynaptic membrane protein that may play a role in LTP, neurotransmitter release, and cytoskeletal organisation, however it is also expressed abundantly in the growth cones of sprouting axons (Skene *et al.,* 1986; Benowitz and Routtenberg, 1997; Benowitz *et al.,* 1998, 1990). Synaptophysin is a calcium binding glycoprotein localised in synaptic vesicles; synaptophysin immunohistochemistry can be used to label synapse density (Wiedenmann and Franke, 1985; Masliah *et al.,* 1991). GAP-43 and synaptophysin are useful markers of degeneration and regeneration in the CNS, as they can label both fibre degeneration and sprouting, and synapse loss and reactive synaptogenesis, respectively (Masliah *et al.,* 1991). Masliah and colleagues (1991) reported a significant decrease in both markers in the middle and outer molecular layers of the dentate gyrus 7 days following entorhinal cortex lesion in the rat, however, there was a 80% recovery of synaptophysin and a complete recovery of GAP-43 immunostaining by 30 days.

1.4.2 Neurogenesis

The discovery of a population of endogenous stem cells that divide and give rise to new neurons (neurogenesis) in adulthood in the mammalian CNS has further challenged the idea that the regenerative capacity of the CNS is limited. The dentate gyrus is one area of the brain where there is a population of dividing neuronal and glial progenitor cells (Cameron and McKay, 2001; van Praag *et al.,* 2002). The S-phase marker 5-bromo-2'deoxyuridine (BrdU) is commonly used to label proliferating stem cells in the dentate gyrus; using this marker it has been suggested that approximately 10 000 new cells are generated in the dentate gyrus each day (Miller and Nowakowski , 1988; Cameron and McKay, 2001). Many of these newly generated cells go on to die 1-2 weeks following generation, however a proportion may survive and go on to form functional neurons (Gould *et al.,* 1999; Shors *et al.,* 2001; vanPraag *et al.,* 2002). Enhanced levels of stem cell proliferation and neurogenesis in the dentate gyrus have been demonstrated following brain injury, such as global and focal cerebral ischaemia, seizures and entorhinal cortex lesion (Gould and Tanapat, 1997; Parent *et al.,* 1997; Liu *et al.,* 1998; Arvidsson *et al.,* 2002; Kokaia and Linvall, 2003).

1.5 Therapeutic Potential of AMPA receptor antagonists and AMPA receptor potentiators

Overwhelming evidence suggests that excitotoxic mechanisms contribute to the pathophysiology of cerebral ischaemia (discussed in section 1.2.2). Based on their efficacy in animal models of ischaemia (McCulloch *et al.*, 1992), NMDA receptor antagonists were advanced to clinical trials in human stroke, however they showed no evidence of efficacy (Dyker and Lees, 1998; Devuyst and Bogousslavsky, 1999; Lees *et al.*, 2001). Their inability to improve functional outcome in the clinic is multifactorial (Gladstone *et al.*, 2002), but may partly be related to an inability to protect white matter. Compared to rodents, which are generally used to demonstrate pre-clinical efficacy, humans have evolved larger amounts of white matter (see section 1.3.1). Whilst MK-801 can protect grey matter following focal cerebral ischaemia in the cat, there is no concomitant protective effect on the axons in white matter (Yam *et al.*, 2000). This is consistent with the lack of evidence for functional NMDA receptors in white matter (Verkhratsky and Steinhauser, 2000). It seems obvious that improved functional outcome following stroke should be dependent on the protection of neuronal perikarya *in addition* to axons and white matter components as the latter are critical for the normal functioning of the nervous system.

AMPA receptor antagonism may represent a promising approach for the treatment of ischaemic stroke. Based on the presence of functional AMPA receptors in white matter (reviewed in section 1.3.3) it seems more likely that AMPA receptor antagonists may be capable of salvaging the cellular components of both white and grey matter. Considerable evidence suggests a role for AMPA receptors in mediating white matter pathology. Thus, oligodendrocytes are vulnerable to AMPA receptor mediated toxicity *in vitro* and *in vivo*, and AMPA receptor antagonism can attenuate *in vitro* white matter preparations from ischaemic-like insults (reviewed in chapter 3). The role of AMPA receptors in mediating white matter pathology *in vivo*, and in particular, axonal pathology will be investigated further in this thesis.

In contrast to glutamate receptor antagonists, the clinical potential of AMPA receptor potentiators (described in section 1.1.4) has only become evident within the past ten years. Based on the role of AMPA receptors in plasticity and LTP (reviewed in

section 1.1.6), potentiating activity at AMPA receptors may have beneficial effects in a number of clinical disorders. Deficits in glutamatergic transmission have been hypothesised in the aged brain, in Alzheimer's disease and in schizophrenia, which are often associated with cognitive deficits (Tamminga, 1998; Carlsson *et al.*, 1999; Segovia *et al.*, 2001; Farber *et al.*, 2002). The ability of AMPA receptor potentiators to enhance action potential discharge rate, LTP and performance in rodent and human models of cognition suggests that they may have positive effects in these clinical conditions (Staubli *et al.*, 1994,a,b; Davies *et al.*, 1997; Ingvar *et al.*, 1997; Vandergriff *et al.*, 2001; Quirk and Nisenbaum, 2002). Pre-clinical animal studies have also suggested that AMPA receptor potentiators may possess anti-depressant effects (Li *et al.*, 2001; Knapp *et al.*, 2002). Whilst AMPA receptor potentiators such as LY404187 are known to enhance AMPA induced currents in prefrontal cortical, hippocampal and spinal neurons (Baumbarger *et al.*, 2001; Vandergriff *et al.*, 2001), there is little other information regarding the anatomical site of action of AMPA receptor potentiators or the functional consequences of AMPA receptor potentiation. This will be investigated in this thesis.

Activation of AMPA receptors is known to promote BDNF synthesis (Zafra *et al.*, 1990; Bessho *et al.*, 1993; Wetmore *et al.*, 1994; Hayashi *et al.*, 1999). Furthermore, AMPA receptor potentiators can enhance the expression of BDNF protein and mRNA *in vitro* (Lauterborn *et al.*, 2000; Legutko *et al.*, 2001). Administration of CX-546, or LY404187 or its active isomer LY451646 results in increased expression of BDNF mRNA and protein in the hippocampus of rats (Lauterborn *et al.*, 2000; Mackowiak *et al.*, 2002). BDNF is proposed to play a role in brain injury, as endogenous BDNF is upregulated following brain injury (Kokaia *et al.*, 1995, 1998; Goutan *et al.*, 1998; Hicks *et al.*, 1999; Dougherty *et al.*, 2000) and exogenously administered BDNF is neuroprotective (Beck *et al.*, 1994; Schabitz *et al.*, 1997). Furthermore, BDNF has been shown to enhance regeneration following brain injury. For example, exogenous administration of BDNF can promote axonal sprouting following spinal cord or optic nerve injury, or neurotoxin-induced lesion of cortical serotonin neurons (Mamounas *et al.*, 2000; Coumans *et al.*, 2001; Klocker *et al.*, 2001; Takano *et al.*, 2002). The inability of BDNF to cross the blood brain barrier precludes its development as a treatment to enhance regeneration in the human CNS; therefore means of enhancing endogenous BDNF levels may be therapeutically beneficial. Based on the ability of AMPA receptor potentiators to enhance BDNF

levels *in vivo,* it can be hypothesised that they may enhance regenerative processes following brain injury. This was investigated in this thesis, using the entorhinal cortex model of degeneration and regeneration.

1.5.1 Aims of Thesis

1. To determine if AMPA receptor mediated excitotoxicity results in axonal damage *in vivo*. To determine if AMPA receptor antagonism can protect both grey *and* white matter damage following focal cerebral ischaemia *in vivo*.

2. To establish a mouse model of AMPA-induced axonal damage. To compare AMPA-induced pathology with malonate (a mitochondrial inhibitor)-induced pathology in the mouse.

3. To determine if PLP and MBP deficient mice exhibit an altered sensitivity to AMPA-induced axonal and neuronal damage *in vivo*.

4. To determine the anatomical site of action of the AMPA receptor potentiator, LY404187.

5. To determine if the AMPA receptor potentiator, LY404187 can enhance regeneration following brain injury.

CHAPTER 2

MATERIALS AND METHODS

2.1 *In vivo* rat model of AMPA toxicity

2.1.1 Stereotaxic Surgery

Adult male Sprague Dawley rats (Harlan Olac, Bicester, UK) used in these studies were housed in groups prior to surgery, fed with the same diet and housed in identical conditions. The rats were anaesthetised initially in a perspex box containing 5 % halothane in a nitrous oxide and oxygen gas mixture (70:30), and then transferred to a David Kopf stereotaxic frame, where the incisor bar was set at -3.5mm (Clark, Electromedical). A facemask was fitted over the snout, and halothane was reduced to 1.5-2.5% for the remainder of the surgical procedure. Rectal temperature was monitored throughout the period of anaesthesia and maintained close to 37°C with the aid of heating lamps.

A midline incision was made in the scalp, and the skin and muscle retracted to reveal the surface of the skull and Bregma. A 26g, blunt ended 2µl Hamilton syringe attached to the stereotaxic frame was aligned over Bregma, and then moved to the appropriate coordinates (AP –0.26mm, ML 2mm; from the stereotaxic atlas of Paxinos and Watson, 1986) where an ink mark was made on the skull. A small burrhole was then made using a dental drill cooled with saline, and the dura was pierced with a dural hook. The Hamilton syringe was lowered 3mm from the surface of the brain into the external capsule (Fig. 2.1), where injections of 0.5µl of S-AMPA (Sigma) or

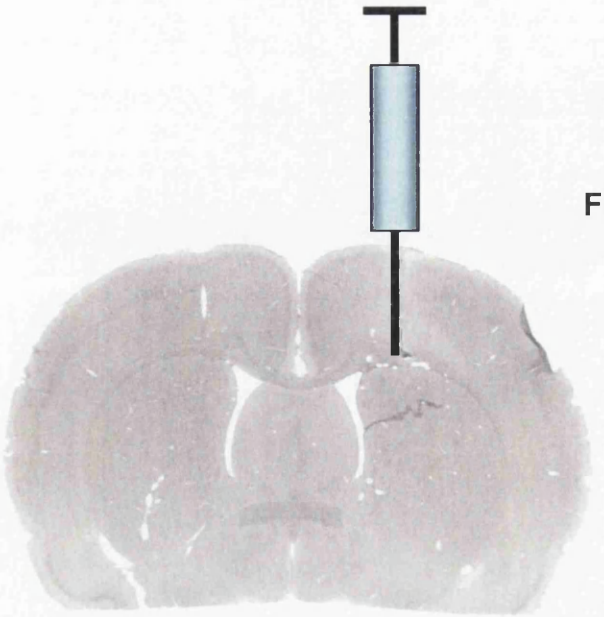

Figure 2.1 Stereotaxic injection into the rat external capsule

Digitised H&E stained section depicting the injection site, at the co-ordinates AP=-0.26, ML=2mm, DV=3mm relative to Bregma

vehicle (PBS, 10mM, pH7.4) were made at the rate of 0.1µl per minute. When the injection was complete, the syringe was left in place for 10 minutes to allow diffusion of the injectate from the needle tip. Following removal of the needle, the scalp was sutured with 4 /0 silk thread (Tyco Healthcare, UK), and 2 mls of saline was administered subcutaneously. A topical antibiotic (Auremycin) was applied liberally over the wound to minimise infection. Anaesthesia was withdrawn, and animals were housed individually for a survival period of 24 hours on post-operative pads in cages containing soft diet.

2.1.2 Intravenous administration of the AMPA antagonist SPD 502

Male Sprague Dawley rats (Harlan Olac, Bicester, UK) were initially anaesthetised in a perspex box with 5% halothane in a 30% oxygen / 70% nitrous oxide mix. When deeply anaesthetised, rats were intubated by introducing a 16 gauge intubation tube, which contained a blunted needle within the tube, into the trachea (Quick-Cath II; 51mm L, Baxter). Once in place, the needle was removed and rats attached to a ventilator delivering anaesthetic containing between 1-2% halothane.

The left femoral artery and vein were cannulated to allow for blood pressure monitoring and drug infusion, respectively. Cannulae were prepared at least 24 hours prior to surgery, consisting of a 2cm length of polythene cannula (external diameter 0.96 mm, internal diameter 0.58mm diameter; SIMS Portex Ltd) inserted into a 20cm length of wider diameter cannula (external diameter 1.4mm, internal diameter 0.63 mm, SIMS Portex Ltd), and secured with a small amount of superglue (RS Components). The femoral vessels were exposed by blunt dissection using forceps, the artery and vein were isolated, and blood flow was temporarily restricted by holding the vessels taut with 4/0 silk thread (Tyco Healthcare, UK). A small incision was made in each vessel using microscissors, and the cannulae, containing heparinised saline, were inserted and advanced 1cm into the vessels. Following insertion into the artery and vein, the cannulae were secured with 4/0 silk thread (Tyco Healthcare, UK), and a small amount of superglue (RS Components). By blunt dissection, a small incision was made at the nape of the neck, and the cannulae, sealed using small metal stoppers, were advanced through the subcutaneous tissue to

the neck, and externalised with the aid of a hollow stainless steel rod. Lignocaine gel (Biorex Labs Ltd) was applied to the femoral incision site, which was then sutured.

Animals were assigned into drug or vehicle groups by Mrs Joan Stewart, and I was blinded to the Animals received an intravenous bolus of drug (SPD 502, formerly known as NS 1209, Neurosearch, 16 mg/kg) (n=5) or vehicle (24 mM NaOH in isotonic saline) (n=6), 15 minutes prior to intracerebral injection of AMPA (25nmol) into the external capsule as described in section 2.1.1. All animals received identical volumes of bolus containing drug or vehicle (1ml/kg) administered over 2 minutes. Rats then received continual infusion of SPD 502 (16mg/kg/hr) or vehicle (6mM NaOH in isotonic saline) for 1 hour. Again, rats received identical volumes of drug or vehicle infusions (4ml/kg/hr). All infusions were made with a Harvard infusion pump (Harvard apparatus syringe pump model '22'). Following the infusion, cannulae were trimmed until just surpassing the incision site at the neck, sealed using blunted 1cm metal stoppers made from needle tips (23 gauge, 0.6mm diameter, Microlance), and then held in place by suturing. Anaesthetic was withdrawn and the endotracheal tube was removed once the animals were capable of spontaneous respiration. Animals were then administered saline and housed in individual cages with soft diet. All animals used in these studies were perfuse fixed 24 hours following the stereotaxic injection.

2.1.3 Perfusion Fixation

Animals were deeply anaesthetised in a perspex box containing 5% halothane in a 30% oxygen / 70% nitrogen mixture, and then transferred to a facemask where halothane levels were reduced to 3% until the end of the saline step of the procedure. An incision was made below the sternum to reveal the diaphragm, which was excised. The ribs were cut at either side of the midline to expose the heart. A blunt needle attached to the perfusion fixation equipment was inserted in the left ventricle and advanced up the aorta. The needle was clamped in place, and the right atrium was pierced to allow for drainage of blood. Between 300 – 400 ml of heparinised saline (1000units/100ml) was administered to the animal until the perfusate ran clear. The animal was then administered 300-400 ml of 4% paraformaldehyde in a 50 mM phosphate buffer solution (Sigma, see appendix 2) until the carcass became rigid. The heads were removed and immersed in paraformaldehyde solution for 24 hours.

The brains were then removed from the skull, and post-fixed in paraformaldehyde for a further 24 hours.

2.1.4 Tissue processing and cryostat cutting

Following post-fixation in paraformaldehyde, the brains were transferred to 30% sucrose in 10 mM phosphate buffered saline. The brains initially floated in this solution, and gradually sank over the course of 3 or 4 days. The brains were then frozen in isopentane cooled to -42°C in dry ice for 2 minutes, mounted on a chuck using cryomatrix (Shandon) and stored at -20°C until ready for sectioning. Sections (30μm) were cut in a cryostat (Bright) at -20°C, and stored in individual cell wells containing cryoprotectant (see appendix 2) at -20°C until further use.

2.2 Focal cerebral ischaemia

Dr Eileen McCracken performed all surgical procedures and tissue processing for this experiment. Male Sprague-Dawley rats were deeply anaesthetised in a perspex box with 5% halothane and 30% oxygen/70% nitrous oxide, intubated and mechanically ventilated on 1-2% halothane in 30% oxygen/70% nitrous oxide for the duration of surgery. Both arterial and venous lines were cannulated to allow blood pressure monitoring and for drug infusion, respectively. Mircovascular clips were placed on the left common carotid artery (CCA) and internal carotid artery (ICA) and the external carotid artery (ECA) was electro-coagulated distal from the bifurcation of the ECA and ICA. A heat blunted 3.0 monofilament was inserted in the ECA and advanced up through the ICA for approximately 22mm until resistance was felt, to block the origin of the middle cerebral artery (MCA) (Longa et al., 1989). Vehicle (saline 24mmol/L NaOH in isotonic saline)(n=8) and drug (SPD 502) (n=7) was administered as an intravenous bolus (16mg/kg) 15 minutes prior to monofilament insertion, and then as a continuous infusion for 4 hours (16mg/kg/hr) with a Harvard infusion pump. Drug cerebrospinal fluid levels were estimated to be 300nM based upon the pharmacokinetics and brain entry of the drug (Morrison, unpublished data, Shire Pharmaceuticals development Ltd, U.K). After 3 hours of ischaemia the monofilament was removed, animals were allowed to recover and placed in a controlled environment for 21 hours. Animals treated with SPD 502 appeared more lethargic than the vehicle treated animals in the initial post-operative period. In the

latter 12 -24 hours of the recovery period both groups of animals behaved in a similar manner. Twenty-four hours after the onset of ischaemia animals were perfused transcardially with 0.9% saline and 4% paraformaldehyde. Rat brains were processed for paraffin embedding and 6μm sections cut for histology and immunohistochemistry. The inclusion criteria for analysis of the tissue were the absence of an intracranial haemorrhage and the presence of neuronal damage.

2.3 *In vivo* mouse model of AMPA toxicity

2.3.1 Stereotaxic surgery

All mice used in these studies were housed in groups prior to surgery, fed with the same diet and housed in identical conditions. The mice were initially anaesthetised in a perspex box containing 3% halothane in an oxygen and nitrous oxide mix (20:50), then transferred to a David Kopf stereotaxic frame (Clark, Electromedical). A mouse facemask was fitted over the snout, and anaesthesia maintained with 3 - 3.5% halothane for the remainder of the surgical procedure. Rectal temperature was monitored throughout the surgical procedure and maintained at 37°C by the use of heating lamps. A midline incision was made which exposed the skull and Bregma. A 2μl Hamilton syringe was aligned over Bregma, and then moved to the appropriate coordinates (-0.25mm AP, 2mm ML; from the stereotaxic atlas of Franklin and Paxinos, 1997, Fig. 2.2), where an ink mark was made on the skull. A burr hole was drilled over this spot, using saline to cool the skull. The dura was pierced using a dural hook, and the syringe was slowly lowered 3.5mm from the surface of the brain. Injections of 0.7μl S-AMPA (Sigma), malonate (Sigma) or vehicle (PBS, 10mM, pH7.4) were made into the caudate nucleus at the rate of 0.1μl per minute. The needle was left in place for 5 minutes to allow for diffusion of the injectate from the needle tip. The syringe was then gradually removed from the brain, and the scalp sutured with 6/0 silk thread (Tyco Healthcare, UK). Following subcutaneous administration of 1ml of sterile saline, anaesthesia was withdrawn and the animals were housed in individual cages for 24 hours with soft diet.

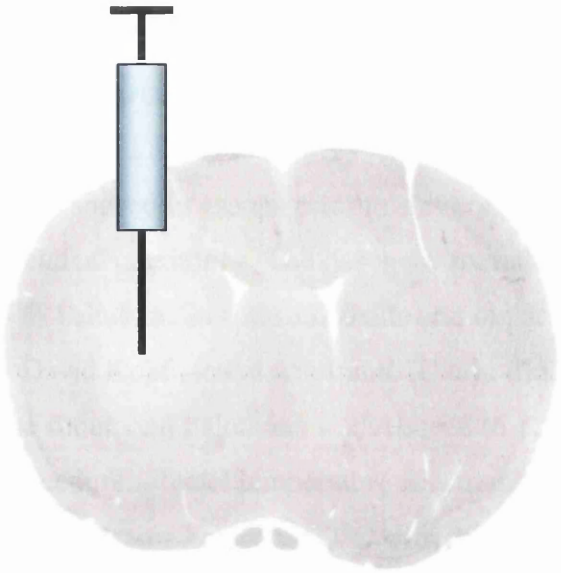

Figure 2.2 Stereotaxic Injection into the mouse caudate nucleus

Digitised H&E stained section demonstrating the injection site, at the co-ordinates AP=-0.5, ML=2mm, DV=3.5mm relative to Bregma

2.3.2 Perfusion Fixation

The mice were deeply anaesthetised in a perspex box containing 3% halothane in a 20% oxygen / 50% nitrous oxide mixture, then transferred to a face mask where anaesthesia was maintained. An incision was made in the abdomen to reveal the diaphragm, which was excised. The ribs were cut at either side of the midline to expose the heart. A needle, attached by tubing to a 20ml syringe, was placed in the heart through the left ventricle, clamped in place, and the right atrium was pierced. Twenty mls of heparinsed saline, then 20ml of 4% paraformaldehyde (appendix 2) was infused continually at the rate of 3.24ml per minute using a Harvard infusion pump. The heads were removed, and post-fixed in paraformaldehyde for 24 hours. The brains were removed from the skull, post-fixed in paraformaldehyde for a further 2 hours, then placed in 50 mM phosphate buffer until paraffin processing.

2.3.3 Paraffin processing and sectioning

The whole mice brains were dehydrated through a series of alcohols, cleared with xylene, then submerged in liquid paraffin at 60°C by an automated tissue processor (VIP, appendix 1). The brains were then embedded in small containers containing liquid paraffin, left to cool, then removed and mounted onto wooden blocks. Sections (6μm) sections were cut using a microtome (Leica RM 2135), and mounted onto poly-L-lysine slides (see appendix 2).

2.4 *In vivo* rat entorhinal cortex lesion model

2.4.1 Stereotaxic Surgery

Adult male Sprague Dawley rats (Harlan Olac, Bicester, UK) used in these studies were housed in groups prior to surgery, fed with the same diet and housed in identical conditions. The rats were anaesthetised initially in a perspex box containing 5 % halothane in a nitrous oxide and oxygen gas mixture (70:30), then transferred to a David Kopf stereotaxic frame (Clark, Electromedical). A facemask was fitted over the snout, and halothane was reduced to 1.5-2.5% for the remainder of the surgical procedure. Rectal temperature was monitored throughout the period of anaesthesia and maintained close to 37°C with the aid of heating lamps.

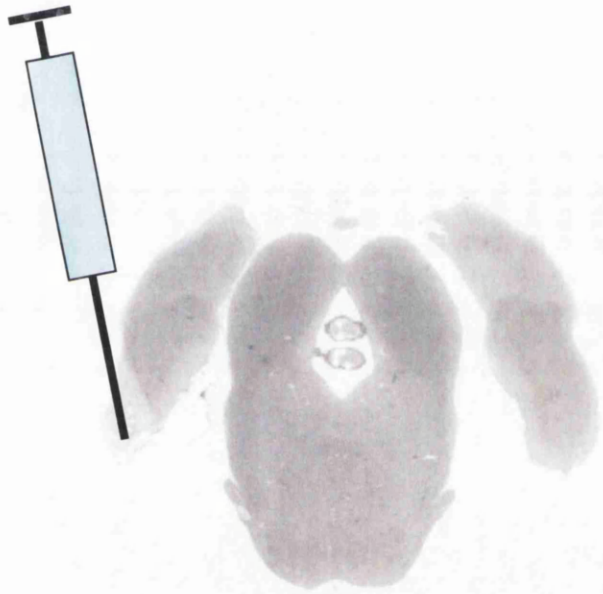

Figure 2.3 Stereotaxic Injection into the rat entorhinal cortex

Digitised H&E stained section demonstrating the injection site, at the co-ordinates AP=-8.3, ML=6.8mm, relative to Bregma. The needle was at an angle of 15°; lowered 3.5mm from the surface of the brain.

A midline incision was made in the scalp, and the tissue and muscle were retracted to reveal the surface of the skull, bregma and the interaural line. Muscle was retracted to reveal the right occiptal bone, down to the base of the skull. A 2µl Hamilton syringe attached to the stereotaxic frame was aligned over bregma, and then moved to the appropriate coordinates (AP -8.3mm, ML 6.8mm, angle 15°C from vertical, Fig. 2.3) where an ink mark was made on the skull. A burr hole was drilled over this area with a dental drill, using saline to cool the skull, and then the dura was pierced with a dural hook. The needle was lowered 3.5 mm ventrally from the surface of the brain. Ibotenic acid (α-amino-3-hydroxy-5-isoazoleacetic acid, Sigma, 10mg/ml) made in PBS (10mM, pH 7.4) was injected into the entorhinal cortex, at the rate of

0.1μl per minute. A total volume of 0.5μl was injected, and then the needle was left in place for a further 10 minutes to allow diffusion of the injectate. The skin was then sutured, anaesthesia discontinued, and 2 ml of sterile saline was administered subcutaneously. Animals were housed individually following surgery, initially on post-operative pads in cages containing soft diet. The following day, animals were transferred to individual cages containing sawdust and returned to the animal unit.

2.4.2 Experimental design and drug administration

The experimental design is illustrated in figure 2.4. Animals were divided into two groups of either 2 (Group A) or 3 (Group B) weeks survival time following the entorhinal cortex lesion (ECL). Drug or vehicle treatment commenced 7 days following ECL. On day 6 post ECL, all animals administered intraperitoneal injection of BrdU (100mg/kg in 0.007NaOH/0.9% saline; 1mg/80μl). Animals from each group were randomly assigned to drug (LY404187, 0.5mg/kg) or vehicle (10% ethanol, 3.75% hydroxy-propyl-β–cyclodextrin) treatment. Each animal received subcutaneous injections of LY404187 (0.5mg/kg) or vehicle twice daily. All animals received identical volumes of either drug or vehicle (1mg/4ml).

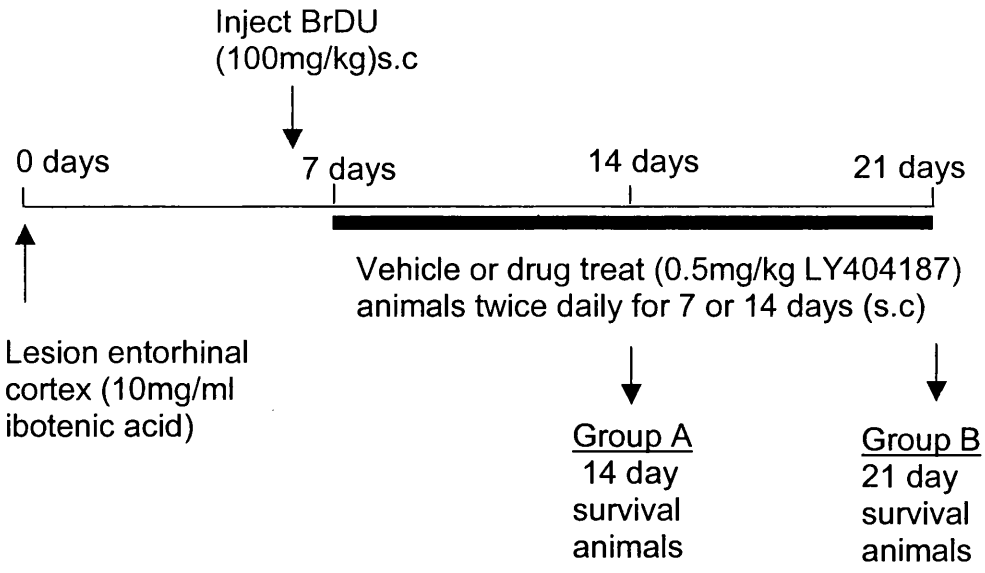

Figure 2.4 Experimental design for entorhinal cortex lesion study

2.4.3 Perfusion Fixation

At the end of the appropriate survival period outlined in figure 2.4, animals were re-anaesthetised and transcardially perfuse fixed with 4% paraformaldehyde as described in section 2.1.3.

2.4.4 Tissue processing and sectioning

Following perfusion fixation, animals were decapitated and the heads immersed in paraformaldehyde solution for 24 hours. The brains were then removed from the skull, and post-fixed in paraformaldehyde for a further 24 hours. The whole rat brains were dehydrated through a series of alcohols, cleared with xylene, then submerged in liquid paraffin at 60°C by an automated tissue processor (VIP, appendix 1). The brains were then embedded in small containers containing liquid paraffin, left to cool, then removed from the and mounted onto wooden blocks. Sections (6μm) were cut using a microtome (Leica RM 2135), and mounted onto poly-L-lysine slides (see appendix A). Sections were initially taken from the entorhinal cortex area to confirm lesion placement, then further sections were cut from the hippocampus at the level of the lateral habenula.

2.5 Immunohistochemistry

2.5.1 General Principle

The immunohistochemistry technique takes advantage of basic immunological principles to enable the detection and localisation of specific tissue constituents (antigens). Antibodies, raised in animals against a particular antigen, will bind specifically to the antigen located in the tissue of interest. The avidin-biotin detection method was used in many of the studies in this thesis to improve the sensitivity and resolution of the technique (Fig. 2.5). As well as using the enzymatic reaction between peroxidase and DAB described in figure 2.5, the incorporation of a fluorescent signal into the avidin (ie, texas red, avidin D) was also used for antibody detection in this thesis.

2.5.2 Immunostaining of free-floating sections

Sections were removed from storage in the -20° C freezers, and transferred from cyroprotectant to individual cell wells using a paintbrush, where they were washed in PBS (10mM solution). Pasteur pipettes were used at all stages during the experiments to remove and add the various solutions to the sections in the cell wells. Three hundred µl of each solution was required per section. The cell wells were placed on a shaker (Luckham R100) at all times, except for the overnight incubation in primary antibody. Immunostaining was then performed using the protocol described in figure 2.6. Optimal working dilutions were determined for each antibody using serial dilution curves. Details of the primary antibody concentrations, blocking sera and secondary antibodies used are shown in table 2.1. When the immunostaining was complete, the sections were floated onto glass slides coated with poly-L-lysine (Appendix 2) with the aid of Tris buffer and a paintbrush. After air drying overnight, the sections were then rinsed in tap water for 20 minutes, then dehydrated through a series of alcohols, placed in histoclear (National Diagnostics), and coverslips mounted using DPX (R.A. Lamb Lab Supplies). Negative controls underwent the same procedure as above except for omission of the primary antibody. No significant staining was detected in these controls.

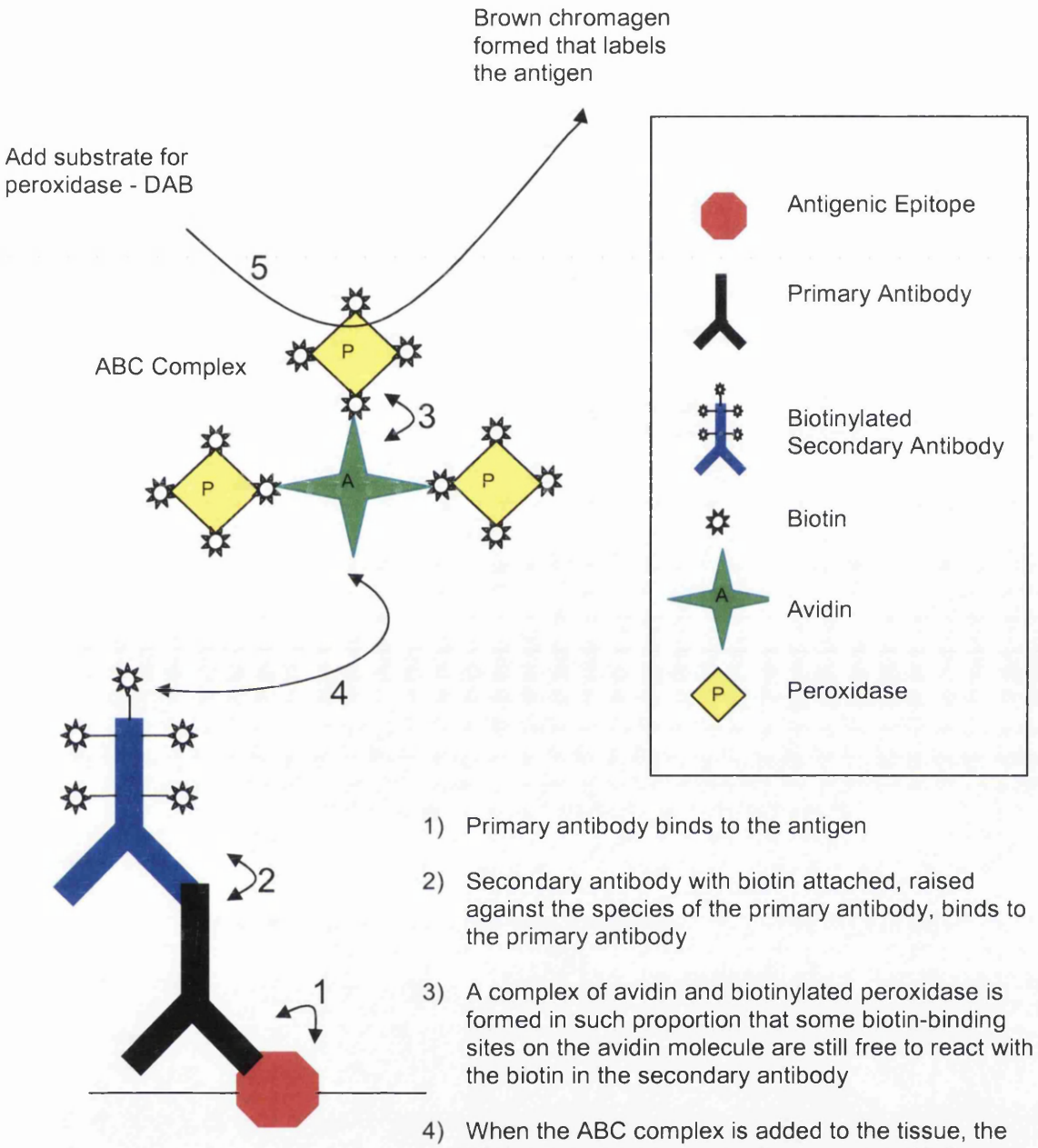

Figure 2.5 The ABC detection method used in immunostaining

This indirect method for antibody detection improves the sensitivity and resolution of the technique. The ABC technique takes advantage of the very high affinity that avidin, a large glycoprotein from egg whites, has for biotin, a low molecular weight protein from egg yolks.

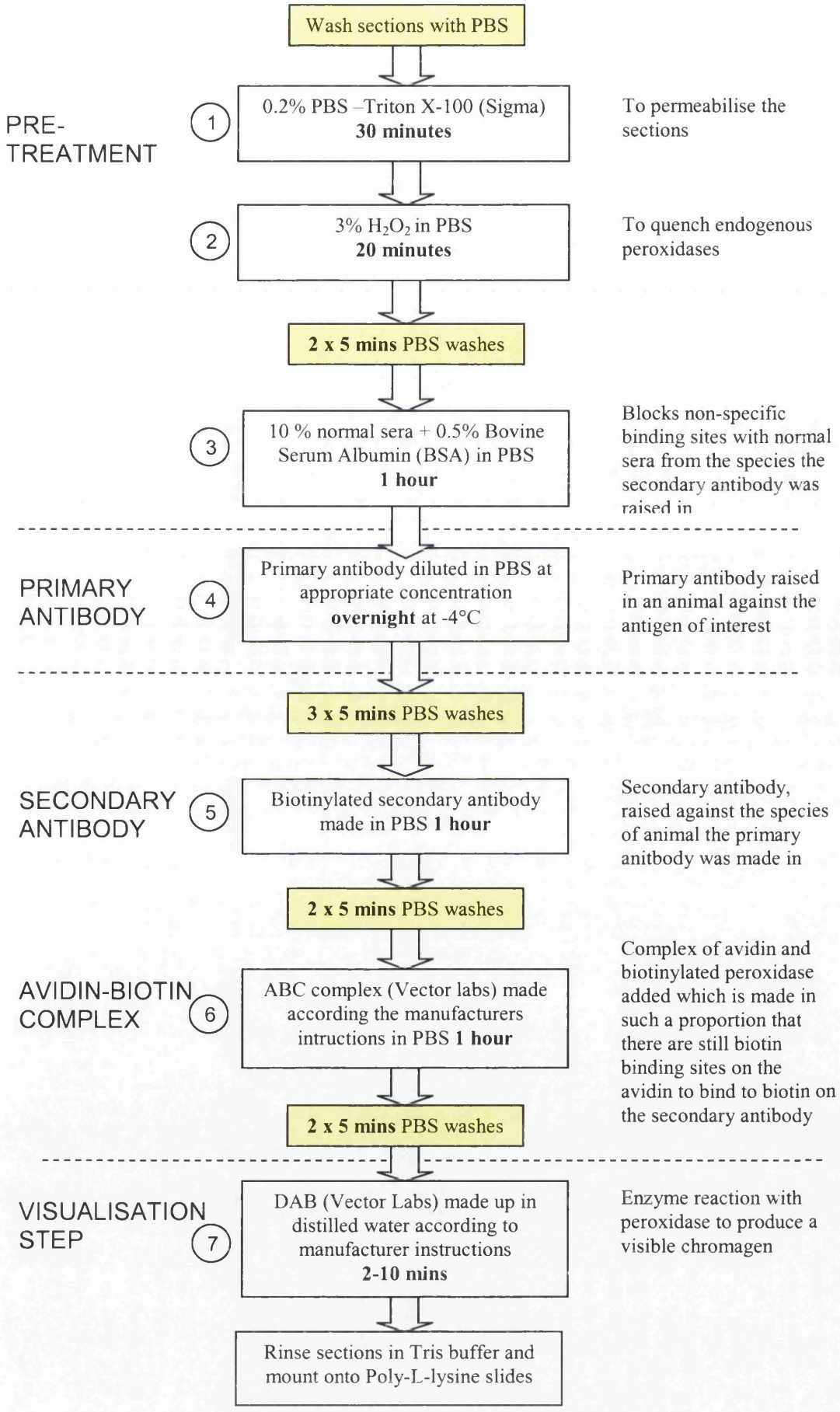

Figure 2.6 Flow chart demonstrating the protocol for immunostaining of free floating sections

2.5.3 Double labelling with free floating sections

Sections were immunostained with the first antibody as outlined in steps 1-6 of figure 2.6. Instead of using DAB in the visualisation step however, SG (Vector Labs, UK) was used to react with peroxidase to produce a grey colour. The sections were rinsed with water, followed by 3 x 5 minute PBS washes and then incubated with the appropriate blocking solution for the second antibody for 1 hour. The sections were then placed in the second primary antibody made in PBS overnight at -4°C. The following day, sections were treated as outlined in steps 5 and 6 in the protocol in figure 2.6. For the visualisation step with the second antibody, VIP (Vector Labs) was used to produce a pink chromagen. Sections were then rinsed in water, and treated in the same way following the DAB visualisation step described in section 2.5.2.

Primary Antibody	Species , type	Source of Primary	Dilution	Blocking Sera	Secondary Antibody
MAP-5 (clone AA6)	Mouse Monoclonal	Sigma	1:2000	10% horse serum, 0.5% BSA in PBS	Biotinylated Anti-Mouse 1:100 (Rat Adsorbed)
NF-200 (Clone NE14)	Mouse Monoclonal	Sigma	1:15000	10% horse serum, 0.5% BSA in PBS	Biotinylated Anti-Mouse 1:100 (Rat Adsorbed)
SMI-32	Mouse Monoclonal	Sternberger Monoclonals Inc.	1:1500	10% horse serum, 0.5% BSA in PBS	Biotinylated Anti-Mouse 1:100 (Rat Adsorbed)
PLP	Mouse Monoclonal	CN Biosciences	1:1000	10% horse serum, 0.5% BSA in PBS	Biotinylated Anti-Mouse (Rat Adsorbed) 1:100
Tau-1	Mouse Monclonal	Chemicon	1:5000	10% horse serum, 0.5% BSA in PBS	Biotinylated Anti-Mouse 1:100 (Rat Adsorbed)
MAG	Goat Polyclonal	Santa-Cruz	1:100	10% horse serum, 0.5% BSA in PBS	Biotinylated Anti-Goat 1:100
GFAP	Mouse Monclonal	Sigma	1:1000	10% horse serum, 0.5% BSA in PBS	Biotinylated Anti-Mouse 1:100 (Rat Adsorbed)
mrf-1 (Microglial response factor-1)	Rabbit Polyclonal	Gift from Dr S. Tanaka	1:50	10% goat serum, 0.5% BSA in PBS	Biotinylated Anti-Rabbit 1:100
Neu-N	Mouse Monoclonal	Chemicon	1:1000	10% horse serum, 0.5% BSA in PBS	Biotinylated Anti-Mouse 1:100 (Rat Adsorbed)

Table 2.1 Primary antibodies used in free floating immunohistochemistry experiments

2.5.4 Double labelling with the Tau-1 antibody and a marker of DNA fragmentation

For Tau-1 and Fluorescein-FragEL™ double labelling, sections were rinsed in PBS, then incubated in 0.2% Triton X-100 in PBS, followed by 1 hour in blocking solution (10% normal horse serum, 0.5% bovine serum albumin in PBS), and then overnight with Tau-1 (1:1000, Chemicon). Following washes, sections were incubated for 1 hour with biotinylated rat adsorbed horse anti-mouse secondary antibody (1:100, Vector Labs), followed by 1 hour with fluorescent avidin D (Texas red, Vector Labs, 1:100), then washed again. Sections were then mounted onto glass slides and left to dry in the dark overnight. Detection of DNA fragmentation the following day was carried out with a Fluorescein-FragEL™ kit (Oncogene Research Products), according to the manufacturer's instructions. Briefly, sections were rehydrated with TBS (20mM Tris pH7.6, 140mM NaCL) for 15 minutes, permeabilized with 2mg/ml proteinase K in 10mM Tris pH8 for 12 minutes and then equilibrated in 5X Equilibration Buffer. DNA Fragmentation was detected by incubating sections with TdT enzyme diluted with Fluorescein-FragEL™ TdT labelling reaction mix for 2 hours at 37°C. At this stage, only 60µl of solution was used per section. To ensure that this covered all the sections evenly, a small section of film (Nescofilm) was placed onto the solution on each section. Sections were then rinsed and mounted using Fluorescein-FragEL™ mounting media.

2.5.5 Immunohistochemistry on paraffin sections

Paraffin sections were placed in histoclear for 2 x 10 minutes to remove the wax, and then two changes of absolute alcohol (for 5 then 10 minutes). The sections were then microwaved in citric acid buffer (10 mM, pH6.0) for 2 x 5 minutes on full power to increase the antigenicity of the tissue (optional). Following a 40-minute cooling period, the sections were placed in 3% hydrogen peroxide (BDH lab supplies) in methanol for 30 minutes, and then thoroughly washed in running water for 40 minutes. Following 2 x 5 minute washes in PBS, the sections were removed from their racks, dried and ringed with a hydrophobic pen (Vector Labs) before proceeding with the same protocol outlined in steps 3 –7 of figure 2.6. Details of the primary antibody concentrations, source, and appropriate blocking solution and

secondary antibody are shown in table 2.2. After the DAB visualisation step, the sections were rinsed in water, then placed in running water for 20 minutes. Following dehydration through a series of graded alcohols, the sections were cleared with histoclear (National Diagnostics) then mounted with coverslips using DPX (R.A.Lamb Lab Supplies).

Antibody	Species, Type	Source of Primary	Dilution	Blocking Sera	Secondary Antibody
NF 200 (clone NE14)	Mouse, monoclonal	Sigma	Rat tissue = 1:8000 Mouse tissue =1:8000	10% horse serum, 0.5% BSA in PBS	Biotinylated Anti-Mouse (Vector) (Rat Adsorbed) 1:100
APP (clone 22CC11)	Mouse, monoclonal	Chemicon	Rat tissue = 1:500 Mouse tissue=1:2000	10% horse serum, 0.5% BSA in PBS	Biotinylated Anti-Mouse (Vector) (Rat Adsorbed) 1:100 (rat) 1:300 (mouse)
MBP	Rat, monoclonal	Chemicon	Rat tissue = 1:12000 Mouse tissue=1:10000	10% rabbit serum, 0.5% BSA in PBS	Biotinylated Anti-Rat (Chemicon) 1:100
PLP	Mouse, monoclonal	Oncogene Reasearch Products	Rat tissue = 1:1000	10% horse serum, 0.5% BSA in PBS	Biotinylated Anti-Mouse (Vector) (Rat Adsorbed) 1:100
MAG	Goat polyclonal	Santa-Cruz	Rat tissue = 1:100 Mouse tissue = 1:150	10% horse serum, 0.5% BSA in PBS	Biotinylated Anti-Goat (Vector) 1:100
Synapto-physin	Mouse, monoclonal	Sigma	Rat tissue = 1:100	10% horse serum, 0.5% BSA in PBS	Biotinylated Anti-Mouse (Vector) (Rat Adsorbed) 1:100
GAP-43	Rabbit, polyclonal	Chemicon	Rat tissue= 1:1000	10% goat serum, 0.5% BSA in PBS	Biotinylated Anti-Rabbit (Vector) 1:100
BrdU	Mouse, monoclonal	Sigma	Rat tissue = 1:100	10% horse serum, 0.5% BSA in PBS	Biotinylated Anti-Mouse (Vector) (Rat Adsorbed) 1:100

Table 2.2 Primary antibodies used in paraffin embedded tissue immunohistochemistry experiments

2.5.6 Quantification of axonal damage following intracerebral injection of AMPA in the rat

Every seventh section throughout the entire extent of the histological lesion (see section 2.6.3) was stained using an antibody raised against MAP 5, a microtubule associated protein present in axons. MAP 5 immunostained sections were captured and digitised with a standard 8-bit CCD video camera connected to an MCID-M4 image analyser (Imaging Research, Canada). The image of each coronal section was printed, at a fixed magnification, onto A4 paper using a laser printer. Areas of axonal damage, which contained axonal bulbs and swellings, were identified in the external capsule using a conventional light microscope, and transcribed onto the digitised images. These areas of axonal damage were then quantified by placing a 2mm spaced transparent grid over each digitised image, and counting the number of grid intersections that fell within the area containing damaged axons. A MAP 5 score for each animal was obtained by summing the scores for each coronal plane through the lesion. The reproducibility of the MAP 5 scoring system was examined and described in appendix 3.

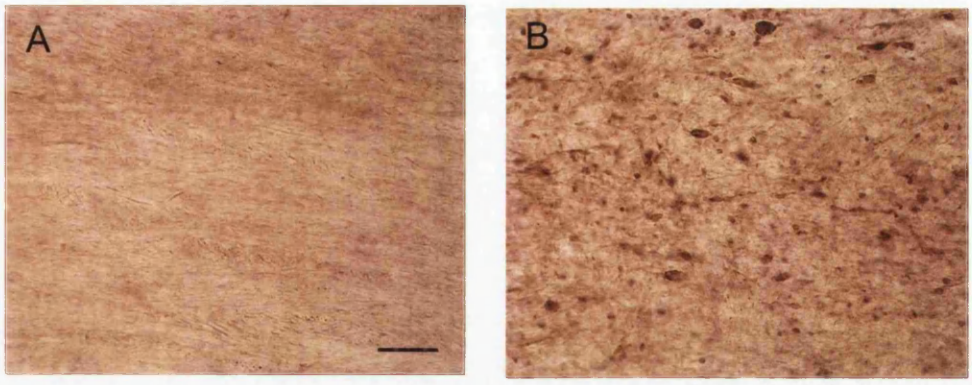

Figure 2.7 AMPA-induced axonal damage in the external capsule in MAP 5 immunostained sections

A. Representative image from the external capsule contralateral to the injection site, where axons appeared smooth, and ordered.

B. Axonal swellings and disruption following intracerebral injection of AMPA

Scale bar = 50μm.

2.5.7 Quantification of oligodendrocyte damage following intracerebral injection of AMPA in the rat

Increased tau immunoreactivity is present in oligodendrocytes in the brains of rats after focal cerebral ischaemia (Dewar and Dawson, 1995; Irving *et al.*, 1997, Valeriani *et al.*, 2000) and following intracerebral injection of glutamate (Irving *et al.*, 1996a). Every fourteenth section throughout the lesion was immunostained with Tau-1. The boundary between areas containing intensely stained tau-positive oligodendrocytes and those containing none or a few faintly stained oligodendrocytes could be easily identified. Each Tau-1 immunostained section was captured using a standard 8-bit CCD video camera and digitised, and the resultant image was printed on A4 paper. With the aid of a light microscope, the area of tissue containing tau-positive oligodendrocytes was delineated on the printed image. The area of tissue containing tau-positive cells was determined, with the aid of the delineated printed diagrams, using the MCID-M4 image analyser that had been calibrated for distance with a 1cm graticule. The volume of tissue containing oligodendrocyte damage was calculated using the integration of the damaged areas with the distance between the sections.

2.5.8 Quantification of myelin damage following intracerebral injection of AMPA in the rat

Every fourteenth section throughout the histological lesion was immunostained using an antibody raised against proteolipid protein (PLP). The boundary between damaged myelin and normal appearing myelin was identified on the PLP immunostained sections. The area of myelin damage was determined using the MCID-M4 image analyser with the aid of a light microscope. The MCID-M4 analyser was calibrated for distance with a 1cm graticule. The volume of myelin damage was calculated using the area of myelin damage on each section integrated with the distance between the sections.

2.5.9 Quantification of axonal damage following intracerebral injection of AMPA in the mouse

Serial sections were taken throughout the lesion according to the cutting schedule described in section 2.6.4. Adjacent sections to those used to examine histological damage were stained using antibodies raised against amyloid prescusor protein (APP,

Chemicon) or the heavy chain, phoshorylated component of neurofilaments (NF 200, Sigma). Each APP or NF 200 immunostained slide was then examined by light microscopy, and the appropriate coronal plane was identified using a stereotaxic mouse atlas (Franklin and Paxinos, 1997). Areas of focal axonal damage were then transcribed onto a copy of the appropriate area from the stereotaxic atlas. Using an MCID-M4 image analyser, calibrated for distance using the scale bar in the stereotaxic atlas (Imaging Research, Canada), the areas of axonal damage were then calculated from each coronal level throughout the lesion. The volume of axonal damage was then calculated based on the distances between each section calculated from the stereotaxic atlas.

2.5.10 Quantification of plasticity using GAP 43 and synaptophysin following entorhinal cortex lesion in the rat

To quantify the GAP 43 and synaptophysin immunoreactivity, Tiff images were captured in grey scale from the molecular layer of the dentate gyrus at x10 magnification, using a Leica microscope and Image ProPlus software. Two images each were captured from the contralateral and ipsilateral dentate gyrus per section, as illustrated below. Two sections were examined per animal, from the anterior and posterior portion of the lateral habenula. Images were also taken from a reference region in each section.

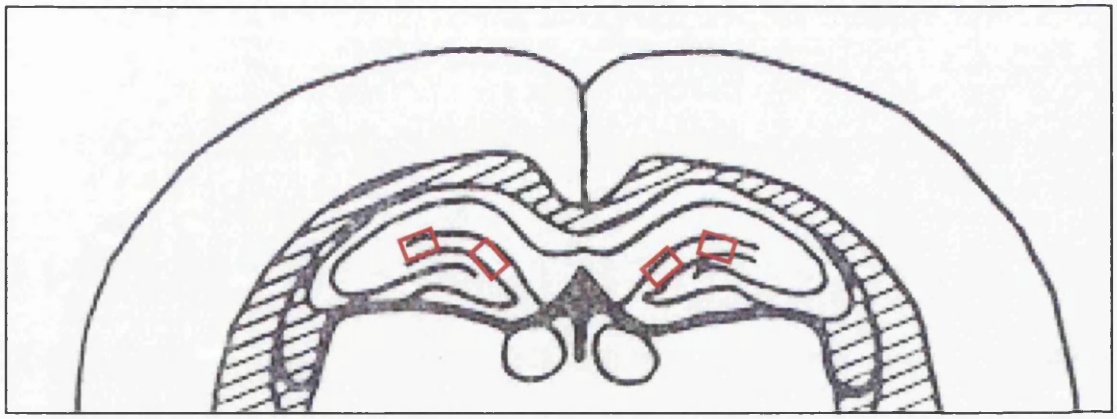

Figure 2.8 Representative diagram of dentate gyrus, illustrating where images were captured for quantification of immunostaining

Two images were captured from the dentate gyrus contralateral and ipsilateral to the ECL. The red boxes illustrate the areas where the images were captured.

For synaptophysin immunostained sections, the reference region was the corpus callosum, which exhibited minimal levels of immunostaining. For GAP 43 immunostained sections, the optic tract was taken as the reference region, as this anatomical area contained the lowest levels of immunostaining at the level of the hippocampus (Benowitz *et al.*, 1988). All images were captured for each antibody on the same day at the same light intensity. Relative optical density was then measured in the inner, middle and outer molecular layers using an MCID/M4 image analyser (Imaging Research, Canada). Ten optical density readings were taken per layer for each image, using a measuring frame with a constant size. To ensure that there were consistent levels of immunostaining, 10 optical density readings were also taken from the appropriate reference region from each section. The optical density readings for the outer, middle and inner molecular layer from each animal were then averaged; and the ipsilateral values were expressed as percentage of the contralateral optical density readings. In addition the average optical density values from the contralateral dentate gyrus were compared for drug and vehicle treated animals to ensure that the drug had no effect on this region.

2.6 Histology

2.6.1 Haematoxylin and Eosin staining

Free floating sections, mounted onto poly-L-lysine slides (Appendix 2), were firstly rehydrated in water for 20 minutes, dehydrated through a series of alcohols, then rehydrated back through a series of graded alcohols and finally back into water. Paraffin sections were placed in the oven at 60°C for 20 minutes, then in histoclear for 2x 5 minutes to remove the wax, dehydrated through graded alcohols, and then into water.

Sections were placed in haematoxylin (Surgipath) for 2-5 minutes, differentiated in acid alcohol, rinsed in water, placed in Scott's tap water for 1 minute, rinsed and placed in eosin (Surgipath) for 3-5 minutes. Sections were then dehydrated through a series of alcohols, cleared in histoclear and mounted with coverslips using DPX.

2.6.2 Counter staining with Haematoxylin

Paraffin embedded sections immunostained using the APP antibody were counterstained with haematoxylin to enable the identification of anatomical landmarks. Following the DAB visualisation stage, sections were rinsed in water for 20 minutes and then placed in haematoxylin (Surgipath) for 30 seconds, and differentiated in acid alcohol. Sections were then placed in Scott's tap water for 1 minute, rinsed in water, dehydrated through a series of alcohols, cleared in histoclear, and mounted with coverslips using DPX.

2.6.3 Quantification of tissue damage following intracerebral injection of AMPA in the rat

Serial sections (30μm) were cut coronally through the lesion, and every seventh section was stained with haematoxylin and eosin (H & E). Each H & E section was captured with an 8-bit standard CCD video camera and the area of pallor was measured using an MCID-M4 image analyser (Imaging Research, Canada). This was integrated using the distance between each section to obtain a volume of tissue damage for every animal.

2.6.4 Quantification of neuronal damage following intrastriatal injection of AMPA or malonate in the mouse

Sections (6μm) were cut coronally through the mice brains using a microtome (Leica RM2135). Twenty sections (2 per slide) from every 40 sections cut were floated onto poly-L-lysine slides for histology and immunostaining. From each cycle in this cutting schedule, the first slide was stained with H & E to examine histological damage. Each H & E slide was then examined microscopically, and the co-ordinates were identified using a stereotaxic mouse atlas (Franklin and Paxinos, 1997). Areas of focal histological damage were then transcribed onto a copy of the appropriate coronal level from the stereotaxic atlas. Using an MCID-M4 image analyser (Imaging Research, Canada), the areas of grey matter damage were then calculated from each level throughout the lesion. The volume of neuronal cell body damage was then calculated based on the distances between each section, calculated from the stereotaxic atlas.

2.7 *In vivo* [^{14}C]-2-deoxyglucose autoradiography

2.7.1 Theory

The [^{14}C]-2-deoxyglucose autoradiographic technique ([^{14}C]-2-DG) allows the quantification of function-related glucose utilisation within anatomically discrete regions of the CNS. Two principles provide the conceptual basis for this approach. Firstly, under normal conditions, the metabolic requirements of the central nervous system are derived almost exclusively from the aerobic metabolism of glucose. Secondly, local functional activity is intimately related to local energy metabolism and use (Sokoloff et al, 1977). Regional measurement of rates of glucose phosphorylation therefore enables energy generation and energy consuming functional events within individual CNS structures to be determined.

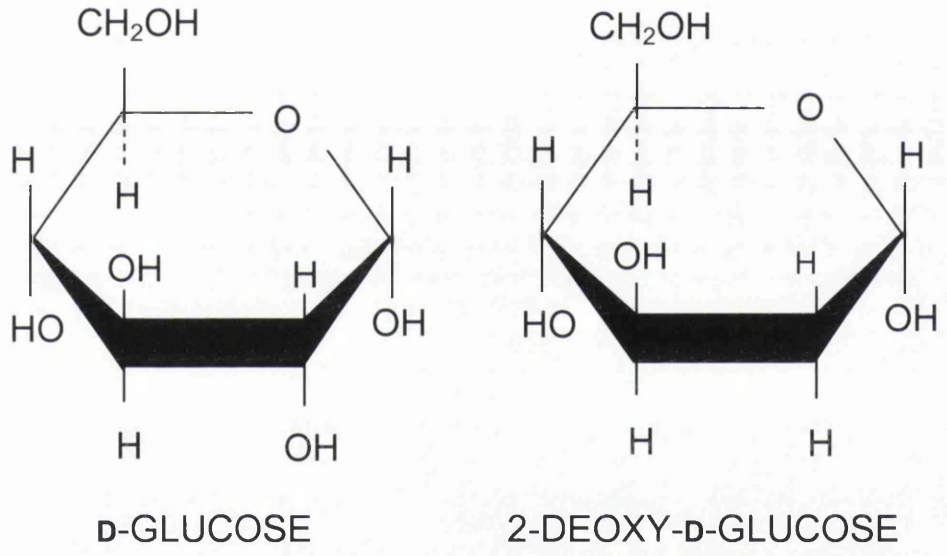

Figure 2.9 The structural difference between glucose and 2-deoxyglucose

2-deoxyglucose differs from glucose only by the replacement of a hydroxyl group on the second carbon atom by a hydrogen atom, yet this structural difference is responsible for the properties that make this technique possible.

The unique properties of 2-deoxyglucose, which differs from glucose only in the replacement of the hydroxyl group on the second carbon by a hydrogen atom (Fig. 2.9), account for the ability of this technique to quantify glucose utilisation in anatomically discrete regions in the CNS. The same carrier transports glucose and 2-deoxyglucose across the blood brain barrier to CNS tissue, where they become

substrates for metabolism, and are both phosphorylated by their respective hexose-6-phosphates. Glucose-6-phosphate is subsequently metabolised and therefore does not accumulate within cerebral tissues. However, 2-deoxyglucose-6-phosphate is not a substrate for the next enzyme in the glycolytic cycle (isomerase), and so it accumulates progressively during the experimental phase. An alternative pathway for 2-deoxyglucose-6-phosphate is glucose-6-phosphatase metabolism, however this does not present a problem in this technique as glucose-6-phosphatase is only present at low levels. 2-deoxyglucose-6-phosphate is effectively trapped in the tissue for the duration of the experiment. Regions within the CNS that have larger rates of glucose utilisation will accumulate more 2-deoxyglucose-6-phosphate. The 2-deoxyglucose used in this technique is isotopically labelled with ^{14}C to enable the quantification of accumulated [^{14}C]-2-deoxyglucose-6-phosphate in discrete anatomical regions with autoradiography.

Sokoloff et al (1977) developed a theoretical model based on the biochemical properties of glucose and 2-deoxyglucose (Fig. 2.10), which allows the rate of glucose utilisation to be calculated using an 'operational equation' (Fig. 2.11). The operational equation calculates the rate of cerebral glucose utilisation in terms of the arterial plasma concentration of glucose (C_P) and [^{14}C]-2-deoxyglucose (C_P^*) during the experimental period, and the total concentration of ^{14}C tracer within cerebral tissue at the end of the experiment (C_i^*). The operational equation depends on the following assumptions:-

(1) Plasma glucose concentration and the rate of glucose consumption remain constant during the experimental period

(2) Tissue is homogeneous within which the concentrations of [^{14}C]-2-deoxyglucose and glucose are uniform and exchange directly with the plasma

(3) [^{14}C]-2-deoxyglucose is present in a tracer amount

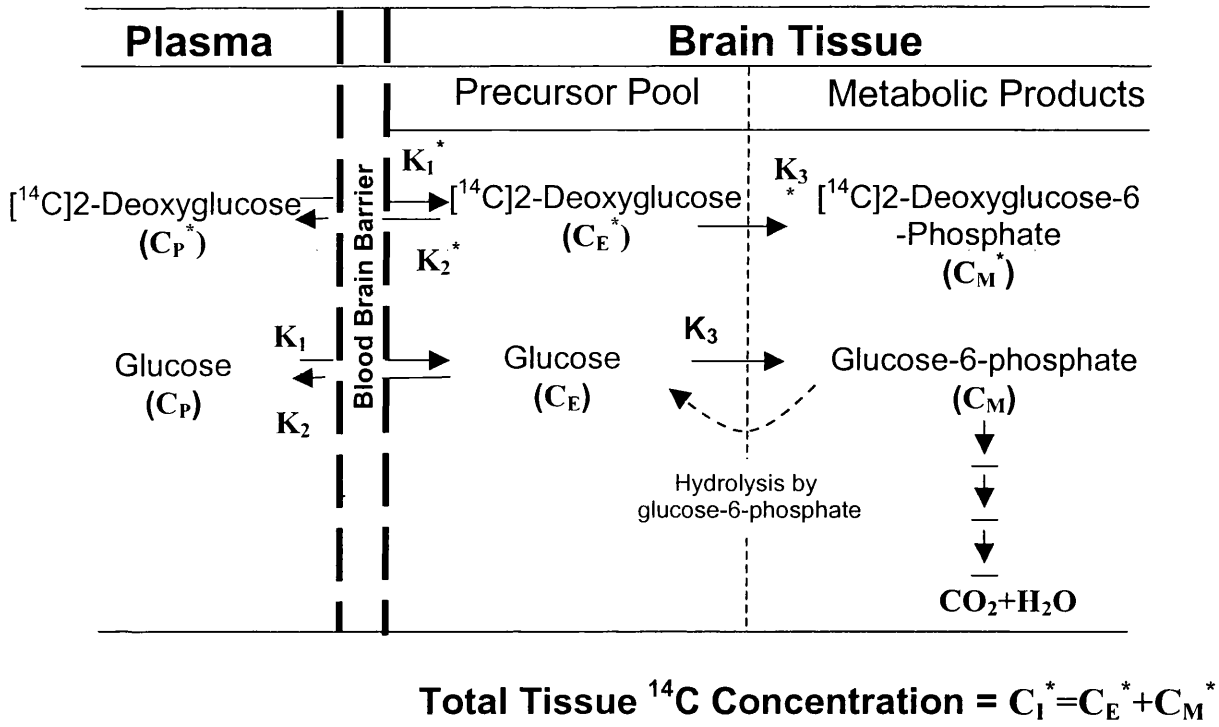

Figure 2.10 Diagrammatic representation of the theoretical model that formed the basis for the 2-deoxyglucose method

C_i represents the total ^{14}C concentration in a single homogenous tissue of the brain

C_P and C_P^* represent the concentrations of glucose and [^{14}C]-2-deoxyglucose in the arterial plasma

C_E and C_E^* represent the concentrations of glucose and [^{14}C]-2-deoxyglucose in tissue pools serving as substrates for hexokinase

C_M^* represents the tissue concentration of [^{14}C]-2-deoxyglucose

K_1^* is the rate constant for carrier-mediated transport of [^{14}C]-2-DG from plasma to tissue

K_2 is the constant for carrier-mediated transport back from tissue to plasma

K_3^* is the constant for phosphorlyation by hexokinase

K_1, K_2 and K_3 are the equivalent rate constants for glucose

(from Sokoloff et al, 1977)

$$R_i = \frac{C_i^*(T) \quad - \quad k_1^* \; e^{-(k_2^*+k_3^*)T} \int_0^T C_P^* e^{(k_2^*+k_3^*)t} dt}{\left[\frac{\lambda \,.\, V_m^* \,.\, K_m}{\phi \,.\, V_m \,.\, K_m^*}\right]\left[\int_0^T \left(\frac{C_P^*}{C_P}\right) dt - e^{-(k_2^*+k_3^*)T} \int_0^T \left(\frac{C_P^*}{C_P}\right) e^{(k_2^*+k_3^*)t} dt\right]}$$

Figure 2.11 The operational equation of [^{14}C]-2-deoxyglucose method

This equation is used to calculate the rate of glucose utilisation in any region cerebral tissue.

T represents the time at the end of the experiment

λ represents the ratio of the distribution space of deoxyglucose in the tissue to that of glucose

Φ is the fraction of glucose which, once phosporylated, continues down the glycolytic pathway

K_m^* and V_m^* and K_m and V_m represent the Michaelis-Menten kinetic constants for hexokinase and deoxyglucose, respectively.

Other symbols are defined in figure 2.10.

(from Sokoloff et al, 1981)

2.7.2 Rat surgical technique

Professor J. McCulloch performed the surgical techniques used in the 2-deoxyglucose experiments. Adult male Sprague Dawley rats were anaesthetised initially in a perspex box filled with 5% halothane in a 30% oxygen/70% nitrous oxide mixture. When deeply anaesthetised, rats were transferred to a facemask where anaesthetic was maintained at 2-2.5% halothane. The right femoral vessels were exposed using blunt dissection, and the femoral artery and vein were separated from the surrounding connective tissue. A small incision was made in each vessel whilst they were held taunt with silk thread to briefly reduce flow. Polythene catheters (external diameter 0.96 mm, internal diameter 0.58mm diameter; SIMS Portex Ltd; 15 cm long) containing heparinised saline were inserted 1cm into the vein and artery and then secured with 2/0 silk suture. Local anaesthetic gel (xylocaine) was applied to the incision site, which was sutured and then held in place with gauze pads and masking tape. The rat's body was then inserted into a 20 cm

length of bandage. A moistened Plaster of Paris was carefully wrapped loosely around the body and hind limbs to immobilise the animal. The animal's body and hind limbs were then taped to a lead brick. A rectal probe was inserted to allow temperature to be monitored. At this stage, the anaesthetic was discontinued and the animals were left for 2 hours before the start of the 2-deoxyglucose procedure to allow the majority of the anaesthetic to clear. Animals were maintained at 37°C during the procedure with the aid of heating lamps. Prior to drug administration, the femoral artery cannula was connected to a blood pressure transducer, to allow the monitoring of blood pressure.

2.7.3 The 2-deoxyglucose technique – rats

Local cerebral glucose utilisation was measured in conscious rats using an experimental design based on the theoretical considerations outlined in section 2.7.1, and the original method described by Sokoloff et al (1977). At time zero, 50μCi [^{14}C]-2-deoxyglucose dissolved in 0.5ml of saline (specific activity 51 mCi/mol. Sigma) was administered into the venous catheter at a constant rate for 30 seconds. Fourteen arterial blood samples (approximately 100μl) were taken over the 45 minute experimental period, beginning at the onset of the administration of ^{14}C-2-DG. Arterial samples were taken more frequently during the early phase of the experiment, then at less frequent intervals later in the experimental phase. Arterial samples were immediately centrifuged (Beckman Microfuge E). Plasma samples were then assayed for glucose levels, using a semi-automated glucose oxidase enzyme assay (Glucose Analyser 2, Beckman), and for ^{14}C concentration by means of liquid scintillation counting. At approximately 45 minutes, the animal was decapitated using a guillotine, and the brain was dissected and frozen in isopentane maintained at -42°C for 10 minutes. The brain was mounted onto a cryostat chuck using mounting media (Cryomatrix, Shandon), and embedding matrix (Thermo Shandon, Shandon) was poured over the brain to provide a protective coating. The brain was then stored at -20°C (maximum of 24 hours) until it was sectioned. Sections (20μm) were cut in a cryostat at -15°C. As a general rule, 3 sections were retained from every 13 sections cut, however, extra sections were retained from regions of interest. The entire brain and cerebellum was sectioned according to this

cutting schedule. Triplicate sections were retained on coverslips, which were secured against a piece of card. These were then exposed to X-ray film (Kodak BioMax MR-1 film, Sigma), with a set of 14 pre-determined [^{14}C]methacrylate standards, which contain different ^{14}C concentrations (equivalent to brain concentrations in 20μm section of 44-2500nCi/g) for 3 days. The films were then developed using an automated film developer.

2.7.4 Densitometric analysis and calculation of cerebral glucose utilisation in rats

An MCID/M4 image analyser (Imaging Research, Canada) was used to determine local levels of ^{14}C-2-DG that had accumulated in 51 anatomical areas, by quantitative densitometry. These areas were identified by visual inspection of the films on a light box prior to densitometry. Optical density measurements taken from the 52 brain areas were converted into ^{14}C levels by reference to the optical density of the 14 [^{14}C]methacrylate standards on the autoradiograms, which were used to calibrate the machine. The size of measuring frame used to capture the optical densities varied for certain anatomical regions depending on the size of the structure, however it remained constantly sized for all treatments for a defined region. The history of the plasma glucose and isotope levels from the duration of the 45 minute 2-deoxyglucose procedure was also entered into the MCID-M4 machine. Cerebral glucose utilisation was then calculated using the operational equation outlined in figure 2.11 by the MCID-M4. For each structure analysed, cerebral glucose utilisation was calculated from an average of 12 densitometric readings (right and left side from 6 sections).

2.7.5 The 2-deoxyglucose technique – mice

Cerebral glucose utilisation was estimated in mice following stereotaxic injection of AMPA (6nmol), malonate (1.35μmol) or vehicle (PBS, 10mM, pH7.4) as described in section 2.3.1. The entire procedure was timed to take exactly 38 minutes (see figure 4.1), then anaesthesia was discontinued, and mice received an intraperitoneal injection of 4.5μCi of ^{14}C-2-deoxyglucose in 400μl of sterile saline. Exactly 42.5 minutes later, mice were re-anaesthetised for 2.5 minutes, decapitated, and a terminal blood sample taken by torso inversion and immediately centrifuged. Brains were dissected from the skull and frozen in isopentane at -42°C for 5 minutes. Plasma

samples were assayed for glucose levels using a semi-automated glucose oxidase enzyme assay (Glucose Analyser 2, Beckman); and for ^{14}C concentration by means of liquid scintillation counting. Coronal sections (20μm) were cut through the brain and cerebellum in a cryostat at -15°C, collected in triplicate on coverslips, and dried quickly on a hotplate at 60°C. Three sections from every six cut were retained, and autoradiograms produced by exposing the sections to X-ray film for 3 days with pre-determined ^{14}C standards (44-2500nCi/g).

2.7.6 Densitometric analysis and estimation of local cerebral glucose utilisation in mice

The technique described in section 2.7.3 for rat ^{14}C-2- DG experiments involved taking 14 blood samples over the 45-minute experimental procedure, and using this information in the operational equation to calculate LCGU. However, in the mouse, only a terminal blood sample was taken, therefore local cerebral glucose utilisation was estimated using a semi-quantitative technique. Levels of ^{14}C in 17 anatomical areas were determined based on the densitometric measurements from the X-ray film. Optical density measurements from the 17 brain areas were converted into ^{14}C levels with reference to the 14 [^{14}C] methacrylate standards on the autoradiograms, which were used to calibrate the machine. The levels of ^{14}C were calculated in 6 sections for each anatomical region, both in the hemisphere ipsilateral to the stereotaxic injection, and the contralateral hemisphere. LGCU was estimated based on the ratio of ^{14}C in the region of interest with ^{14}C in a reference region, the hypothalamus.

$$\text{Estimated LCGU} = \frac{\text{Tissue } ^{14}C \text{ in region of interest}}{\text{Tissue } ^{14}C \text{ in reference region (Hypothalamus)}}$$

2.8 Western Blotting

2.8.1 Tissue homogenisation and preparation

Western blotting techniques were used to determine the levels of glutamate receptor subunits in PLP knockout and wild type littermates. Whole mouse brains (post natal day 20) were dissected and a membrane-enriched fraction was prepared according to the protocol of Norton and Poduslo (1973), by Dr Mark McLaughlin. The brains were homogenised in 7 mls of solution A (see appendix A) using a Polytron homgeniser at high speed for 10 seconds. The homogenates were then placed in a Beckman SW41 centrifuge tube, and 3mls of solution B (see appendix 2) was layered on top of the samples and centrifuged at 70000g (25000rpm) for 90 minutes at 4°C, yielding a pellet, supernatant and myelin fraction. The supernatant and myelin fraction were removed, then the pellet fraction was homogenised in solution B and snap frozen in liquid nitrogen and stored at -80°C until further use. The pellet fraction is membrane enriched and was selected for western blot analysis of the glutamate receptor subunits GluR1-4.

2.8.2 Quantification of protein content of samples

The protein concentration of the samples was determined using a BCA protein assay reagent (Pierce). This assay is based on the biuret reaction where proteins reduce Cu^{2+} to Cu^{1+} to generate a purple product. The intensity of the colour is proportional to the protein concentration and can be measured using spectrophotometry. A series of protein (bovine serum albumin) standards ranging from 0.1 – 0.8 mg/ml were reacted with the protein assay reagent, to produce solutions with a spectra of different colours from pale green through to purple. Light absorbency measurements from these standards were then determined in a spectrophotometer (Cecil) at a wavelength of 562 nm. From these values, a graph was constructed (figure 2.12). The homogenates for the western blotting were simultaneously reacted with the protein assay reagent, and absorbency was measured in the spectrophotometer. Samples were assayed in duplicate then averaged. Using linear regression analysis, the protein content of the samples was determined from their relative absorbencies.

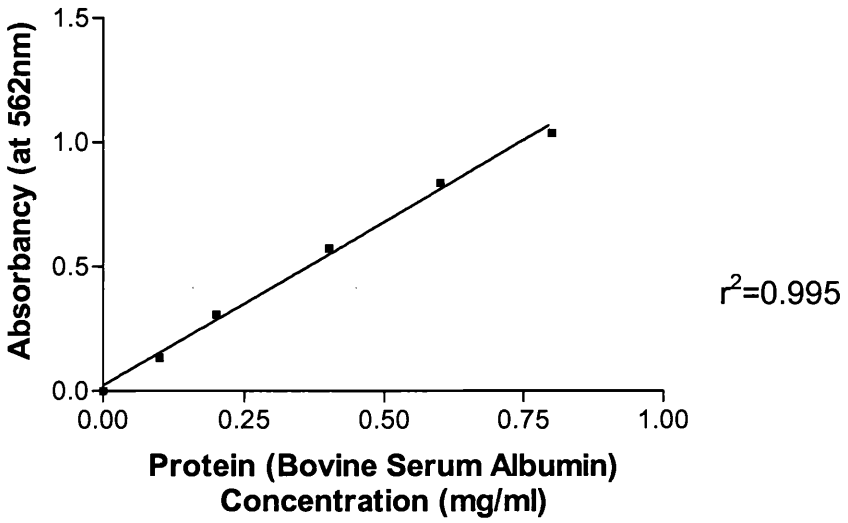

Figure 2.12 Standard Curve for determining protein concentration

The relative absorbancy of BSA standards at 562 nm increases with increasing concentration of BSA. Linear regression was used to determine protein concentration of the homogenates for the western blotting experiments.

2.8.3 SDS-PAGE electrophoresis

Once the protein concentration of each of the homogenates had been determined, the samples were prepared for gel electrophoresis. Equal amounts of sample were prepared by adding the appropriate volume of water and laemelli buffer (240µl of 3x sample buffer, 30µl of 1M DTT) to the homogenates to obtain 25µl of sample. Samples were mixed thoroughly, heated to 90°C for 4 minutes to denature the proteins, then spun briefly.

Mini gel apparatus was used in these experiments. The glass plates were thoroughly cleaned with ethanol, and the gaskets were clamped in place. A 10% resolving gel (see appendix 2) was prepared and immediately poured between the glass plates. A small amount of 0.1% SDS was poured onto of the gel to ensure that it polymerised evenly. When the resolving gel had set, the SDS was washed off, and a stacking gel (see appendix 2) was prepared. This was poured on top of the resolving gel, the combs inserted (to allow wells to form for the samples), and left to set. When set, the combs were removed, and the wells were rinsed thoroughly with PAGE buffer

(see appendix 2). The rubber gaskets were then removed, and the gel was transferred to the electrophoresis apparatus, which was filled with PAGE buffer. Each sample was then loaded (25µl per lane) into the individual wells, with broad range colour markers (Sigma) also being loaded periodically. The gel was run for 1.5 hours at a constant current of 20 mA (Biorad).

2.8.4 Western Blotting

The gel was carefully removed from the glass plates, the stacking gel discarded, and excess gel trimmed from the sides. A small diagonal segment was removed from the left-hand corner so that the correct orientation of the gel could be determined. The gel was then incubated in cathode buffer for 5 – 10 minutes. The methanol in the cathode buffer fixes the proteins. A section of PVDF membrane (Hybond P, Amersham) and 6 pieces of 3MEM blotting paper per gel were prepared with the same dimensions as the gel (7cm x 10cm). The PVDF membrane was hydrated in methanol for 10 seconds, then incubated in distilled water for 5 minutes followed by anode II buffer (appendix 2) for at least 10 minutes. One, two and three sheets of 3MEM blotting paper were soaked in anode I buffer, anode II buffer and cathode buffer, respectively (Fig. 2.13, appendix 2). Each piece of blotting paper, PVDF membrane and gel was then placed on the transfer equipment, according to the order shown in figure 2.13. Proteins were then transferred from the gel onto the membrane at a constant current of 100mA for 1 hour (Biorad powerpack).

Following the protein transfer, the PVDF membrane was rinsed in 1X TBS-tween, then incubated with blocking solution (5% Marvel in 1X TBS-tween) for 1 hour to block non-specific binding sites. The blots were then incubated in primary antibody (see table 2.3) on a shaker overnight at 4°C. The following day, the blots were rinsed for 3 x 20 minutes in 1X TBS, then incubated with the appropriate HRP conjugated secondary antibody diluted in blocking solution for 1 hour. Following 3 x 20 minute washes with 1X TBS-Tween, antibody detection was performed using enhanced chemiluminescence (ECL, Pierce), prepared according to the manufacturers instructions. The ECL reagents contain luminol, which reacts with the horseradish peroxidase in the secondary antibody producing light emission, which can be

detected using X-ray film. The membranes were removed from the 1X TBS-tween, excess solution blotted off, then placed in ECL solution for 1 minute. Excess ECL solution was removed by placing the membranes between two sheets of blotting paper, then they were wrapped with cling film and secured in X-ray cassettes with tape. The blots were exposed to X-ray radiographs in the dark for 1-5 minutes depending on each antibody. Following development in a automatic X-ray processor, the proteins detected with the appropriate antibody appeared as dark bands on the X-ray film.

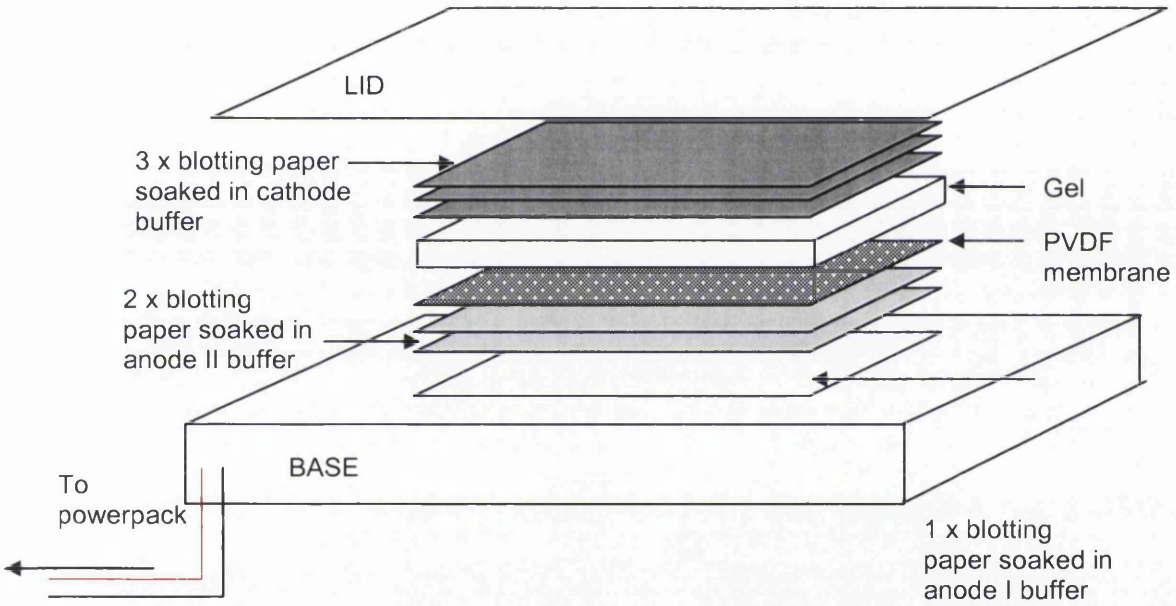

Figure 2.13 Arrangement of blotting paper, gel and PVDF membrane on semi-dry transfer system

As each layer was placed on the transfer equipment, it was rolled with a glass pipette to remove air bubbles

2.8.5 Quantification of protein levels

The films were scanned using a Hewlitt Packard scanner (ScanJet 6200C), and proteins were quantified for differences in light intensity using NIH imaging software.

Primary Antibody	Species, Type	Source of Primary	Dilution of Primary	Blocking Sera	Secondary Antibody
GluR1	Rabbit Polyclonal	Chemicon	1:100	5% Marvel in TBS	HRP Anti-Rabbit (Sapu) 1:4000
GluR2/3	Rabbit, polyclonal	Chemicon	1:66	5% Marvel in TBS	HRP Anti-Rabbit (Sapu) 1:4000
GluR2	Rabbit, Polyclonal	Chemicon	1:200	5% Marvel in TBS	HRP Anti-Rabbit (Sapu) 1:4000
GluR4	Rabbit, Polyclonal	Chemicon	1:50	5% Marvel in TBS	HRP Anti-Rabbit (Sapu) 1:4000
Actin	Mouse, Monoclonal	Sigma	1:100 000	5% Marvel in TBS	HRP Anti-Mouse (Sigma) 1:5000

Table 2.3 Primary antibodies used in the western blotting experiments

CHAPTER 3

THE ROLE OF AMPA RECEPTORS IN MEDIATING AXONAL DAMAGE *IN VIVO*

3.1 Introduction

AMPA receptor-mediated excitotoxicity causes neuronal perikaryal death *in vitro* and *in vivo*, and AMPA receptor antagonists attenuate neuronal perikaryal damage following cerebral ischaemia (Meldrum and Garthwaite, 1990; Gill, 1994). In addition to their presence on neuronal perikarya, functional AMPA receptors are also present in the cellular components of white matter, such as oligodendrocytes and myelin.

Considerable evidence suggests a role for AMPA receptor-mediated excitotoxicity in causing oligodendrocyte death. Exposure of oligodendrocyte cultures to AMPA or glutamate results in cell death (Oka *et al.*, 1993; Yoshioka *et al.*, 1995; McDonald *et al.*, 1998a, b; Sanchez-Gomez and Matute, 1999; Alberdi *et al.*, 2002), whilst intracerebral injection of AMPA into the external capsule of rats results in a 60% reduction of oligodendrocytes (McDonald *et al.*, 1998a). Chronic and acute *in vivo* administration of the AMPA receptor agonist kainate onto the rabbit optic nerve results in oligodendrocyte cell death and myelin disruption (Matute *et al.*, 1997; Matute, 1998).

Myelinated axons are dependent upon interactions between the oligodendrocyte/myelin sheath and the axon cylinder for normal functioning. Excitotoxic events at the oligodendrocyte may have detrimental effects on axons, and hence the functioning of the nervous system. *In vitro* evidence suggests that AMPA receptor-mediated mechanisms may cause axonal damage. Exposure of spinal cord segments to anoxia and trauma results in a loss of compound action potential and structural damage to the axon cylinder, which is attenuated by AMPA-receptor antagonists, and exacerbated by the addition of AMPA or kainate (Agrawal and Fehlings, 1997; Li *et al.*, 1999). However, while application of glutamate to spinal cord dorsal column segments *in vitro* does not affect the structural integrity of axons, functional integrity of the tract is impaired, demonstrated by reduced compound action potential (Li and Stys, 2000). This is attenuated by the AMPA receptor antagonists NBQX and GYKI52466, suggesting that AMPA-receptor mediated mechanisms cause axonal dysfunction (Li and Stys, 2000). In contrast to the spinal cord, exposure of rat brain slices to oxygen glucose deprivation results in both a loss of axonal compound action potential and neurofilament derangement, and both are prevented by blockade of AMPA receptors with NBQX or GYKI52466 (Baltan Tekkok and Goldberg, 2001).

It remains to be established if axons in the brain are vulnerable to AMPA receptor-mediated damage *in vivo*.

3.1.1 Aims of study

The aims of the present study were firstly to determine if intracerebral injection of AMPA causes structural damage to the axonal cytoskeleton, and to confirm if this occurs through AMPA receptor-mediated mechanisms. The effects of AMPA on myelin, oligodendrocytes and neurons were also examined. In addition, it was determined if AMPA receptor antagonism has the potential to salvage axons as well as neuronal perikarya following focal cerebral ischaemia.

3.2 Methods

3.2.1 Intracerebral injection of AMPA

Male Sprague-Dawley rats (Harlan Olac, UK) weighing 300-425g received stereotaxic injections of 0.5μl of S-AMPA (Sigma, UK) (2.5nmol, n=19) (25 nmol, n=5) or vehicle (10 mM PBS pH 7.4, n=11) into the external capsule according to the protocol outlined in section 2.1.1. To further characterise the response of myelin to intracerebral injection of AMPA, a separate set of animals received intracerebral injection of 0.5μl of S-AMPA (2.5nmol, n=5) (25nmol, n=5) or vehicle (n=4).

3.2.2 Intracerebral injection of AMPA with intravenous administration of the AMPA receptor antagonist, SPD-502

Male Sprague Dawley rats (340-375g) received an intravenous bolus of drug (SPD-502, 16 mg/kg; n=5) or vehicle (saline; n=6), 15 minutes prior to intracerebral injection of S-AMPA (25nmol) into the external capsule as described in section 2.1.1. Rats then received a continual infusion of SPD 502 (16mg/kg/hr) or vehicle for 1 hour, according to the protocol in section 2.1.2. All drug administration and subsequent analysis was performed whilst blinded to the treatment.

3.2.3 Intracerebral injection of AMPA with the NMDA receptor antagonist, MK-801

To determine if axonal damage induced by intracerebral injection of AMPA occurred through NMDA receptor mediated mechanisms, the NMDA receptor antagonist MK-

801 was co-injected with AMPA into the external capsule as described previously (McDonald *et al.*, 1998). Male Sprague-Dawley rats (295-335g) received stereotaxic co-injection of 0.5µl S-AMPA (25nmol) and MK-801 (5nmol, n=6); S-AMPA (25nmol, n=5); or vehicle (n=5) into the external capsule and were allowed to recover for 24 hours as described in section 2.1.1. All drug administration and subsequent analysis was performed whilst blinded to the treatment given for each animal.

3.2.4 Immunohistochemistry and histology following stereotaxic injection

Animals were re-anaesthetised 24 hours following the stereotaxic injection, then perfused transcardially with 0.9% heparinised saline followed by 4% paraformaldehyde in 50mM phosphate buffer as described in section 2.1.3. Brains were then processed with sucrose, then 30µm sections were cut in a cryostat, as described in section 2.1.4. Immunohistochemistry was performed on the free floating sections as described in section 2.5.2. MAP 5, NF 200 and SMI 32 immunostaining was used to examine axonal pathology; Tau-1 and PLP immnostaining was used to examine oligodendrocyte and myelin pathology respectively. Double labelling with Tau-1 and either GFAP (a marker of astrocytes), neuN (a marker of neurons) or mrf-1 (a marker of microglia) was carried out according to the protocol outlined in section 2.5.3. Double labelling with Tau-1 and TUNEL was also performed according to the protocol in section 2.5.4. with sections from animals that had received intracerebral injection of AMPA (25nmol; n=5). Free floating sections were also mounted onto poly-L-lysine slides and stained using conventional H & E staining to examine histological damage (2.6.1). Quantification of axonal, oligodendroglial, myelin and tissue damage is outlined in sections 2.5.6., 2.5.7., 2.5.8., and 2.6.3., respectively.

3.2.5 Focal cerebral ischaemia

Dr Eileen McCracken performed all surgical procedures and tissue processing for this experiment. Male Sprague-Dawley rats were deeply anaesthetised, and the right middle cerebral artery was occluded using the intraluminal thread technique, as described in section 2.2. Vehicle (saline)(n=8) and drug (SPD 502) (n=7) were administered as an intravenous bolus (16mg/kg) 15 minutes prior to monofilament insertion and then as a continuous infusion for 4 hours (16mg/kg/hr). Twenty-fours hours following the MCAO, animals were perfuse fixed, then brains were processed and paraffin embedded (section 2.2).

3.2.6 Immunohistochemistry and histology on ischaemic tissue

Sections (6μm) from 8 pre-determined coronal levels throughout the brain (Osborne et al., 1987) were stained with H & E to determine neuronal cell body damage (section 2.6.1). The volume of neuronal perikaryal damage was quantified by Dr Eileen McCracken, using a protocol described by Osborne *et al.*, 1987. Adjacent sections were immunostained with APP and NF 200 to examine axonal pathology according to the protocol outlined in section 2.5.5. Dr Eileen McCracken performed APP immunostaining and quantification of axonal damage in APP immunostained sections. Axonal damage visible in APP immunostained sections was quantified using a scoring system based on the presence or absence of damaged axons in 65 individual regions of white matter (Imai *et al.*, 2002). I performed the analysis of the NF 200 immunostaining. The area of axonal damage visible in each NF 200 immunostained section was plotted onto a copy of the appropriate coronal level from a rat stereotaxic atlas (Paxinos and Watson, 1998). The volume of axonal damage in the NF 200 immunostained sections was calculated by integration of the areas of damage on each coronal plane with the distance between each level. For descriptive analysis of damage to myelinated fibre tracts, sections were immunostained using antibodies raised against myelin basic protein (MBP), proteolipid protein (PLP) and myelin associated glycoprotein (MAG), according to the protocol outlined in section 2.5.5.

3.2.7 Statistical Analysis

To determine if there was any significant difference between the AMPA (2.5nmol or 25nmol) or vehicle-injected animals, one-way analysis of variance was used with *post-hoc* Student's *t*-test and Bonferonni corrections for multiple comparisons. To determine if there was any significant difference between vehicle, AMPA or AMPA and MK-801 treatement, one-way analysis of variance was used with *post-hoc* Student's *t*-test and Bonferonni corrections for multiple comparisons. To determine if there was any significant difference between SPD 502- and saline- treated animals following intracerebral injection of AMPA, two-tailed, unpaired Student's *t*-test was used. Data are presented as mean ± standard error of the mean (SEM).

To determine if there were any differences in the volume of axonal (NF 200) or neuronal damage between vehicle treated and SPD 502 treated animals following focal cerebral ischaemia, two-tailed unpaired Student's *t*-test was used. Data are presented as mean ± SEM.

3.3 Results

3.3.1 AMPA-induced axonal damage

In the external capsule contralateral to the site of injection, axons in MAP-5 immunostained sections ran in a smooth, organised manner (Fig. 3.1A). In contrast, the ipsilateral external capsule of animals that received injection of AMPA contained damaged axons, visualised in MAP 5 stained sections as swollen and bulbous like profiles (Fig. 3.1B). SMI 32 and NF 200 immunostaining also revealed the presence of axonal swellings and bulbs in the ipsilateral external capsule of AMPA-treated animals (Fig. 3.1D and 3.1F), which had a rougher, disorganised appearance compared to the contralateral hemisphere (Fig. 3.1C and 3.1E). Animals that received intracerebral injection of vehicle exhibited minimal axonal damage confined to a small area immediately adjacent to the injection site (Fig. 3.3A). Quantification of axonal damage in the external capsule of MAP 5 immunostained sections showed that AMPA caused significantly more axonal damage compared to injection of the vehicle (Fig. 3.3B), and this was dose-dependent. The presence of damaged axons and dendrites, often with a characteristic beaded appearance, in the cortex overlying the injection site, was observed in AMPA treated animals in MAP 5 immunostained sections (Fig. 3.2B). SMI 32 and NF 200 immunostained sections also revealed axonal swellings and bulbs in the cortex overlying the injection site (Fig. 3.2D and 3.2F).

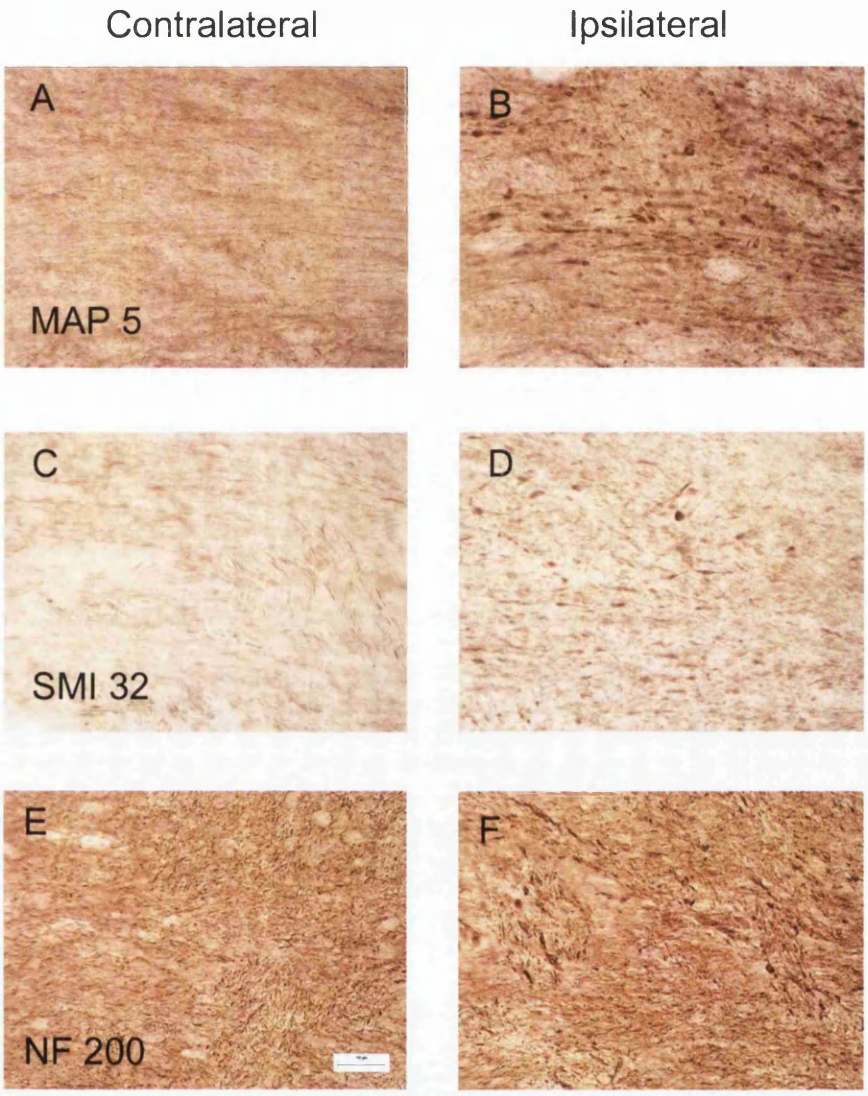

Figure 3.1 Immunohistochemical staining in the external capsule following intracerebral injection of AMPA (25nmol)

In the external capsule contralateral to the injection site, axons in MAP 5, SMI 32 and NF 200 immunostained sections appeared to be running in smooth, organised networks (A, C and E respectively). Following intracerebral injection of AMPA, axonal disruption was evident in MAP 5, SMI 32 and NF 200 immunostained sections (B, D and F respectively).

Scale Bar = 50μm.

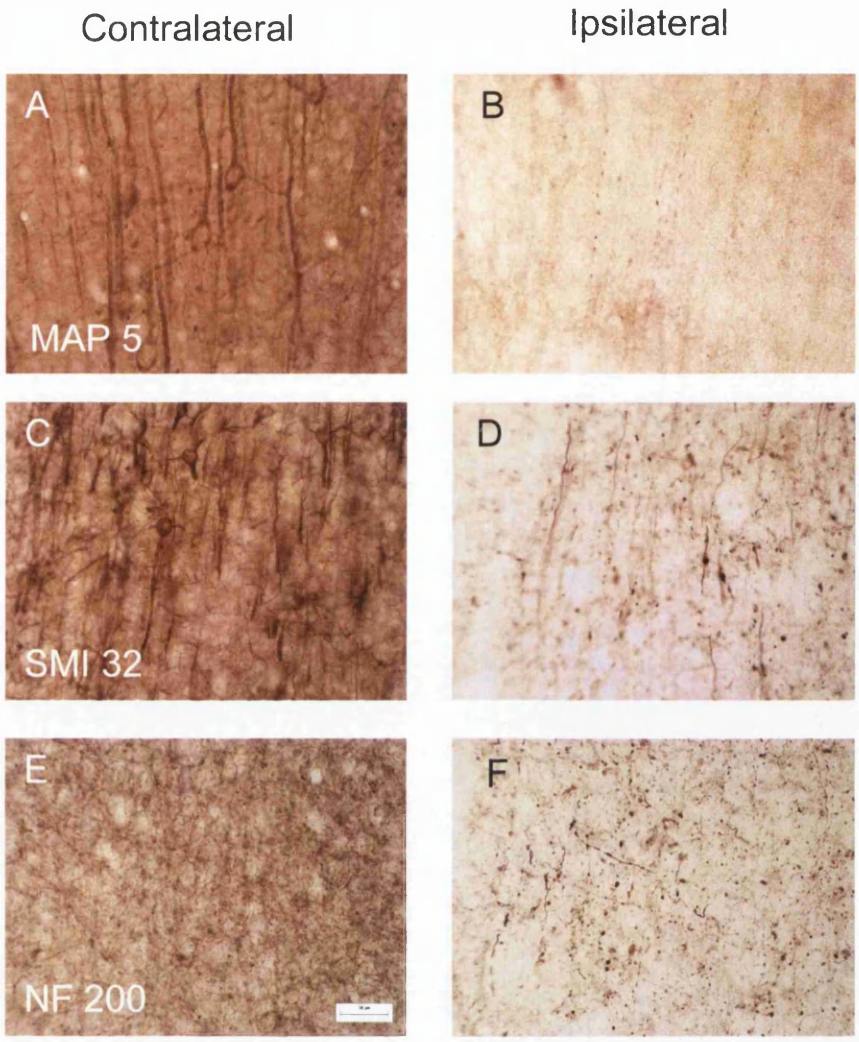

Figure 3.2 Immunohistochemical staining in the cortex following intracerebral injection of AMPA (25nmol)

In the cortex contralateral to the injection site, axons in MAP 5, SMI 32 and NF 200 immunostained sections appeared to be running in smooth, organised networks (A, C and E respectively). Following intracerebral injection of AMPA, axonal disruption was evident in MAP 5, SMI 32 and NF 200 immunostained sections (B, D and F respectively).

Scale Bar = 50μm

A

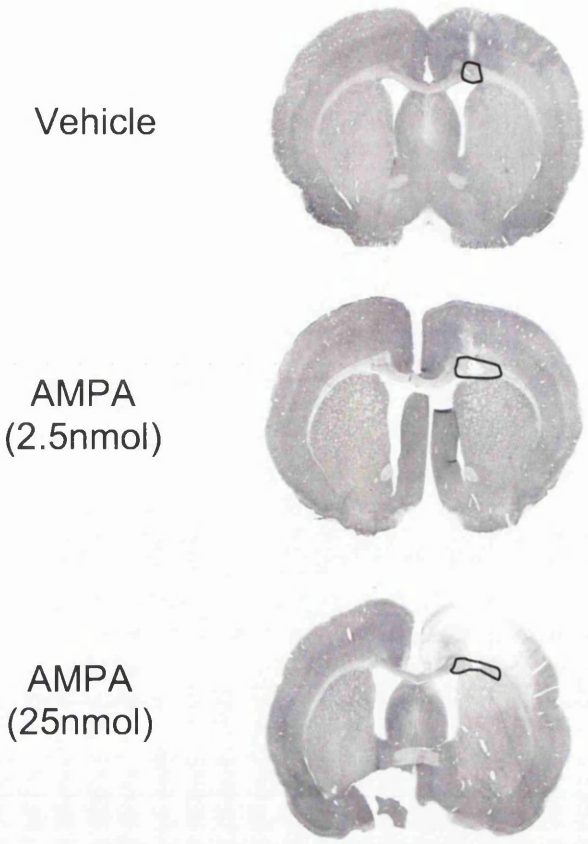

B

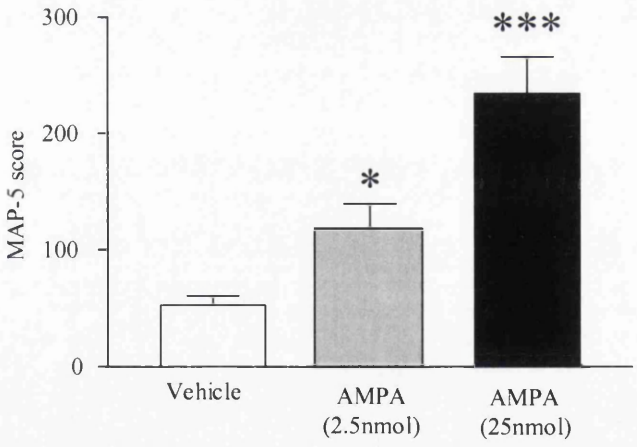

Figure 3.3 Axonal damage in MAP 5 immunostained sections following intracerebral injection of AMPA

A. Digitised MAP 5 immunostained sections from a single coronal level of representative animals following injection of vehicle or AMPA (2.5 or 25nmol). The extent of axonal damage in the external capsule is represented within the solid black line.

B. Quantification of axonal damage in the MAP 5 immunostained sections. Data are presented mean ± SEM. *P<0.05, ***P<0.001, for comparison with vehicle treated group (one way ANOVA with *post hoc* Student's *t* test and Bonferonni correction). Vehicle, n=11; 2.5nmol, n=9; 25nmol, n=5.

3.3.2 AMPA-induced oligodendrocyte pathology

Tau-1 immunoreactivity in the hemisphere contralateral to the site of injection had a diffuse pattern of staining, with minimal staining of cell bodies in both white (Fig. 3.4C) and grey matter (Fig. 3.4A). AMPA-treated animals exhibited intensely stained cells with the characteristic morphology of oligodendrocytes (figure 3.4B) in tau immunostained sections. Tau-positive cells were not observed to be double labelled with either GFAP (a marker of astrocytes), mrf-1 (a marker of microglia)or neu-N (a marker of neurons) (Fig. 3.5).

Tau-positive oligodendrocytes were present predominantly in the cortex overlying the external capsule, but only occasionally within the external capsule itself following injection of the lower dose of AMPA (2.5nmol, Fig. 3.6A). Following injection of the higher dose of AMPA (25nmol), tau-positive oligodendrocytes were observed in an anatomically more extensive area of cortex, often being localised to the boundary of the lesion. Tau-positive cells were rarely observed in the external capsule following injection of the higher dose of AMPA (25nmol; Fig. 3.4D, 3.6A). Animals that received an injection of vehicle contained few tau-positive cells, which were confined to the area adjacent to the needle tract (Fig. 3.6A). Quantification of the volume of tissue containing tau-positive oligodendrocytes showed that AMPA caused significantly more oligodendrocyte damage compared to the vehicle, and that this damage increased in a dose dependent manner (Fig. 3.6B).

Tau-positive cells were not observed to be double labelled with TUNEL, a marker of DNA fragmentation (TdT FragEL) (Fig. 3.7).

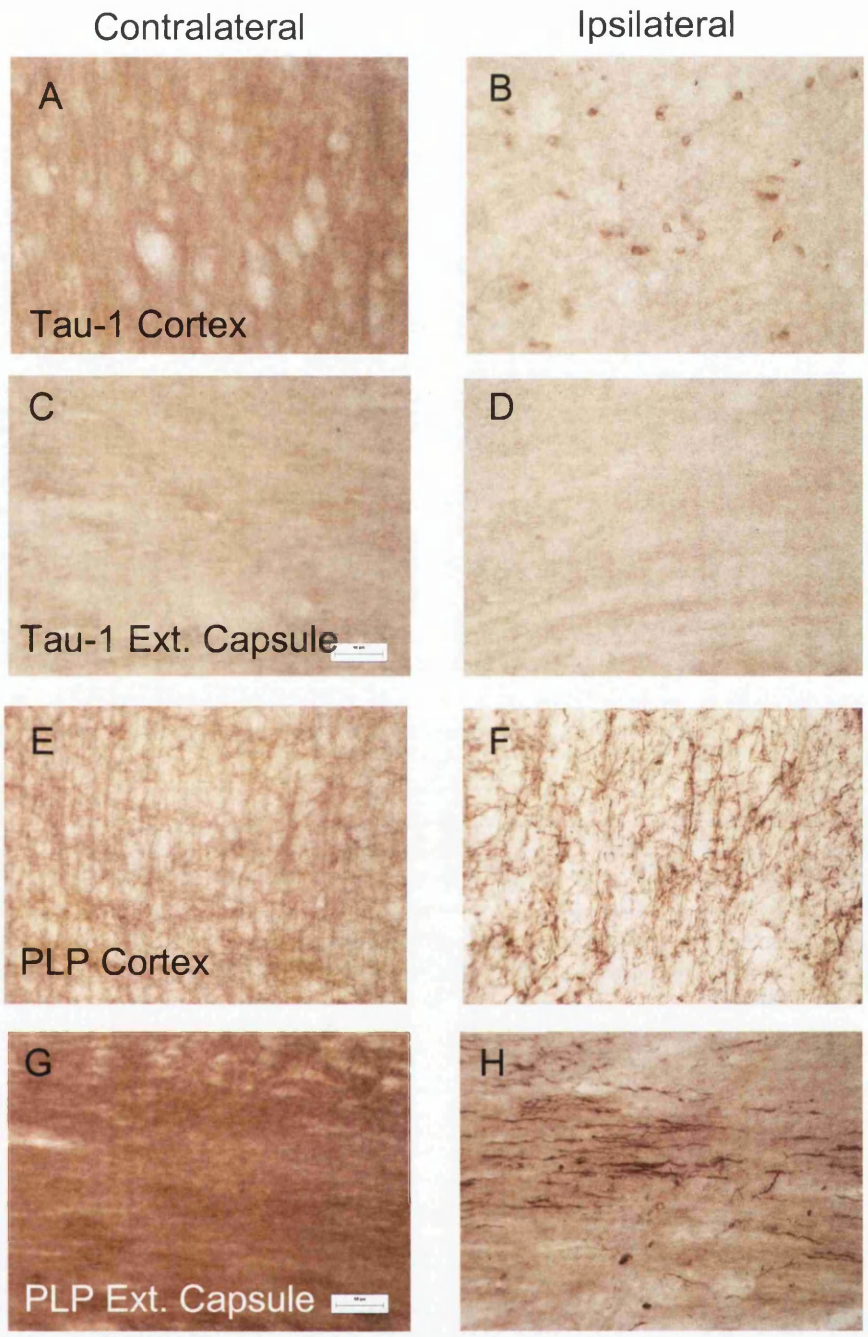

Figure 3.4 Oligodendrocyte and myelin damage in the cortex and external capsule of immunostained sections following intracerebral injection of AMPA (25nmol)

There was diffuse Tau-1 immunoreactivity, with minimal staining of cell bodies in the cortex (A) and external capsule (C) contralateral to the injection site. Tau-positive oligodendrocytes were present in the cortex overlying the injection site (B), but were rarely observed in the external capsule (D) following injection of AMPA (25nmol). Myelinated fibres immunostained with PLP formed organised profiles in the cortex (E) and external capsule (G) in the hemisphere contralateral to the injection site. AMPA (25nmol) caused disruption of PLP immunostained fibres in the cortex (F), and in the external capsule there was a loss of immunostaining accompanied by the presence of intensely stained swollen fibres. Scale bar = 50μm

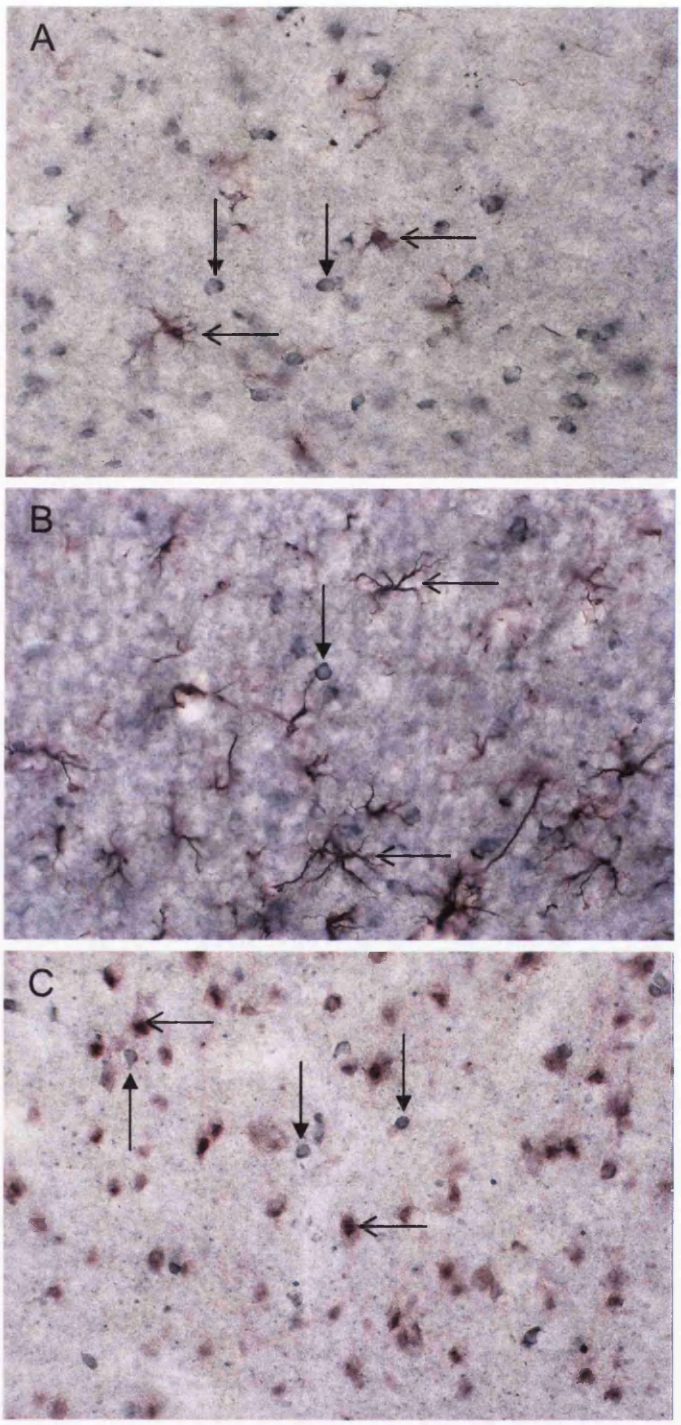

Figure 3.5 Double labelling immunohistochemistry

A. Tau-1 (grey, closed arrow heads) and mrf-1, a marker of microglia (pink, open arrow heads).

B. Tau-1 (grey, closed arrow heads) and GFAP, a marker of astrocytes (pink, open arrow head).

C. Tau-1 (grey, closed arrow heads) and Neu-N, a marker of neurons (pink, open arrow head).

All images were taken from the cortex overlying the injection site (x400 magnification).

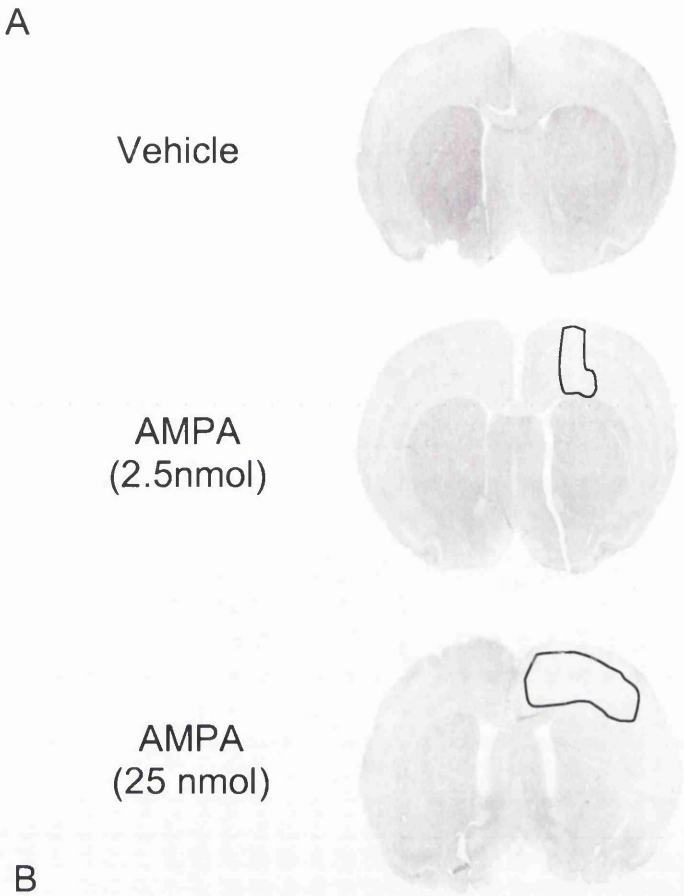

Figure 3.6 Oligodendrocyte pathology following intracerebral injection of AMPA

A. Digitised representative Tau-1 immunostained sections from a single coronal level. Tissue containing tau-positive oligodendrocytes are contained within the solid black line.

B. Quantification of the volume of tissue containing tau-positive oligodendrocytes following intracerebral injection of vehicle or AMPA (2.5 or 25nmol). Data are presented mean ± SEM. *P<0.05, ***P<0.001 for comparison with vehicle treated group. (One way ANOVA followed by Student's *t*-test with Bonferroni correction). Vehicle, n=11; 2.5nmol, n=9; 25nmol, n=5.

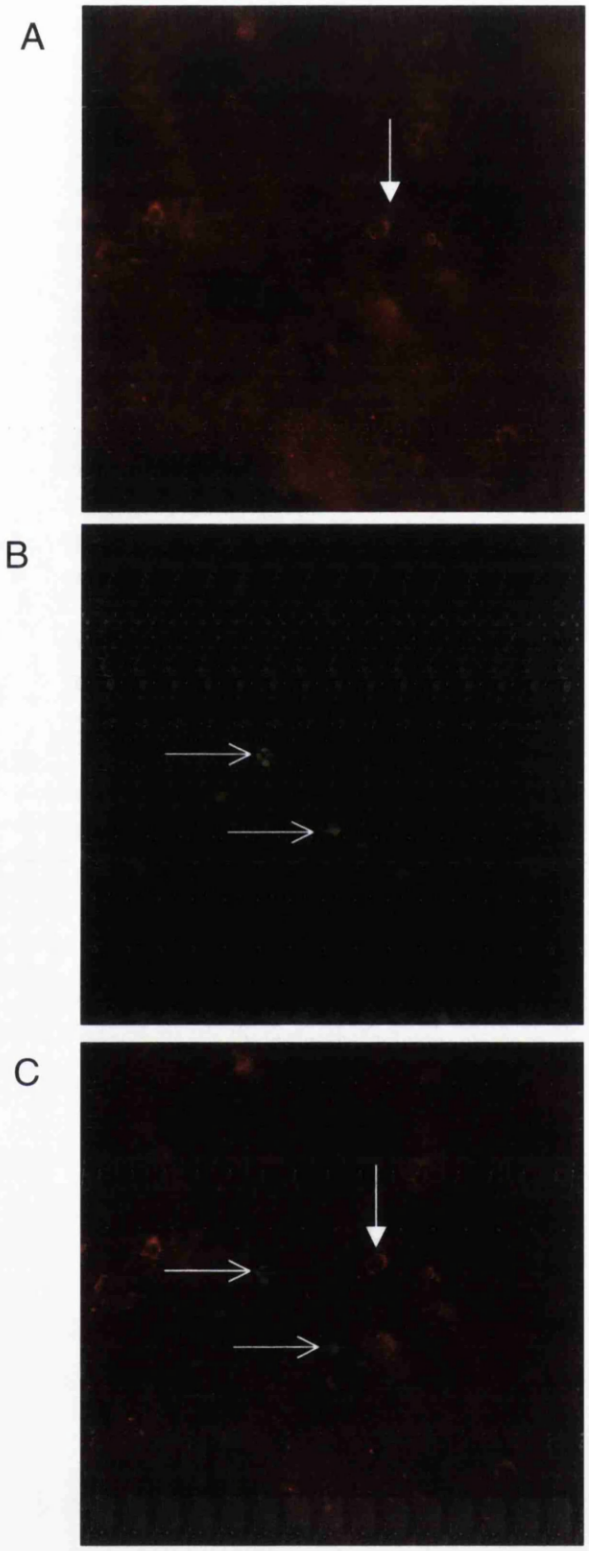

Figure 3.7 Double labelling with Tau-1 and a marker of DNA fragmentation (TUNEL)

A. Tau-positive cell (red, closed arrow head).

B. TUNEL positive cells (green, open arrow head)

C. Combined channel showing that tau-positive cells (red, closed arrow head) are not visibly double labelled with TUNEL positive cells (green, open arrow head).

All images were taken from the cerebral cortex overlying the injection site (x400 magnification).

3.3.3 AMPA-induced myelin pathology

A separate set of animals were used to examine the responses of myelin to intracerebral injection of AMPA. PLP immunostained sections showed uniform, smooth staining of the myelin in the external capsule contralateral to the injection site (Fig. 3.4G). AMPA caused a loss of PLP immunostaining, accompanied by the presence of intensely stained swollen myelinated fibres in the external capsule (Fig. 3.4H). PLP immunostained sections revealed organised networks of myelinated fibres in the cortex overlying the injection site (Fig. 3.4E). Following injection of AMPA, there was a loss of this organised appearance of myelinated fibres in the cortex, with fibres severely disrupted and swollen (Fig. 3.4F). Quantification of the volume of tissue containing myelin damage on PLP immunostained sections revealed that there was significantly more myelin damage following injection of AMPA (25nmol) compared to injection of vehicle (Fig. 3.8).

These data show that intracerebral injection of AMPA causes damage to axons and myelin; however, explicit comparisons were not made between the amounts of axonal and myelin damage as these were assessed in different groups of animals.

3.3.4 AMPA-induced tissue damage

H & E staining of the external capsule contralateral to the injection site revealed that oligodendrocyte-like cells ran in organised profiles (Fig 3.9A). Following injection of AMPA, the oligodendrocytes appeared abnormal and disorganised, and vacuolation was evident in the external capsule (Fig. 3.9B). In the cortex, AMPA caused neuronal cell body necrosis, indicated by the presence of shrunken, eosinophilic cells (Fig. 3.9D). The lower dose of AMPA (2.5nmol) caused neuronal perikaryal damage in the cortex surrounding the injection site (Fig. 3.10A), whereas the higher dose of AMPA caused neuronal damage in a larger area of cortex, as well as a small area in the dorsal caudate nucleus beneath the injection site (Fig. 3.10A). The H & E sections of vehicle-treated animals revealed minimal neuronal cell body damage limited to a small area overlying the external capsule at the injection site (Fig. 3.10A) The dose-dependent increase in neuronal perikaryal damage induced by AMPA is reflected in the volume of tissue damage (Fig. 3.10B).

A

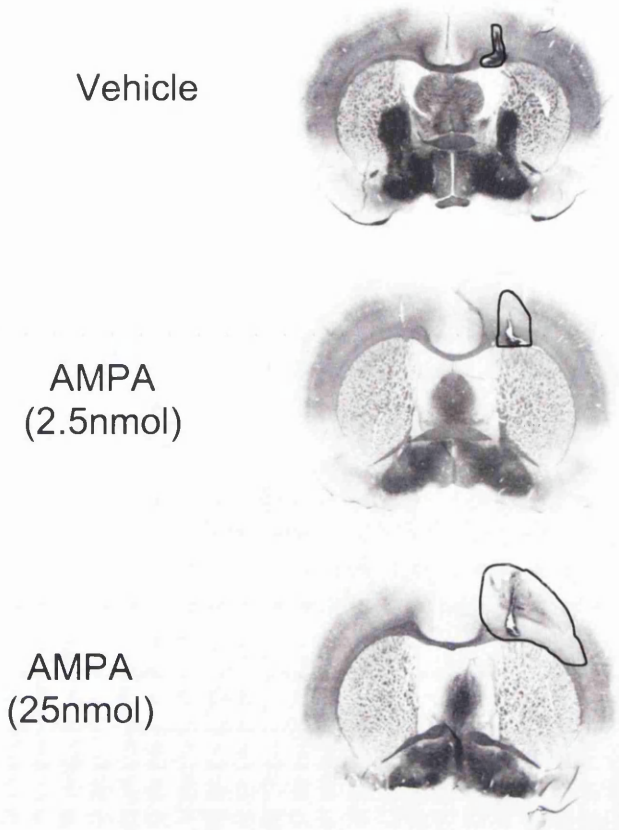

B

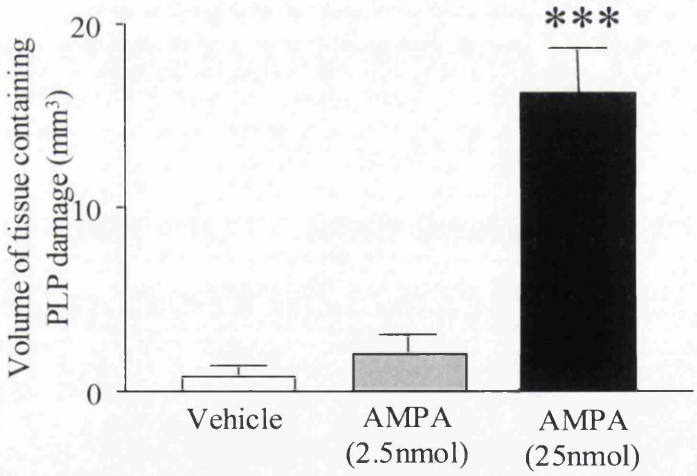

Figure 3.8 Myelin damage in PLP immunostained sections

A. Representative PLP immunostained sections from a single coronal level showing the extent of myelin damage within the black line following injection of AMPA (2.5nmol or 25nmol) or vehicle

B. Quantification of myelin damage in PLP immunostained sections. Data are presented as mean ± SEM ***P<0.001 for comparison with vehicle treated gourp (One way ANOVA followed by Student's *t*-test with Bonferroni correction). Vehicle, n=4; 2.5nmol, n=5; 25nmol, n=5. Direct comparisons cannot made between the amount of myelin damage with the amount of axonal damage (Fig. 3.3), as these were assessed in separate groups of animals.

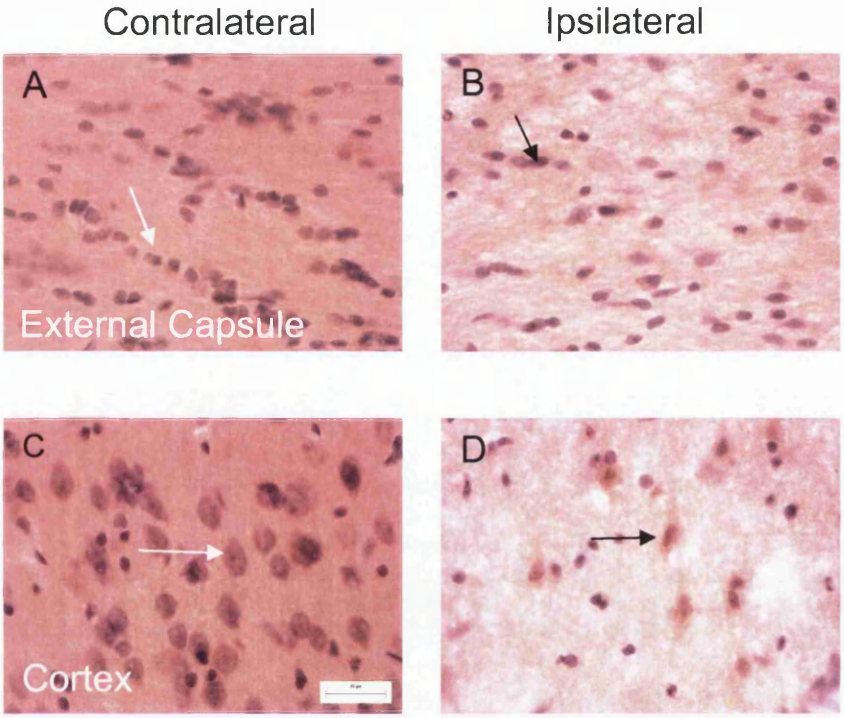

Figure 3.9 Histological changes in the external capsule and cortex following intracerebral injection of AMPA (25nmol).

Oligodendrocyte-like cells (white arrows) ran in an organised manner in the external capsule contralateral to the injection site (A). In contrast, oligodendrocytes appeared abnormal (black arrows) and vacuolation was present in the external capsule following intracerebral injection of AMPA (B). Neurons (white arrows) appeared morphologically normal in the cortex overlying the injection site (C). Following injection of AMPA, neurons appeared shrunken and eosinophilic (black arrows) in the cortex overlying the injection site (D). Sections were stained with H & E.
Scale bar = 25μm.

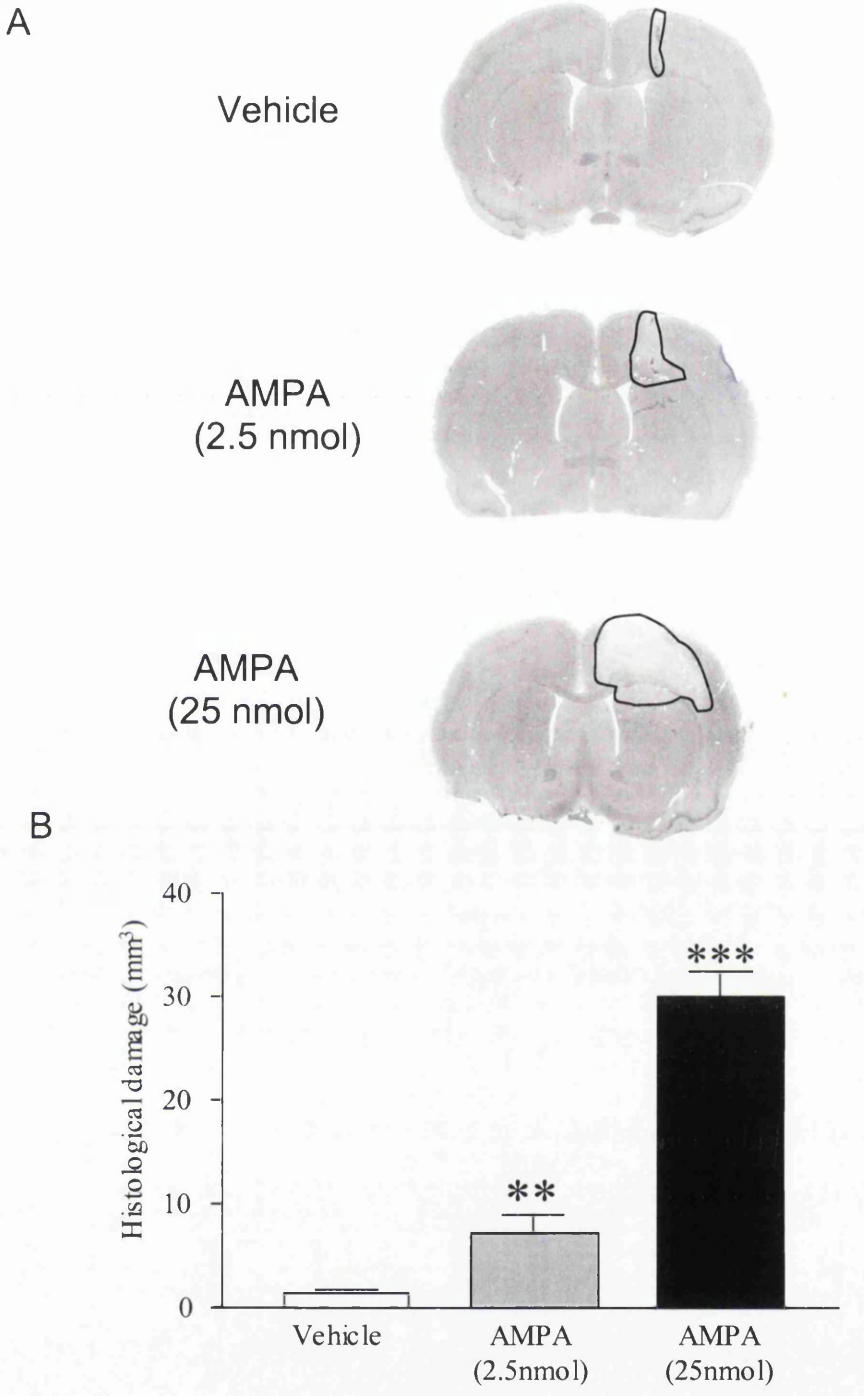

Figure 3.10 Tissue damage following intracerebral injection of AMPA

A. Digitised H & E stained section showing the area of tissue damage within the solid black line, following injection of AMPA (2.5nmol or 25 nmol) or vehicle.

B. Quantification of the volume of tissue damage in the H & E stained sections. Data are presented mean ± SEM. **P<0.01 ***P<0.001 for comparison with vehicle treated groups (One way ANOVA followed by Student's *t*-test with Bonferroni correction). Vehicle, n=11; 2.5nmol, n=9; 25nmol, n=5.

3.3.5 Stereotaxic injection of AMPA with intravenous administration of the AMPA receptor antagonist SPD 502

Axonal damage was evident in MAP 5, NF 200 and SMI 32 immunostained sections in the external capsule following injection of AMPA (25nmol) with intravenous administration of vehicle. Following SPD 502 treatment, axonal damage was anatomically less extensive. Quantification of AMPA- induced axonal damage in MAP 5 immunostained sections showed that SPD 502-treated animals contained significantly less axonal damage when compared to saline treated control animals (Fig. 3.11A). Tau-positive oligodendrocytes were evident in the cortex of AMPA-treated control animals, however SPD 502 administration significantly reduced the volume of tissue containing AMPA-induced tau-positive oligodendrocytes (Fig. 3.11B). The extent of myelin damage in PLP immunostained sections was significantly reduced following administration of SPD 502 compared with saline-treated control AMPA animals (Fig. 3.11C). The volume of tissue damage quantified from H & E stained sections was significantly reduced following pre-treatment with SPD 502 (Fig. 3.11D) compared to controls.

3.3.6 Co-injection of AMPA (25nmol) with the NMDA receptor antagonist MK-801 (5nmol)

Intracerebral injection of AMPA (25nmol) or AMPA (25nmol) with MK-801 (5nmol) caused a significantly greater amount of axonal damage compared to injection of the vehicle. However, there was no significant change in the pattern or anatomical extent of axonal damage between the AMPA (25nmol) and AMPA (25nmol) with MK-801 (5nmol) groups (Fig 3.12A). Tau-positive cells were rarely observed in the vehicle treated animals; however, tau-positive cells were detected in the cortex following administration of AMPA (25nmol) or AMPA (25nmol) and MK-801 (5nmol). There were no significant differences in the volume of tissue containing tau-positive oligodendrocytes in the AMPA (25nmol) compared to the AMPA (25nmol) with MK-801 (5nmol) treated animals (Fig. 3.12B). Similarly, there were no significant differences in the amount of myelin damage between the AMPA (25nmol) and AMPA (25nmol) with MK-801 (5nmol) groups (Fig. 3.12C). Co-injection of AMPA (25nmol) with MK-801 (5nmol) had no significant effects on the amount of tissue damage quantified from H & E stained sections compared to injection of AMPA (25nmol; Fig. 3.12D).

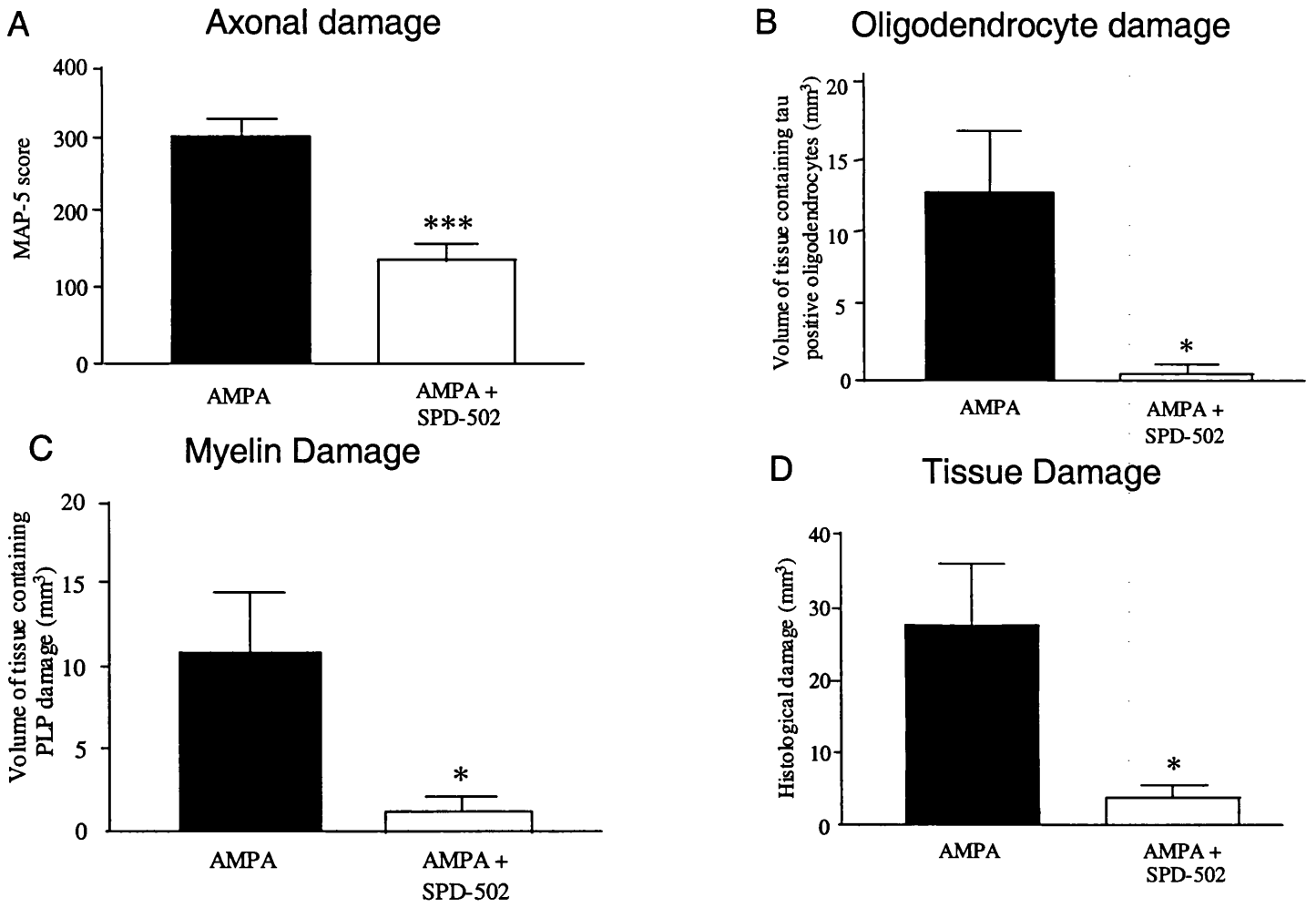

Figure 3.11 Quantification of axonal, oligodendrocyte, myelin and tissue damage following intracerebral injection of AMPA (25nmol) with intravenous administration of vehicle or SPD 502

Data are presented mean ± SEM. AMPA + Vehicle, n=5, AMPA + SPD 502, n=6. Student's *t*-test *P<0.05, ***P<0.001.

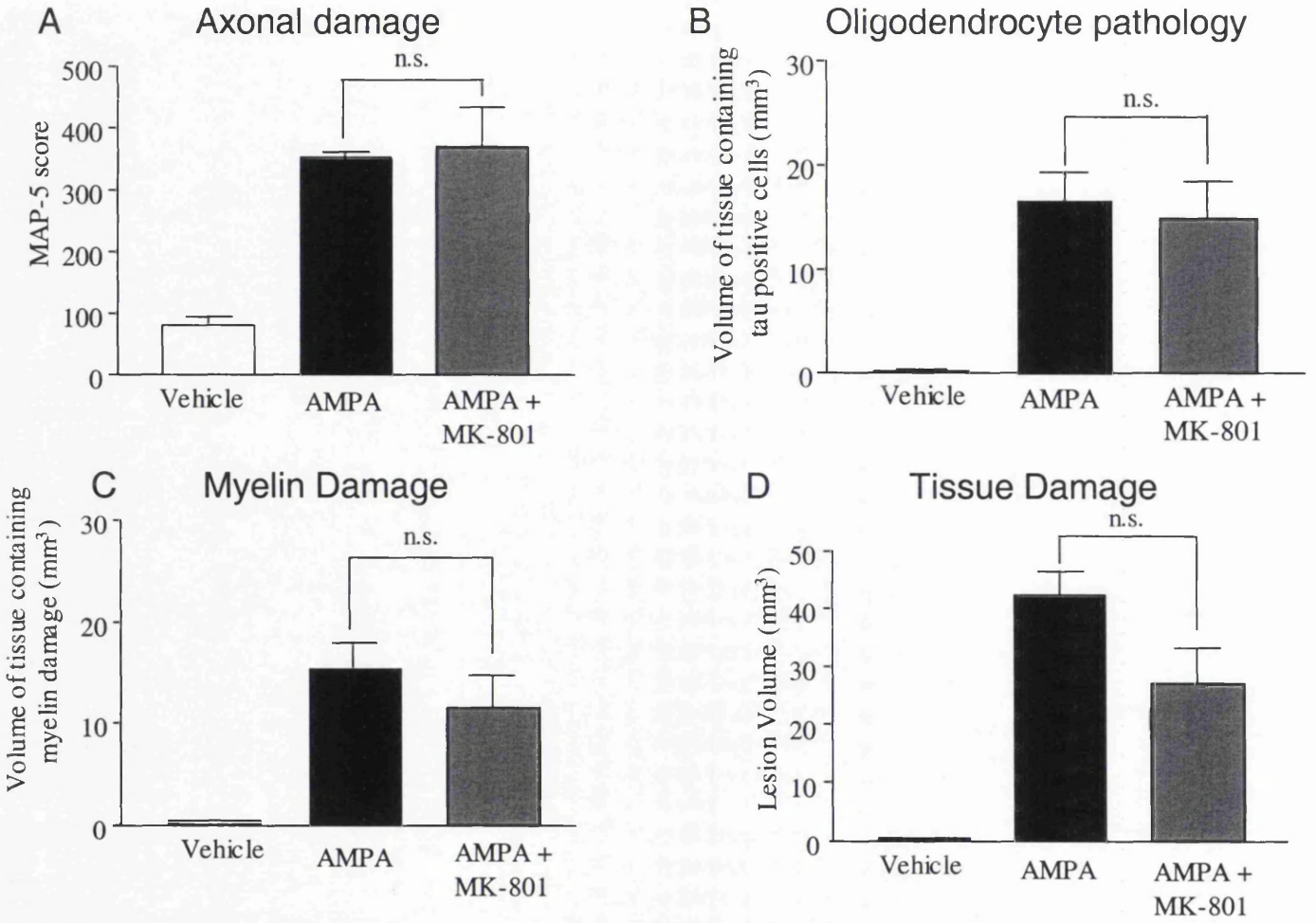

Figure 3.12 Quantification of axonal, oligodendrocyte, myelin and tissue damage following intracerebral injection of vehicle, AMPA (25nmol) or AMPA (25nmol) + MK-801 (5nmol)

Data are expressed mean ± SEM. Vehicle (PBS), n=5; AMPA (25nmol), n=5; AMPA + MK-801, n=6;. One way ANOVA with *post hoc* Student's *t*-test and Bonferroni correction for multiple comparisons.

3.3.7 Effect of SPD 502 on axonal damage visualised in NF 200 immunostained sections following focal cerebral ischaemia

In the hemisphere contralateral to the occluded MCA, NF 200 immunostained axons were evident running in a smooth, regular pattern (Fig. 3.13A, C, E, G). In contrast, in the hemisphere ipsilateral to the occluded MCA, axons appeared swollen and disrupted, indicating disrupted cytoskeletal structure (Fig. 3.13B, D, F, H). The anatomical extent of axonal damage visualised in a representative animal following vehicle treatment is presented in Fig. 3.14. Axonal damage was often observed in the cortex, external and internal capsule, caudate nucleus, globus pallidus, hypothalamus, thalamus and median forebrain bundle following vehicle treatment. Treatment with the AMPA receptor antagonist, SPD 502 (16mg/kg) reduced the anatomical extent of axonal damage visualised in NF 200 immunostained sections (Fig. 3.15). Quantification of the amount of axonal damage demonstrated that SPD 502 significantly reduced the amount of total hemispheric axonal damage (Fig. 3.16A). Subdividing this into cortical and subcortical damage revealed that SPD 502 significantly reduced the amount of cortical axonal damage (Fig. 3.16B), however there was no significant concomitant protective effect on axons in the subcortex (Fig. 3.16C).

3.3.8 Effect of SPD 502 on axonal damage visualised in APP immunostained sections following focal cerebral ischaemia

In the hemisphere contralateral to the occluded MCA, APP immunoreactivity was present at a diffuse, low level (Fig. 3.17B). In the ipsilateral hemisphere, intense APP immunoreactivity was present in swollen axons and bulbs (Fig. 3.17C). APP-immunoreactive axons were present predominately within the myelinated fibre tracts of the caudate nucleus, internal and external capsules, median forebrain bundle and fornix (Fig. 3.14). The anatomical extent of APP immunoreactive axons was reduced following SPD 502 treatment (Fig. 3.15). Quantitative analysis of the axonal damage in the APP-immunostained sections demonstrated that treatment with SPD 502 significantly reduced that amount of axonal damage (Fig. 3.17A).

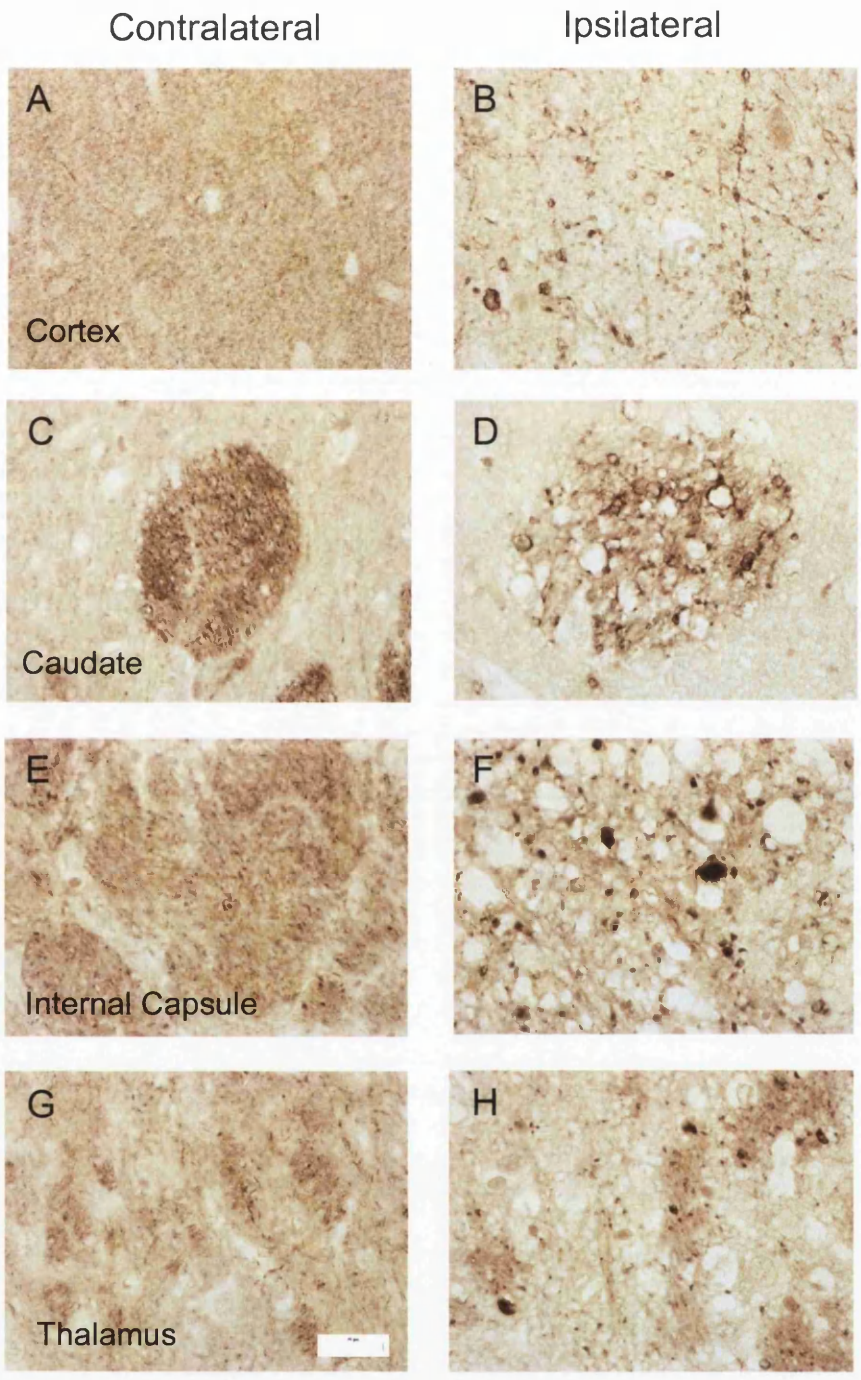

Figure 3.13 NF 200 immunostaining following transient focal cerebral ischaemia

In the hemisphere contralateral to the occluded hemisphere, axons ran in smooth, organised profiles in the cortex (A) and subcortical regions such as the caudate nucleus (C), internal capsule (E) and thalamus (G), which contrasts with the axonal swellings and bulbs evident in ipsilateral hemisphere (B, D, F, H).

Scale Bar = 25μm.

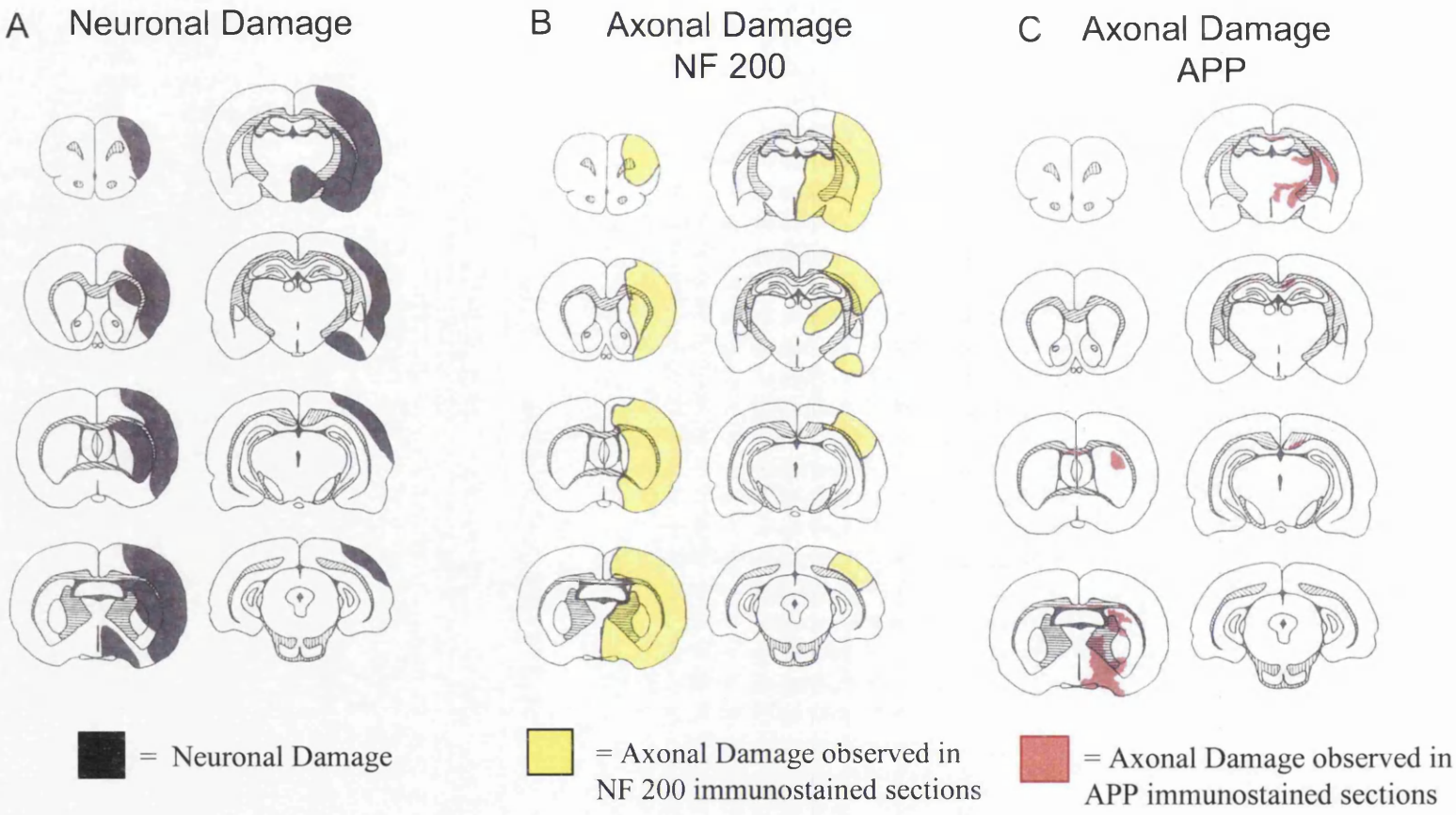

Figure 3.14 Anatomical extent of neuronal and axonal damage (in NF 200 and APP immunostained sections) in an animal following 3 hours of ischaemia, 21 hours reperfusion and saline treatment

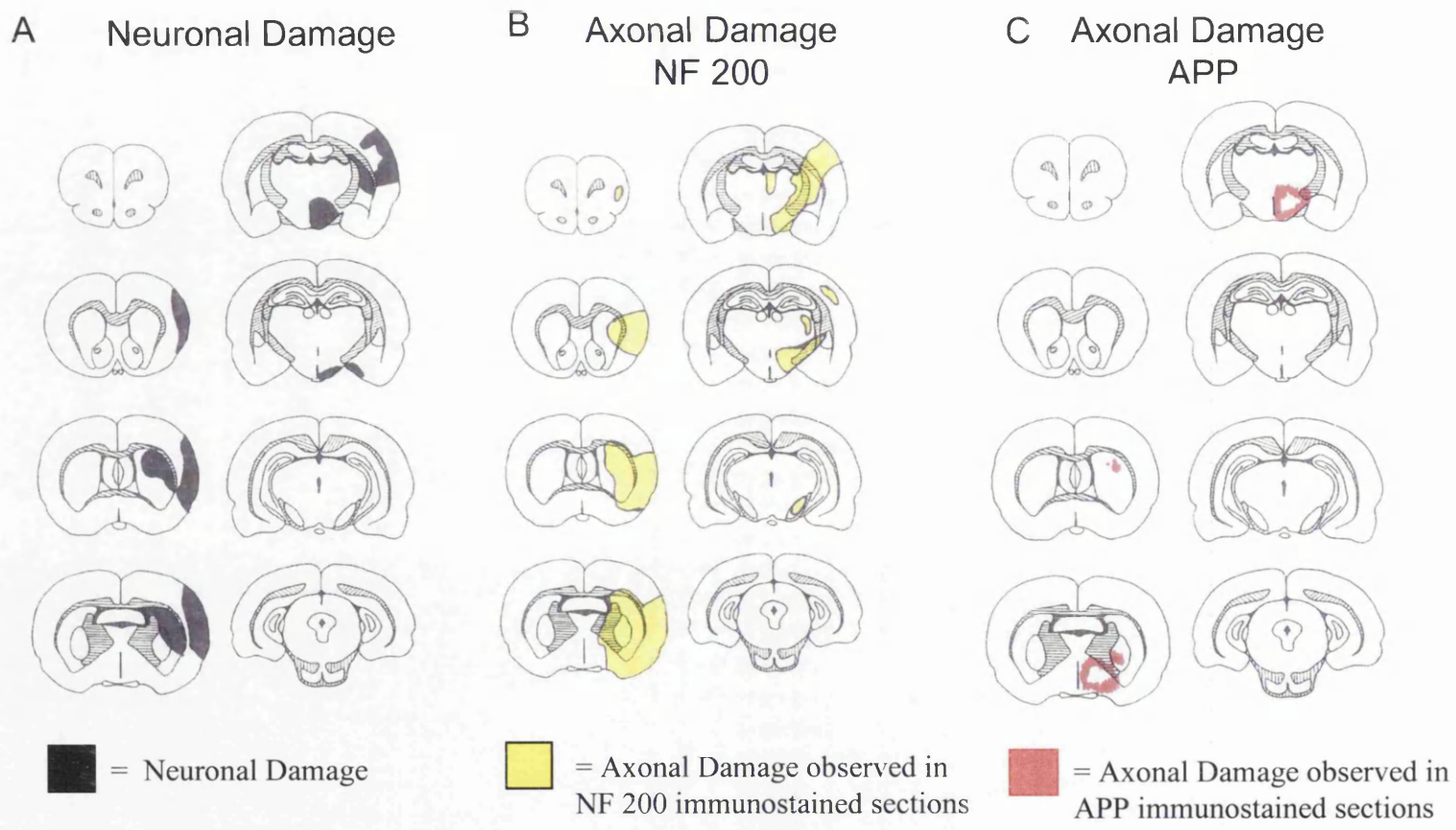

Figure 3.15 Anatomical extent of neuronal and axonal damage (in NF 200 and APP immunostained sections) in an animal following 3 hours of ischaemia, 21 hours reperfusion and AMPA receptor antagonist SPD 502 treatment

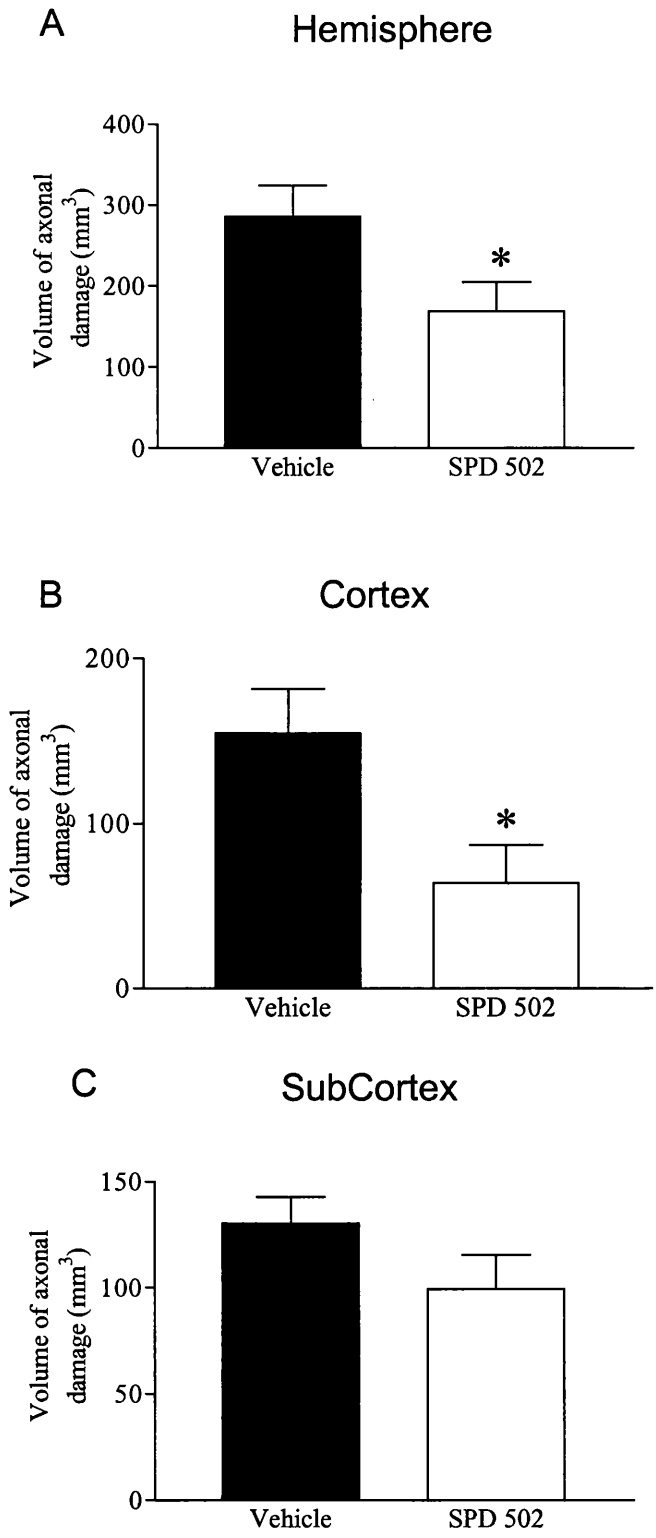

Figure 3.16 Quantification of axonal damage observed in NF 200 immunostained sections following 3 hours of focal cerebral ischaemia, 21 hours of reperfusion and treatment with vehicle or the AMPA receptor antagonist SPD 502

A. Hemisphere B. Cortex C. Subcortex

Data are expressed mean ± SEM. Vehicle, n=8; SPD 502, n=7.

*P=<0.05, two-tailed Student's *t*-test

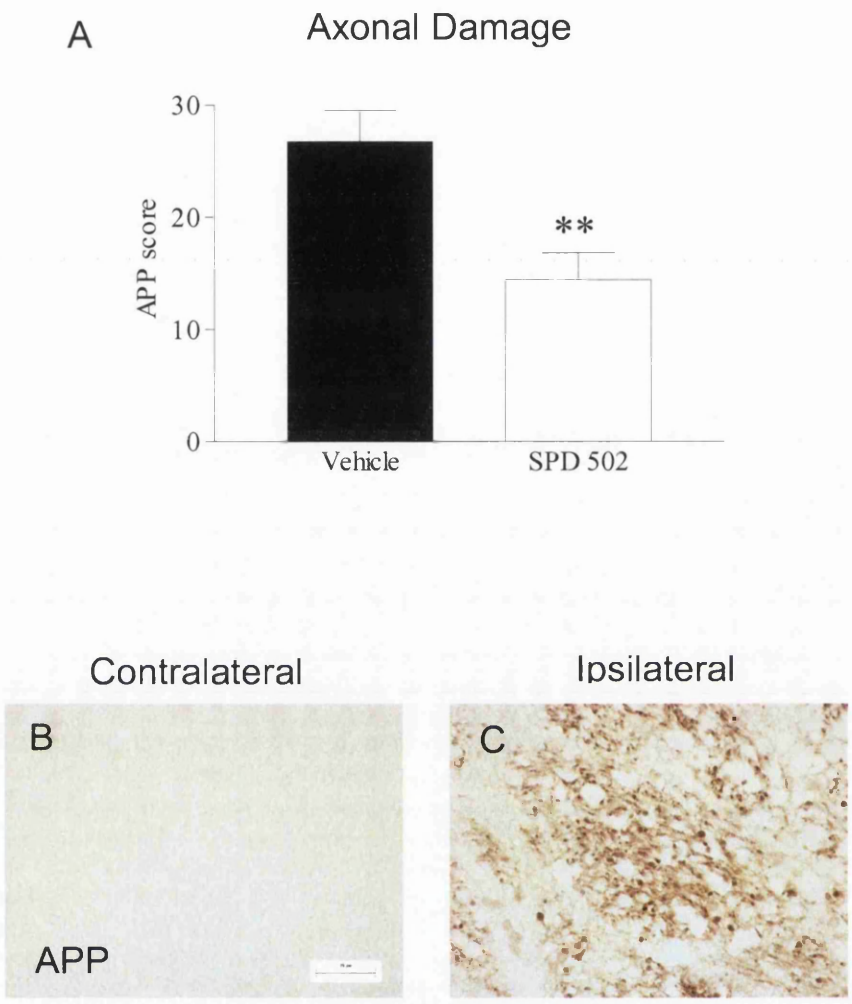

Figure 3.17 Axonal pathology assessed in APP immunostained sections following 3 hours of focal cerebral ischaemia and 21 hours of reperfusion

A. Axonal damage quantified from APP immunostained sections according to the protocol outlined by Imai et al., 2002. Vehicle, n=8; SPD 502 n=7. **P<0.01, two-tailed Mann-Whitney test

B. Representative images from APP immunostained sections in the hemisphere contralateral to the MCA occlusion, where no damaged axons were evident.

C. APP accumulation in damaged axons in the ipsilateral hemisphere. Scale bar = 25μm.

(data presented in McCracken et al, 2002)

3.3.9 Effect of SPD 502 on myelin-protein immunostaining following focal cerebral ischaemia

In the hemisphere contralateral to the occluded MCA, PLP and MBP immunostaining revealed individual networks of fibres running in organised networks in the cortex (Fig. 3.18A, C), whilst subcortical white matter tracts had a smooth, organised profile (Fig. 3.19A, C). In the ipsilateral hemisphere, PLP and MBP immunostained fibres appeared swollen and disrupted in the cortex (Fig. 3.18B, D), and subcortical white matter tracts appeared disrupted and vacuolated (Fig. 3.19B, D). In the SPD 502 treated animals, the extent of myelin disruption was anatomically less extensive compared with the vehicle treated group. Myelinated fibres stained with MAG appeared ordered and even in the contralateral hemisphere (Fig. 3.18E; Fig. 3.19E), however there was a reduction of MAG immunostaining in the occluded hemisphere, particularly within the core of MCA territory (Fig. 3.18F; Fig. 3.19F). Although the appearance of MAG immunostaining was similar in the SPD 502 treated animals; the loss of immunostaining was less extensive in these animals.

3.3.10 Effect of SPD 502 on neuronal damage following focal cerebral ischaemia

In the hemisphere ipsilateral to the occluded MCA, the cerebral cortex, caudate nucleus and anterior hypothalamus clearly exhibited the characteristics of ischaemic neuronal necrosis, whereas the contralateral hemisphere showed no evidence of neuronal pathology (Fig. 3.20B, C). The anatomic extent of neuronal damage in a representative animal from the vehicle and SPD 502 treated groups are presented in figures 3.14 and 3.15. Treatment with SPD 502 significantly reduced the anatomical extent of neuronal damage in the hemisphere and cortex, however there was no difference between SPD 502 and vehicle treated groups in the subcortex (Fig. 3.20A).

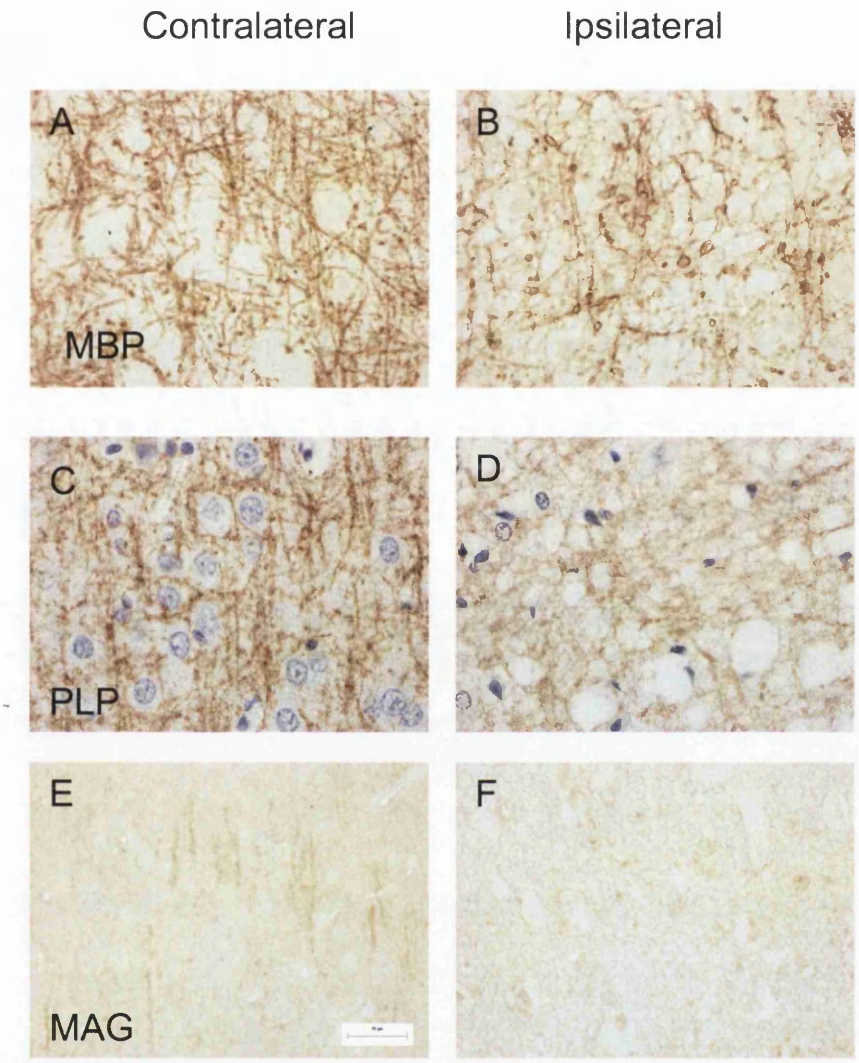

Figure 3.18 Immunostaining of myelin proteins in the cerebral cortex following 3 hours of focal cerebral ischaemia and 21 hours of reperfusion

Representative images from the cerebral cortex in the hemisphere contralateral to the MCA occlusion in MBP (A), PLP (C) and MAG (E) immunostained sections. In the cortex ipsilateral to the MCA occlusion, there was a disruption of the pattern of MBP (B) and PLP (D) and MAG (F) immunostaining. PLP immunostained sections have been counterstained with haematoxylin

Scale bar = 25μm.

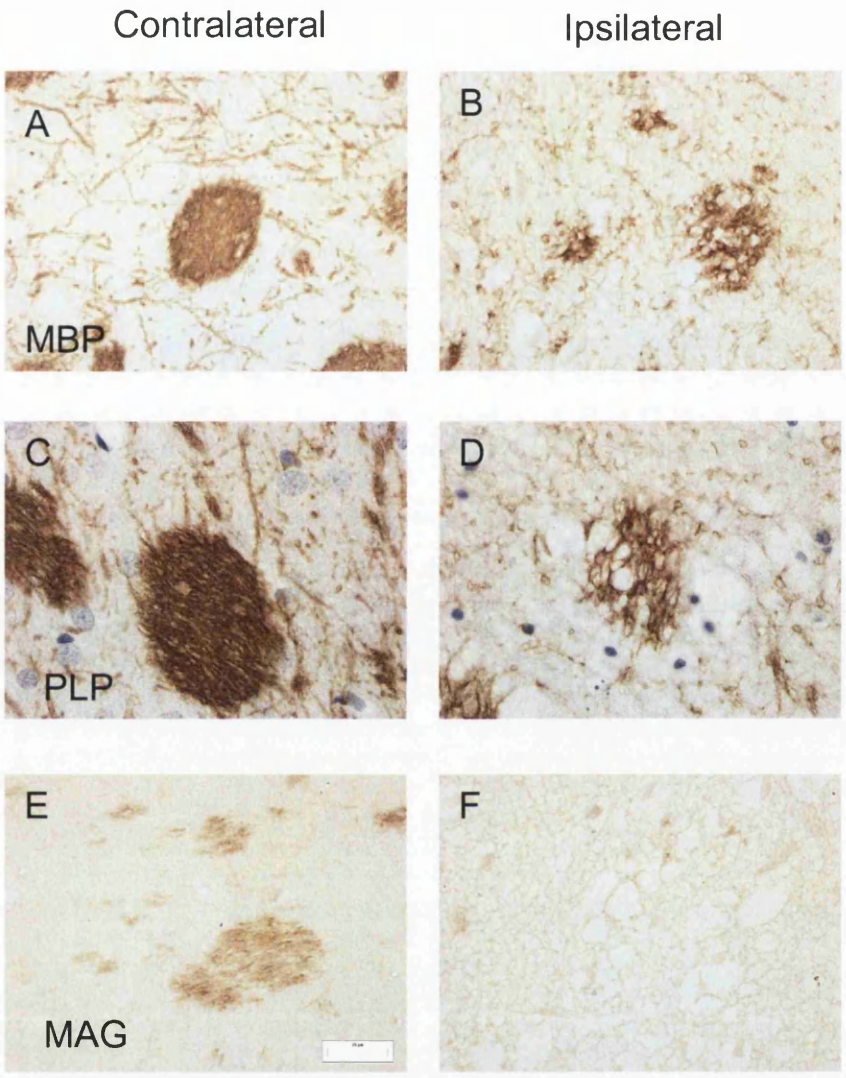

Figure 3.19 Immunostaining of myelin proteins in the caudate nucleus following 3 hours of focal cerebral ischaemia and 21 hours of reperfusion

Representative images from the caudate nucleus in the hemisphere contralateral to the MCA occlusion in MBP (A), PLP (C) and MAG (E) immunostained sections. In the caudate nucleus ipsilateral to the MCA occlusion, there was a disruption of the pattern of MBP (B) and PLP (D) immunostaining, and a loss of MAG immunostaining (F). PLP immunostained sections have been counterstained with haematoxylin.

Scale bar = 25μm.

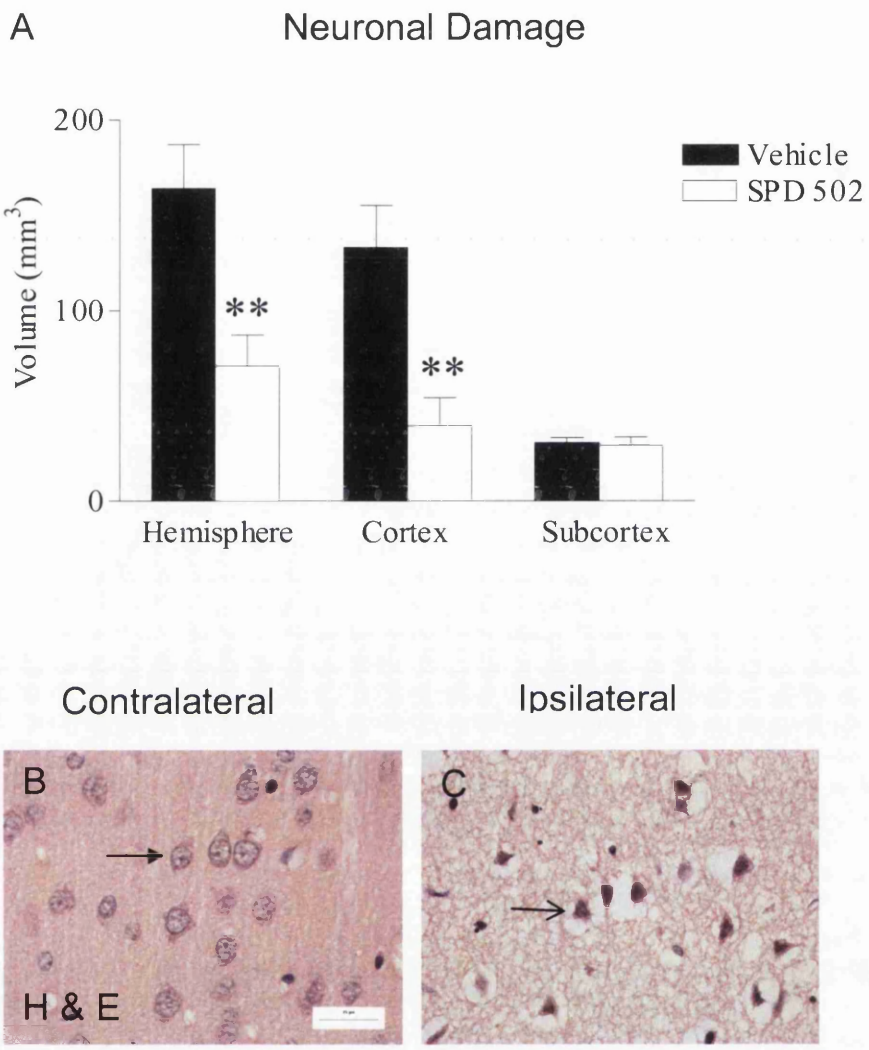

Figure 3.20 Effects of SPD 502 on neuronal damage following 3 hours of focal cerebral ischaemia and 21 hours of reperfusion

A. Neuronal Damage. Data are expressed mean ± SEM. Vehicle, n=8; SPD 502 n=7. **P<0.01, two-tailed Students *t*-test

B. Representative images illustrating morphologically normal neurons (closed arrow head) in the hemisphere contralateral to the occluded MCA

C. Ischaemic neurons (open arrow head) in the hemisphere ipsilateral to the occluded MCA.

Scale bar – 25μm

(data presented in McCracken et al, 2002).

3.4 Discussion

In the present study, it was demonstrated that intracerebral injection of AMPA causes damage to the cytoskeleton of axons *in vivo*. The AMPA-induced axonal damage was attenuated with systemic administration of an AMPA-receptor antagonist, SPD 502, suggesting that AMPA receptor-mediated mechanisms cause axonal damage. Furthermore, intracerebral injection of AMPA also induced oligodendrocyte, myelin, and neuronal perikaryal damage *in vivo*. Myelinated axons and oligodendrocytes contained within grey matter of the cortex are also vulnerable to AMPA mediated toxicity. These data indicate the importance of AMPA receptor-mediated mechanisms in causing damage to multiple cellular elements. The AMPA receptor antagonist SPD 502 significantly reduced the amount of axonal and neuronal damage following focal cerebral ischaemia, suggesting that AMPA receptor antagonism has the potential to salvage the cellular components of white and grey matter.

AMPA causes cytoskeletal disruption in axons

Excitotoxic lesions were thought historically to cause "axon sparing" lesions (Simson *et al.*, 1977). This view reflects an era when damage was evaluated using conventional histological staining. The more sensitive immunocytochemical methods used in this study reveal that intracerebral injection of AMPA causes damage to microtubules and neurofilaments, cytoskeletal components of the axon. Application of kainate, an agonist of both AMPA and kainate subtypes of glutamate receptor, onto the rabbit optic nerve *in vivo* also causes damage to the axonal cytoskeleton, evident as axonal swellings, and disrupted neurofilaments (Matute, 1998).

AMPA-induced oligodendrocyte damage - significance of increased Tau-1 immunoreactivity

Oligodendrocyte pathology, demonstrated by increased Tau-1 immunoreactivity in oligodendrocytes within the cortex, was observed following intracerebral injection of AMPA in this model. However, tau positive-oligodendrocytes were not observed within the external capsule at the injection site of these animals. The reasons for this discrepancy between the responses of the oligodendrocytes in the cortex and external capsule are unknown. Whilst increased immunoreactivity of tau in oligodendrocytes has been demonstrated as a sensitive marker of oligodendrocyte damage following intracortical perfusion of glutamate (Irving *et al.*, 1996a), experimental focal cerebral

ischaemia (Dewar and Dawson, 1995; Irving *et al.,* 1997; Valeriani *et al.,* 2000) and human stroke or head injury (Irving *et al.,* 1996b), at present it remains unclear if this is indicative of a restorative, protective function, or if it signifies oligodendroglial degeneration. If tau positive-oligodendrocytes were involved in a protective response, oligodendrocytes near the injection site may be too severely injured for this response to occur. In support of this, intracerebral injection of AMPA (20nmol) has previously been shown to reduce the amount of Rip-positive oligodendrocytes by 60% (McDonald *et al.,* 1998a), suggesting oligodendroglial death in this region. This hypothesis is also supported by the demonstration that tau-positive oligodendrocytes were not double labelled with a marker of DNA fragmentation. In addition, the lack of tau-positive oligodendrocytes in the external capsule may also reflect the temporal progression of pathology, and it remains possible that tau positive oligodendrocytes may have been present in the external capsule at earlier time points than 24 hours. However, this discrepancy may also be explained by differences in intrinsic properties of oligodendrocytes in these diverse environments. For example, they may contain different AMPA receptor subunit compositions, and oligodendrocytes within grey matter in the cortex may also react differently to excitotoxins when compared to those in the white matter (Jamin *et al.*, 2001).

Mechanisms of AMPA-induced axonal damage – involvement of oligodendrocytes and the myelin sheath

At present, there is no evidence that functional AMPA receptors are located on axonal cylinders therefore it seems unlikely that AMPA is directly toxic to axons. Instead, axonal pathology is likely to result from actions occurring at the AMPA receptors located on the myelin sheath and/or the oligodendrocyte. Axonal dysfunction caused by application of AMPA or glutamate onto isolated spinal cord preparations *in vitro* is thought to be mediated through Ca^{2+} permeable GluR4 subunits localised in the myelin sheath (Li & Stys, 2000). In the present study we also demonstrate that AMPA causes myelin and oligodendrocyte pathology *in vivo*. Previous studies have also shown that intracerebral injection of AMPA into a similar anatomical area causes oligodendrocyte damage *in vivo* (McDonald *et al.,* 1998a).

It is currently unclear how AMPA receptor-mediated excitotoxicity at the myelin sheath and oligodendrocyte results in axonal damage. The integrity of myelinated

axons is dependent on their stable interactions with oligodendroglia and myelin sheaths, and disruption of these interactions is associated with axonal damage. This is illustrated by the high prevalence of axonal damage associated with myelin disorders (Bjartmar *et al.,* 1999). For example, over-expression or lack of expression of MAG or PLP in the myelin sheath causes axonal damage in humans (PLP, Garbern *et al.*, 2002) and rodents (Griffiths *et al.*, 1998; Yin *et al.,* 1998). Similarly, axonal damage is prevalent in multiple sclerosis and Charcot Marie Tooth disease (Dyck *et al.,* 1989; Ferguson *et al.,* 1997; Trapp *et al.,* 1998; Hanemann *et al.,* 2001; Stefano *et al.,* 2001). Disruptions in the cytoskeleton of mice containing mutant PMP 22 (trembler) or MBP deficiency further reinforce the constant influence that myelinating glial have over axonal integrity (deWaugh *et al.,* 1992; Brady *et al.,* 1999; Kirkpatrick *et al.,* 2001). AMPA receptor-mediated damage to the oligodendrocyte and myelin could therefore impact on the structural integrity of the axon cylinder.

In support of this, studies have recently been performed in an *in vitro* Campenot chamber, where axons can be separated from oligodendrocytes, allowing axonal-oligodendroglial relationships to be examined. Axons cultured in the absence of oligodendrocytes are not damaged by exposure to kainate, whereas axons co-cultured with oligodendrocytes are damaged by kainate (Underhill *et al.,* 2001; 2002a). These *in vitro* data suggest axonal damage is mediated through over-activation of AMPA receptors on oligodendrocytes. This may be caused by the diffusion of toxic substances released as a consequence of oligodendroglial excitotoxicity. For example, oligodendrocyte progenitors have been shown to produce free radicals following exposure to AMPA (Liu *et al.,* 2002), and free radical-mediated mechanisms are known to cause axonal damage *in vivo* (McCracken *et al.*, 2000, 2001). A recent study has suggested that AMPA-induced axonal damage is mediated by free radical mediated mechanisms arsing at the oligodendrocyte, which can be blocked with catalase, which breaks down H_2O_2 (Underhill *et al.,* 2002b). Oligodendrocytes also express inducible nitric oxide in pathological situations (Merrill *et al.,* 1997; Gahm *et al.,* 2002;) and by-products of nitric oxide, such as peroxynitrite, also cause axonal damage *in vivo* and *in vitro* (Smith *et al.,* 2001; Touil *et al.,* 2001; Garthwaite *et al.,* 2002).

Mechanisms of AMPA-induced axonal damage – involvement of the neuronal cell body and NMDA receptor mediated mechanisms

In addition to AMPA-receptor mediated axonal damage in the external capsule, axonal damage in the overlying cortex was also demonstrated. Neuronal damage was also present in the cortex; therefore the possibility that axonal damage is secondary to neuronal perikaryal damage cannot be excluded. This could occur by diffusion of toxic substances from neurons, or by axonal degeneration resulting from damage to the perikarya. However, the protective effect of AMPA receptor blockade on axons following oxygen/glucose deprivation *in situ* was not an indirect consequence of neuronal perikarya protection, as no concomitant protective effect on neuronal perikarya was demonstrated (Baltan Tekkok and Goldberg, 2001). Instead, the protection of axons was likely to reflect the local protection of cellular elements in white matter tracts (Baltan Tekkok and Goldberg, 2001). Myelin damage induced by kainic acid is detected prior to neuronal perikaryal damage, suggesting that the pathological processes at these two sub cellular sites occur independently (Hopkins *et al.*, 2000). Thus, it would appear unlikely that the AMPA-induced axonal damage observed in the present study is a consequence of neuronal cell body damage in the overlying cortex. Time course studies may establish if axonal and neuronal perikaryal damage occur as independent events.

Another possibility is that AMPA may have induced secondary NMDA receptor excitotoxicity. However, it was demonstrated in the current study that co-injection of AMPA with the NMDA receptor antagonist MK-801 did not significantly reduce the amount of axonal damage. Similarly, co-injection of AMPA (20nmol) with MK-801 (5nmol) did not reduce the amount of oligodendroglial loss in the external capsule (McDonald *et al.*, 1998a). Intracerebral injection of NMDA does not induce oligodendrocyte death (McDonald *et al.*, 1998a), and NMDA receptor antagonism does not reduce axonal or oligodendrocyte damage after cerebral ischaemia (Irving *et al.*, 1997; Yam *et al.*, 2000). Therefore, it seems unlikely that NMDA receptor-mediated mechanisms contribute to AMPA-induced axonal damage.

AMPA receptor blockade with SPD 502 protects axons and oligodendrocytes from focal cerebral ischaemia in vivo

The *in vivo* AMPA toxicity studies indicated that AMPA induces damage to the cellular components of both white and grey matter *in vivo*. The *in vivo* cerebral ischaemia study therefore provided 'proof of concept' that AMPA receptor antagonism can protect against grey *and* white matter damage. In addition to the protection of axons and neurons, SPD 502 also significantly reduced the anatomic extent of ischaemically-damaged oligodendrocytes, determined by Tau-1 immunoreactivity (McCracken *et al.*, 2002). The protective effect of AMPA blockade was demonstrated in the cerebral cortex, however axons and neurons were not protected in the deep subcortical areas, where the reduction in cerebral blood flow is most pronounced (Komjati *et al.*, 2001). The protective effect of AMPA blockade on oligodendrocyte pathology was also significant in the cortex but minimal in subcortical areas (McCracken *et al.*, 2001).

Interestingly, the anatomical distribution of damaged neurons and axons labelled with APP or NF 200 immunostaining were comparatively different following focal cerebral ischaemia (see Fig. 3.14 and 3.15). APP immunoreactive axons were the least anatomically widespread, and usually located at the boundary of the lesion. This is perhaps expected, considering that the accumulation of APP is dependent on normal axon function and energy dependent axonal transport. In contrast, areas of damaged axons visible in NF 200 immunostained sections were anatomically more extensive, and coincidental with neuronal damage. In addition, swollen axons were also evident in NF 200 immunostained sections in anatomical areas where neurons appeared morphologically normal, particularly the thalamus. The lack of APP immunopositive axons in these areas highlights the sensitivity of NF 200 immunostaining, and emphasises the need for multiple markers for the evaluation of axonal damage. Similar findings have been reported using APP and NF 200 immunohistochemistry in another model of focal cerebral ischaemia (Bingham *et al.*, 2003). Sherriff and colleagues (1994a) carried out a comparison of the sensitivity of APP and NF 68 immunohistochemistry on post mortem head injured patients, and concluded that APP immunostaining was the most sensitive marker of damaged axons. However, only one anatomical area was examined in this study (corpus callosum) in contrast to the many areas examined in the current study. In addition, the heavy chain component of

neurofilament examined in the current study may be a more sensitive marker than NF 68. It is unclear if the presence of swollen axons in areas such as the thalamus, which contained morphologically normal neurons, signifies reversible or irreversible axonal damage. It is possible that they may be mildly swollen and damaged, but that this may be resolved beyond 24 hours. Time course studies would be useful to further examine this phenomenon. If they do represent irreversibly damaged axons, two possibilities exist. They may signify axons degenerating as a result of neuronal perikaryal damage, for instance cortico-thalamic fibres degenerating as a consequence of neuronal perikaryal damage in the overlying cortex.

Mechanisms of AMPA induced excitotoxicity in vivo

The current study, combined with *in vitro* and *in situ* experiments, which have shown that AMPA receptor antagonism can protect axons and oligodendrocytes from oxygen and/or glucose deprivation, provide compelling evidence for the role of AMPA-mediated mechanisms in causing white matter ischaemic damage. However, one question remains – what is the endogenous source of glutamate that causes white matter excitotoxicity in the absence of neuronal glutamatergic synapses? Stys and colleagues have examined this phenomenon in isolated white matter preparations devoid of neuronal cell bodies. Exposing dorsal column segments to anoxia or trauma, they demonstrated a loss of axonal function, which could be attenuated with AMPA receptor antagonists (Li *et al.*, 1999). However, inhibitors of Na^+-dependent glutamate transport also attenuated the axonal pathology, and prevented the depletion of cytosolic glutamate from axon cylinders and oligodendrocytes (Li *et al.*, 1999). Therefore, it seems likely that under anoxic conditions, ionic imbalances may result in reverse operation of the Na^+ dependent glutamate transporter that could cause elevated levels of glutamate within white matter (Stys, 1998; Li *et al.*, 1999). This hypothesis is consistent with the presence of glutamate transporters within white matter (Li *et al.*, 1999). A diagrammatic representation of mechanisms of white matter damage during ischaemic conditions is presented in figure 3.21.

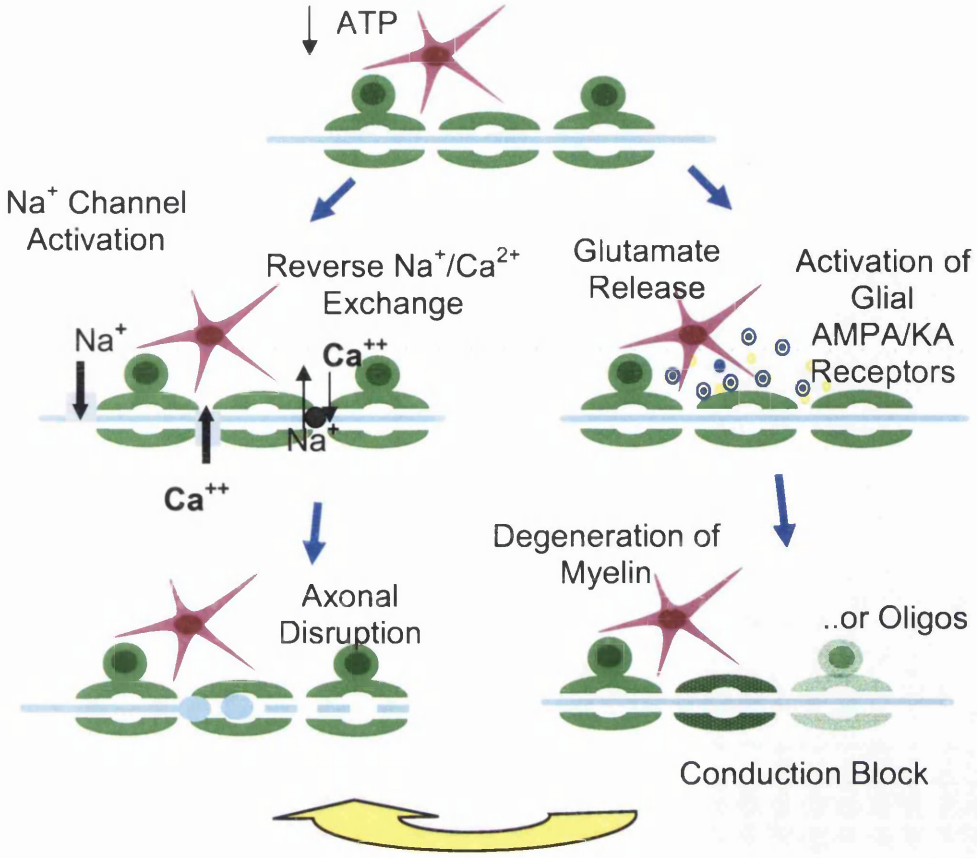

Figure 3.21 Hypothesised mechanisms of hypoxic-ischaemic white matter damage

Disruption of energy supplies results in a depletion of ATP, which causes ionic imbalances due to malfunctioning of the Na^+/K^+-ATPase. This results in Na^+ influx through activation of Na^+ channels, and Ca^{2+} influx through voltage sensitive Ca^{2+} channels and reversal of Na^+/Ca^{2+} exchange. This results in axonal malfunctioning, swelling and the activation of Ca^{2+} mediated destruction. In addition, the ionic imbalances can lead to release of glutamate through reversal of Na^+-dependent glutamate transporters. This can cause excitotoxicity at the myelin sheath and oligodendrocyte, which results in axonal dysfunction.

From Baltan Tekkok and Goldberg (2001).

The data presented in this chapter provide compelling evidence that AMPA receptor mediated mechanisms cause white matter damage. The next chapter describes the characterisation of an *in vivo* model of AMPA-induced axonal damage in mice. This was a prerequisite for the studies investigating the effects of AMPA –induced axonal damage in transgenic mice, which are described in chapter 5.

CHAPTER 4

ESTABLISHING A MOUSE MODEL OF AMPA RECEPTOR-MEDIATED EXCITOTOXICITY & COMPARISON WITH MALONATE-INDUCED PATHOLOGY IN THE MOUSE

4.1 Introduction

The myelin sheath is interspersed with proteins that have an integral role in myelin formation and maintenance. Proteolipid protein (PLP) and myelin basic protein (MBP) are the two major protein components of CNS myelin. In addition to supporting the architecture of the myelin sheath, these proteins have an integral role in glial-axonal interactions. Evidence supporting this came from the discovery of axonal abnormalities in transgenic mice that are deficient in PLP or MBP, which will be described in more detail in chapter 5. *Plp* gene knockout mice and MBP deficient mice (*shiverer* mice) are currently under investigation at the Glasgow University Vet School campus, by a group led by Professor Ian Griffiths. The abnormal glial-axonal relationships that PLP and MBP deficient mice contain provide a useful model to examine the role of oligodendrocytes and myelin in AMPA-induced axonal damage. It may also be possible that the degeneration exhibited by these mice may arise from 'secondary' excitotoxicity. Therefore, investigations were undertaken to determine if *Plp* gene knockout and *shiverer* mice exhibit altered sensitivity to AMPA-induced axonal damage compared with wild type mice. These studies will be described in chapter 5. Preceding these investigations however, a model of AMPA induced axonal pathology was characterised in the mouse (C57/BLJ), and this work will be described in detail in the current chapter.

At the same time that the mouse model of AMPA-mediated axonal damage was established, Mr Dan Cuthill carried out contemporaneous studies in this department to establish a mouse model of malonate-mediated energy failure. Malonate competitively inhibits succinate dehydrogenase (SDH), a mitochondrial enzyme that plays a central role in energy metabolism. Energy failure due to mitochondrial dysfunction contributes to the pathology observed following cerebral ischaemia and head injury, and may also contribute to the pathogenesis of chronic neurodegenerative diseases (Fiskum *et al.*, 1999). Irreversible inhibition of SDH with the plant myotoxin 3-Nitropropionic acid produces striatal neuronal damage (Ludolph *et al.*, 1991; Beal *et al.*, 1993a) and axonal damage, assessed with APP immunohistochemistry (McCracken *et al.*, 2001). Infusion of malonate into the caudate nucleus of rats also produces neuronal damage (Beal *et al.*, 1993b; Greene *et al.*, 1993) and accumulation of APP in damaged axons at the boundary of the lesion (Dewar *et al.*, 2000).

4.1.1 Aims of study

The primary aim of this study was to establish an *in vivo* mouse model of AMPA receptor mediated axonal and neuronal damage. The effects of intrastriatal injection of malonate on axonal and neuronal damage were also evaluated and compared with AMPA-induced damage. As interesting discrepancies were observed in the pattern of pathology observed in AMPA and malonate injected animals, the acute effects of either toxin on cerebral glucose utilisation were examined 1 hour post-injection.

4.2 Methods

4.2.1 Stereotaxic Surgery

Adult C57/BLJ (23-33g) mice received stereotaxic injection of AMPA (1.5nmol, n=5; 3nmol, n=6 or 6nmol, n=5) or vehicle (10 mM PBS, pH 7.4, n=5); and malonate (0.34μmol, n=5; 0.68μmol, n=5 or 1.35μmol, n=5) or vehicle (10 mM PBS, pH 7.4, n=5) into the caudate nucleus as outlined in section 2.3.1. Mr Daniel Cuthill performed all the stereotaxic injections of malonate in the pathology experiment. Twenty-four hours later, animals were perfused transcardially with saline (0.9%) then paraformaldehyde (4%); post-fixed, processed and paraffin embedded (section 2.3.2).

4.2.2 Histology and Immunocytochemistry

Sixteen sections (6μm) from every forty sections cut were retained on poly-L-lysine slides (2 sections per slide) for histology and immunostaining. One slide from each cycle was stained with H & E to examine neuronal perikaryal damage (section 2.6.1), and adjacent sections were immunostained using antibodies raised against NF 200 and APP to examine axonal pathology (section 2.5.5). Mr Daniel Cuthill performed all histological and immunostaining procedures for malonate-injected brains. All malonate-lesioned brains were quantified by Mr Daniel Cuthill, while I performed the analysis of the AMPA-lesioned brains. Inter-rater variability was assessed in eight animals from each group (See appendix 4). Quantification of axonal and neuronal damage is outlined in section 2.5.9 and 2.6.4. In addition to the focal area of neuronal and axonal damage induced by AMPA, widespread damage was also

observed, for instance in various thalamic nuclei in the hemisphere ipsilateral and contralateral to the injection site. This widespread damage, which could clearly be differentiated from the focal damage caused by AMPA, was not included in the volumetric quantification of damage. The rostral and caudal limit for integration of the lesion induced by AMPA were 2.8mm and -4.26mm respectively from Bregma. The rostral and caudal limit for integration of the lesion induced by malonate were 1.98mm and –1.58mm respectively from Bregma.

4.2.3 *In vivo* ^{14}C-2-deoxyglucose autoradiography

To further characterise the acute affects of intrastriatal injection of AMPA or malonate, the effects of these toxins on glucose utilisation were investigated one hour post-injection. The protocol for stereotaxic injection of AMPA, malonate or vehicle followed by ^{14}C-2-deoxyglucose autoradiography is illustrated in figure 4.1. Fifteen C57/BLJ (26-32g) were anaesthetised and received stereotaxic injection of AMPA (6nmol, n=5), malonate (1.35μmol, n=5), or vehicle (PBS, 10mM, pH, 7.4, n=5) into the caudate nucleus as previously described (section 2.3.1). Each animal was then administered ^{14}C-2deoxygucose as described in section 2.7.5. The subsequent ^{14}C-2-deoxyglucose protocol is described in section 2.7.5 and 2.7.6. Levels of ^{14}C were calculated in 17 brain areas, in both the hemispheres ipsilateral and contralateral to the injected caudate nucleus. Local cerebral glucose utilisation was estimated as the ratio of ^{14}C in the region of interest to that in the hypothalamus. The hypothalamus was chosen as reference region as it has few direct afferent and efferent connections with the injection site. To validate the use of the hypothalamus as a reference area, the relationship between ^{14}C in this region with plasma ^{14}C and plasma glucose was examined.

4.2.4 Statistical analysis

To determine if there was any significant difference between AMPA (1.5, 3 and 6nmol) and vehicle treated animals, one-way analysis of variance was used with *post hoc* Student's *t* test and Bonferonni corrections for multiple comparisons. To determine if AMPA (6nmol) induced altered levels of glucose utilisation in the hemisphere ipsilateral and contralateral to the injected caudate, two-tailed, paired Student's *t* test was used.

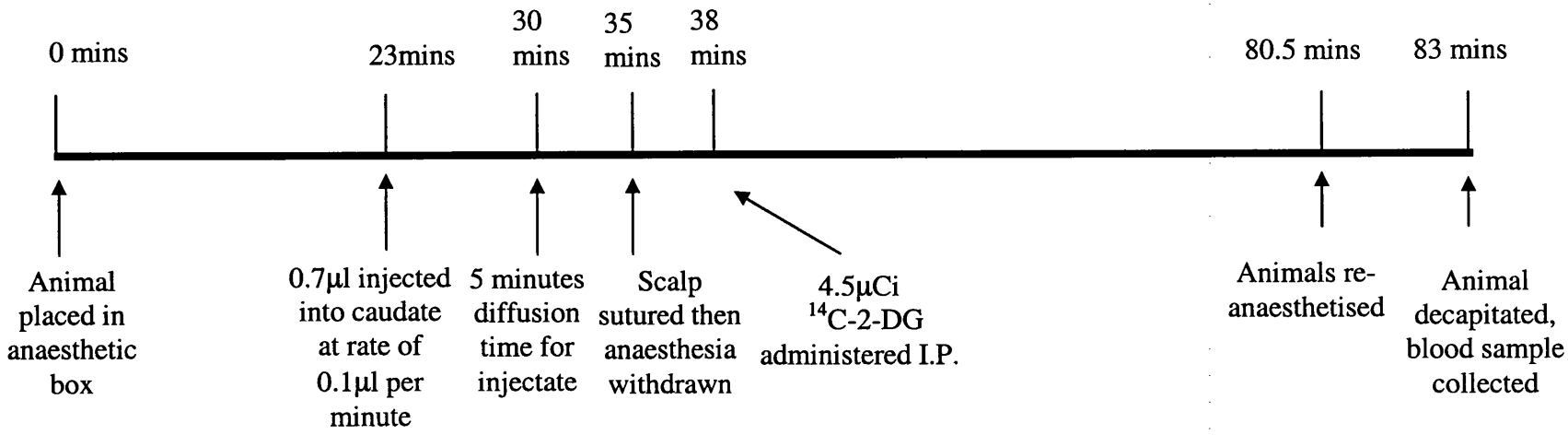

Figure 4.1 Protocol for stereotaxic injection and ^{14}C-2-deoxglucose administration

Mice were anaesthetised and then injected with 0.7μl of AMPA (6nmol), malonate (1.34μmol) or vehicle (PBS) into the caudate nucleus, followed by an intraperitoneal injection of ^{14}C-deoxglucose, according to the protocol above.

4.3 Results

4.3.1 AMPA-induced axonal damage assessed in NF 200 immunostained sections

Injection Site

In the caudate nucleus and overlying external capsule contralateral to the injection site, NF 200 immunostained axons within white matter tracts appeared uniform and organised, and individual axons in the overlying cortex ran in organised networks (Fig. 4.2A, C, E). The caudate nucleus of animals that received injection of AMPA contained a rougher, disrupted pattern of immunostaining. Disrupted, severely swollen axons were evident in the centre of the lesion (Fig. 4.2B), whereas the surrounding areas contained vacuolated, disrupted white matter tracts with less severely swollen axons (Fig. 4.2D). A disorganised pattern of immunostaining was also observed in the overlying cortex (Fig. 4.2F) and external capsule, where bulbous like axonal profiles were evident. Increasing AMPA dosage caused axonal damage in an anatomically more extensive area of caudate and cortex (Fig. 4.4B-D). Animals that received intrastriatal injection of vehicle exhibited minimal axonal damage, mainly confined to a small area immediately adjacent to the needle tract in the caudate nucleus and overlying external capsule and cortex (Fig. 4.4A).

Distant Brain Areas

Disrupted, swollen axons immunostained with NF 200 were also observed in the globus pallidus, internal capsule and substantia nigra (Fig. 4.3) following intrastriatal injection of AMPA. In the volumetric analysis of axonal damage, the damage in these areas could not be differentiated from the local damage caused by AMPA in the caudate; therefore they were included in the quantification. Quantification of axonal damage in NF 200 immunostained sections revealed that AMPA caused a dose dependent increase in axonal damage compared to injection of vehicle (Fig. 4.4E). AMPA also induced scattered axonal damage in several thalamic nuclei that were distant from the focal lesion, in the hemispheres ipsilateral and contralateral to the injection site. These areas were not included in the volumetric quantification of axonal damage because of their diffuse nature. There was an increased frequency of axonal damage in these distant brain areas with increasing AMPA dosage (Table 4.1). Contralateral axonal damage in the caudate nucleus, globus pallidus, internal capsule or substantia nigra was not observed.

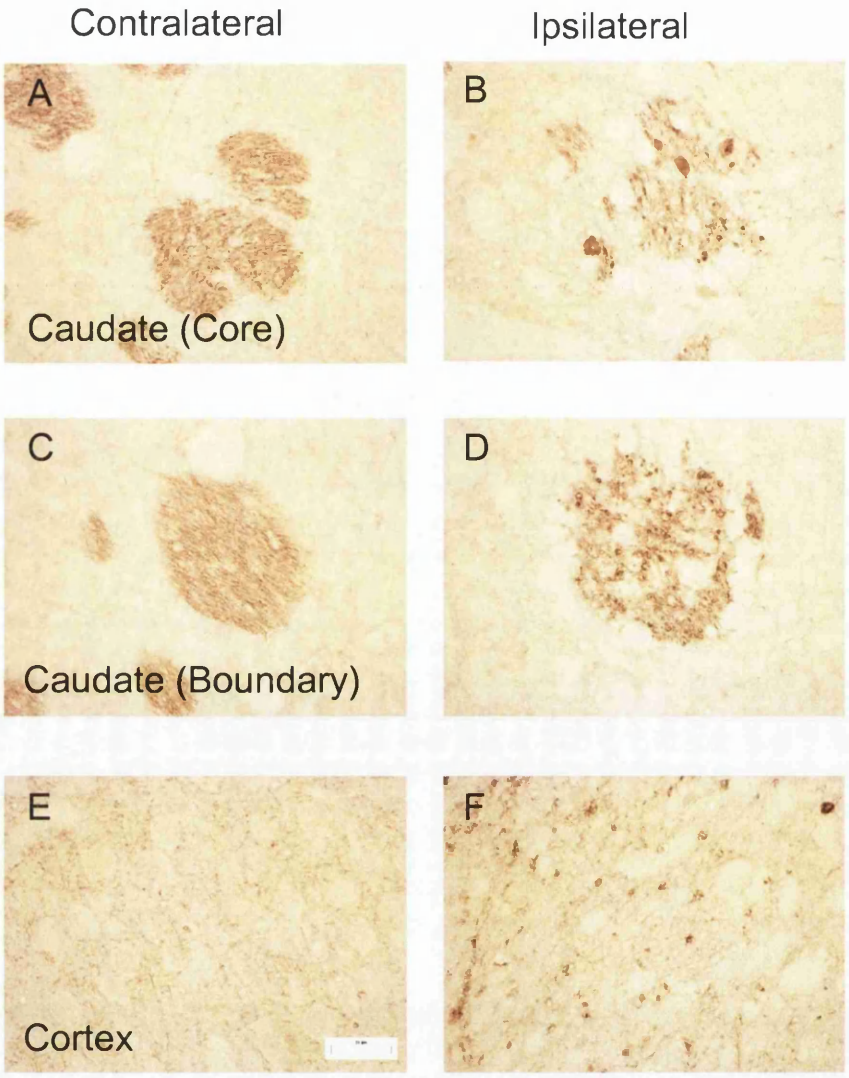

Figure 4.2 NF 200 immunostaining in the caudate nucleus and cortex following intrastriatal injection of AMPA (6nmol)

In the caudate nucleus and cerebral cortex contralateral to the injection site, axons ran in a smooth, organised profile (A, C, E). Axonal swellings and a disrupted pattern of immunostaining were evident in the core (B) and boundary of the lesion (D) in the caudate nucleus, and the overlying cerebral cortex (F). Scale bar = 25μm.

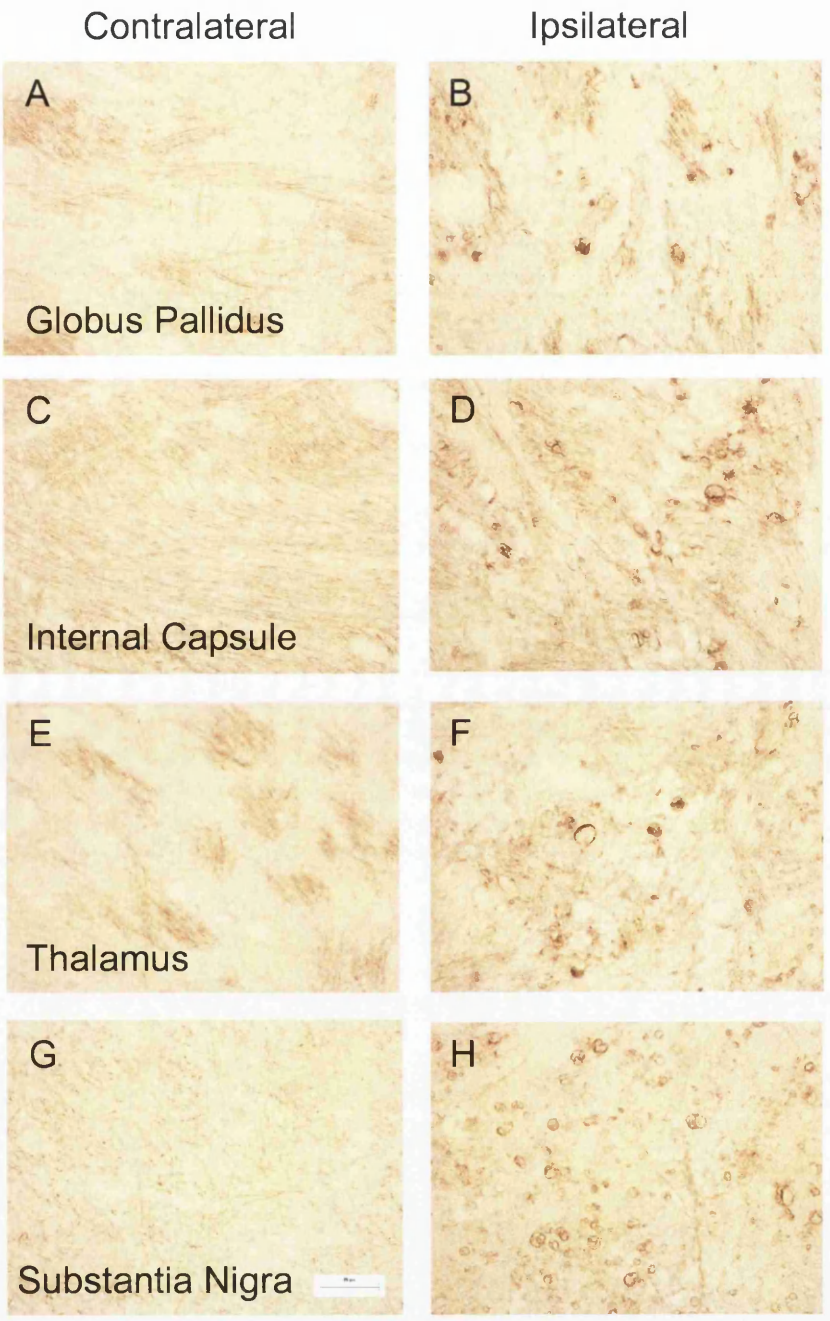

Figure 4.3 NF 200 immunostaining in extrastriatal brain areas following intrastriatal injection of AMPA (6nmol)

In the globus pallidus, internal capsule, thalamus and substantia nigra contralateral to the injection site of this animal, axons ran in a smooth, organised profile (A, C, E, F). Axonal swellings were evident in these areas in the hemisphere ipsilateral to the injection site (B, D, F, H).

Scale bar = 25μm.

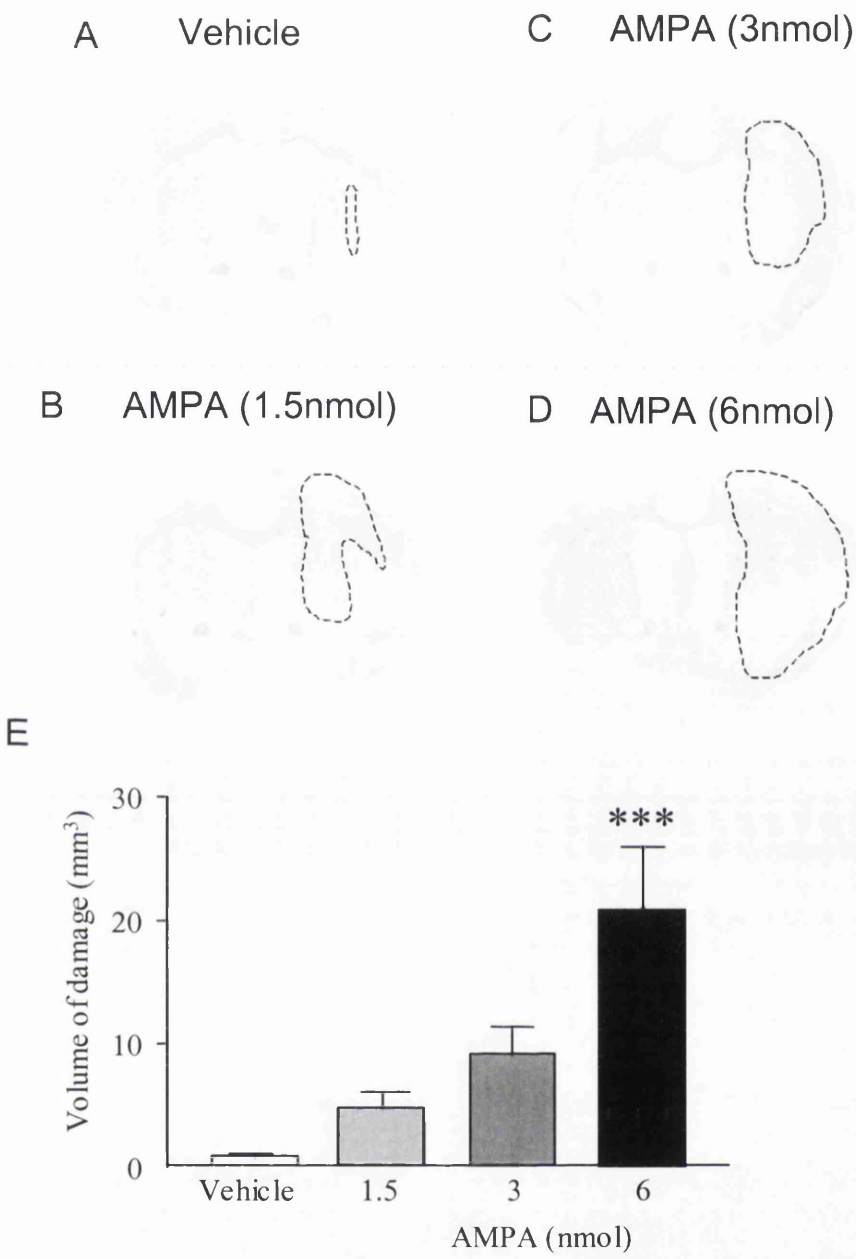

Figure 4.4 Axonal damage assessed in NF 200 immunostained sections following intrastriatal injection of AMPA

Digitised NF 200 immunostained sections (A-D), demonstrating the anatomical extent of axonal damage following stereotaxic injection of Vehicle (PBS) or AMPA (1.5-6nmol). The area of disrupted immunostaining is contained within the dashed line. Quantification of the volume of axonal damage in NF 200 immunostained sections. One way ANOVA followed by Student's *t* test with Bonferonni correction). ***P<0.001 for comparison with vehicle treated group. Vehicle, n=5; AMPA (1.5nmol), n=5; AMPA (3nmol), n=6; AMPA (6nmol), n=5.

Anatomical Area		AMPA		
	Vehicle	1.5nmol	3nmol	6nmol
Globus Pallidus (ipsilateral)	1 of 5	3 of 5	6 of 6	5 of 5
Internal Capsule (ipsilateral)	1 of 5	3 of 5	6 of 6	5 of 5
Thalamus (ipsilateral)	0 of 5	1 of 5	4 of 6	5 of 5
Thalamus (contralateral)	0 of 5	0 of 5	1 of 6	3 of 5
Substantia Nigra	1 of 5	3 of 5	6 of 6	5 of 5

Table 4.1 The incidence of damaged axons assessed in NF 200 immunostained sections in 4 brain areas following intrastriatal injection of AMPA

4.3.2 AMPA-induced axonal damage assessed in APP immunostained sections

Injection Site

In the hemisphere contralateral to the injection site, APP immunoreactivity was present at a low, diffuse level. Intracerebral injection of AMPA caused increased APP immunoreactivity in swollen axons (Fig. 4.5). However, this was confined to a small area in the caudate nucleus and external capsule adjacent to the needle tract, in a similar pattern to vehicle treated animals (Fig. 4.7). APP immunoreactive axons were rarely observed in the overlying cortex of any animal. This contrasted with the pattern of axonal disruption and swellings evident in NF 200 immunostained sections (Fig. 4.4).

Distant Brain Areas

Increasing AMPA dosage did not increase the anatomical extent of APP immunoreactive axons (Fig. 4.6, 4.7). Occasionally, small APP immunoreactive swellings were observed in the globus pallidus, internal capsule, thalamus, and substantia nigra following injection of AMPA. These were rarely present, and contrasted starkly with number of swellings evident in the same areas of NF 200 immunostained sections. These intermittent, distant APP immunoreactive axons were not included in the volumetric analysis of axonal damage in APP immunostained sections. Quantification of the volume of tissue containing damaged axons in APP immunostained sections demonstrated that there was no significant difference between AMPA and vehicle treated animals (Fig. 4.7E).

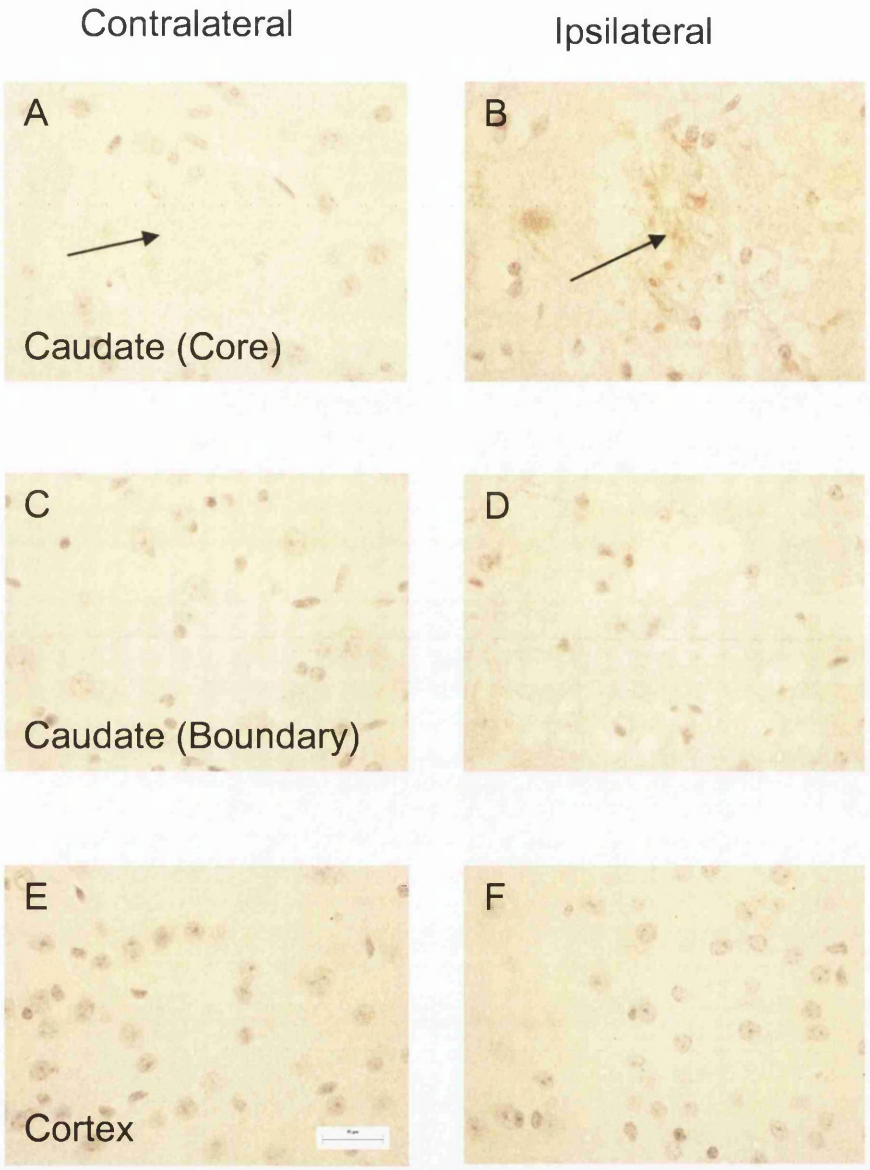

Figure 4.5 APP immunostaining in the caudate nucleus and cortex following intrastriatal injection of AMPA (6nmol)

In the caudate nucleus and cerebral cortex contralateral to the injection site, APP immunoreactivity was present at a low, diffuse level (A, C, E). APP immunoreactive swollen axons were present at the centre of the lesion in the caudate, (B) but not in the boundary of the lesion (D) in the caudate nucleus, or the overlying cortex (F). The arrows in (A) and (B) indicate white matter tracts in the caudate nucleus. All sections were counterstained with haematoxylin. Scale bar = 25μm.

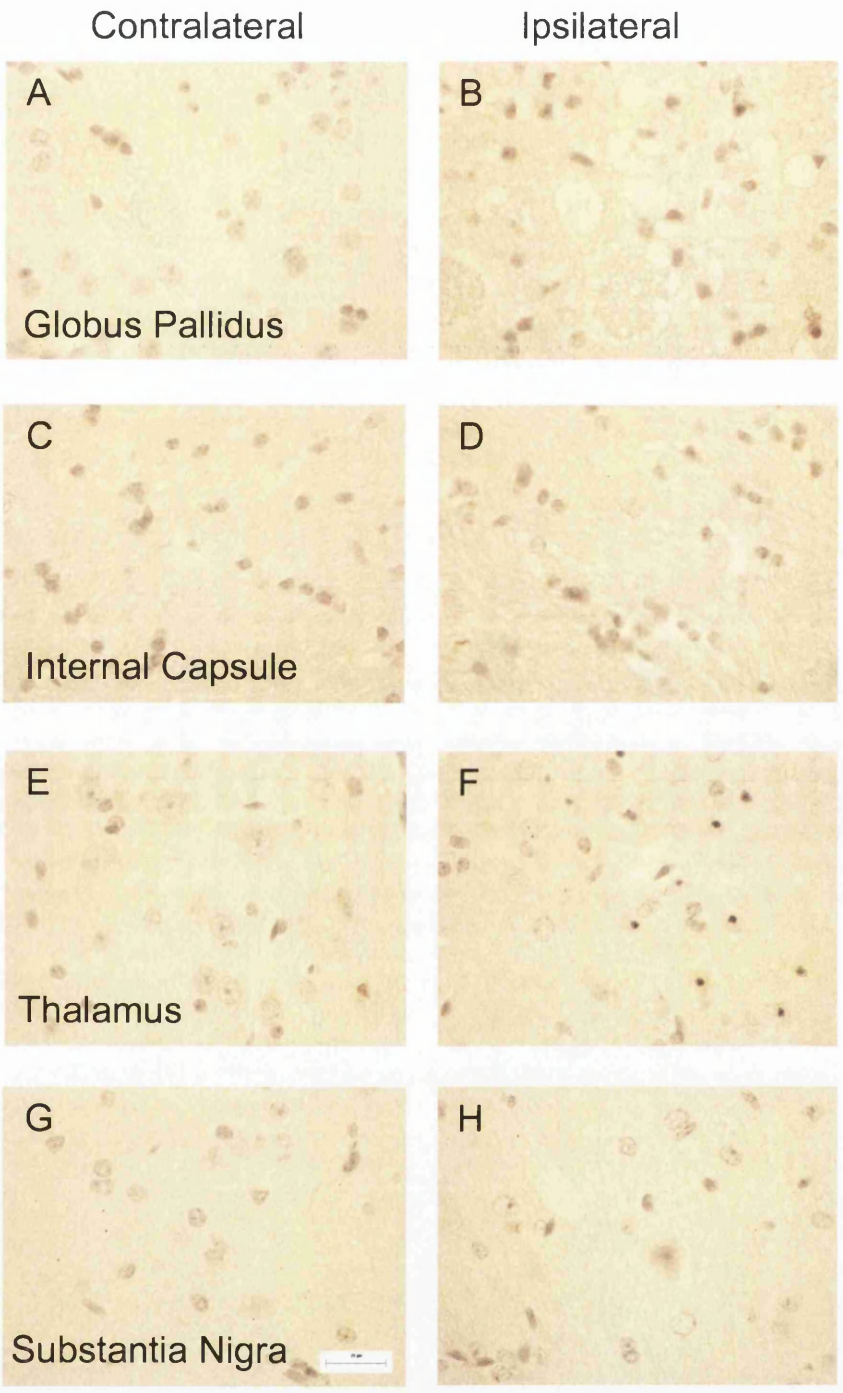

Figure 4.6 APP immunostaining in 4 brain areas following intrastriatal injection of AMPA (6nmol)

In the globus pallidus, internal capsule, thalamus and substantia nigra contralateral to the injection site, APP immunoreactivity was present at a low, diffuse level (A, C, E, G respectively). APP immunoreactive axons were rarely present in these structures in the hemisphere ipsilateral to the injection (B, D, F, H), in contrast to the changes observed in NF 200 immunostained sections (Fig 4.3). All sections were counterstained with haematoxylin

Scale bar = 25μm.

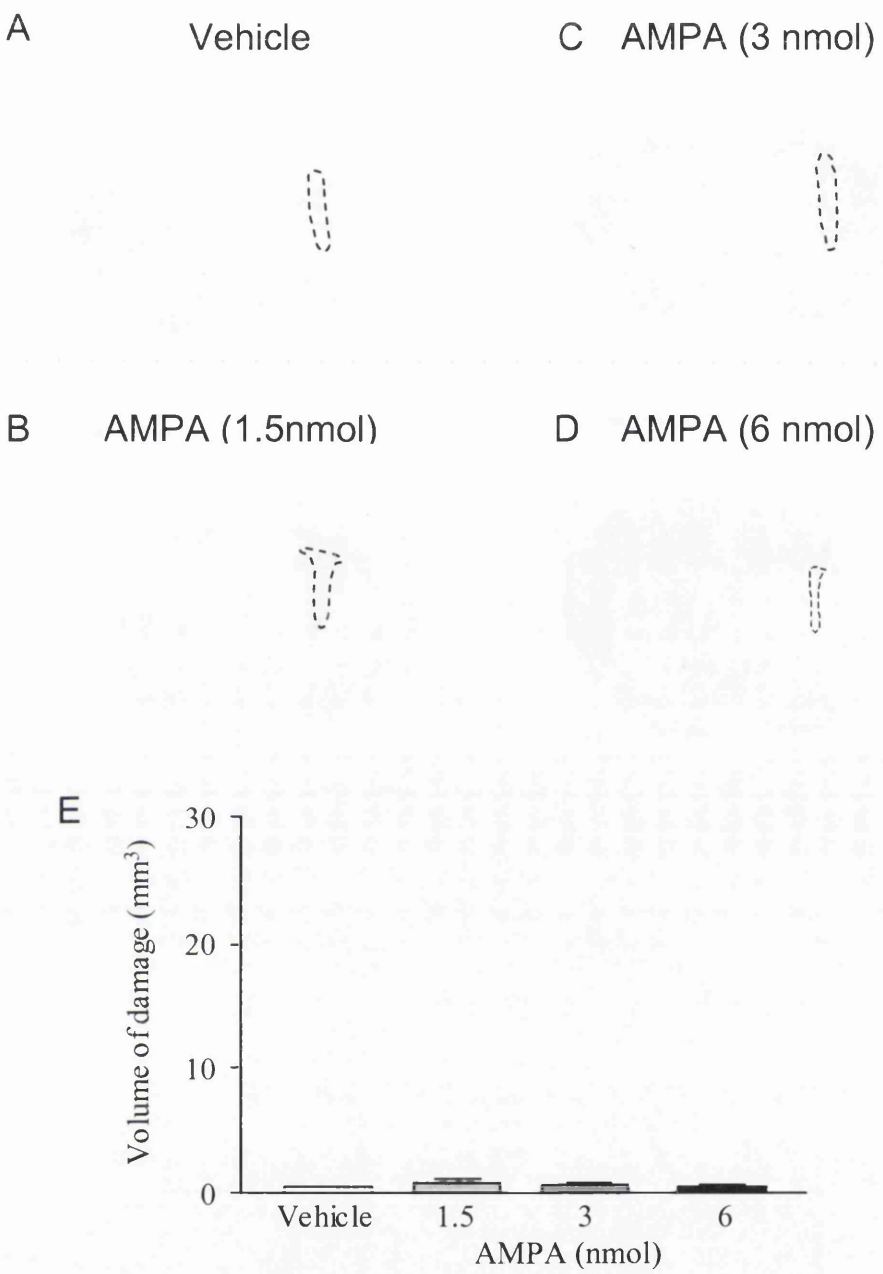

Figure 4.7 Axonal damage assessed in APP immunostained sections following intrastriatal injection of AMPA

Digitised APP immunostained sections (A-D), demonstrating the anatomical extent of axonal damage following stereotaxic injection of Vehicle (PBS) or AMPA (1.5-6nmol). The area of disrupted immunostaining is contained within the dashed line. Quantification of the volume of axonal damage in APP immunostained sections (E). One way ANOVA followed by Student's *t* test with Bonferonni correction) $P>0.05$ for comparison with vehicle treated group. Vehicle, n=5; AMPA (1.5nmol), n=5; AMPA (3nmol), n=6; AMPA (6nmol), n=5.

The data are presented on a graph with the same Y-axis to that used in Figure 4.4E, to highlight the discrepancies between NF 200 and APP immunostaining.

4.3.3 AMPA-induced neuronal damage

Minimal neuronal damage was observed in H & E stained sections from vehicle treated animals, confined to a small area in the caudate nucleus and cortex. Injection of AMPA caused neuronal perikaryal damage, evident in the caudate nucleus and overlying cortex. The anatomical extent of neuronal damage in the caudate nucleus and cortex increased with increasing doses of AMPA (Fig. 4.8B-D), and the lesion often extended into the globus pallidus and thalamus. Quantification of the neuronal damage within the focal lesion demonstrated that AMPA caused a dose-dependent increase in neuronal damage (Fig. 4.8E). In addition to the neuronal damage associated with the focal lesion, AMPA caused widespread neuronal damage in many other areas (Fig. 4.9), such as the hippocampus, thalamic nuclei and the dorsal endopiriform nuclei, in both the hemisphere ipsilateral and contralateral to the injection site. Damaged neurons in these areas were shrunken with an intensely eosinophilic cytoplasm, and were usually intermingled with morphologically normal neurons. The incidence of distant neuronal damage following intrastriatal injection of AMPA is described in figure 4.9A.

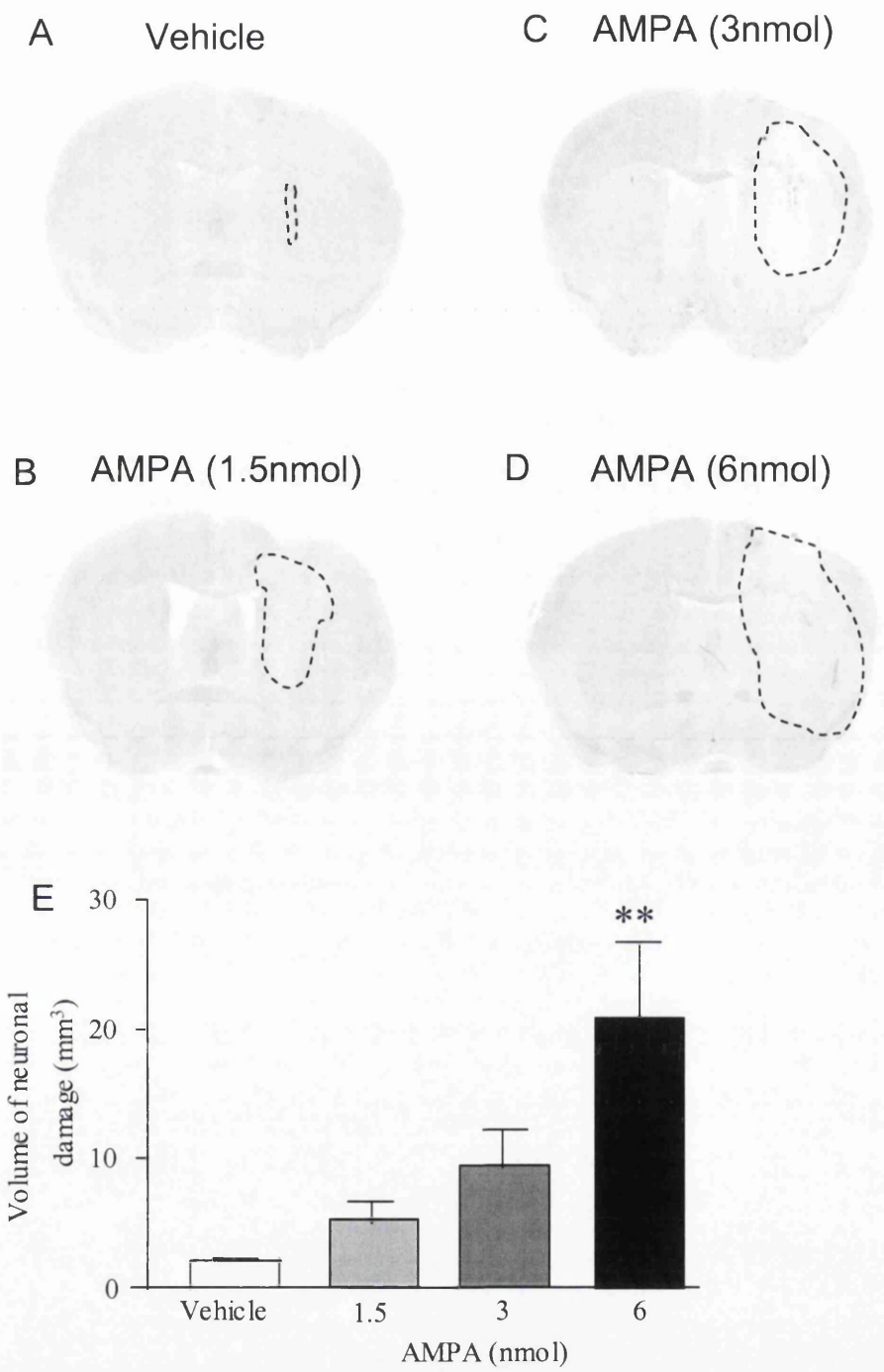

Figure 4.8 Neuronal damage following intrastriatal injection of AMPA

Digitised H & E sections (A-D) demonstrating the anatomical extent of histological damage following stereotaxic injection into the caudate nucleus of Vehicle (PBS) or AMPA (1.5-6nmol). Damage in the cerebral cortex overlying the injection site is likely to be due to diffusion of AMPA along the needle tract. Quantification of the volume of neuronal damage (E). Data are presented mean ± SEM. One way ANOVA followed by Student's *t*-test with Bonferonni correction). **P<0.01 for comparison with vehicle treated group. Vehicle, n=5; AMPA (1.5nmol), n=5; AMPA (3nmol), n=6; AMPA (6nmol), n=5.

A

Anatomical Area		AMPA		
	Vehicle	1.5nmol	3nmol	6nmol
Globus Pallidus (ipsilateral)	1 of 5	3 of 5	5 of 6	5 of 5
Thalamus (ipsilateral)	0 of 5	1 of 5	4 of 6	5 of 5
Thalamus (contralateral)	0 of 5	0 of 5	1 of 6	5 of 5
Hippocampus (ipsilateral)	0 of 5	0 of 5	2 of 6	3 of 5
Hippocampus (contralateral)	0 of 5	0 of 5	1 of 6	3 of 5
Amydala (ipsilateral)	0 of 5	0 of 5	1 of 6	2 of 5
Amydala (contralateral)	0 of 5	0 of 5	1 of 6	1 of 5
Endopiriform cortex (ipsi)	0 of 5	0 of 5	2 of 6	2 of 5
Endopiriform cortex (contra)	0 of 5	0 of 5	1 of 6	1 of 5
Piriform cortex (ipsilateral)	0 of 5	0 of 5	2 of 6	4 of 5
Substantia Nigra (ipsilateral)	0 of 5	0 of 5	5 of 6	5 of 5

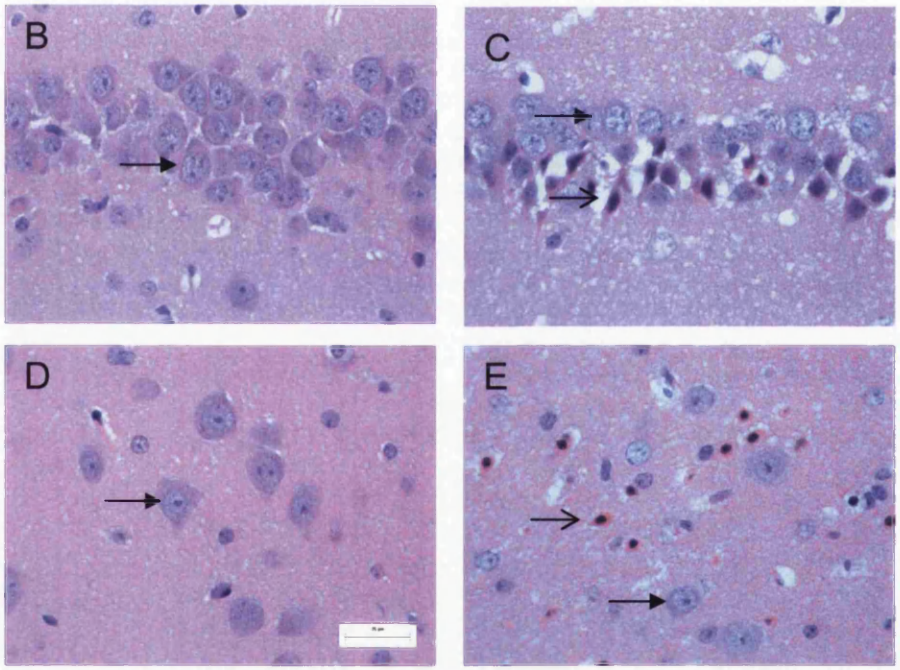

Figure 4.9 Selective neuronal damage in widespread brain areas caused by intracerebral injection of AMPA

Table (A) illustrating the number of animals that contained selective neuronal damage in 6 brain areas following injection of vehicle or AMPA (1.5nmol, 3nmol, 6nmol).

Representative images illustrating morphologically normal neurons in the CA1 sector of the hippocampus (B) and thalamus (D) of vehicle treated animals; and shrunken, eosinophilic neurons in the CA1 sector of the hippocampus (C) and thalamus (E) following intrastriatal injection of AMPA (6nmol).

Closed arrow heads point to morphologically normal neurons, open arrow heads point to damaged neurons.

Scale bar = 25μm.

4.3.4 Malonate-induced axonal damage assessed in NF 200 immunostained sections

In contrast to the organised pattern of immunostaining observed in the hemisphere contralateral to the injection site, malonate (0.34μmol) resulted in the occurrence of axonal swellings and bulbs in the injected caudate nucleus and overlying external capsule (Fig. 4.10). In the centre of the lesion, there was generally an area of increased immunostaining, where axons appeared less severely disrupted (Fig. 4.10B), in contrast to the boundary of the lesion where axons were severely swollen and disrupted following injection of malonate (0.68, 1.34μmol) (Fig. 4.10D). Disorganised, swollen axons were increasingly evident in the globus pallidus and external capsule following injection of the higher doses of malonate (Fig. 4.11; Table 4.2). There was minimal disruption of axons in the overlying cerebral cortex following injection of malonate (Fig. 4.10F; 4.12A), except for mechanical damage caused by the needle tract and an occasional, small rim of damage overlying the external capsule in animals that had received the higher doses of malonate (0.68, 1.35μmol). Animals that received stereotaxic injection of vehicle contained minimal disruption of immunostaining, confined to a small area adjacent to the needle tract in the caudate nucleus and overlying cortex. Quantification of the volume of tissue containing damaged axons in the NF 200 immunostained sections revealed that malonate caused a dose-dependent increase in axonal damage (Fig. 4.12B)

Anatomical Area		Malonate		
	Vehicle	0.34μmol	0.68μmol	1.34μmol
Globus Pallidus	0 of 5	2 of 5	5 of 5	5 of 5
Internal Capsule	0 of 5	1 of 5	5 of 5	5 of 5
Thalamus (ipsilateral)	0 of 5	0 of 5	0 of 5	0 of 5
Thalamus (contralateral)	0 of 5	0 of 5	0 of 5	0 of 5

Table 4.2 Incidence of axonal damage assessed in NF 200 and APP immunostained sections in two brain structures following intrastriatal injection of malonate

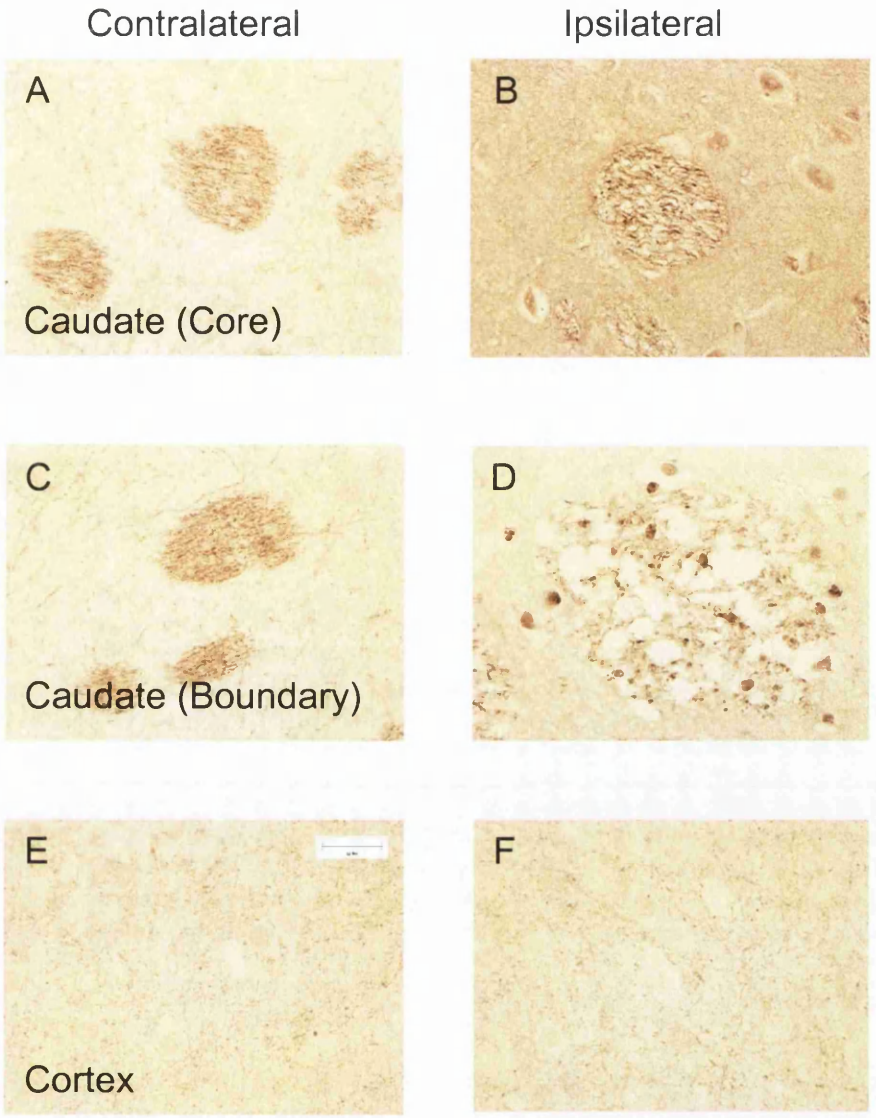

Figure 4.10 NF 200 immunostaining in the caudate nucleus and cortex following intrastriatal injection of malonate (1.35μmol)

In the caudate nucleus and cerebral cortex contralateral to the injection site, axons ran in a smooth, organised profile (A, C, E). In the core of the lesion, less axonal swellings were evident (B) than in the boundary of the lesion (D). Minimal disruption of axons was evident in the cortex overlying the caudate nucleus (F). Scale bar = 25μm.

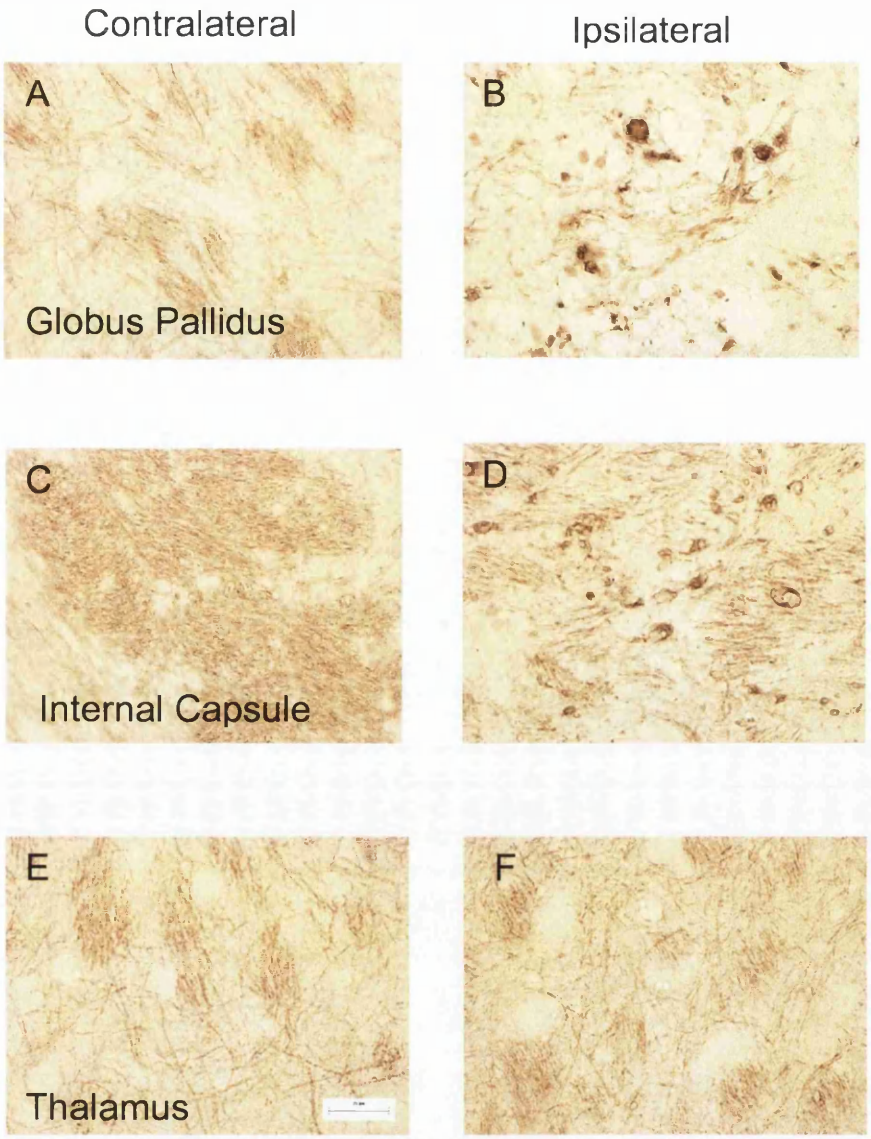

Figure 4.11 NF 200 immunostaining following intrastriatal injection of malonate (1.35μmol)

In the globus pallidus (A), internal capsule (C) and thalamus (E) contralateral to the injection site, axons ran in a smooth, organised profile. Swollen, disrupted axons were evident in the ipislateral globus pallidus (B) and internal capsule (D), however swollen axons were rarely observed in the thalamus (F).

Scale bar = 25μm.

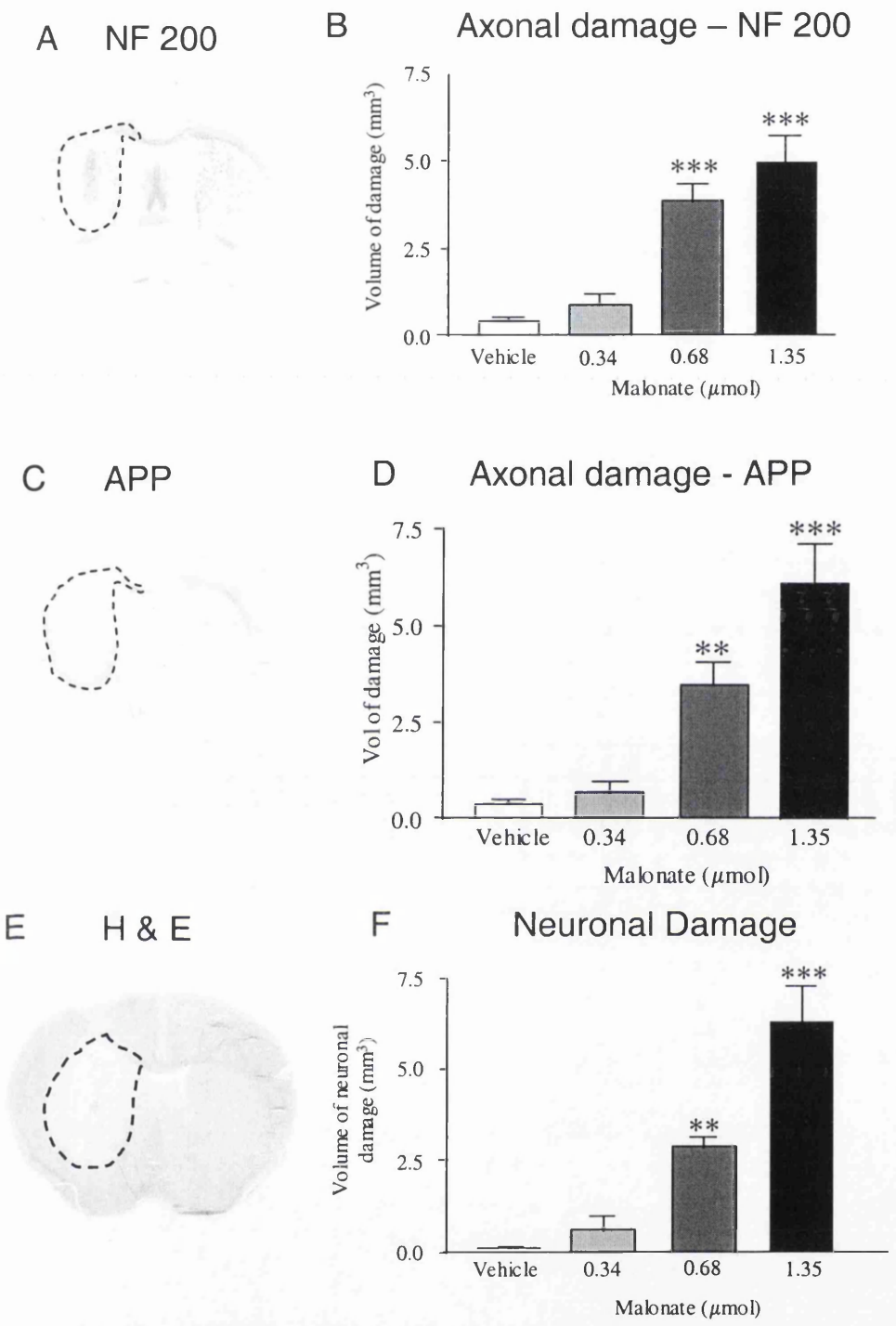

Figure 4.12 Quantification of axonal and neuronal damage following intrastriatal injection of malonate

Digitised NF 200 (A), APP (C) and H & E (E) stained sections, demonstrating the anatomical extent of axonal and neuronal damage (within the dashed line) following intrastriatal injection of malonate (1.35μmol).

Quantification of axonal damage in NF200 (B) and APP (D) immunostained sections revealed that there was a dose dependent increase in axonal damage using both these markers (in contrast to AMPA, see figures 4.4 and 4.7). Quantification of neuronal damage (F) revealed that there was a dose dependent increase in neuronal damage. One-way ANOVA followed by Student's *t* test with Bonferroni correction. n=5 per group. **P<0.01, ***P<0.001 for comparison with vehicle treated group.

4.3.5 Malonate-induced axonal damage assessed in APP immunostained sections

In the hemisphere contralateral to the injection site, APP immunoreactivity was present at a low, diffuse level (Fig. 4.13 A, C, E). Intrastriatal injection of malonate resulted in the presence of intense APP immunoreactivity in swollen and bulbous axons in the caudate nucleus (Fig. 4.13D) and overlying external capsule. The anatomical extent of APP-immunoreactive axons increased with increasing malonate dosage. Following intrastriatal injection of malonate at the highest doses (0.68, 1.35μmol), APP immunoreactive fibre bundles were predominantly present in the boundary of the lesion, whilst the core of the lesion contained relatively few immunoreactive axons (Fig. 4.13A). APP immunoreactive axons were also present in the external capsule overlying the lesion, and occasionally spread across the corpus callosum following malonate administration (0.68, 1.34μmol; Fig. 4.12C). The incidence of axonal damage in the internal capsule and globus pallidus was the same as that observed in NF 200 immunostained sections (Table 4.2). Animals that received intrastriatal injection of vehicle contained minimal APP immunoreactive axons confined to a small area adjacent to the needle tract. Malonate caused a dose-dependent increase in axonal damage quantified from APP immunoreactive sections (Fig. 4.12D).

4.3.6 Malonate-induced neuronal damage

Vehicle treated animals contained minimal neuronal damage confined to a small area immediately adjacent to the needle tract in the caudate nucleus and cortex. Malonate caused an increased area of neuronal perikaryal damage in the caudate nucleus, and the lesion extended into the globus pallidus in two animals following injection of malonate (0.34μmol), and in all animals following injection of the higher doses (0.68, 1.35μmol). Intracerebral injection of malonate did not cause increased neuronal perikaryal damage in the overlying cortex compared with controls (Fig. 4.12E), except for a small area overlying the external capsule in one animal following injection of the highest dose (1.35μmol). Neuronal damage in distant areas such as thalamic nuclei and the hippocampus was not observed following intrastriatal injection of malonate. Quantification of the volume of tissue containing neuronal damage revealed that malonate caused a dose dependent increase when compared with controls (Fig. 4.12F).

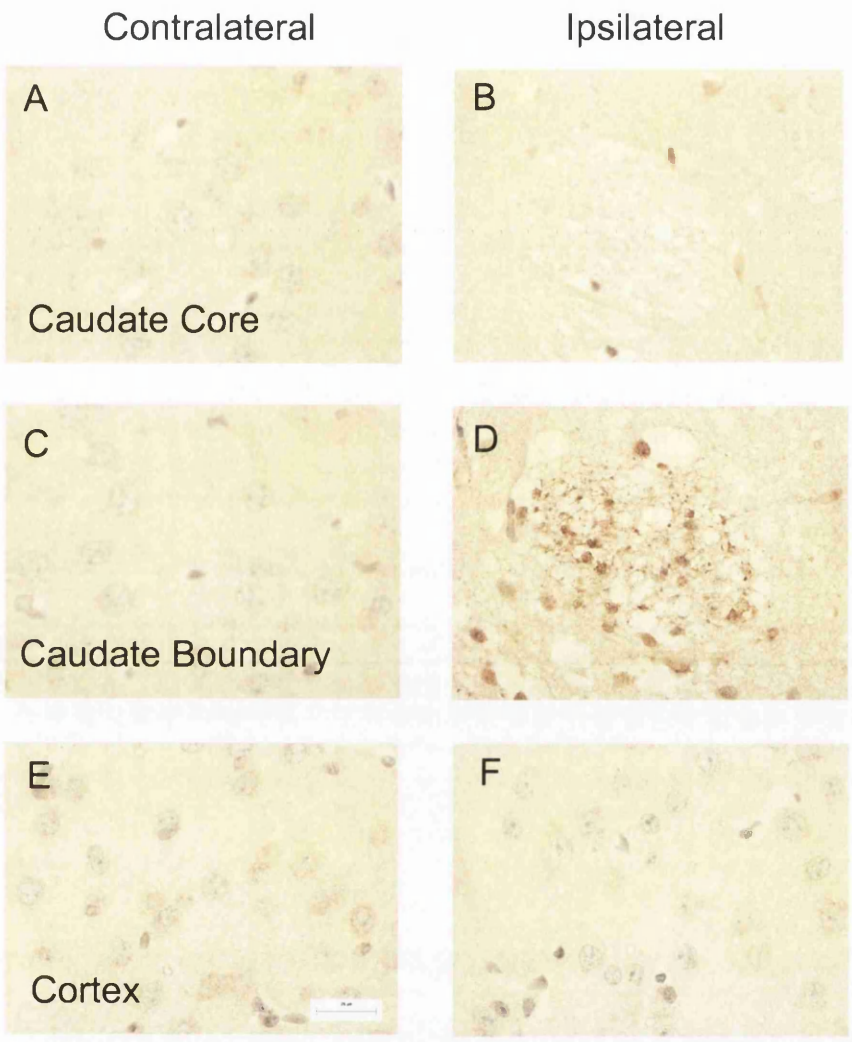

Figure 4.13 APP Immunostaining in the caudate and cortex following intracerebral injection of malonate (1.35μmol)

In the caudate nucleus contralateral to the injection site (A, C), APP immunoreactivity was present at a diffuse, low level. In the core of the malonate-induced lesion, there were less APP immunoreactive axons (B) compared to the boundary of the lesion (C). APP immunoreactive axons were rarely observed in the overlying cortex (F) following malonate injection.

Scale Bar = 25μm.

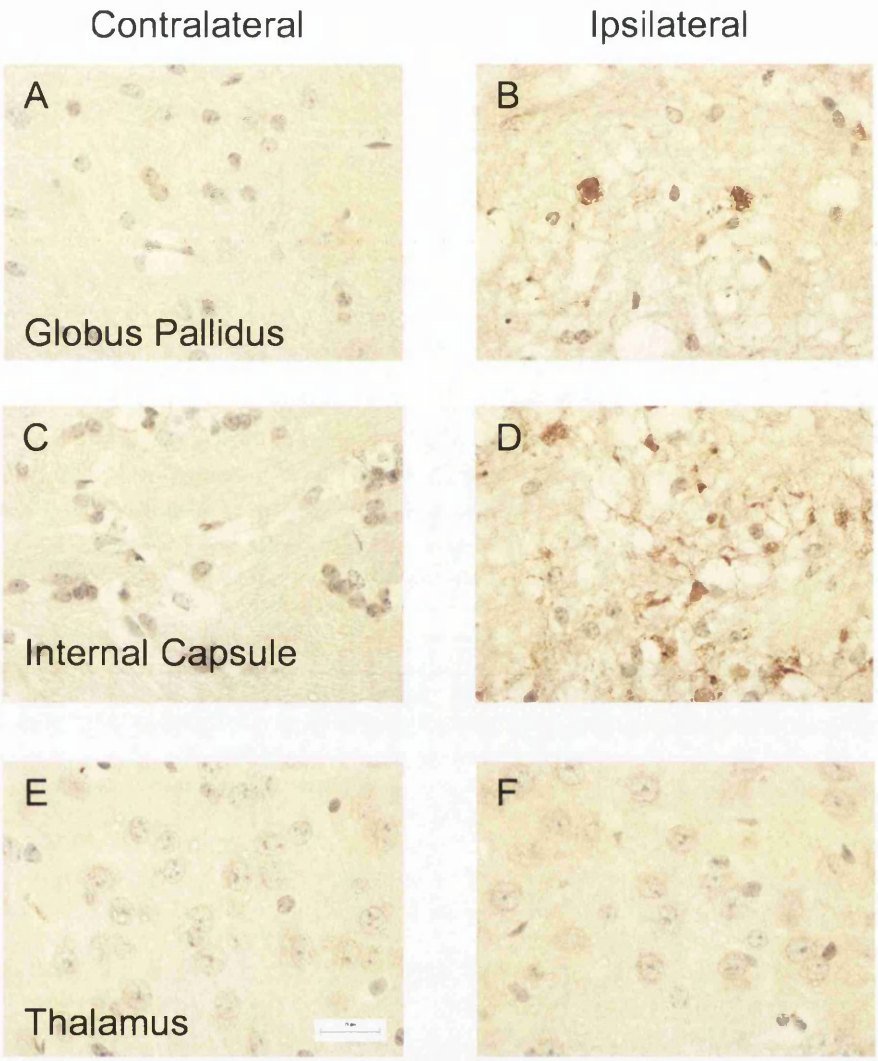

Figure 4.14 APP Immunostaining following intracerebral injection of malonate (1.35μmol)

In the globus pallidus (A), internal capsule (C) and thalamus (E) contralateral to the injection site, APP immunoreactivity was present at a diffuse, low level. APP immunoreactive axons were present in the globus pallidus (B) and internal capsule (D) following intracerebral injection of malonate (1.35μmol), but were rarely observed in the thalamus (F).

Scale bar = 25 μm

4.3.7 ^{14}C-2-deoxyglucose autoradiography

Mean plasma ^{14}C and glucose concentrations did not differ significantly following intrastriatal injection of AMPA, malonate or vehicle (Fig. 4.15). The levels of ^{14}C in the hypothalamus did not differ significantly between the three groups (Fig. 4.16A). In individual animals, the relationship between hypothalamic ^{14}C levels and terminal plasma ^{14}C/ glucose ratios was similar, irrespective of treatment (Fig. 4.16B). These data suggest that intrastriatal injection of AMPA and malonate did not alter the level of glucose utilisation in the hypothalamus, therefore this region was selected as the reference region.

The ratio of tissue ^{14}C in the 17 structures relative to hypothalamic ^{14}C for all three groups is presented in table 4.3. Local cerebral glucose utilisation (LCGU) did not differ significantly between structures in the hemisphere ipsilateral and contralateral to the injection site following intrastriatal injection of vehicle; with the exception of the piriform cortex and cerebellar cortex, where LCGU was increased; and the mediodorsal and ventrolateral thalamic nuclei, where LCGU was significantly lower than the contralateral side.

Following intrastriatal injection of AMPA (6nmol), LCGU was significantly increased in 11 of the 17 structures compared with the contralateral hemisphere. LCGU was increased by the greatest magnitude in the caudate nucleus (Fig. 4.17), and the increase seemed to be homogeneous throughout all affected areas of the caudate (Fig. 4.21). Other areas included thalamic nuclei (Fig. 4.18); the globus pallidus, entopeduncular nucleus and substantia nigra (Fig. 4.19); and white matter areas such as the external capsule, corpus callosum and internal capsule (Fig. 4.20). No significant changes were observed in the remaining structures, and no decreases in LCGU were observed.

Following intrastriatal injection of malonate (1.35μmol), LCGU was significantly reduced in the caudate nucleus (Fig. 4.17). The decrease in LGCU in the caudate nucleus was surrounded by a zone where LGCU appeared to be increased (not quantified, see Fig. 4.21). In contrast, LGCU was significantly increased in the entopeduncular nucleus, and 4 white matter areas; the corpus callosum, external capsule, anterior commissure and the internal capsule (Fig. 4.19, 4.20) following

intrastriatal injection of malonate. There were no significant changes in LCGU in the remaining 11 areas.

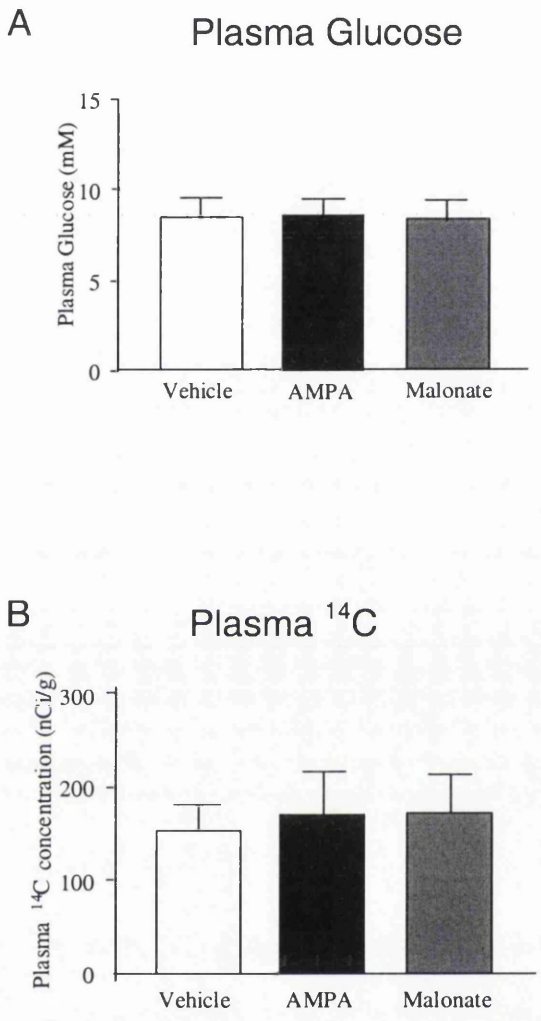

Figure 4.15 Terminal plasma glucose and ^{14}C levels

Plasma glucose (A) and ^{14}C levels (B) at the end of the 45 minute deoxyglucose experimental period in animals that had received injection of AMPA (6nmol), malonate (1.34µmol) or vehicle (PBS). Data are presented mean ± SEM. There was no significant difference between the plasma glucose (A) and ^{14}C levels (B) in the three groups. ($P>0.05$, one way ANOVA) n=5 per group.

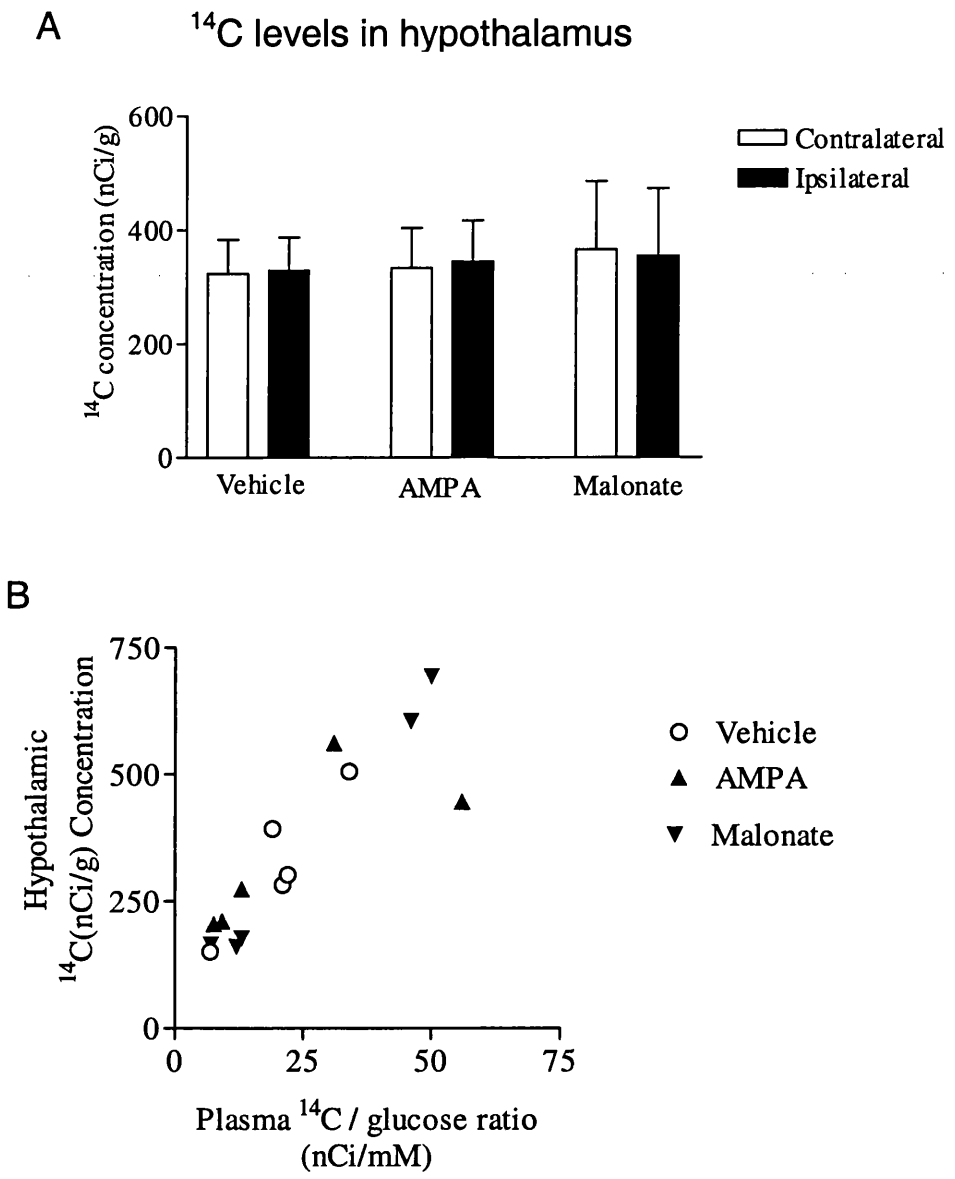

Figure 4.16 Hypothalamic ^{14}C concentration, and its relationship with the terminal plasma ^{14}C : glucose ratio

(A) There was no significant difference between the ^{14}C concentration in the hypothalamus ipsilateral and contralateral to the injected hemisphere following injection of AMPA (6nmol), malonate (1.34μmol) and vehicle into the caudate nucleus ($P>0.05$, Student's paired *t* test). No significant differences were detected in glucose utilisation values in the contralateral hypothalamus between animals in different treatment groups ($P>0.05$, one way ANOVA).

(B) The relationship was similar between hypothalamic ^{14}C concentration and plasma ^{14}C : glucose between groups, irrespective of injectate.

n=5 per group.

	Vehicle		AMPA		Malonate	
	Contralateral	Ipsilateral	Contralateral	Ipsilateral	Contralateral	Ipsilateral
Caudate Nucleus	1.60 ± 0.058	1.57 ± 0.04	1.64 ± 0.085	4.07 ± 0.35 **	1.29 ± 0.048	0.80 ± 0.069 ***
Sensory Motor Cortex	1.93 ± 0.111	1.88 ± 0.119	1.80 ± 0.107	2.25 ± 0.302	1.5 ± 0.0302	1.36 ± 0.095
External Capsule	1.04 ± 0.053	1.09 ± 0.071	1.09 ± 0.088	2.51 ± 0.092 ***	1.46 ± 0.119	2.18 ± 0.058 **
Corpus Callosum	0.98 ± 0.047	0.98 ± 0.064	1.15 ± 0.11	1.77 ± 0.122 *	2 ± 0.136	2.30 ± 0.104 *
Anterior Commissure		0.91 ± 0.087		0.87 ± 0.033		2.72 ± 0.135 ***
Globus Pallidus	1.15 ± 0.082	1.14 ± 0.089	1.04 ± 0.043	2.19 ± 0.1 ***	1.15 ± 0.138	1.27 ± 0.082
Piriform Cortex	1.50 ± 0.109	1.62 ± 0.114 *	1.47 ± 0.018	1.57 ± 0.036 *	1.31 ± 0.046	1.38 ± 0.015
Internal Capsule	1.01 ± 0.056	1.02 ± 0.057	0.92 ± 0.057	1.34 ± 0.179 *	0.89 ± 0.055	1.38 ± 0.075**
Entopeduncular Nucleus	0.97 ± 0.047	1.01 ± 0.036	1.08 ± 0.023	1.84 ± 0.096 **	1.01 ± 0.033	1.64 ± 0.136 *
Thalamus: Mediodorsal	2.03 ± 0.141	1.87 ± 0.137 *	1.94 ± 0.113	2.61 ± 0.263 *	1.64 ± 0.088	1.62 ± 0.139
Dorolateral	1.94 ± 0.144	1.81 ± 0.097	1.96 ± 0.110	2.06 ± 0.177	1.69 ± 0.161	1.63 ± 0.167
Ventrolateral	1.70 ± 0.124	1.64 ± 0.113 *	1.62 ± 0.076	2.24 ± 0.274 *	1.39 ± 0.047	1.46 ± 0.053
Hippocampus	1.94 ± 0.140	1.90 ± 0.135	1.73 ± 0.169	1.69 ± 0.187	1.78 ± 0.153	1.73 ± 0.171
Amygdala	1.01 ± 0.032	1.01 ± 0.033	0.97 ± 0.035	1.03 ± 0.014	0.99 ± 0.021	1.01 ± 0.033
Substantia Nigra:						
Pars compacta	1.44 ± 0.093	1.60 ± 0.112	1.43 ± 0.030	1.56 ± 0.057 *	1.35 ± 0.102	1.34 ± 0.046
Pars reticulata	1.12 ± 0.118	1.11 ± 0.126	1.16 ± 0.078	1.68 ± 0.079 **	1.08 ± 0.01	1.21 ± 0.056
Cerebellar Cortex	1.17 ± 0.092	1.24 ± 0.096 **	1.21 ± 0.070	1.24 ± 0.076	1.09 ± 0.060	1.13 ± 0.043
Number of animals	5		5		5	

Table 4.3 **Relative cerebral glucose utilisation following intrastriatal injection of vehicle, AMPA or malonate**

Data are presented mean (± SEM) ratio of tissue ^{14}C in regions of interest to tissue ^{14}C in the hypothalamus for structures in the hemisphere ipsilateral and contralateral to the caudate nucleus 1 hour following injection of vehicle (PBS), AMPA (6nmol) or malonate (1.34μmol). *P<0.05, **P>0.01, ***P>0.001 for comparison between ipsilateral and contralateral hemispheres within each group (Student's paired *t* test).

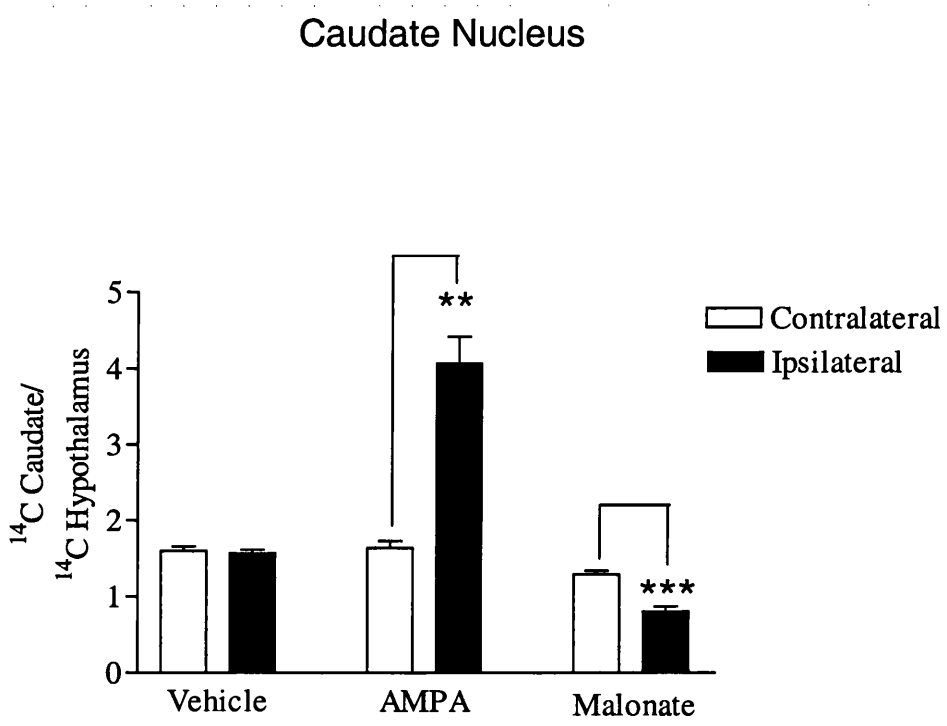

Figure 4.17 LCGU in the caudate nucleus following injection of vehicle, AMPA (6nmol) or malonate (1.34μmol)

Data are presented mean ± SEM. ** P<0.01,*** P<0.001 for comparison between ipsilateral and contralateral hemisphere (Student's paired *t* test). n=5 per group.

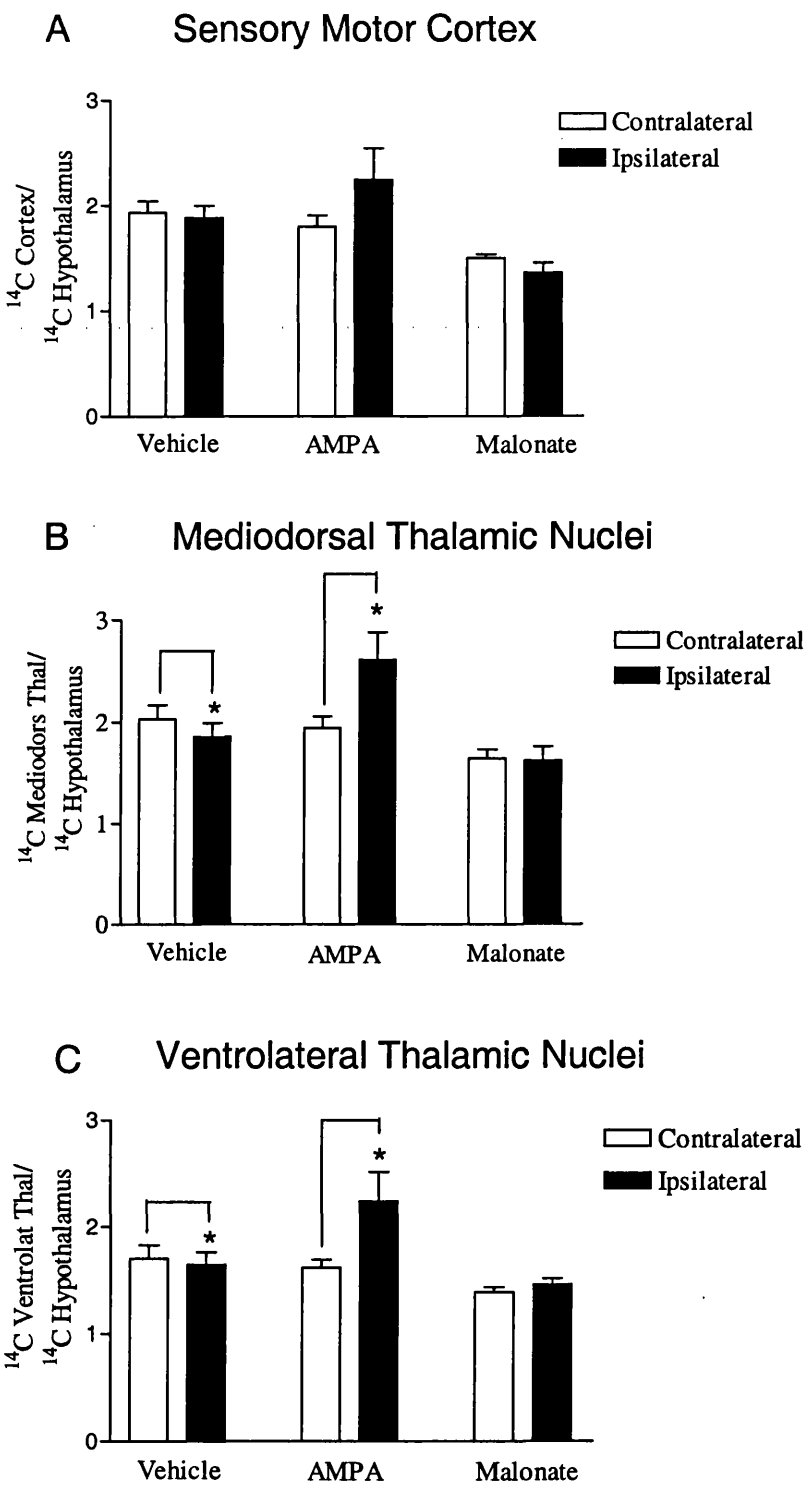

Figure 4.18 LCGU in the cortex and thalamus following intrastriatal injection of vehicle, AMPA (6nmol) or malonate (1.34μmol)

A. Sensory Motor Cortex B. Mediodorsal Thalamic Nuclei

C. Ventrolateral Thalamic Nuclei

Data are presented mean ± SEM. *P<0.05 for comparison between ipsilateral and contralateral hemisphere (Student's paired *t* test). n = 5 per group.

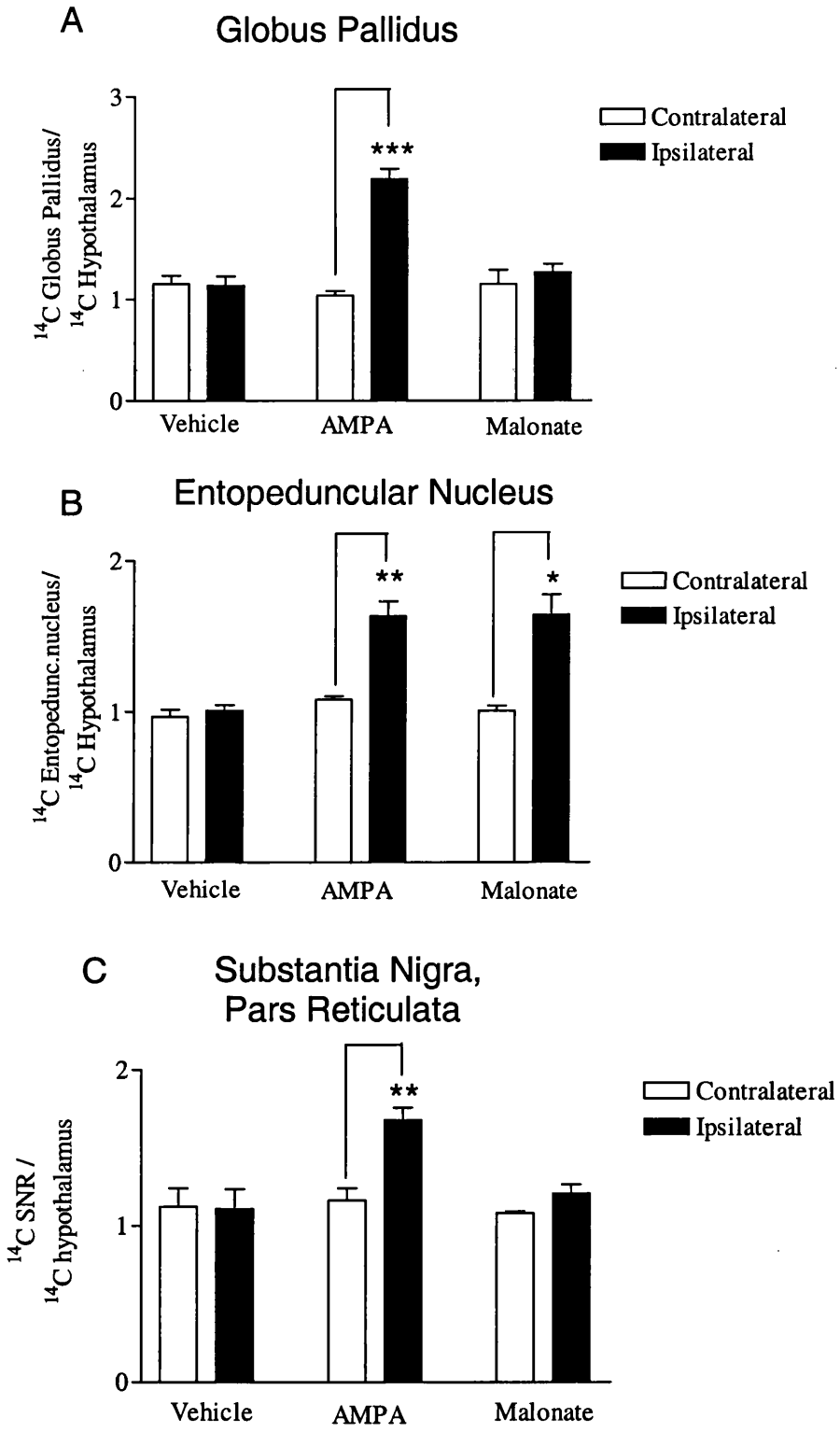

Figure 4.19 LCGU in extrastriatal areas following intrastriatal injection of vehicle, AMPA (6nmol) or malonate (1.34μmol)

A. Globus Pallidus B. Entopeduncular Nuclei

C. Substantia Nigra, pars reticulata

Data are presented mean ± SEM. *P<0.05, **P<0.01, ***P<0.001 for comparison between ipsilateral and contralateral hemisphere (Student's paired *t* test).

n= 5 per group.

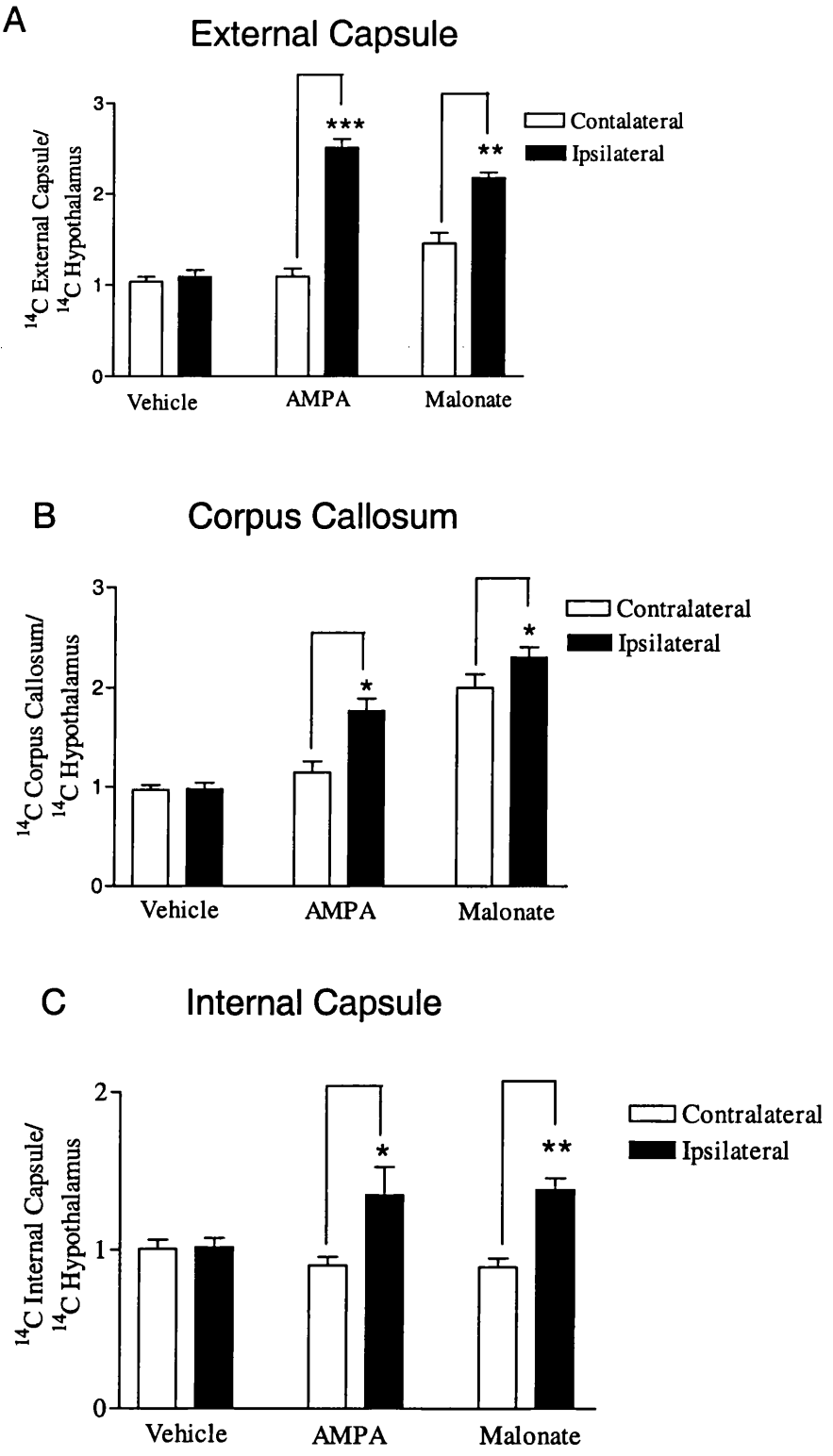

Figure 4.20 LCGU in white matter areas following intrastriatal injection of vehicle, AMPA (6nmol) or malonate (1.34μmol)

A. External Capsule B. Corpus Callosum

C. Internal Capsule

Data are presented mean ± SEM. *P<0.05, **P<0.01,*** P<0.001 for comparison between ipsilateral and contralateral hemisphere (Student's paired

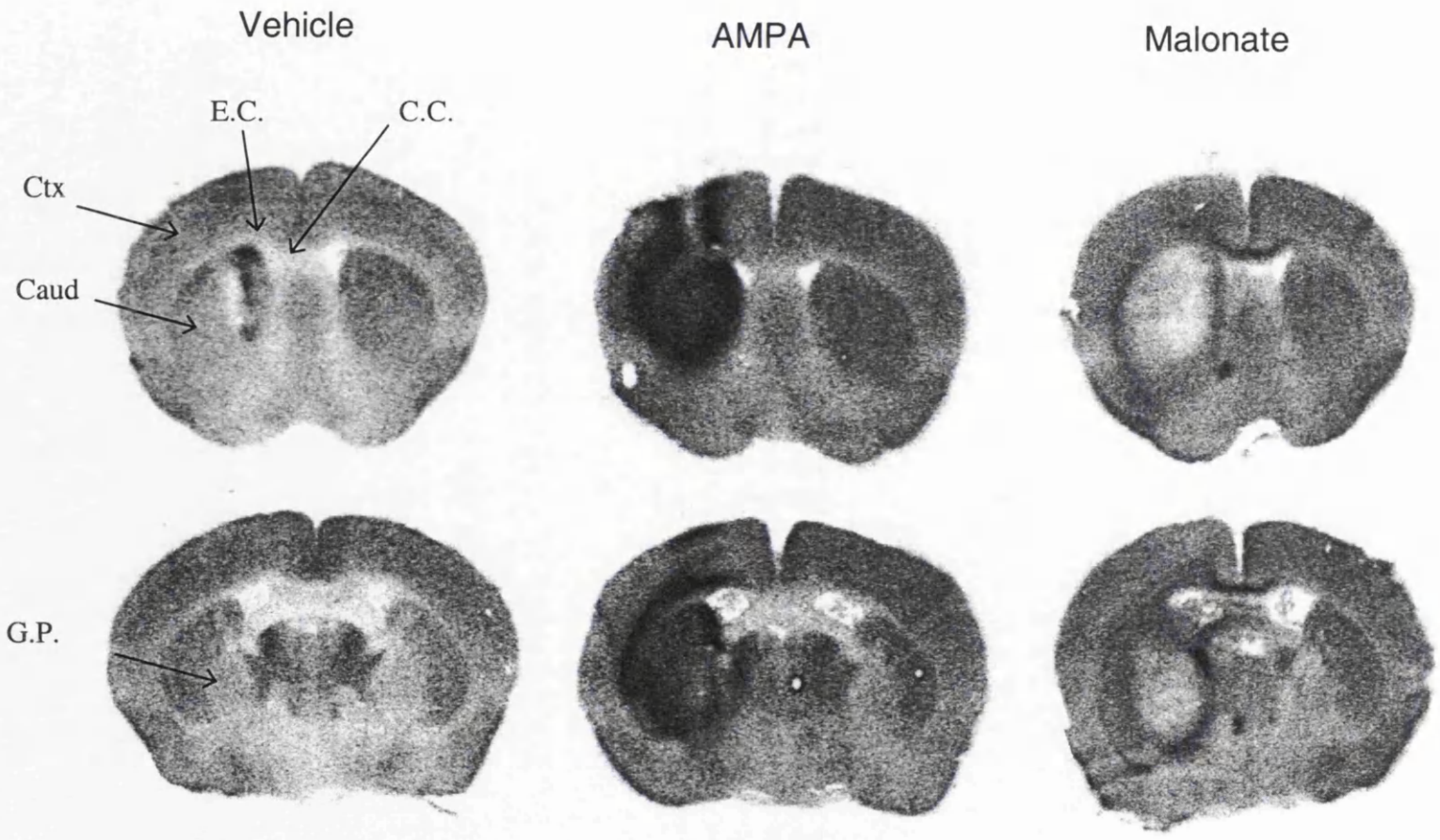

Figure 4.21. Representative autoradiograms illustrating changes in local cerebral glucose utilisation following intrastriatal injection of vehicle, AMPA or malonate

Autoradiograms derived from representative animals following intrastriatal injection of vehicle (PBS), AMPA (6nmol) or malonate (1.35μmol). Arrows indicate caudate nucleus (Caud), external capsule (E.C.), corpus callosum (C.C.), cerebral cortex (Ctx) and globus pallidus (G.P.); areas where alterations in glucose utilisation were detected.

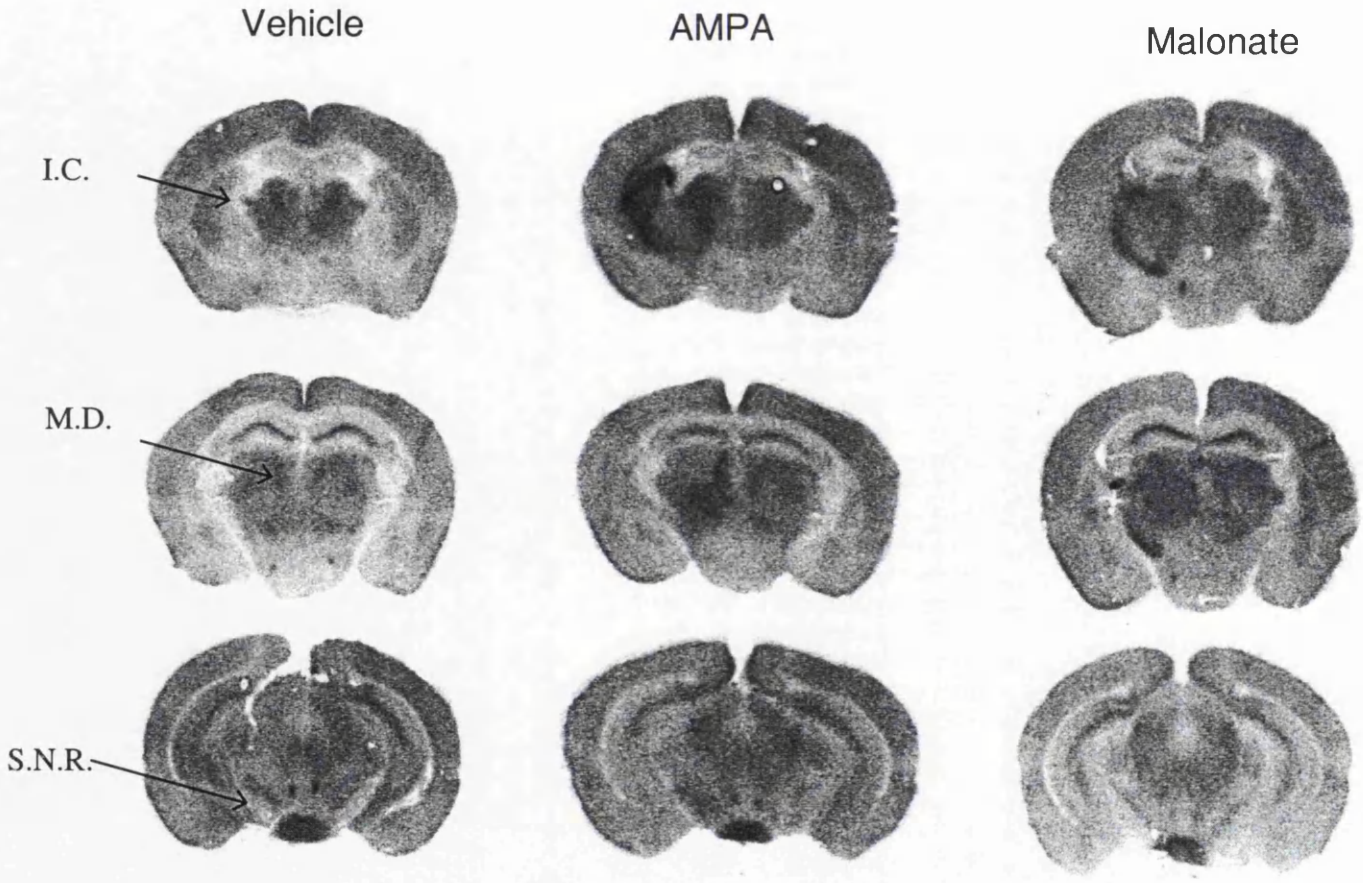

Figure 4.22. Representative autoradiograms illustrating changes in local cerebral glucose utilisation following intrastriatal injection of vehicle, AMPA or malonate

Autoradiograms derived from representative animals following intrastriatal injection of vehicle (PBS), AMPA (6nmol) or malonate (1.35μmol). Arrows indicate internal capsule (I.C.), mediodorsal thalamic nucleus (M.D.) and the substantia nigra, pars reticulata (S.N.R.); areas where alterations in glucose utilisation were detected.

4.4 Discussion

To summarise, the data presented in this chapter demonstrate that intrastriatal injection of AMPA in the mouse caused a dose dependent increase in neuronal damage, and axonal damage quantified from NF 200 immunostained sections. However, AMPA did not induce an increase in axonal damage assessed with APP immunostaining. This contrasts with intrastriatal injection of malonate, which caused increased axonal damage assessed with both markers. The contrasting pattern of glucose utilisation in the acute period following injection of either toxin suggests that AMPA and malonate act by divergent mechanisms.

Differences in AMPA-induced pathology in NF 200 and APP immunostained sections

The reasons for the discrepancy between the extent of axonal pathology in NF 200 and APP immunostained sections is unclear. Numerous studies have utilised neurofilament *or* APP immunohistochemistry to examine axonal pathology following brain injury (described in section 1.3.2), however these markers are rarely used together or compared. A recent study used dual label immunofluorescence to compare the distribution of neurofilament compaction/disruption with the accumulation of APP in damaged axons following experimental traumatic brain injury (Stone *et al.,* 2001). Compaction of neurofilament side arms was initially hypothesised to cause the impairment of axoplasmic transport that results in APP accumulation (Povlishock *et al.,* 1997). However, dual labelling revealed that neurofilament compaction and APP accumulation were generally localised to distinct populations of axons, and were less commonly double labelled (Stone *et al.,* 2001), and ultrastructural analysis confirmed this finding. Axons immunopositive for neurofilament compaction appeared thin, elongated, contained swollen mitochondria and were often vacuolated and segmented. In contrast, APP immunopositive axons contained accumulated organelles, which became progressively larger over time. Double labelling with APP and an antibody raised against calpain-mediated breakdown products (Ab38) in another study revealed that only 30-50% of the axons labelled with Ab38 were APP immunopositive (Buki *et al.,* 1999b). These findings, together with pilot data which revealed that APP immunopositvity and neurofilament disruption occurred in separate populations of axons in human head-injured patients, led the authors to conclude that APP immunohistochemistry may underestimate the

full spectrum of axonal pathology following traumatic brain injury (Stone *et al.*, 2001). Discrepancies between the populations of damaged axons labelled with NF 200 and APP are also described in the previous and subsequent chapter of this thesis.

The distinct populations of axons labelled by NF 200 and APP immunohistochemistry following brain injury may represent different mechanisms of injury. APP accumulation within an axon requires energy-demanding, kinesin-dependent axonal transport. Therefore it is conceivable that in situations where energy metabolism is impaired, or kinesin is not functioning, that APP will not accumulate. APP accumulation in damaged axons can occur very quickly, up to 15 minutes following experimental traumatic brain injury (Stone *et al.*, 2001). This suggests that the axonal cylinder is rapidly and directly damaged at an area that will go on to accumulate APP. The 2-deoxyglucose studies described in this chapter suggest that, when compared with malonate-induced damage where considerable APP accumulation does occur, AMPA-induced toxicity progresses more slowly. In addition, AMPA is unlikely to be directly toxic to axons, as there is no evidence that AMPA receptors are present on the axon cylinder. Instead, AMPA-induced axonal damage is likely to be secondary to excitotoxic events occurring at the oligodendrocytes, myelin sheath or neuronal perikarya. The neurofilament disruption and compaction that occurred following experimental traumatic brain injury was associated with disruption of the myelin sheath and infoldings of the axolemma (Stone *et al.*, 2001). Normal cytoskeletal composition in axons is dependent upon intact myelin (Brady *et al.*, 1999), therefore disruption of myelin following brain insults may lead to derangement of the neurofilament network; this may account for the cytoskeletal abnormalities following injection of AMPA.

'Distant' pathology following intrastriatal injection of AMPA

In addition to causing axonal and neuronal pathology in the caudate nucleus, axonal and/or neuronal damage was also evident in anatomical areas distant from the injection site, such as the thalamus, substantia nigra and hippocampus. Neuronal pathology has previously been reported in similar 'distant' anatomical areas following intrastriatal injection of kainate (Wuerthele *et al.*, 1978; Wooten and Collins, 1980; Ciani *et al.*, 1994). Because these brain areas are remote from the injection site, it is unlikely that diffusion of the toxin accounts for the pathology in

these distant areas. In support of this, intrastriatal injection of [^{3}H]-kainate resulted in hippocampal damage that was not accompanied by diffusion of the isotope to this area (Scherer-Singler and McGreer, 1979). Instead, the 'distant' pathology resulting from intrastriatal injection of AMPA is likely to result from the excessive excitation of brain areas that have excitatory polysynaptic connections with the striatum. Striatal neurons project to the cortex via the globus pallidus, substantia nigra and thalamus (see Fig. 4.23). Furthermore, all regions of the striatum receive a cortical input. Activation of these pathways, excessive release of endogenous glutamate in these structures and the resultant excessive neuronal activity are likely to result in the pathology observed in distant areas following intrastriatal injection of AMPA. In support of this, increases in glucose utilisation were demonstrated in the cortex, globus pallidus, thalamus and substantia nigra, 1 hour following intrastriatal injection of AMPA. The excessive activation of striatonigral pathways may also be enhanced by a loss of inhibitory GABAergic inputs from the striatum, as infusion of the GABA agonist muscimol reduces pathology observed in the substantia nigra following intrastriatal injection of ibotenic acid (Saji and Reis, 1987).

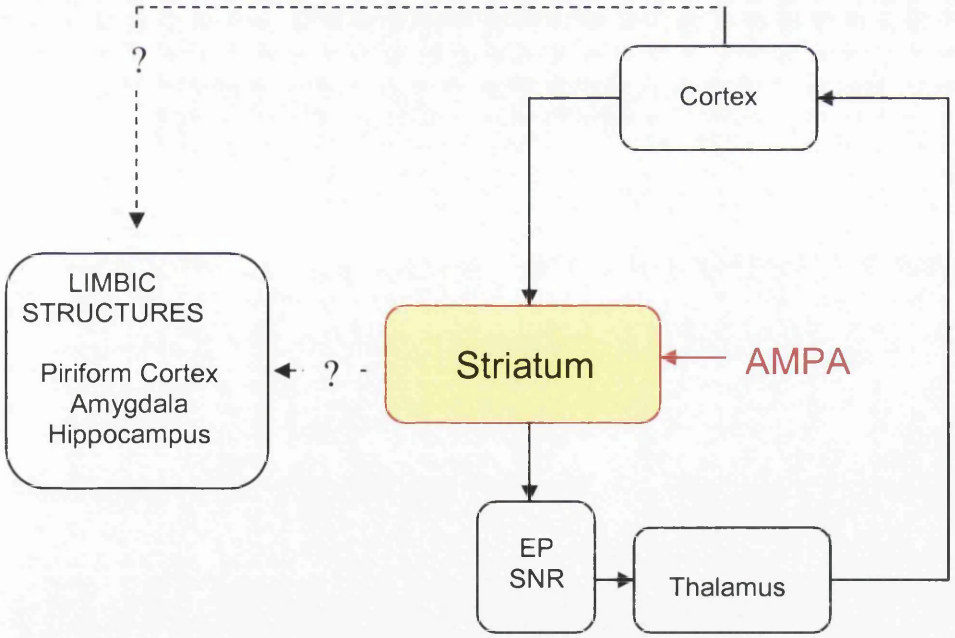

Figure 4.23 Anatomical areas that may be involved in the pathology induced by AMPA
EP = Entopeduncular Nucleus; SNR= Substantia Nigra, pars reticulata

The cortex is thought to play an integral role in intrastriatal kainate-induced pathology, as decortication protects against toxicity, whereas lesioning the substantia nigra or thalamus does not protect against kainate toxicity (McGeer *et al.*, 1978;

Biziere and Coyle, 1979). Extensive cortical damage is present when AMPA is co-injected with the cytokine interleukin-1 (IL-1), which is not present when AMPA is injected alone (Lawrence *et al.,* 1998). However, this cortical damage can be attenuated with intracortical infusion of the NMDA receptor antagonist D-AP5, suggesting the activation of endogenous glutamatergic pathways between the striatum and cortex (Allan and Rothwell, 2000). The cortical damage induced by co-injection of AMPA and IL-1 in the rat is thought to be mediated, in part, by polysynaptic striatal outputs to the cortex via the hypothalamus (Allan *et al.,* 2000, see figure 4.23).

Other anatomical structures where neuronal pathology was observed following intrastriatal injection of AMPA are the piriform cortex, amygdala and hippocampus, which form part of the limbic system. Damage in the limbic system is also observed following intrastriatal injection of kainate (Wuerthele *et al.,* 1978; Ciani *et al.,* 1994). The pattern of pathology observed in the limbic system following intrastriatal injection of AMPA is similar to that observed following administration of convulsants, and suggests seizure like excessive activation of the limbic circuits. Dramatic increases in glucose utilisation correlate with seizure propagation following intrastriatal injection of kainate (Lothman and Collins, 1981). The administration of anti-convulsants such as diazepam reduces neuronal death in limbic brain distant from the site of administration following administration of kainate or AMPA and IL-1β (Zaczek *et al.,* 1978; Ben-Ari *et al.,* 1980; Patel *et al.,* 2002). It is unclear how intrastriatal injection of AMPA induces damage in the limbic system when there are no major anatomical connections between the striatum and these limbic system areas. The pathologic response of these areas may arise indirectly, as a result of connections between the limbic system and the cortex/thalamus (Fig. 4.23).

Enhanced levels of glucose utilisation following intrastriatal injection of AMPA

Glucose utilisation was markedly increased in the caudate nucleus 1 hour following intrastriatal injection of AMPA. Similar increases in glucose utilisation have been reported 15 minutes and 1 hour following intracerebral injection of AMPA or kainate (Wooten and Collins, 1980; Browne *et al.,* 1998). A number of energy demanding processes could account for the increased glucose utilisation (enzyme synthesis, transmitter synthesis and reuptake, etc). However, dynamic alterations in glucose utilisation are thought to predominantly reflect the energy demanding process of ion

transport at nerve terminals (Schwartz *et al.*, 1979). The increase in glucose utilisation induced by AMPA in the caudate nucleus is likely to be caused by energy demanding ion pumps responding to excessive activation of AMPA/kainate receptors. Greatly increased neuronal activity assessed using electrophysiological methods follows intracerebral injection of kainate (Ben-Ari *et al.*, 1980; Sawamura *et al.*, 2001).

As mentioned earlier, increased glucose utilisation was also observed in the globus pallidus, entopeduncular nucleus, thalamus, substantia nigra and cortex following intrastriatal injection of AMPA. This supports the notion that the pathology observed in these areas results from the excessive release of endogenous excitatory amino acids and sustained neuronal activation in these polysynaptic pathways connected to the striatum.

Glucose utilisation was also elevated in several white matter areas. This applied not only to white matter areas in close proximity to the injection site, such as the corpus callosum and external capsule, but also to the internal capsule. Whilst the majority of glucose utilisation in grey matter is thought to predominately reflect activity at neuronal synaptic terminals, this cannot account for the increased glucose utilisation in white matter. It may be possible that AMPA has diffused or tracked up the needle tract to the external capsule and corpus callosum, activated AMPA receptors present on oligodendrocytes and astrocytes within the white matter, resulting in increased activity at ion pumps. However, this is unlikely to account for the increased glucose utilisation observed in the internal capsule.

Excessive activation of the internal capsule is likely to result in massive voltage dependent Na^+ and Ca^{2+} influx into the axons, therefore enhanced rates of glucose utilisation are presumably a reflection of enhanced activity at axonal ion pumps (Aiello and Bach-y-Rita, 2000). Stimulation of the hindlimb cortical area of the rat cortex results in frequency dependent increases in glucose utilisation in the corpus callosum and contralateral cortex, suggesting that changes in white matter energy metabolism reflect changes in electrical activity (Weber *et al.*, 2002). Ultrastructural analysis of brain tissue from rodents exposed to consultant agents revealed that axonal pathology preceeded changes in neuronal perikarya and dendrites (Auer *et al.*, 1986). Furthermore, swollen mitochondria with damaged cristae were evident within

swollen axons. Again, these changes were associated with hypermetabolism (Ingvar *et al.,* 1987), and were presumed to be related to influx of Na^+ into the excessively activated axon cylinder. It would appear likely therefore, that the swollen axons evident in the 'distant' brain areas 24 hours following intrastriatal injection of AMPA is caused by hypermetabolism of the polysynaptic circuits associated with striatum, influx of Na^+ and Ca^{2+}, loss of ionic membrane potentials and possible swelling of mitochondria. Increased Ca^{2+} and mitochondrial dysfunction has also been implicated in the production of reactive oxygen species, which can cause oxidative damage to cells (Kristian and Siesjo, 1998). The anticonvulsant agent carbamzepine, which acts by blocking sodium channels, reduces seizure activity and hyperactivity following intracerebral injection of kainate (Zaczek *et al.,* 1978). It would be interesting to determine if sodium channel blocking agents could reduce hypermetabolism and axonal pathology observed following intrastriatal injection of AMPA.

Glucose utilisation was not significantly altered in any of the limbic structures 1 hour following intrastriatal injection of AMPA, however by 24 hours neuronal pathology was observed in these areas. Furthermore, despite the presence of damaged neurons in limbic structures at 24 hours, axons were minimally disrupted, and were rarely swollen to the same extent as axons in structures such as the thalamus, cortex, globus pallidus and substantia nigra, in which glucose utilisation was elevated by 1 hour. These observations suggest that the pathology in the limbic system may occur at a later timepoint, and is secondary to the changes in the striato-thalamo-cortical pathways. All mice in the 2-deoxyglucose studies received steady levels of the anaesthetic agent halothane for 38 minutes prior to administration of the 2-deoxyglucose. The depressant effects of the anaesthesia may have inhibited activation of the limbic system in the acute period following intrastriatal injection of AMPA.

Caution should always be applied when interpreting the results of ^{14}C- 2-deoxyglucose experiments in pathological situations such as AMPA-receptor mediated excitotoxicity. Under physiologically normal circumstances, levels of deoxyglucose accumulation are the basis for the estimation of local glucose phosphorylation, which in turn is intimately related to energy consumption. In pathological situations such as seizure induction, dynamic alterations can occur in

the value of rate constants and the 'lumped constant' (Ingvar and Siesjo, 1983; Greenberg *et al.,* 1992). This in turn may alter the normal relationship between deoxyglucose uptake and glucose phosphorylation. The methodology employed in the current study is still valid to determine which anatomical structures have altered levels of glucose utilisation in the acute period following intrastriatal AMPA injection. However, the increased levels of glucose utilisation may not bear the direct relationship with energy production as it would under normal circumstances. Anaerobic metabolism, which yields considerably lower net energy gains per molecule of glucose, may increase in pathological circumstances. This occurs during experimental seizure induction, where levels of lactate are elevated (Ingvar *et al.,* 1987). Therefore, it is possible that at least some of the elevation in glucose utilisation observed following AMPA administration may not reflect increased levels of energy utilisation *per se*, but instead may also reflect enhanced anaerobic glycolysis supplying the normal energy demands. Measuring levels of metabolites such as lactate, the product of anaerobic metabolism, would establish the contribution of anaerobic glycolysis or increased energy demand to the elevation of glucose utilisation observed following intrastriatal administration of AMPA. It is interesting to note that accumulation of lactate may also contribute to axonal pathology, as intracerebral injection of acidic lactate results in axonal swellings (Meller *et al.,* 1993).

Comparison of AMPA-induced pathology with malonate–induced pathology

The similarities and differences in the pattern of pathology observed following intrastriatal injection of AMPA or malonate are summarised in table 4.3.

Intrastriatal injection of malonate results in a significant increase in the amount of APP immunoreactive axons, whereas AMPA does not. This is likely to be a reflection of the ability of malonate to be directly toxic to axons, which contain numerous mitochondria. By inhibiting energy production in the axon cylinder, the ATP-dependent anterograde transport of APP will cease. This explains why APP immunoreactive axons are mainly located at the boundary of the malonate-induced lesion, as presumably intact cell bodies located out with the area affected by malonate transport APP along axons to the point of damage. In contrast, AMPA does not immediately cause energy inhibition, but instead acts through excitotoxic

mechanisms that are not directly toxic to the axon cylinder. A diagrammatic comparison of the different effects of AMPA and malonate on axons is shown in figure 4.24.

	AMPA	Malonate
Neuronal pathology in caudate nucleus	√	√
Neuronal/axonal pathology in the cerebral cortex	√	X
Axonal pathology (NF 200) in caudate nucleus	√	√
Axonal pathology (APP) in caudate nucleus	X	√
'Distant' pathology	√	X
Effects on glucose utilisation in the caudate at 1 hr	↑	↓

Table 4.4 Similarities and differences in AMPA or malonate-induced pathology

Whereas AMPA caused widespread damage in 'distant' brain areas, malonate mainly induced damage confined to the caudate nucleus and globus pallidus. As malonate does not primarily act by exciting glutamate receptors in the caudate, it does not result in the activation of the polysynaptic circuits shown in figure 4.23, therefore there is no 'distant' pathology, at least at the doses used in this experiment.

Intrastriatal injection of malonate resulted in a core area of suppressed glucose utilisation, surrounded by a rim of increased 2-deoxyglucose accumulation in the caudate nucleus. The pattern of altered glucose utilisation following malonate administration is similar to that observed following focal cerebral ischaemia (Ginsberg, 1990). The decreased glucose utilisation in the caudate nucleus indicates that a suppression of energy utilisation and neuronal function has occurred as soon as 1 hour following malonate administration. In both focal cerebral ischaemia and malonate-induced damage, mitochondrial function is disturbed. This is due to O_2 deprivation in the former case, and as a result of succinate dehydrogenase inhibtion

in the latter case. Either way, inhibition of mitochondrial function results in increased rates of anaerobic glycolysis and the production of lactate. Therefore, the enhanced levels of glucose utilisation in the boundary of the caudate are likely to reflect enhanced levels of anaerobic glycolysis. However, increased aerobic energy utilisation may also account for some of the 2-deoxyglucose accumulation in the caudate. Excitotoxic mechanisms, which result in elevated neuronal activity and hence energy consumption, are thought to contribute to the ensuing pathology caused by malonate (Greene *et al.,* 1993). NMDA receptor antagonism attenuates malonate-induced damage (Greene *et al.,* 1993), and recent data generated in our laboratory have shown that the AMPA receptor antagonist LY293558 can reduce neuronal pathology following intrastriatal injection of malonate (Cuthill, unpublished observations).

In addition to altering levels of glucose utilisation in the caudate nucleus, malonate also caused increases in glucose utilisation in the entopeduncular nucleus and internal capsule. It is unclear if activation of these areas arises due to their anatomical connectivity with the caudate nucleus, or if it results from diffusion of malonate or other pathogenic mediators of malonate-induced damage. Elevated glucose utilisation in these two brain areas following intrastriatal injection of AMPA correlated with activation of other areas such as the substantia nigra, thalamus and cortex; which was proposed to occur due to the activation of the polysynaptic circuits described earlier. However, the thalamus, cortex and substantia nigra have unaltered levels of glucose utilisation following intrastriatal injection of malonate. Therefore, it seems likely that diffusion of toxic substances may result in the elevated glucose utilisation and subsequent pathology in these areas. Examining the anatomical extent to which radioactively labelled malonate diffuses, or the pattern of glucose utilisation or pathology following intrastriatal injection of malonate with glutamate receptor antagonism would gain further insights into this phenomenon.

Four out of the 5 areas that contained markedly elevated levels of glucose utilisation following intrastriatal injection of malonate were white matter areas. These included the anterior commissure, external capsule and corpus callosum that were in close proximity to the injection site. Similar, marked elevations in glucose utilisation in white matter tracts have been reported following experimental hypoxemia in the rat, where 2-deoxyglucose accumulation was more pronounced in white matter than

adjacent grey matter areas (Pulsinelli and Duffy, 1979). The authors proposed that the disproportionately greater change in glucose utilisation in white matter compared to grey matter was caused by enhanced anaerobic glycolysis, due to an increased vulnerability of white matter to hypoxia, perhaps related to a greater reduction in blood flow to white matter (Pulsinelli and Duffy, 1978). However, recent data has suggested that white matter is relatively resistant to anoxia, *because* it can utilise energy from anaerobic glycolysis (Ransom *et al.*, 2002). Furthermore, mice optic nerves are reported to be more resistant to anoxia than rat optic nerves (Ransom *et al.*, 2002). This may account for the fact that axonal pathology was consistently observed extending across the corpus callosum into the contralateral white matter following intrastriatal injection of malonate in the rat (Dewar *et al.*, 2001), but was rarely observed following the same treatment in the mouse, despite increased glucose utilisation in the same area. Evidently, further investigation of the metabolic responses of white matter compared to grey matter following brain injury is required. With the exception of the corpus callosum and anterior commissure of malonate-treated animals, all areas that had elevated glucose utilisation 1 hour following intrastriatal injection of malonate or AMPA had axonal pathology in these areas at 24 hours. This suggests that alterations in the metabolic state of these anatomical areas occurs, and perhaps contributes to axonal pathology.

The pathological consequences of intrastriatal injection of AMPA in the mouse have now been characterised. The following chapter will determine if PLP and MBP deficient mice exhibit an altered sensitivity to intrastriatal injection of AMPA.

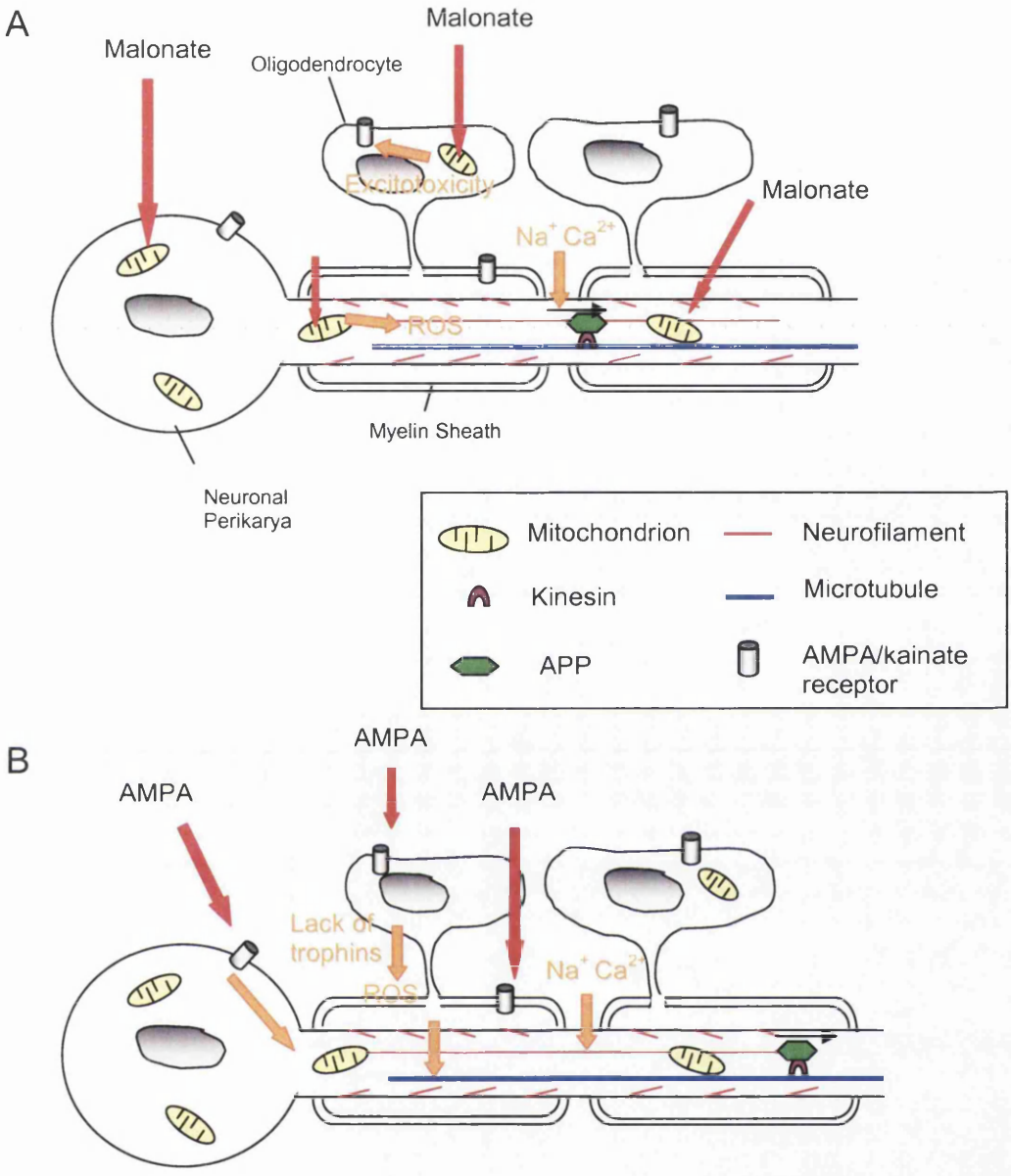

Figure 4.24 Comparison of the mechanisms of AMPA or malonate mediated toxicity

A. Malonate acts directly by inhibiting energy production by competitive inhibition of a mitochondrial enzyme, succinate dehydrogenase. Energy inhibition may lead to the production of reactive oxygen species (ROS), excitotoxicity, and the influx of Na^+ and Ca^{2+}, which in turn may have detrimental effects to the axon (orange arrows).

B. AMPA acts directly by over-activating AMPA receptors located on the neuronal perikarya, oligodendrocytes and myelin sheath (red arrow). Excitotoxic events at these cellular elements may lead to axonal damage via the diffusion of toxic factors such as reactive oxygen species, lack of trophic support from the oligodendrocytes or the influx of Na^+ and Ca^{2+} (orange arrows).

CHAPTER 5

AMPA-INDUCED AXONAL DAMAGE IS ATTENUATED IN PLP, BUT NOT MBP DEFICIENT (*shiverer*) MICE

5.1 Introduction

PLP deficient mice develop compacted myelin, and have a normal life span (Boison and Stoffel, 1994; Klugmann *et al.*, 1997). However, 6-8 weeks following birth, swollen axons are detected in PLP deficient mice, using electron microscopy (Klugmann *et al.*, 1997). The axonal damage is more prominent in animals older than one year, and by 16 months, impairment of motor function is observed (Griffiths *et al.*, 1998). Axonal swellings have also been reported in human patients lacking PLP (Garbern *et al.*, 2002). PLP deficient oligodendrocytes transplanted into the spinal cord of *shiverer* mice induces axonal swellings (Edgar *et al.*, 2001). This suggests that the axonal swellings are due to the presence of PLP deficient oligodendrocytes, and not as a consequence of loss of PLP splice variants from the neuronal cell body. This suggests that interactions with myelin are important for normal functioning of the axon, and that PLP is involved in this process.

Due to a naturally arising mutation on the *MBP* gene, MBP cannot be synthesised in *shiverer* mice (Readhead *et al.*, 1987). These mice lack compact myelin, develop a tremor, progressively increasing seizures, and die prematurely (50-100 days after birth). Unlike PLP deficient mice, there is no evidence that *shiverer* mice possess axonal swellings. However, abnormalities in axons of *shiverer* mice have been reported. Increased rates of slow axonal transport, altered amounts of neurofilaments and microtubules and altered levels of neurofilament phosphorylation have been reported in shiverer mice (Brady *et al.*, 1999). These axonal abnormalities were also observed in transgenic mice containing two copies of a wild type MBP transgene, which results in an intermediate amount of compact myelin (Kirkpatrick *et al.*, 2001). This suggests that it is not merely the lack of compact myelin that accounts for the axonal abnormalities, but MBP-mediated glial-axonal signals.

The abnormal axo-glial relationships that *Plp* knockout and *shiverer* mice possess may provide a useful model to examine the role of excitotoxic events at the myelin sheath and oligodendrocyte in mediating AMPA-induced axonal damage. In addition, it remains possible that the axonal abnormalities observed in PLP and MBP deficient mice may be mediated, in part, by secondary excitotoxic processes. Therefore the current study was undertaken to determine if PLP and MBP deficient mice exhibit altered sensitivity to AMPA-induced axonal damage.

5.1.1 Aims of Study

The aim of the current study was to examine if *Plp* knockout and *shiverer* mice exhibited an altered sensitivity to AMPA-induced toxicity *in vivo* compared with their wild type counterparts. Axonal damage was assessed in neurofilament and APP immunostained sections. APP immunostaining of *Plp* knockout animals unexpectedly revealed axonal damage in widespread brain areas. To further examine this phenomenon, and to determine that is was not a consequence of the AMPA injection, APP and NF 200 immunostaining was performed on naïve 2, 3, 4 month and 1 year old *Plp* knockout and wild type mice. In addition, the levels of the AMPA receptor subunits GluR1-4 were assessed in *Plp* knockout and wild type mice.

5.2 Methods

5.2.1 Generation of PLP knockout mice, *shiverer* mice and PCR analysis

The *Plp* gene knockout mice were generated by Klugmann et al (1997) at the University of Heidelberg, Germany. A targeting vector, under the control of the herpes simplex virus (HSV) promoter, was designed to disrupt the *Plp* gene. This was introduced into R1 embryonic stem cells by electroporation, together with the *thymidine kinase* gene, also under the HSV promoter, to select against random vector insertion. Cells containing the *Plp* gene-null allele were microinjected into blastocyts from C57BL/6J mice. Plp +/- heterozygote females were crossed with wild type C57/BL/6J males to give wild type (+/y) and *Plp* knockout (-/y) male offspring. *Shiverer* mice, that lack MBP due to a naturally arising mutation, were maintained on the C3H/101 strain. These mice were donated by K-A Nave. All mice were maintained and bred at the Parasitology Unit, University of Glasgow Veterinary school. *Plp* knockout mice and *shiverer* mice were identified by Polymerase Chain Reaction (PCR) genotyping using DNA extracted from tail biopsies as described previously (Thomson *et al.*, 1999). Dr Julia Edgar performed all PCR genotyping and tail biopsies.

5.2.2 Examination of axonal damage in naïve *Plp* knockout and wild-type animals from different age groups

Wild-type or *Plp* knockout mice were placed in a perspex chamber with increasing levels of CO_2 for 5 minutes, then 0.9% saline followed by 4% paraformaldehyde was administered transcardially. Perfuse fixation of the naïve mice was performed by Dr Julia Edgar, whilst subsequent tissue processing, sectioning, immunostaining and analysis was performed by myself. The different age groups examined were: 2 month old (PLP knockout, n=2; wild-type, n=2), 3 month old (PLP knockout, n=3; wild type n=3), 4 month old (PLP knockout, n=1; wild-type, n=1) and 1 year old (PLP knockout, n=1; wild-type, n=1). Coronal sections were taken from eight levels throughout the brain, corresponding with the anatomical landmarks at the following levels (relative to Bregma in mm) from the stereotaxic atlas of Paxinos and Franklin, 1997: 1.98, 1.1, 0.14, -0.58, -1.06, -1.7, -3.08, -3.88. Sections from each level were stained with H & E for histological assessment, and immunostained using antibodies raised against NF 200 and APP to examine axonal pathology. The extent and degree of axonal pathology in the three month old *Plp* knockout and wild type mice was characterised at each coronal level using a scoring system described in Figure 5.1 and 5.2.

5.2.3 Stereotaxic injection of AMPA

Three month old male wild-type (n=7) or *Plp* knockout mice (n=6) (26-32g); and three month old male *shiverer* (n=5) or wild type mice (n=6) (23-33g) received stereotaxic injection of AMPA (1.5nmol) into the caudate nucleus as previously described (Section 2.3.1). Twenty-four hours later, animals were perfuse-fixed with saline (0.9%) then paraformaldehyde (4%); post-fixed, processed and paraffin embedded (section 2.3.2).

5.2.4 Histology, immunostaining and quantification of damage following stereotaxic injection of AMPA

Twenty coronal sections (6μm) from every forty sections cut were retained on poly-L-lysine slides (2 sections per slide) for histology and immunostaining. One slide from each cycle was stained with H & E to examine neuronal perikaryal damage (section 2.6.1), and adjacent sections were immunostained using antibodies raised

against phosphorylated NF 200 and APP to examine axonal pathology (2.5.5). Quantification of axonal and neuronal damage is outlined in section 2.5.9 and 2.6.4. The rostral and caudal limit for integration of the lesion induced by AMPA were 2.8mm and –4.26mm respectively, from Bregma in the *Plp* knockout or wild type mice. The rostral and caudal limit for integration of the lesion induced by AMPA in the *shiverer* or wild type mice was 2.22mm and –3.16mm respectively, from Bregma. AMPA also induced neuronal and axonal damage in anatomical areas 'distant' from lesion site in certain animals. This distant damage, which could be clearly differentiated from the focal lesion induced by AMPA was not included in the volumetric quantification of damage.

5.2.5 Quantification of AMPA receptor subunits GluR1-4 in *Plp* knockout and wild type mice

Whole mouse brains from postnatal day 20 *Plp* knockout (n=3) or wild-type mice (n=3) were homogenised, then a membrane-enriched fraction was prepared by Dr Mark McLaughlin as described in section 2.8.1. The protein content of the homogenates was determined using a BCA protein assay (section 2.8.2), then samples underwent SDS-PAGE electrophoresis (section 2.8.3). All samples were loaded onto the mini-gel apparatus together with colour markers of known molecular weights, to ensure that the protein bands detected were of the correct molecular weight. The separated proteins were then transferred onto a PVDF membrane using western blotting (section 2.8.4), and levels of GluR1, GluR2, GluR2/3, GluR4 and actin were detected using the appropriated antibodies, as outlined in table 2.3 Antibody detection was performed using enhanced chemiluminescence, and the optical density of the bands was quantified using Scion Image for windows (Scion Corporation).

5.2.6 Statistics

All data were analysed for statistically significant differences using unpaired, two-tailed Student's *t* test. Data are presented mean ± SEM.

5.3 Results

5.3.1 NF 200 immunostaining of naïve *Plp* knockout and wild-type mice

White matter tracts in NF 200 immunostained sections from wild type mice appeared to be smooth and uniformly stained. In contrast, in PLP knockout animals, white matter tracts appeared were less uniform, and more interspersed. Axonal swellings were present in several anatomical areas, however the magnitude of the swellings varied between regions. A scoring system was devised to describe these changes (Fig. 5.1, Table 5.1). The anatomical areas that contained the greatest amount of swollen axons were the reticular and dorsolateral thalamic nuclei. No differences were observed in the anatomical incidence and amount of axonal swellings in *Plp* knockout mice aged 2, 3 or 4 months. There appeared to be a greater number of axonal swellings, which also appeared to be larger, in the 12-month-old PLP knockout mouse, particularly in all parts of the cerebral cortex and in the superior colliculus. In contrast, axonal swellings were rarely observed in the wild type mice of any age.

5.3.2 APP immunostaining of naïve *Plp* knockout and wild-type mice

APP immunostained sections from wild type mice exhibited a diffuse, low level of staining. In contrast, APP immunopositive axons, which were swollen and bulbous like, were evident in several anatomical areas in the brains of naïve PLP knockout mice. The magnitude of the axonal swellings varied in different anatomical areas. The anatomical incidence and magnitude of the axonal swellings evident in APP immunostained sections is shown in table 5.1 using the scoring system described in figure 5.2. The anatomical areas that contained the greatest amount of axonal swellings were: the anterior commissure, internal capsule (dorsal section), fimbria, stria terminalis, and the reticular and dorsolateral thalamic nuclei. No difference was observed in the anatomical incidence or magnitude of damaged axons between mice aged 2, 3 or 4 months. Whilst the anatomical areas that contained APP immunopositive axons did not differ in the *Plp* knockout mouse aged 12 months, the amount of damaged axons within each area increased, and furthermore, some axons appeared to have larger swellings when compared with the younger mice. Axonal swellings were only rarely observed in wild type mice of any age.

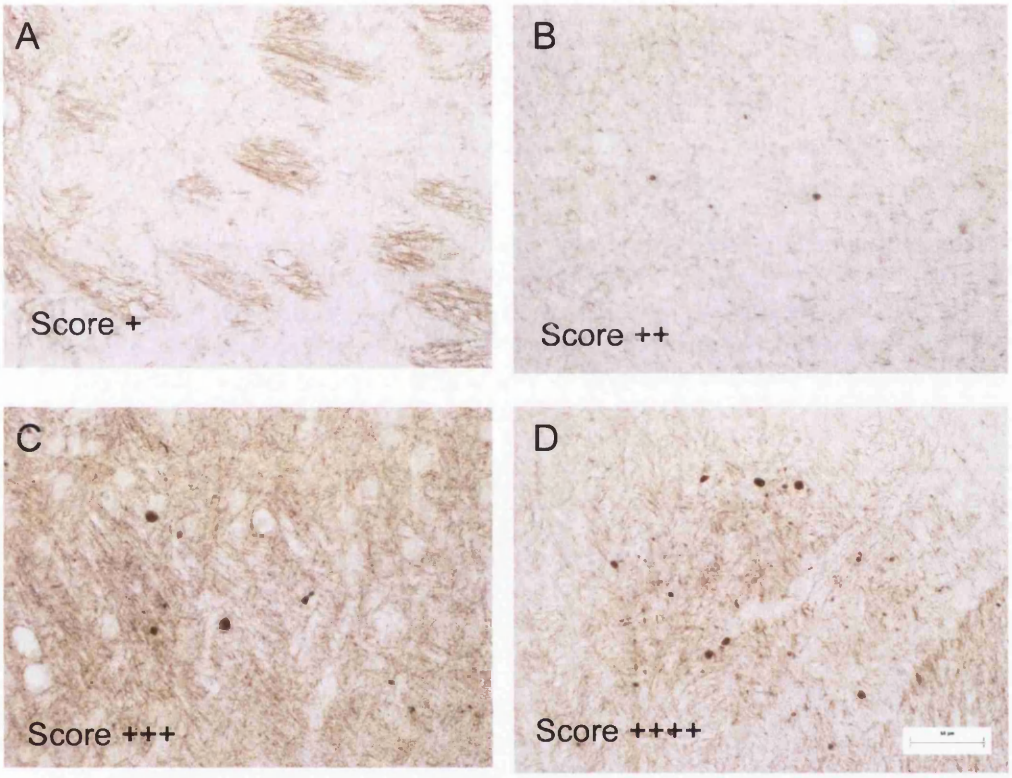

Figure 5.1 NF 200 immunoreactivity in the brains of naive *Plp* knockout mice: method of scoring

Anatomical areas were assigned a score depending on the amount of damaged axons observed. The score ranged from +, where only occasional axonal swellings were observed, to ++++, where axonal swellings were abundant. Scale bar = 50μm.

(A) Caudate nucleus (+)

(B) Sensory Motor Cortex (++)

(C) Superior Colliculus (+++)

(D) Dorsolateral Thamalmic Nuclei (++++)

Anatomical Area		NF 200	APP
Cortex	Sensory Motor	++	+
	Parietal	++	+
	Cingulate: Anterior	+	+
	: Posterior	++	+
Caudate Nucleus	Caudal	+	+
	Rostral	++	++
Corpus Callosum		++	+++
External Capsule		++	+++
Anterior Commissure		++	++++
Globus Pallidus		++	++
Internal Capsule		++	++++
Optic Tract		++	++
Thalamic Nuclei	Anteroventral	+++	++
	Dorsomedial	+	+
	Dorsolateral	++++	++++
	Reticular	++++	++++
	Ventrolateral	+	+
Stria Terminalis		++	++++
Fimbria		+++	++++
Hippocampus		++	++
Lateral Habenula		++	++
Substantia Nigra		+++	+
Superior Colliculus: Deep Gray layer		+++	+
Superior Colliculus: Other layers		++	+

Table 5.1 The anatomical presence and extent of axonal swellings observed in *Plp* knockout mice aged three months

The scoring system, explained in figures 5.1 and 5.2, describes the magnitude of axonal swellings in the anatomical areas listed above in both NF 200 and APP immunostained sections.

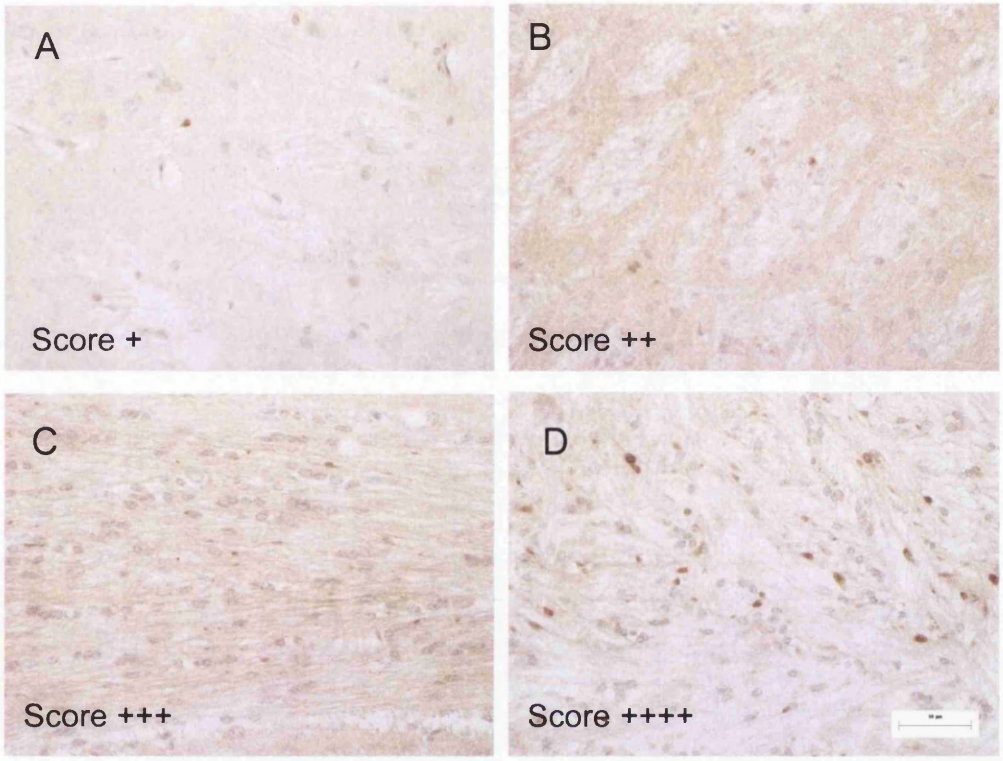

Figure 5.2 APP immunoreactivity in the brains of naive *Plp* knockout mice: method of scoring

Anatomical areas were assigned a score depending on the amount of damaged axons observed. The score ranged from +, where only occasional axonal swellings were observed, to ++++, where axonal swellings were abundant. Scale bar = 50μm.

(A) Caudate nucleus (+)
(B) Globus Pallidus (++)
(C) Corpus Callosum (+++)
(D) Internal Capsule (++++)

5.3.3 Histological staining of naïve *Plp* knockout and wild-type mice

The white matter tracts in all wild type animals appeared uniform, and all oligodendrocyte like cells had a regular spherical appearance, and ran in organised profiles (Fig 5.3A, C, E). In *Plp* knockout animals of all ages, all white matter tracts appeared to be disrupted and less uniform (Fig. 5.3B, D, E). There appeared to be an increase in the number of glial cells within certain white matter tracts in animals aged 4 and 12 months, such as the fimbria, corpus callosum and internal capsule, when compared to the wild type mice. Neurons in *Plp* knockout and wild type animals of all ages appeared to be morphologically normal.

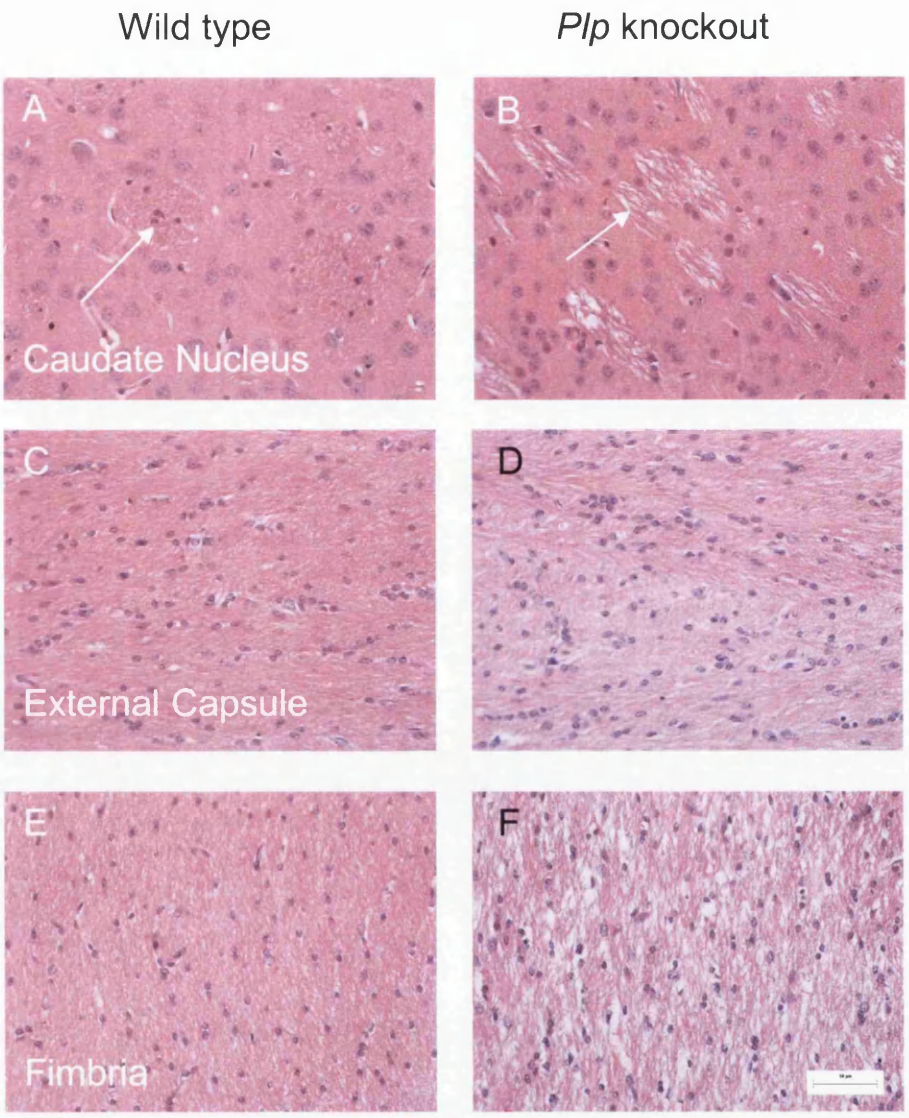

Figure 5.3 Histological staining of naive *Plp* knockout and wild type mice

Representative images from the caudate nucleus (A), external capsule (C) and fimbira (E) of 3 month old wild type mice and *Plp* knockout mice (B, D and F respectively). The arrows in (A) and (B) point to the white matter tracts of the caudate nucleus. Note the perforated apperance of the white matter tracts in *Plp* knockout mice.

Scale bar = 50μm.

5.3.4 Axonal damage assessed in NF 200 immunostained sections following intracerebral injection of AMPA in *Plp* knockout or wild type mice

In the contralateral hemisphere of *Plp* knockout animals, the white matter tracts in NF 200 immunostained sections appeared to be more perforated than white matter tracts in the contralateral hemisphere of wild type mice (Fig 5.4A and 5.4C). Intracerebral injection of AMPA resulted in a disrupted pattern of NF 200 immunostaining, and the presence of axonal swellings in the caudate nucleus in *Plp* knockout and wild type mice. These swellings appeared to be larger near the needle tract, and smaller near the boundary of the lesion. Axonal swellings were also evident in the cortex and external capsule overlying the injection site (Fig. 5.5A). The area of tissue containing damaged axons extended to the globus pallidus, internal capsule and substantia nigra of certain animals (see Table 5.2). As reported in section 5.3.1, axonal swellings are also evident in widespread anatomical areas in NF 200 immunostained sections from naïve *Plp* knockout mice. The anatomical areas that are normally damaged by intrastriatal injection of AMPA (1.5nmol; see chapter 4) generally contained low/intermediate levels of axonal swellings in the naïve PLP knockout brains. This enabled the distinction of axonal damage induced by AMPA from the naturally occurring axonal damage, with continual reference to the contralateral hemisphere. Quantification of the amount of AMPA-induced axonal damage in the NF 200 immunostained sections revealed that *Plp* knockout animals contained significantly less axonal damage compared to wild type animals (Fig. 5.5).

Anatomical Area	Wild Type	*Plp* knockout
Globus Pallidus (ipsilateral)	5 of 7	2 of 6
Internal Capsule (ipsilateral)	5 of 7	1 of 6
Thalamus (ipsilateral)	2 of 7	0 of 6
Thalamus (contralateral)	1 of 7	0 of 6
Substantia Nigra	5 of 7	1 of 6

Table 5.2 Incidence of axonal damage in NF 200 immunostained sections following intrastriatal injection of AMPA in *Plp* knockout or wild type animals

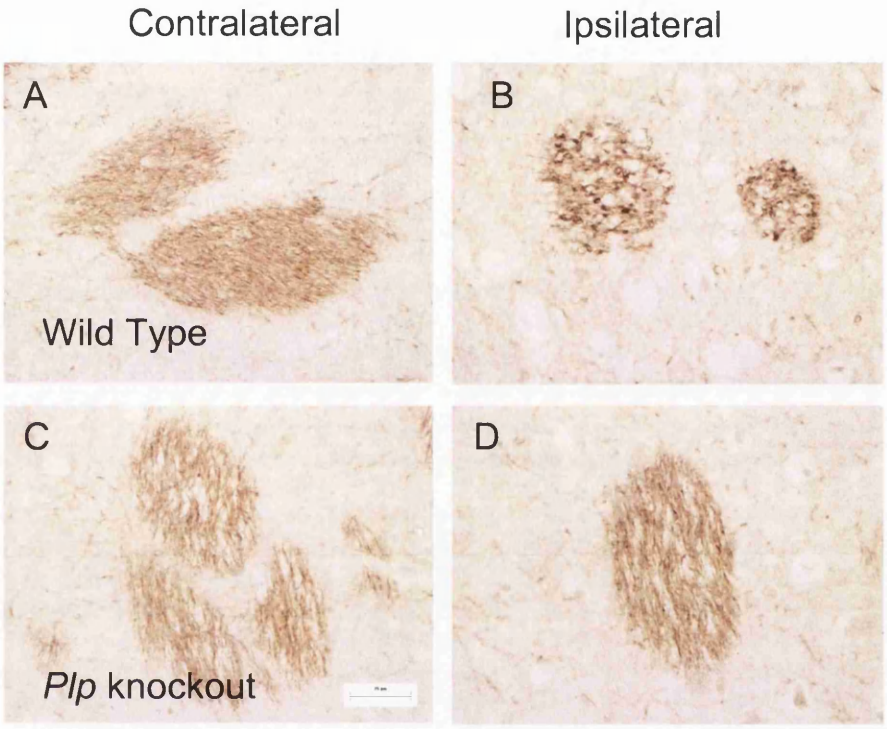

Figure 5.4 NF 200 immunostaining of the caudate nucleus of *Plp* knockout and wild type animals

The white matter tracts of the contralateral caudate nucleus appeared smooth and uniformly stained in wild type animals (A). In contrast, in the contralateral caudate nucleus of *Plp* knockout animals, the axons appeared to be less uniform, and more perforated (C). Axons in the boundary of the lesion in the caudate nucleus of wild type animals appeared disrupted (B). In contrast, an equivalent area of the caudate nucleus of *Plp* knockout did not contain AMPA-induced axonal damage (D).

Scale bar = 25μm.

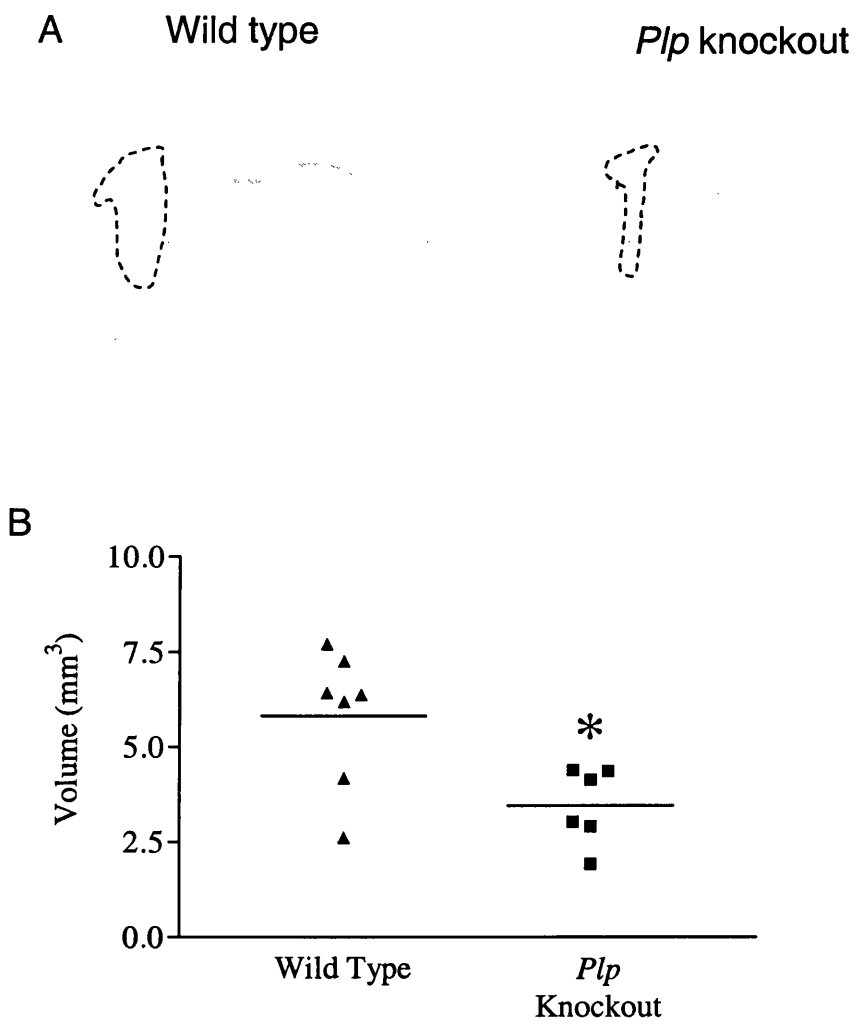

Figure 5.5 Axonal damage quantified from NF 200 immunostained sections in wild type and *Plp* knockout animals following intrastriatal injection of AMPA (1.5nmol)

A. Digitised NF 200 stained sections demonstrating the anatomical extent of axonal disruption and swellings (contained within the dashed line) in a wild type and *Plp* knockout animal.

B. Quantification of the volume of tissue containing axonal damage. *P<0.05 Student's unpaired *t* test.
Bar represents mean of each group.

5.3.5 Axonal damage assessed in APP immunostained sections following intracerebral injection of AMPA in *Plp* knockout or wild type mice

APP immunopositive axons were evident in the caudate nucleus and subcortical white matter following intracerebral injection of AMPA. However, in both *Plp* knockout and wild type mice, this was generally confined to area adjacent to the needle tract (Fig. 5.6A and B). The occurrence of widespread axonal swellings in APP immunostained sections from the brains of *Plp* knockout mice was described in section 5.3.2. However, the injection site (rostral caudate nucleus) rarely contained damaged axons in naïve PLP knockout brains, thus enabling the AMPA-induced lesion to be quantified. There was no significant difference in the amount of AMPA-induced axonal damage quantified from APP immunostained sections in PLP knockout compared with wild type mice (Fig. 5.6B).

5.3.6 Neuronal damage assessed in H & E sections following intracerebral injection of AMPA in *Plp* knockout or wild type mice

Intracerebral injection of AMPA induced the presence of shrunken, eosinophilic neurons in the caudate nucleus and overlying cortex. The lesion extended into the globus pallidus of certain animals (listed in table 5.3). Quantification of the volume of tissue containing neuronal damage showed that there was a reduction in the amount of neuronal damage in PLP knockout animals; however, this did not reach accepted levels of significance (P=0.06, Fig 5.7B). In addition to the focal lesion induced by AMPA, selective, widespread neuronal damage was observed in anatomical areas such as the endopiriform cortex and thalamic nuclei (Table 5.3). However, this was only observed in PLP wild type animals.

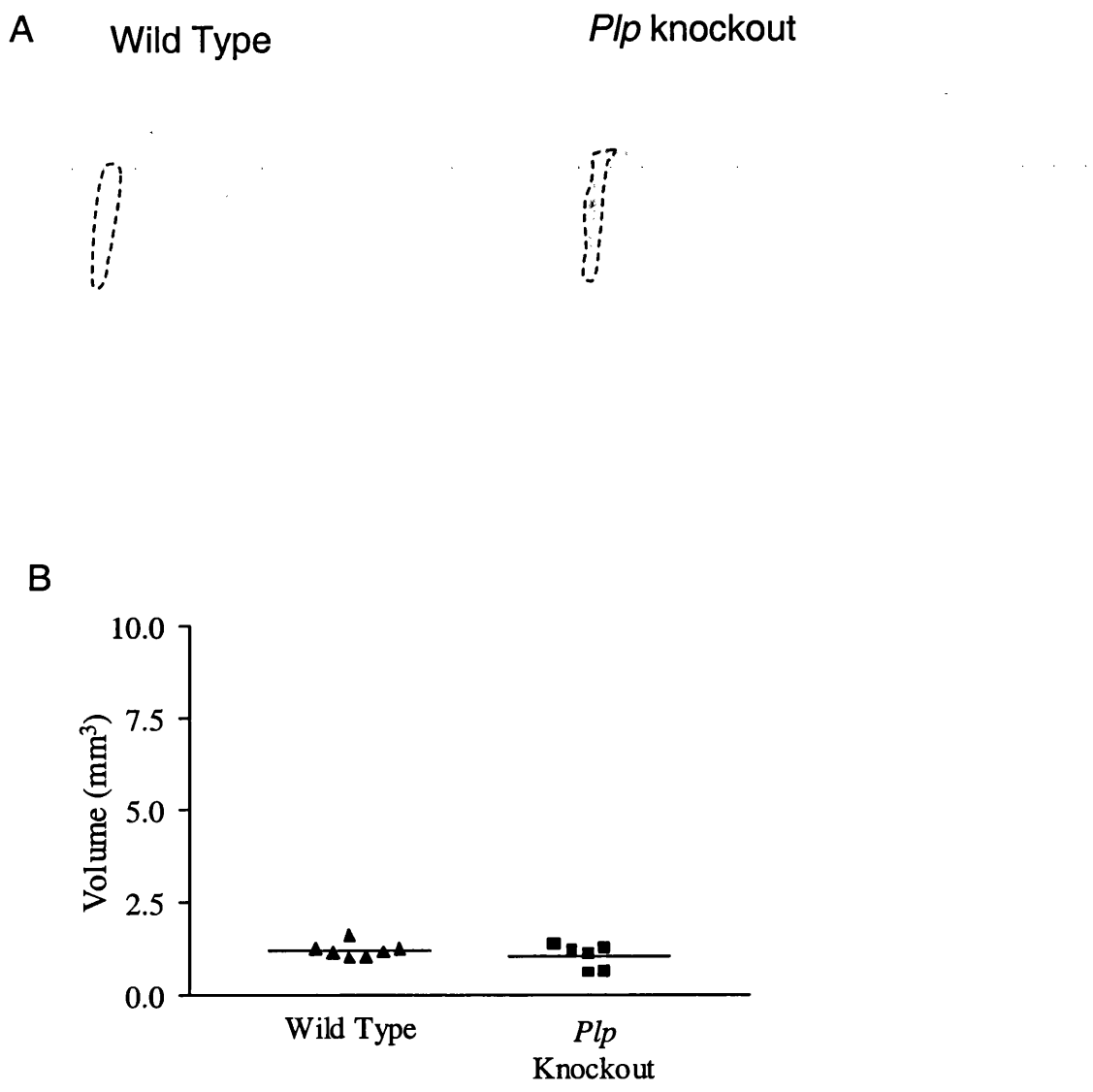

Figure 5.6 Axonal damage quantified from APP immunostained sections in *Plp* knockout and wild type animals following intrastriatal injection of AMPA (1.5nmol)

A. Digitised APP immunostained sections demonstrating the anatomical extent of APP immunopositive swellings (contained within the dashed lines) in a wild type and *Plp* knockout mouse.

B. Quantification of the volume of tissue containing APP immunopositive swellings

P>0.05, Student's *t* test.

Bar represents mean of each group.

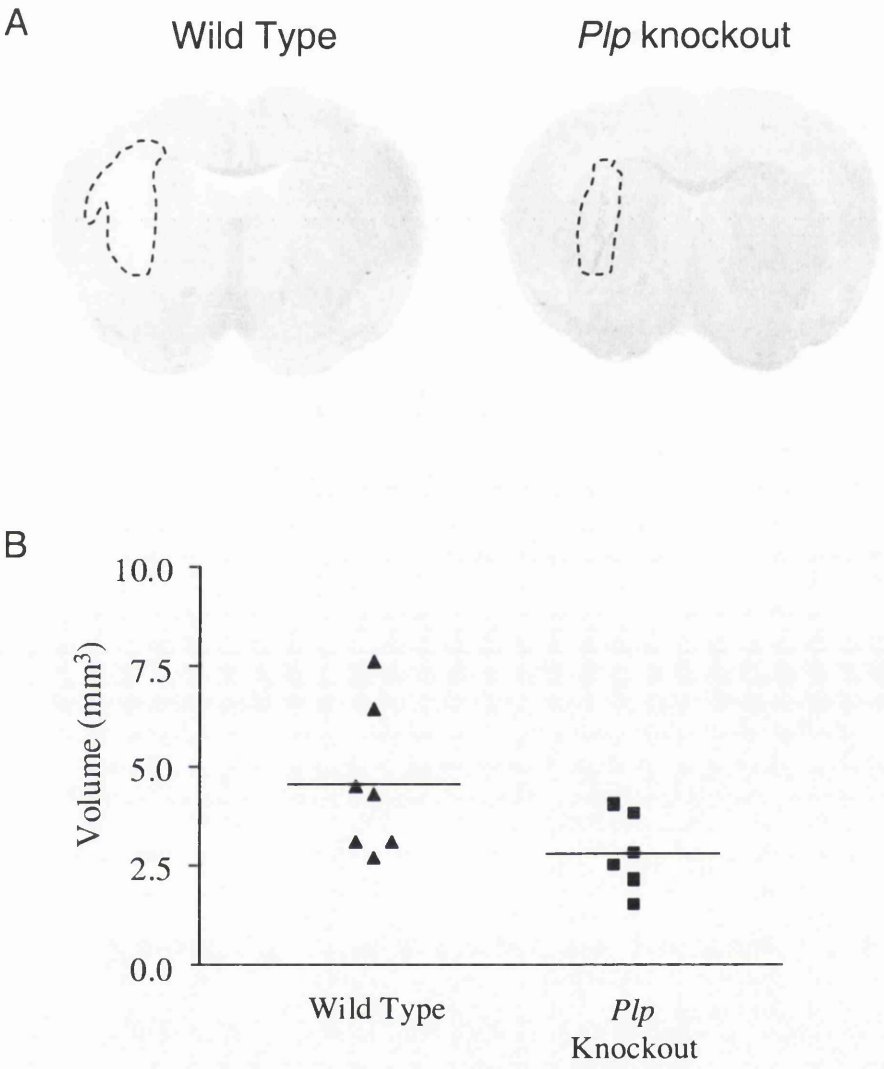

Figure 5.7 Neuronal damage in wild type and *Plp* knockout animals following intrastriatal injection of AMPA (1.5nmol)

A. Digitised H & E stained sections demonstrating the anatomical extent of histological damage in a wild type and *Plp* knockout animal.

B. Neuronal damage is reduced in *Plp* knockout animals compared to wild type animals, however this did not reach accepted levels of significance

P=0.06, Student's *t* test.

Bar represents mean of each group.

Anatomical Area	Wild Type	*Plp* Knockout
Globus Pallidus (ipsilateral)	5 of 7	2 of 7
Thalamus (ipsilateral)	2 of 7	0 of 7
Thalamus (contralateral)	1 of 7	0 of 7
Hippocampus (ipsilateral)	0 of 7	0 of 7
Hippocampus (contralateral)	0 of 7	0 of 7
Amydala (ipsilateral)	0 of 7	0 of 7
Amydala (contralateral)	0 of 7	0 of 7
Endopiriform cortex (ipsi)	3 of 7	0 of 7
Endopiriform cortex (contra)	0 of 7	0 of 7
Piriform cortex (ipsilateral)	1 of 7	0 of 7
Substantia Nigra	4 of 7	2 of 7

Table 5.3 The incidence of selective neuronal damage in widespread brain areas following intrastriatal injection of AMPA in *Plp* knockout or wild type animals.

5.3.7 Levels of GluR1-4 assessed by western blotting in P20 whole brain homogenates from *Plp* knockout or wild type mice

There was no significant difference in the levels of GluR1, GluR2, GluR2/3 or GluR4 in the membrane enriched samples prepared from 20 day old *Plp* knockout or wild type mice (Fig. 5.8 and 5.9). There was no significant difference in the levels of actin detected from the same samples; thus confirming equal loading of the samples (Fig. 5.8, and 5.9).

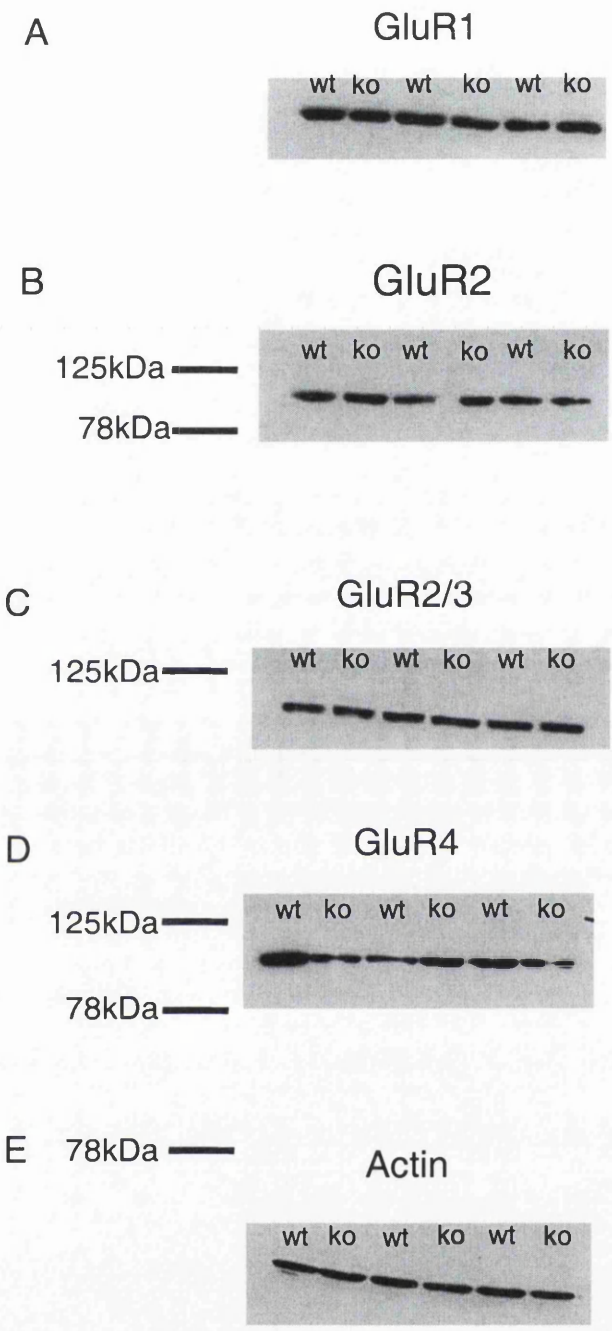

Figure 5.8 Levels of glutamate receptor subunits in wild-type or *Plp* knockout brain homogenates (Post natal day 20)

GluR1 (A), GluR2 (B), GluR2/3 (C), GluR4 (D) and actin (E) immunoreactivity on western blots following gel electrophoresis of *Plp* knockout (ko) or wild-type (wt) mouse brain homogenates. The molecular weights of colour markers included with the samples are indicated on the left hand side.

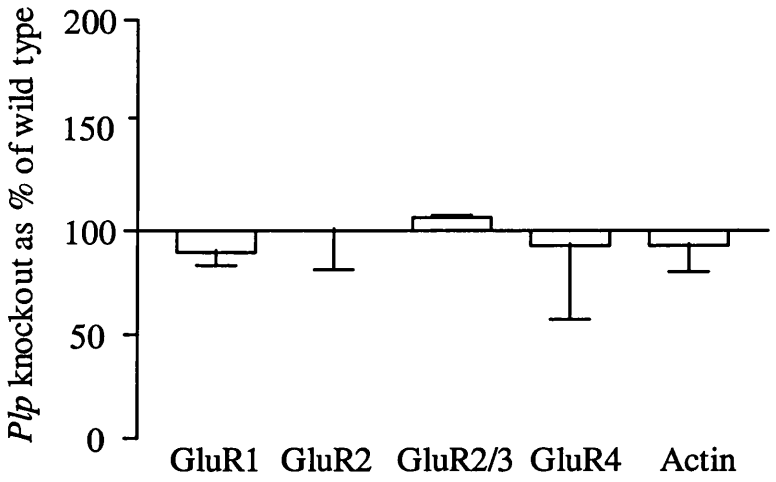

Figure 5.9 Quantification of AMPA receptor subunit levels in *Plp* knockout brains

Quantification of the levels of GluR1-4 in *Plp* knockout mice brains, expressed as a percentage of wild type counterparts. Levels of actin were also detected from the same samples to test for equal loading. There was no significant difference between the levels of GluR1, GluR2, GluR2/3, GluR4 or actin in the brains of the *Plp* knockout or wild type counterpart mice. ($P>0.05$, Students unpaired *t* test, n=3 per group).

5.3.8 Axonal damage assessed in NF 200 immunostained sections following intracerebral injection of AMPA in *shiverer* or wild type mice

In wild type mice, the contralateral hemisphere exhibited a similar pattern of NF 200 immunostaining as previously described for C57 mice (section 4.3.1). In contrast, in the contralateral hemisphere of *shiverer* mice, a rougher, clumped, disrupted pattern of immunostaining was evident. This was most striking in basal forebrain areas such as the substantia innomita and the median forebrain bundle. Other areas such as the internal capsule and substantia nigra contained an irregular, clumped pattern of immunostaining when compared with wild type mice. The contralateral caudate nucleus exhibited very subtle alterations in NF 200 immunoreactivty when compared with wild type mice, appearing slightly rougher (Fig. 5.10A, C). Following intracerebral injection of AMPA, quantification of the volume of axonal damage in NF 200 immunostained sections revealed that there was a slight increase in *shiverer* mice compared to wild type, however this did not reach accepted levels of significance (Fig. 5.11). There was also an increase in the amount of axonal damage in 'distant' brain areas (table 5.4).

Anatomical Area	Wild Type	*shiverer*
Globus Pallidus (ipsilateral)	2 of 6	3 of 5
Internal Capsule (ipsilateral)	2 of 6	3 of 5
Thalamus (ipsilateral)	1 of 6	2 of 5
Thalamus (contralateral)	0 of 6	0 of 5
Substantia Nigra	2 of 6	3of 5

Table 5.4 Incidence of axonal damage in NF 200 immunostained sections following intrastriatal injection of AMPA in wild type or *shiverer* animals

5.3.9 Axonal damage assessed in APP immunostained sections following intracerebral injection of AMPA in *shiverer* or wild type mice

Intracerebral injection of AMPA induced the appearance of APP immunopositive axons in the caudate nucleus and overlying external capsule. However, in both *shiverer* and wild type mice, this was generally confined to area adjacent to the needle tract (Fig. 5.11A). There was no significant difference in the amount of AMPA-induced axonal damage quantified from APP immunostained sections in *Plp* knockout compared with wild type mice (Fig. 5.11B).

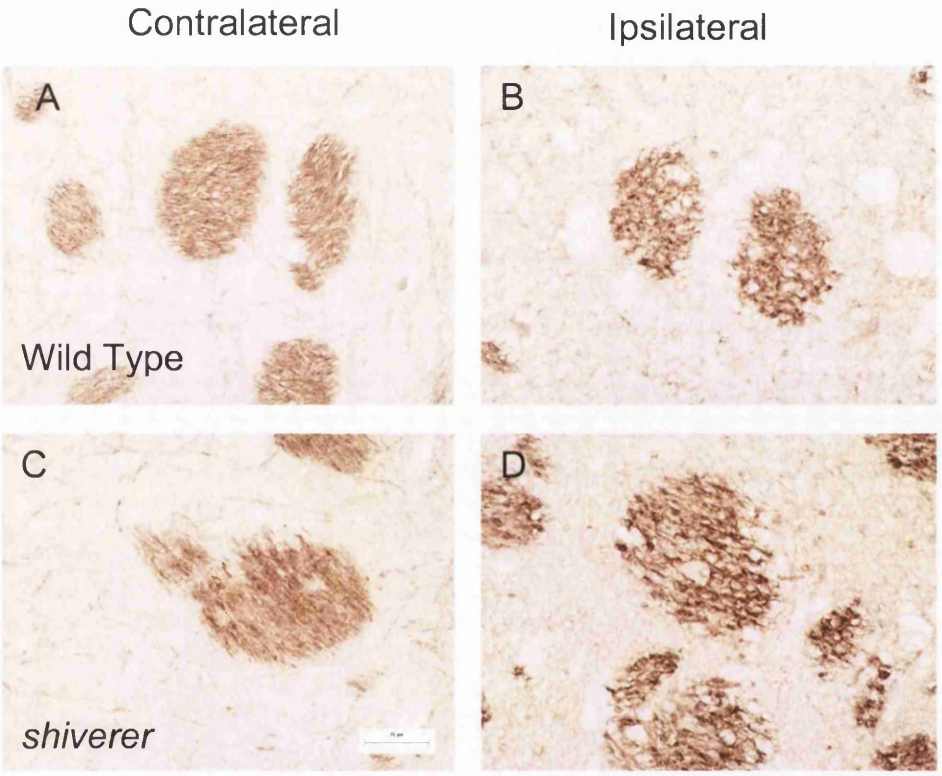

Figure 5.10 NF 200 immunostaining in the caudate nucleus of wild type and *shiverer* mice

White matter tracts in the hemisphere contralateral to the injection site appeared smooth and uniform in wild type mice (A), but slightly more disrupted and clumped in *shiverer* mice (C). In the boundary of the AMPA-induced lesion, swellings and a disrupted pattern of NF 200 immunostaining were evident in both wild type and *shiverer* mice.

Scale bar = 25μm.

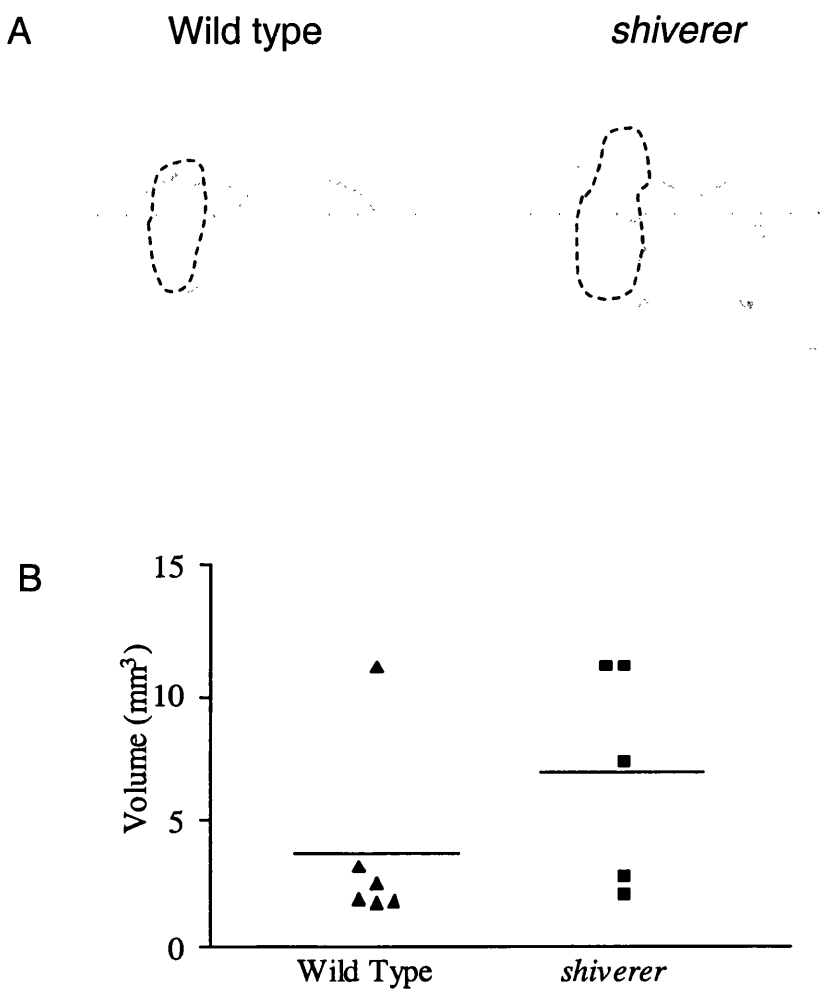

Figure 5.11 Axonal damage quantified from NF 200 immunostained sections in wild type and *shiverer* mice following intrastriatal injection of AMPA (1.5nmol)

A. Digitised NF 200 immunostained sections demonstrating the anatomical extent of axonal swellings (contained within the dashed line).

B. Quantification of the volume of tissue containing axonal damage. P>0.05, Student's unpaired *t* test.
Bar represents mean of groups.

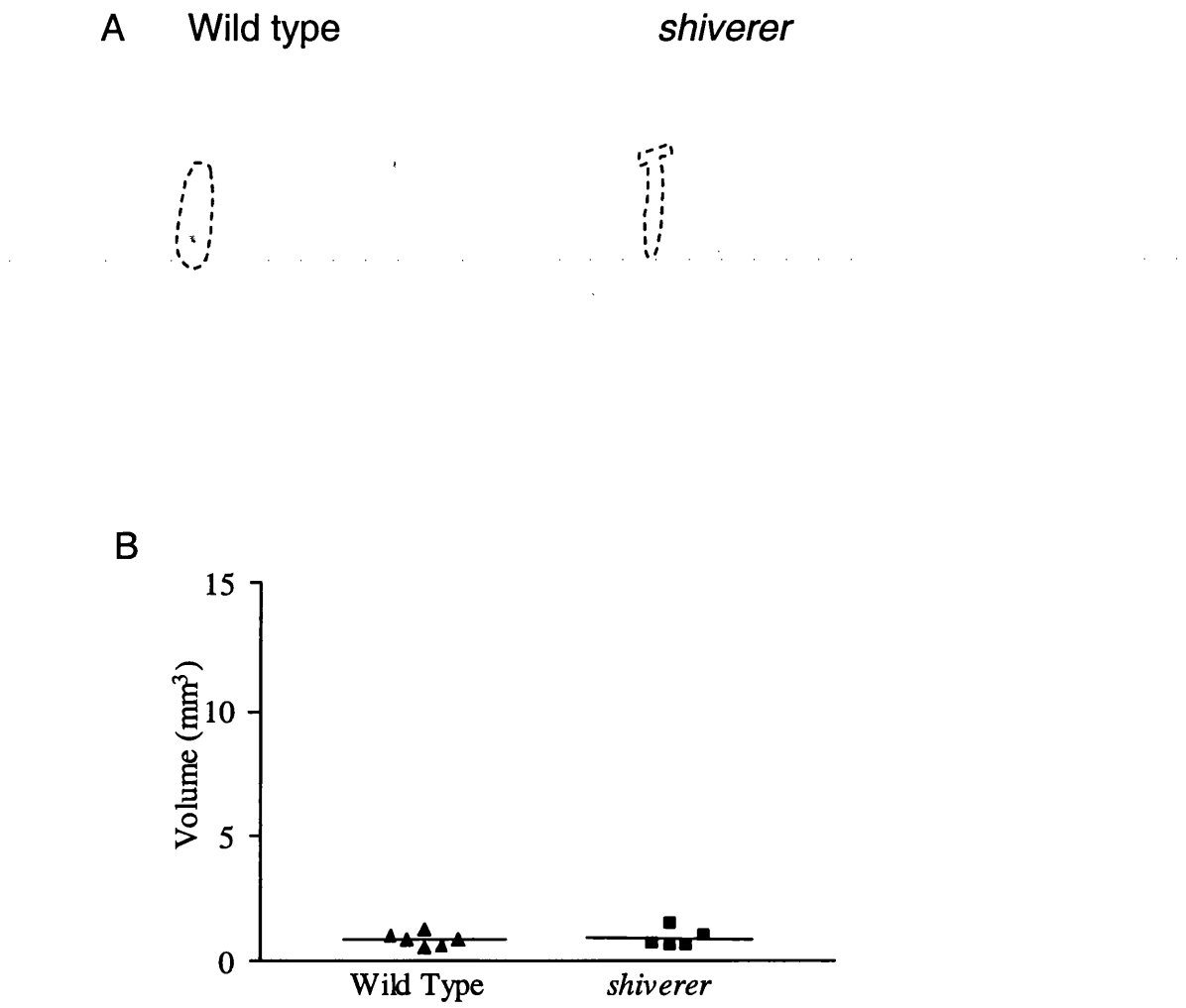

Figure 5.12 Axonal damage quantified from APP immunostained sections in wild type and *shiverer* mice following intrastriatal injection of AMPA (1.5nmol)

A. Digitised APP immunostained sections demonstrating the anatomical extent of axonal damage in wild type and *shiverer* mice. Tissue containing APP immunopositive swellings is contained within the dashed line.

B. Quantification of the extent of axonal damage in the APP immunostained sections. P>0.05, Sudent's unpaired *t* test. Bar indicates mean of each group.

5.3.10 Neuronal damage assessed in H & E stained sections following intracerebral injection of AMPA in *shiverer* or wild type mice

Quantification of neuronal damage revealed that there was no significant difference between *shiverer* and wild type mice following intracerebral injection of AMPA. Similarly, analysis of selective neuronal damage in widespread brain areas induced by AMPA revealed that there were no striking differences between *shiverer* and wild type mice.

Anatomical Area	Wild Type	*shiverer*
Globus Pallidus (ipsilateral)	2 of 6	3 of 5
Thalamus (ipsilateral)	2 of 6	2 of 5
Thalamus (contralateral)	0 of 6	1 of 5
Hippocampus (ipsilateral)	0 of 6	0 of 5
Hippocampus (contralateral)	0 of 6	0 of 5
Amydala (ipsilateral)	0 of 6	2 of 5
Amydala (contralateral)	0 of 6	0 of 5
Endopiriform cortex (ipsi)	2 of 6	2 of 5
Endopiriform cortex (contra)	0 of 6	0 of 5
Piriform cortex (ipsilateral)	1 of 6	1 of 5
Substantia Nigra	2 of 6	3 of 5

Table 5.5 The incidence of selective neuronal damage in widespread brain areas following intrastriatal injection of AMPA in *shiverer or* wild type animals.

A Wild Type *shiverer*

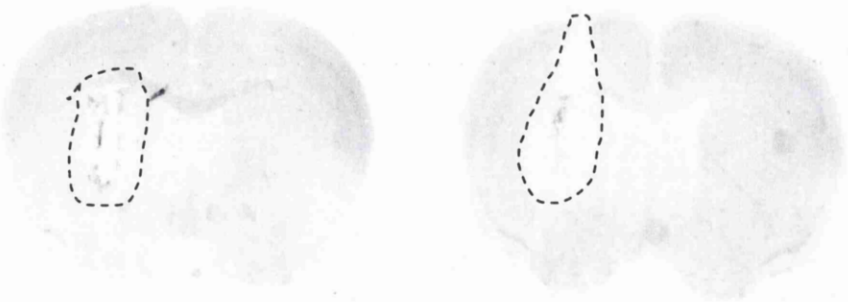

B

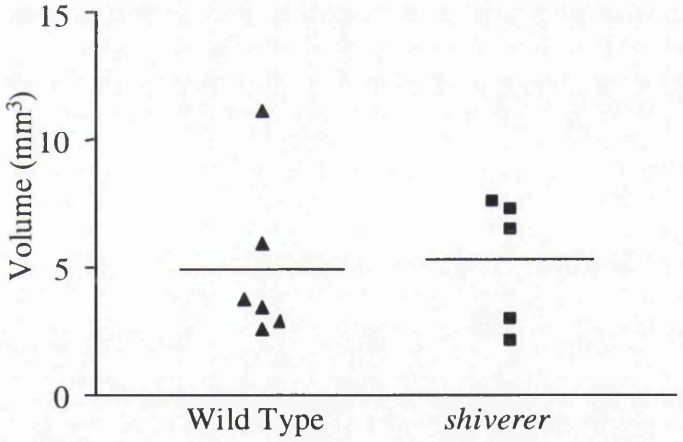

Figure 5.13 Neuronal damage in wild type and *shiverer* animals following intrastriatal injection of AMPA (1.5nmol)

A. Digitised H & E sections demonstrating the anatomical extent of histological damage in a wild type and *shiverer* animal. The extent of histological damage is contained within the dashed line.

B. Quantification of neuronal damage in wild type and *shiverer* mice. P>0.05, Student's unpaired *t* test.
Bar indicates mean of each group.

5.4 Discussion

To summarise, the immunocytochemical studies deployed here revealed axonal damage in widespread anatomical areas in the brains of naïve *Plp* knockout mice; furthermore, there was a differential distribution of axonal swellings labelled with either APP or NF 200 immunostaining. AMPA-induced axonal damage was attenuated in *Plp* knockout mice compared to wild type mice. This was not associated with a change in the levels of AMPA receptor subunit in naïve *Plp* knockout mice at postnatal day 20. Finally, there was no significant difference in the level of AMPA-induced axonal or neuronal damage in the brains of *shiverer* compared to wild type mice.

Axonal damage in naïve PLP deficient mice

The immunocytochemical methods used to detect axonal damage following intracerebral injection of AMPA revealed the presence of APP and neurofilamentous swellings in widespread brain areas in *Plp* knockout mice. To further examine this phenomenon, and to determine that it was not a consequence of the AMPA injection, the presence of axonal swellings in APP and NF 200 immunostained sections was confirmed in certain anatomical areas of naïve *Plp* knockout mice. The reason for selective vulnerability of axons in particular anatomical areas is unknown. EM studies have revealed that axonal swellings are preferentially localised to small diameter axons, particularly at distal juxtaparanodes (area between node of ranvier and internode) (Griffiths *et al.,* 1998). The distal location of the axonal swellings, and accumulation of mitochondria and dense bodies within the swellings suggested that a deficit in retrograde axonal transport occurs (Griffiths *et al.,* 1998; Garbern *et al.,* 2002); and a series of elegant experiments support this hypothesis. Increased levels of dynein, the motor protein responsible for retrograde transport, are present in 2 month old *Plp* knockout mice (Edgar *et al.,* 2001). Decreased levels of a fluorescent tracer are found in the retina of *Plp* deficient mice following stereotaxic injection into the superior colliculus, when compared with wild type mice (Julia Edgar, personal communication.), suggesting aberrant retrograde transport. The selective vulnerability of the distal juxtaparanode may arise because of the organisation of the cytoskeleton in this region. Microtubules density is increased in small diameter compared to large diameter axons At paranodal regions, the diameter of axons is further reduced, the packing density of NFs is increased, and

phosphorylation of NFs is reduced (Kirkpatrick and Brady, 1999). Thus, the cytoskeletal organisation at certain axonal regions may somehow predispose them to swelling and degeneration in the absence of PLP.

By analogy with the conditions that predispose selective axons to degenerate in ALS, a role for Ca^{2+} binding proteins may account for the selective vulnerability of certain axons in *Plp* knockout mice. Thus, motor neurons that lack expression of the Ca^{2+} binding proteins calbindin and parvalbumin are more vulnerable to degeneration than motor neurons that express these proteins (Alexianu *et al.*, 1994). Immunocytochemical studies would determine if these proteins were associated with degenerating axons in *Plp* knockout mice.

Immunostaining with NF 200 revealed axonal swellings in the brains of *Plp* knockout mice, which is consistent with the presence of neurofilamentous swellings in EM analysis of *Plp* knockout mice (Griffiths *et al.*, 1998). NFs are transported by slow anterograde axonal transport. The presence of APP immunopositive swellings in naïve PLP deficient brains is a novel finding. As APP is predominately associated with fast anterograde transport (Koo *et al.*, 1990), this suggests a defect in fast anterograde transport may also occur in *Plp* knockout mice. Therefore, the neurofilamentous and APP–immunopositive swellings may label axons where slow and fast axonal transport is compromised, respectively. However, levels of kinesin, the motor protein responsible for anterograde transport, are normal at the ages in which APP immunopositive swellings are reported here (Edgar *et al.*, 2001). In addition, there was no difference in the amount of labelled anterograde tracer in the superior colliculus following injection into the retina in *Plp* mice aged four months (Julia Edgar, personal communication). Recent reports have suggested that up to 20% of APP may be transported by retrograde axonal transport (Stamer *et al.*, 2003). Taken collectively, this suggests that accumulation of APP within axons may also be caused by aberrant retrograde axonal transport. Further investigation is required to clarify this phenomenon. For example, it would be interesting to perform double labelling of APP with retrograde or anterograde radioactive tracers. A method that has been described for the ultrastructural visualisation of APP antibodies (Stone *et al.*, 1999) would determine which calibre of axons that APP immunopositive swellings are located in, and whether they were predominately present at the distal juxtaparanode.

Following acute brain injury, axonal swellings are thought to either resolve themselves, or undergo secondary axotomy within hours or days of the injury (Maxwell *et al.*, 1997). Between 1 and 2 weeks following focal cerebral ischaemia, there is a reduction in the amount of APP-immunopositive axonal swellings (Irving *et al.*, 2001). However, the presence of large amounts of APP immunopositive axonal swellings in naïve *Plp* knockout animals, at all ages examined, suggests that these axons probably do not undergo immediate degeneration/axotomy. Instead, the axon may 'suffer the swelling'. Increased expression of APP following traumatic brain injury has been associated with deposits of amyloid-β petitide (Aβ), the hallmark lesion of Alzheimer's disease (Graham *et al.*, 1996; Smith *et al.*, 1999; Stone *et al.*, 2002). However, the absence of plaque formation in *Plp* knockout mice in spite of the presence of large quantities of APP in swollen axons (Julia Edgar, personal communication) suggests that another factor initiated following traumatic brain injury, such as caspase-3 activation (Stone *et al.*, 2002) is required for the formation of Aβ-containing plaques.

AMPA-induced axonal damage is attenuated in Plp knockout mice

The reduction in AMPA-induced axonal damage in *Plp* knockout mice suggests that PLP-mediated interactions between the oligodendrocyte/myelin sheath and the axon may be important for mediating AMPA-induced axonal damage. PLP may act as an ion channel, allowing the flow of ions from glia to axon. In addition, the direct transfer of molecules from glia to axons has been demonstrated in invertebrates, and PLP may play a role in mediating these interactions (de Cozar *et al.*, 1987; Kitagawa *et al.*, 1993; Sheller *et al.*, 1995). Thus, it remains possible that toxic factors or ionic imbalances induced by AMPA at the myelin sheath could be transferred from glia to the axon by PLP-mediated interactions, or via a PLP channel pore. These interactions may not have occurred in the *Plp* knockout mice. However, direct conclusions about the role of glia in mediating AMPA-induced axonal damage cannot be drawn from the current study. Firstly, it remains possible that attenuation of damage evident in *Plp* knockout mice may not be caused directly by *Plp* deficiency, but may arise from another factor. For example, the histological and ultrastructural appearance of PLP deficient white matter is not normal, and lacks the normal apposition of extracellular myelin surfaces that occurs in wild type mice. It may be possible that AMPA injected into the brains of *Plp* knockout mice cannot diffuse in this abnormal white matter as it does in wild type mice. Secondly, a

concomitant reduction in neuronal perikaryal damage also occurs in *Plp* knockout mice following AMPA administration. This suggests that axonal damage evident following AMPA administration may be secondary to changes in the neuronal perikarya. Analysis of the relative contribution of neurons and oligodendrocytes to AMPA-induced axonal damage is extremely complex *in vivo.* It is feasible that neither cellular element is exclusively responsible for mediating AMPA-induced axonal damage, but that they may both contribute to the pathology. Further *in vitro* experiments with *Plp* deficient tissue may clarify this issue. For example, the differential vulnerability of neuronal, oligodendoglial and astrocytes cultures to AMPA toxicity could be determined. It would also be interesting to compare these results with the vulnerability of mixed cultures of neurons and glia to AMPA toxicity. The campenot chamber, which allows the separation of neuronal perikarya from axons and oligodendrocytes, could also be utilised to understand more about axo-glial relationships mediating excitotoxicity in *Plp* knockout mice.

As PLP is predominantly expressed in oligodendrocytes and myelin, it was hypothesised that AMPA-induced axonal damage may have been altered without a concomitant effect on neurons. However, there are a number of means by which PLP could influence neurons. PLP RNA is expressed in a population of oligodendrocyte progenitor cells (OPCs; Mallon *et al.,* 2002). Recent data has shown that GluR2 and the glutamate receptor interaction protein (GRIP) are co-localised in NG2 expressing OPCs (Stegmuller et al, 2003). Furthermore, OPCs form functional synapses with neurons (Bergles *et al.,* 2000), which are thought to be important for glial-neuronal signalling. Splice variants of PLP have also been localised to the neuronal perikarya of certain neurons, where they have been implicated with modulating neuronal viability (Bongarazone *et al.,* 1999; Boucher *et al.,* 2002). In *shiverer* mice, altered patterns of gene expression occur in the neuronal perikarya, which suggests that there must be a retrograde signalling pathway from glia to neurons (Brady *et al.,* 1999). A similar pathway may allow PLP to influence neuronal perikarya.

As with many chronic neurodegenerative disorders, regardless of the underlying cause of the pathology, it is possible PLP deficiency may initiate a cascade of pathogenic mediators that could contribute to the ensuing damage. If *Plp* knockout mice had exhibited an increased sensitivity to AMPA-induced axonal damage, then it

could be presumed that excitotoxic mechanisms contribute to axonal pathology in these mice. As the opposite was demonstrated in the current study, this argues against a pathogenic role for 'slow' excitotoxicity in *Plp* knockout mice. The reduction in AMPA-induced pathology in *Plp* knockout mice may be related to perturbations in glutamate homeostasis. For instance, there may be a reduction in the amount of AMPA receptors, an increase in the amount of glutamate transporters, or reduced levels of endogenous glutamate release at glutamatergic synapses in *Plp* knockout mice. An extensive down regulation of NMDA receptors occurs in the brainstem of the myelin-deficient rat, a spontaneously occurring *Plp* mutant (Miller *et al.*, 2003). Whilst there was no significant difference in the levels of AMPA receptor subunits in P20 *Plp* knockout mice, the AMPA toxicity studies performed here utilised three-month-old mice. A decrease in the levels of AMPA receptor subunit may occur in three-month-old mice, and therefore further western blotting studies are required to determine this. These should be complimented by immunocytochemical or *in situ* hybridisation investigations, as western blotting experiments with whole brain homogenates may not be sensitive enough to discriminate subtle alterations in the cellular distribution of glutamate receptors in *Plp* knockout or wild type mice. There may be a switch in the Ca^{2+} permeability of AMPA receptors in *Plp* knockout mice, due to differential editing of AMPA receptors, or a switch in AMPA receptor subunit conformation. Electrophysiological studies could be performed to determine if there is a difference in the functional properties of AMPA receptors in *Plp* knockout and wild type mice.

In additions to altered glutamate homeostasis, there are other mechanisms that may account for the reduction in pathology observed in *Plp* knockout mice. Cultured PLP deficient oligodendrocytes survive for a longer time period than PLP expressing oligodendrocyte cultures (Yang and Skoff, 1997), suggesting that lack of PLP may have beneficial effects. The PLP deficient brains may have developed compensatory mechanisms that account for its ability to remain functional despite the great number of axonal swellings present. For example, it is possible that the axonal pathology in *Plp* knockout mice may induce increased levels of reactive oxygen species, and consequently, the mice may have upregulated endogenous anti-oxidant capacities, such as the anti-oxidant superoxide dimutase (SOD) enzymes. As ROS are implicated in the pathogenesis of excitotoxicity, increased levels of endogenous anti-oxidant enzymes would be protective. The immunocytochemical studies in the

naïve *Plp* knockout mice revealed that axons in the injection site, the caudate nucleus, are less vulnerable to axonal swelling than axons in other brain areas, This may be related to increased levels of Ca^{2+} buffering enzymes, such as calbindin. These enzymes may play a role in protection against excitotoxicity, based on the importance of Ca^{2+}-mediated processes in excitotoxicity.

AMPA-induced pathology in shiverer mice

There was no evidence to suggest that *shiverer* mice were more vulnerable to AMPA-induced neuronal damage. However the data does suggest that axons may be more vulnerable to AMPA-induced damage, although this did not reach accepted levels of significance. This may be related to an increased vulnerability of MBP deficient oligodendrocytes/myelin to AMPA-induced toxicity. It would be interesting to compare the volume of oligodendrocyte/myelin damage, assessed with Tau-1 or MBP immunohistochemistry, with the volume of neuronal/axonal damage in the brains of *shiverer* and wild type mice. Again, the vulnerability of mixed or isolated cultures of *shiverer* or wild type neurons, astrocytes and oligodendrocytes and campenot preparations to AMPA-induced toxicity would provide further information about the relative contribution of these cell types to AMPA-induced axonal damage. Axons may be more vulnerable to AMPA-induced toxicity based on their altered architecture in the absence of compact myelin. For example, there is an upregulation of K^+ channels in *shiverer* mice, which suggests that other ion channels may also be upregulated (Wang *et al.,* 1995). This may render the axon more vulnerable to ionic imbalances. There may also be an increased expression of AMPA receptors in white matter, and immunocytochemical studies could be deployed to examine this.

It was originally hypothesised, based on the pro-convulsant properties of AMPA, that it may exacerbate the seizures that are associated with the *shiverer* phenotype. On the contrary however, seizures were not observed in any of the *shiverer* animals injected with AMPA, although a systematic analysis was not performed. This may have been related to the anti-convulsant actions of the anaesthetics used for the surgical procedures. However, seizures were not present at 24 hours, a timepoint when anaesthetic would have been cleared from the CNS. It may be possible that the AMPA-induced neuronal pathology present by this time point had interrupted the anatomical circuitry required for seizure generation. Again, further investigation,

perhaps with vehicle treated animals or sham animals would gain a greater insight into this phenomenon.

In conclusion, the current study suggests that PLP-mediated interactions between the oligodendrocyte/myelin and axons may be important for mediating AMPA-induced excitotoxicity. The focus of the thesis will now move from the toxic potential of glutamate and excitotoxicity, to examining AMPA receptor potentiators, which may have beneficial effects by enhancing glutamatergic transmission.

CHAPTER 6

MAPPING THE FUNCTIONAL EFFECTS OF THE AMPA RECEPTOR POTENTIATOR LY404187 WITH ^{14}C-2-DEOXGLUCOSE AUTORADIOGRAPHY

6.1 Introduction

Activation of AMPA receptors contributes to the induction of long-term potentiation (LTP), which is suggested to be a major neural substrate for the formation and development of learning and memory (Lynch and Baudry, 1984; Morris *et al.,* 1990; Bliss and Collinridge, 1993). Deficits in glutamatergic neurotransmission and AMPA receptor antagonism often result in cognitive deficits (Filliat *et al.,* 1998; Tamminga, 1998; Carlsson *et al.,* 1999; Riedel *et al.,* 1999; Segovia *et al.,* 2001). In contrast enhancing glutamatergic neurotransmission or AMPA receptor-mediated transmission appears to enhance cognition and may therefore be therapeutically beneficial where cognitive function is impaired. As predicted from their ability to enhance LTP *in vivo* (Staubli *et al.,* 1994b), many of these compounds have demonstrated cognitive enhancing effects in rodent models of cognition (Granger *et al.,* 1993, 1996; Staubli *et al.,* 1994a, Thompson *et al.,* 1995; Zivkovic *et al.,* 1995; Hampson *et al.,* 1998).

A novel series of biarylpropylsulfonamide AMPA receptor potentiators have recently been developed (Ornstein *et al.,* 2000), which are highly potent, selective and centrally active (Baumbarger *et al.,* 2001a,b; Gates *et al.,* 2001; Linden *et al.,* 2001; Miu *et al.,* 2001; Vanergriff *et al.,* 2001). LY404187 is a representative compound of this series and these molecules have efficacy in rodent models of depression and cognition (Quirk and Nisenbaum, 2002). These compounds also appear to increase BDNF expression in the hippocampus (Mackowiak *et al.,* 2002). However a detailed analysis of the anatomical basis of AMPA receptor potentiators is not known. *In vivo* 2-deoxyglucose autoradiography is an effective tool for evaluating the functional consequences of central neurotransmitter system manipulation (section 2.7.1).

6.1.1 Aims of Study

The aim of the current study was to determine the effects of the AMPA receptor potentiator LY404187 on cerebral glucose utilisation using ^{14}C-2-deoxyglucose autoradiography, to gain an insight into the specific anatomical sites of action of AMPA receptor potentiators. In addition, to determine if the functional effects of LY404187 occurred through AMPA receptor-mediated mechanisms, the AMPA

receptor antagonist, LY293558, was administered prior to administration of LY404187 (0.5mg/kg) in another group of animals.

6.2 Methods

6.2.1 Surgical Preparation of animals for ^{14}C- 2-deoxyglucose autoradiography

Male Sprague Dawley rats (345-405g, n=38) were anaesthetised, cannulated, and restrained by Professor J. McCulloch according to protocol outlined in section 2.7.2.

6.2.2 Drug Administration and ^{14}C- 2-deoxglucose technique

The AMPA receptor potentiator LY404187 (0.05, 0.5, 5mg/kg) or vehicle (30% ethanol, 35 % hydroxy-propyl-β–cyclodextrin) were administered subcutaneously 15 minutes prior to administration of the ^{14}C-2-deoxyglucose (n=28). Ten animals received intravenous administration of the AMPA receptor antagonist, LY293558 (25mg/kg), dissolved in NaOH and 5.5% glucose solution (final pH 8.5, isotonic solution), 5 minutes prior to subcutaneous administration of the AMPA receptor potentiator, LY404187 (0.5mg/kg) or vehicle. Fifty μCi [^{14}C]-2-deoxyglucose dissolved in 0.5ml of saline (specific activity 51 mCi/mol, Sigma) was administered into the venous catheter at a constant rate for 30 seconds. The subsequent experimental protocol is outlined in section 2.7.3. Local cerebral glucose utilisation was calculated in 52 anatomical brain areas based on the operational equation outlined in section 2.7.1 using an MCID-M4 image analysis system, as described in section 2.7.4.

6.2.3 Statistical Analysis

All 2-deoxglucose data for each anatomical region were analysed for statistical significance by one-way analysis of variance, then *post-hoc* Student's *t*-test. A Bonferroni correction factor of 6 was applied to the probability values, to take into consideration the multiple comparisons between drug treated and control groups.

6.3 Results

6.3.1 Effect of AMPA receptor potentiator LY404187 on physiological parameters

Prior to drug administration, rats were generally inquisitive, with periods of movement and grooming. LY404187 produced no overt changes in this behavioural pattern. In contrast, administration of the AMPA receptor antagonist LY293558 produced sedative affects, reduced motor activity, with a loss of responsiveness to auditory stimuli. This sedative effect continued following the administration of the AMPA receptor potentiator, LY404187. LY404187 produced no significant changes in rectal temperature, blood glucose levels or arterial blood pressure (Table 6.1). There was a transient rise in blood pressure following administration of the AMPA receptor antagonist, LY293558, however this returned to control levels approximately 20 minutes later.

6.3.2 LY404187 and cerebral glucose utilisation

The effects of the AMPA receptor potentiator LY404187 (0.05, 0.5, 5mg/kg) compared with administration of the vehicle are presented in tables 6.2 – 6.6. LY404187 (0.5mg/kg) produced significant increases in glucose utilisation in 28 of the 52 anatomical areas examined. In contrast, LY404187 (0.05 or 5mg/kg) did not produce any significant increases in glucose utilisation, with the exception of the cerebellar cortex, where a significant increase in glucose utilisation was detected following administration of the high dose of LY404187 (5mg/kg). Administration of LY404187 (0.05, 0.5 or 5 mg/kg) did not result in significant decreases in glucose utilisation in any of the anatomical areas studied. The areas in which LY404187 (0.5mg/kg) caused elevations in glucose utilisation included the hippocampus (molecular layer), several of the cortical areas examined (Fig.6.1, 6.5, 6.6, 6.7); the locus coeruleus, median raphe nucleus and the lateral habenula (Fig.6.2. 6.5, 6.8); and the lateral geniculate nucleus, visual cortex and superior colliculus (Fig 6.3). Other brain areas such as the hypothalamus and pons (Fig. 6.4) were relatively unaffected by LY404187 (0.5mg/kg). A hierarchy of responsiveness to LY404187 (0.5mg/kg) in grey matter areas is presented in table 6.7.

		AMPA receptor potentiator LY404187				AMPA receptor antagonist LY293558	
	Time after drug	Vehicle	0.05mg/kg	0.5mg/kg	5mg/kg	LY293558 + Vehicle	LY293558 + LY404187
Rectal Temperature (°C)	0	36.2 ± 0.3	36.7 ± 0.2	36.9 ± 0.2	36.0 ± 0.2	36.4 ± 0.2	36.7 ± 0.4
	10	36.5± 0.3	37.2 ± 0.2	37.0 ± 0.1	37.0 ± 0.2	36.4 ± 0.2	36.5 ± 0.3
	50	36. ± 0.1	37.0 ± 0.2	36.9 ± 0.2	36.7 ± 0.2	36.6 ± 0.3	35.8 ± 0.4
Mean arterial blood pressure (mmHg)	0	136 ± 3	133 ± 8	139 ± 3	136± 3	142 ± 6	141± 1
	10	138 ± 2	138 ± 3	139 ± 3	138 ± 2	152 ± 3**	151 ± 3*
	50	141 ± 1	140 ± 0	140 ± 3	139 ± 3	140 ± 6	144 ± 3
Arterial plasma glucose (mM)	Pre-drug	11 ± 1	11 ± 1	9 ± 1	10 ± 1	10 ± 1	11 ± 1
	15	11 ± 1	12 ± 1	9 ± 1	10 ± 0	10 ± 0	10 ± 1
	50	12 ± 1	15 ± 2	9 ± 1	11 ± 1	10 ± 1	10 ± 1
Number of animals		10	3	7	8	5	5

Table 6.1 Effect of the AMPA receptor potentiator LY404187 on physiological parameters

Data are presented mean ±SEM. No significant difference was detected between vehicle and drug treated groups (P>0.05 one way ANOVA). Time after drug refers to time following administration of the AMPA receptor potentiator, LY404187. *P,0.05, **P<0.01.

	AMPA receptor potentiator LY404187				AMPA receptor antagonist LY293558 (25mg/kg)	
Anatomical area	Vehicle	0.05mg/kg	0.5mg/kg	5mg/kg	LY293558 + Vehicle	LY293558 + LY404187
Primary Visual System						
Visual Cortex (layer IV)	100 ± 4	95 ± 5	117 ± 5*	102 ± 6	63 ± 3 ***	62 ± 6 ***
Lateral Geniculate Body	86 ± 4	91 ± 11	108 ± 4**	86 ± 6	56 ± 2 ***	51 ± 2 ***
Superior Colliculus	85 ± 4	81 ± 4	107 ± 5**	84 ± 4	65 ± 3 *	61 ± 4 *
Primary Auditory System						
Auditory Cortex (layer IV)	152 ± 6	148 ± 12	179 ± 6	151 ± 8	106 ± 12 **	86 ± 7 ***
Medial Geniculate Body	114 ± 5	110 ± 1	137 ± 4*	116 ± 6	82 ± 10 **	75 ± 7 ***
Inferior Colliculus	164 ± 8	157 ± 5	192 ± 6	163 ± 9	101 ± 10 ***	89 ± 6 ***
Superior Olivary Nucleus	121 ± 6	108 ± 3	151 ± 5 **	121 ± 6	84 ± 8 **	83 ± 8 **
Cochlear Nucleus	121 ± 3	123 ± 4	137 ± 8	128 ± 4	105 ± 5	101 ± 5
Number of animals	10	3	7	8	5	5

Table 6.2 Effects of the AMPA receptor potentiator LY404187 on cerebral glucose utilisation in anatomical areas of the visual and auditory system

Data are presented as mean ± SEM (μmol/100g/min)

*P<0.05, **P<0.01, ***P<0.001 for statistical comparison between vehicle and drug treated groups (ANOVA, Students unpaired *t*-test with Bonferroni correction factor of 6).

There was no significant difference between animals pre-treated with the AMPA antagonist LY293558 (25mg/kg) followed by either vehicle or the AMPA potentiator LY404187 (0.5mg/kg)

	AMPA receptor potentiator LY404187				AMPA receptor antagonist LY293558 (25mg/kg)	
Anatomical area	Vehicle	0.05mg/kg	0.5mg/kg	5mg/kg	LY293558 + Vehicle	LY293558 + LY404187
Parietal Cortex						
Layer II/III	89±2	90±6	104±6	89±6	61 ± 3 **	60 ± 4 ***
Layer IV	103±3	101±6	128±6**	105±7	71 ± 1 ***	65 ± 4 ***
Layer V/VI	84±3	88±8	100±5*	84±5	56 ± 2 ***	53 ± 3 ***
Ventral Parietal Cortex (GP)						
Layer II/III	87±3	89±5	107±4***	89±3	59 ±4 ***	59 ± 2 ***
Layer IV	106±4	107±6	137±5***	113±5	71 ± 5 ***	70 ± 2 ***
Layer V/VI	78±3	86±8	96±4**	80±3	54 ± 3 ***	53 ± 2 ***
Sensory Motor Cortex						
Layer II/III	88±3	87±5	107±6*	91±6	61 ± 3 **	58 ± 4 ***
Layer IV	109±4	110±6	136±7**	115±7	72 ± 3 ***	67 ± 5 ***
Layer V/VI	80±3	84±7	98±5*	82±5	53 ± 3 ***	52 ± 4 ***
Frontal Cortex						
Layer II/III	90±4	95±11	106±4	90±5	61 ± 3 ***	60 ± 4 ***
Layer IV	105±4	109±7	136±7**	112±8	67 ± 4 ***	67 ± 3 ***
Layer V/VI	80±4	88±9	99±4*	81±4	52 ± 4 ***	51 ± 3 ***
Prefrontal Cortex	114±6	108±10	135±7	116±6	77 ± 3 **	74 ± 7 **
Anterior Cingulate Cortex	103±3	104±4	130±6***	107±5	71 ± 3 ***	64 ± 5 ***
Number of Animals	10	3	7	8	5	5

Table 6.3 Effects of the AMPA receptor potentiator LY404187 on cerebral glucose utilisation in cerebral cortex areas

Data are presented as mean ± SEM (μmol/100g/minutes)

*P<0.05, **P<0.01, ***P<0.001 for statistical comparison between vehicle and drug treated groups (ANOVA, Students unpaired *t*-test)

There was no significant difference between animals pre-treated with the AMPA antagonist LY293558 (25mg/kg) followed by either vehicle or the AMPA potentiator LY404187 (0.5mg/kg)

	AMPA receptor potentiator LY404187				AMPA receptor antagonist LY293558 (25mg/kg)	
Anatomical area	Vehicle	0.05mg/kg	0.5mg/kg	5mg/kg	LY293558 + Vehicle	LY293558 + LY404187 (0.5mg/kg)
Caudate nucleus, dorsolateral	98 ± 5	96 ± 6	116 ± 3	100 ± 7	68 ± 3 **	65 ± 6 **
Caudate nucleus, ventromedial	83 ±4	83 ± 7	98 ± 3	86 ± 5	66 ± 3	60 ± 4 **
Globus Pallidus	47 ± 3	49 ± 3	57 ± 3*	48 ± 2	34 ± 2 **	33 ± 1 **
Substantia nigra:						
Pars compacta	74 ± 4	68 ± 9	85 ± 3	74 ± 3	59 ±6 *	52 ± 2 **
Pars reticulata	48 ± 2	45 ± 2	53 ± 3	47 ± 2	42± 5	34 ± 2 **
Thalamus:						
Mediodorsal	95 ± 5	101 ± 8	121 ± 4 **	108 ± 8	73 ± 5	69 ± 3 *
Ventrolateral	79 ± 5	83 ± 7	96 ± 4*	77 ± 4	54± 2 **	50± 3 ***
Laterodorsal	113 ± 5	118 ± 10	134 ± 6	113 ± 8	64 ± 3 ***	62 ± 3 ***
Posterior	90 ± 4	96 ± 9	105 ± 3*	90 ± 4	58 ± 3 ***	57 ± 2 ***
Subthalamic Nuclei	84 ± 4	79 ± 5	100 ± 2*	84 ± 5	61 ± 3 **	54 ± 3 ***
Red nucleus	75 ± 4	77 ± 1	86 ± 2	75 ± 4	53 ± 3 ***	51 ± 2 ***
Inferior Olivary Nucleus	78 ± 2	82 ± 6	92 ± 8	78 ± 3	63 ± 5	59 ± 3
Cerebellar cortex	60 ± 2	57 ± 1	73 ± 3***	71 ± 3**	45± 2 ***	44 ± 2 ***
Cerebellar nucleus	87 ±3	90 ± 5	101 ± 4	91 ± 7	72 ± 4	69 ± 5
Vestibular nucleus	105 ± 3	106 ± 5	122 ± 3**	106 ± 4	83 ± 4***	80 ± 2***
Number of Animals	10	3	7	8	5	5

Table 6.4 Effects of the AMPA receptor potentiator LY404187 on cerebral glucose utilisation in extrapyramidal and sensory-motor areas

Data are presented as mean ± SEM (μmol/100g/min)

*P<0.05, **P<0.01, ***P<0.001 for statistical comparison between vehicle and drug treated groups (ANOVA, Students unpaired *t*-test)

There was no significant difference between animals pre-treated with the AMPA antagonist LY293558 (25mg/kg) followed by either vehicle or the AMPA potentiator LY404187 (0.5mg/kg)

Anatomical area	Vehicle	AMPA receptor potentiator LY404187 0.05mg/kg	0.5mg/kg	5mg/kg	AMPA receptor antagonist LY 293558 (25mg/kg) LY293558 + Vehicle	LY293558 + LY404187 (0.5mg/kg)
Hippocampus (stratum lacunosum moleculare)	86 ± 4	88 ± 2	102 ± 2 *	84 ± 3	67 ± 6 **	56 ± 3 ***
Dentate gyrus	68 ± 3	70 ± 1	80 ± 3	66 ± 3	53 ± 5 *	44 ± 3 ***
Lateral habenula	114 ± 4	116 ± 4	137 ± 3 *	129 ± 7	68 ± 5 ***	69 ± 5 ***
Dorsal raphe nucleus	82 ± 4	82 ± 3	99 ± 2 **	85 ± 4	58 ± 2 ***	52 ± 4 ***
Median raphe nucleus	92 ± 5	89 ± 1	106 ± 3	88 ± 5	56 ± 3 ***	51 ± 3 ***
Amydala	42 ± 2	44 ± 4	50 ± 3	43 ± 2	38 ± 1	32 ± 3 *
Septal nucleus	57 ± 3	54 ± 4	65 ± 3	55 ± 3	38 ± 2 **	35 ± 2 ***
Nucleus accumbens	82 ± 4	78 ± 1	93 ± 4	83 ± 4	52 ± 4 ***	50 ± 4 ***
Pons	54 ± 2	50 ± 3	59 ± 2	51 ± 3	39 ± 2 ***	38 ± 3 ***
Locus Coeruleus	65 ±3	68±0	87±4 ***	66±3	50 ± 1 *	49 ± 4 *
Hypothalamus	48 ± 3	46 ± 1	52 ± 4	42 ± 2	35 ± 3 *	31 ± 2 **
Number of Animals	10	3	7	8	5	5

Table 6.5 Effects of the AMPA receptor potentiator LY404187 on cerebral glucose utilisation in anatomical areas of limbic and functionally non-specific areas

Daa are presented as mean ± SEM (μmol/100g/min)

*P<0.05, **P<0.01, ***P<0.001 for statistical comparison between vehicle and drug treated groups (ANOVA, Students unpaired *t*-test with Bonferroni correction factor of 6).

There was no significant difference between animals pre-treated with the AMPA antagonist LY293558 (25mg/kg) followed by either vehicle or the AMPA potentiator LY404187 (0.5mg/kg)

STRUCTURE	AMPA receptor potentiator LY404187				AMPA receptor antagonist LY 293558 (25mg/kg)	
	Vehicle	0.05mg/kg	0.5mg/kg	5mg/kg	LY 293558 + Vehicle	LY293558 + LY404187 (0.5mg/kg)
Internal capsule	30 ± 2	27 ± 4	39 ± 2*	27 ± 2	21± 1*	18 ± 2 **
Corpus callosum	33 ± 2	34 ± 6	35 ± 2	33 ± 2	26 ± 1	24 ± 2*
Genu of the corpus callosum	25 ± 2	23 ± 5	28 ± 2	24 ± 3	21 ± 1	17 ± 1
Cerebellar white matter	27 ± 2	25 ± 3	32 ± 2	27 ± 2	20 ± 1*	18 ± 2*
Number of Animals	10	3	7	8	5	5

Table 6.6 Effects of the AMPA receptor potentiator LY404187 on cerebral glucose utilisation in white matter tracts

Data are presented as mean ± SEM (μmol/100g/min)

**P<0.05, **P<0.01 for statistical comparison between vehicle and drug treated groups (ANOVA, Students unpaired *t*-test with Bonferroni correction factor of 6).

here was no significant difference between animals pre-treated with the AMPA antagonist LY293558 (25 mg/kg) followed by either vehicle or the AMPA potentiator LY404187 (0.5mg/kg)

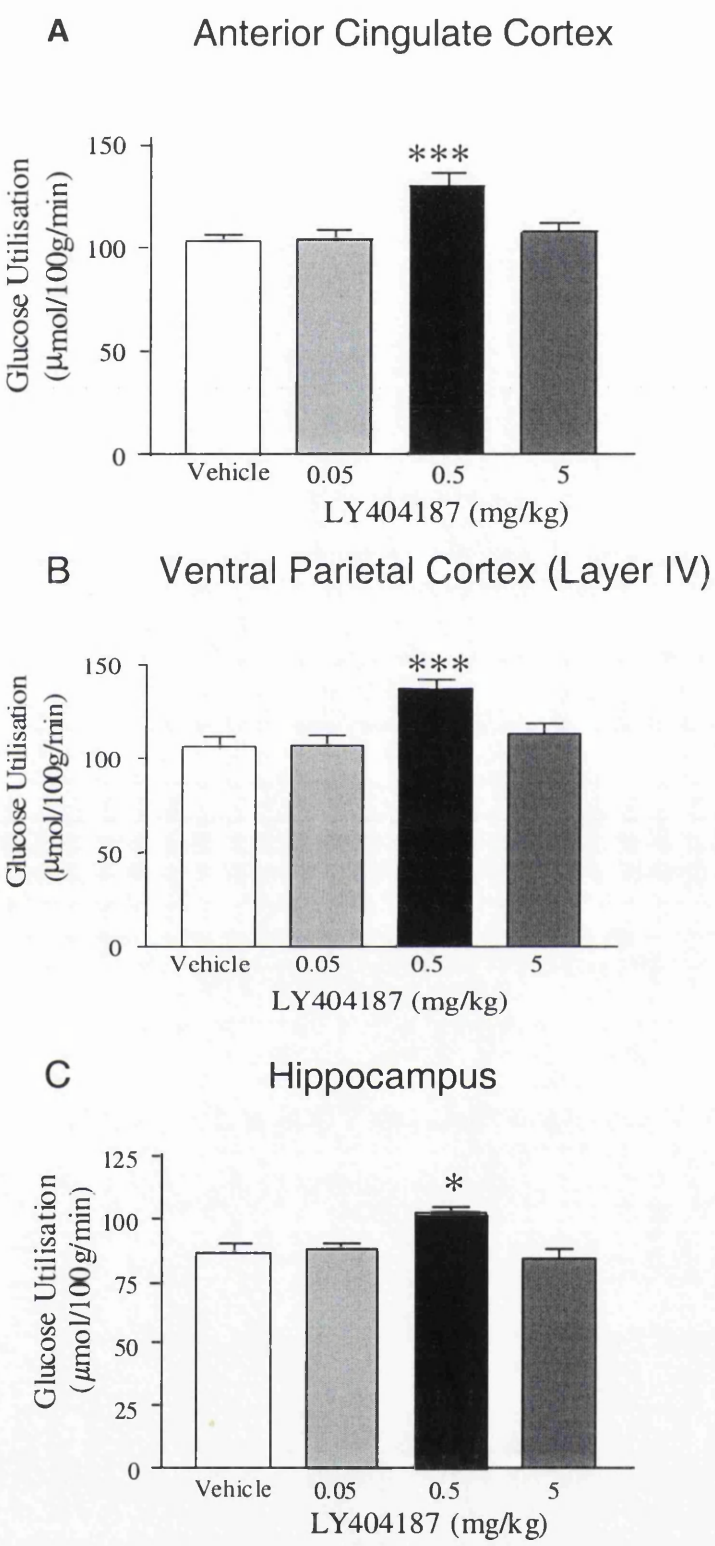

Figure 6.1 The effects of the AMPA potentiator LY404187 on cerebral glucose utilisation in cortical areas and hippocampus

A. Anterior Cingulate Cortex B. Ventral Parietal Cortex (Layer IV)

C. Superior Colliculus

Data are presented as mean ± SEM (n=3-10 per group). *P<0.05, ***P<0.001 for statistical comparison between vehicle and drug treated groups (ANOVA followed by post-hoc Students unpaired *t*-test with Bonferroni correction factor of 6).

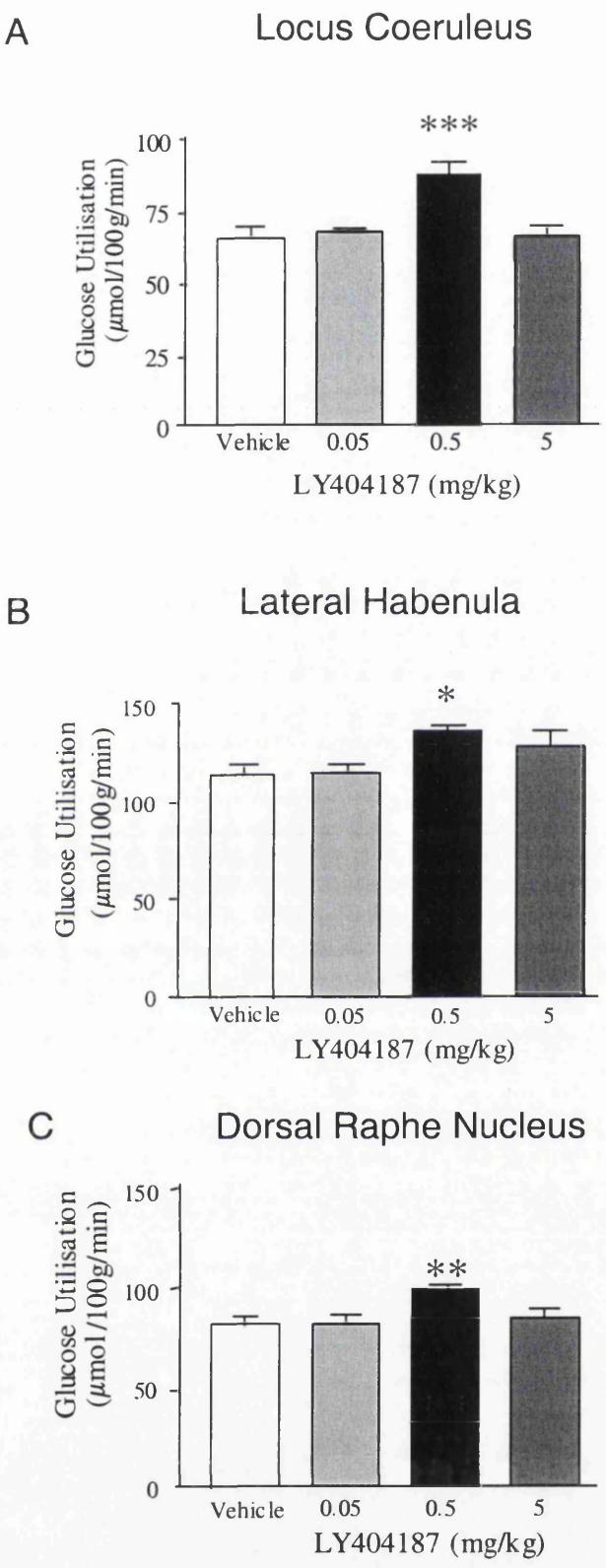

Figure 6.2 The effects of LY404187 on cerebral glucose utilisation in components of the monoaminergic system

A. Locus Coeruleus B. Lateral Habenula C. Dorsal Raphe Nucleus

Data are presented as mean ± SEM (n=3-10 per group). *P<0.05, **P<0.01, ***P<0.001 for statistical comparison between vehicle and drug treated groups (ANOVA followed by post-hoc Students unpaired *t*-test with Bonferroni correction factor of 6).

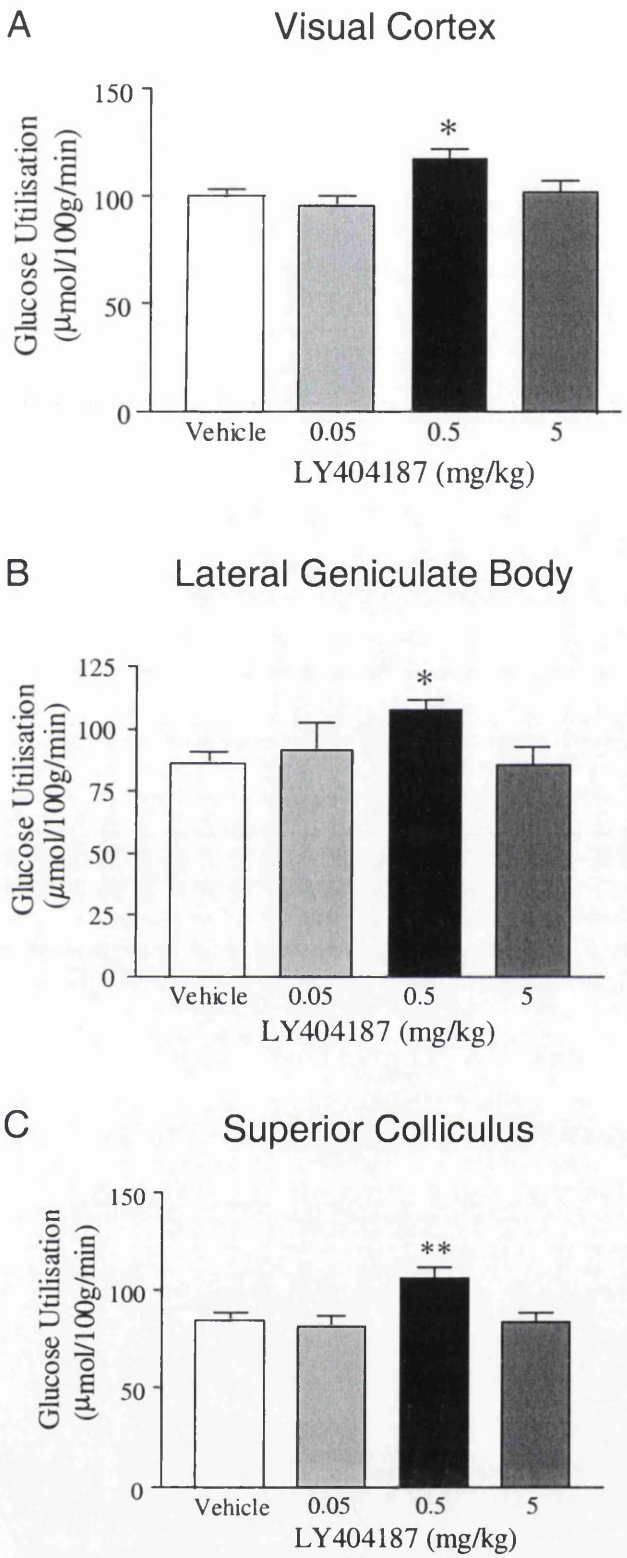

Figure 6.3 The effects of the AMPA potentiator LY404187 on cerebral glucose utilisation in the visual system

A. Visual cortex (layer IV); B. Lateral Geniculate Body;

C. Superior Colliculus

Data are presented as mean ± SEM (n=3-10 per group). *P<0.05, **P<0.01, for statistical comparison between vehicle and drug treated groups (ANOVA followed by post-hoc Students unpaired *t*-test with Bonferroni correction factor of 6).

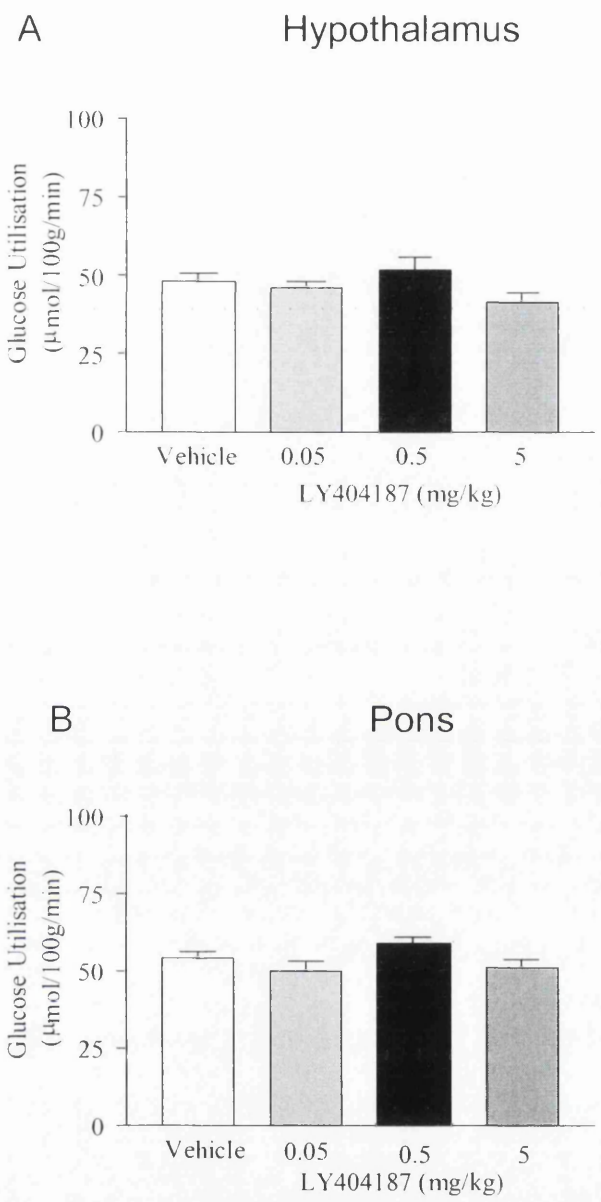

Figure 6.4 The effects of the AMPA potentiator LY404187 on cerebral glucose utilisation in the hypothalamus and pons

A. Hypothalamus B. Pons

Data are presented as mean ± SEM (n=3-10 per group). P>0.05 for statistical comparison between vehicle and drug treated groups (ANOVA followed by post-hoc Students unpaired *t*-test with Bonferroni correction factor of 6).

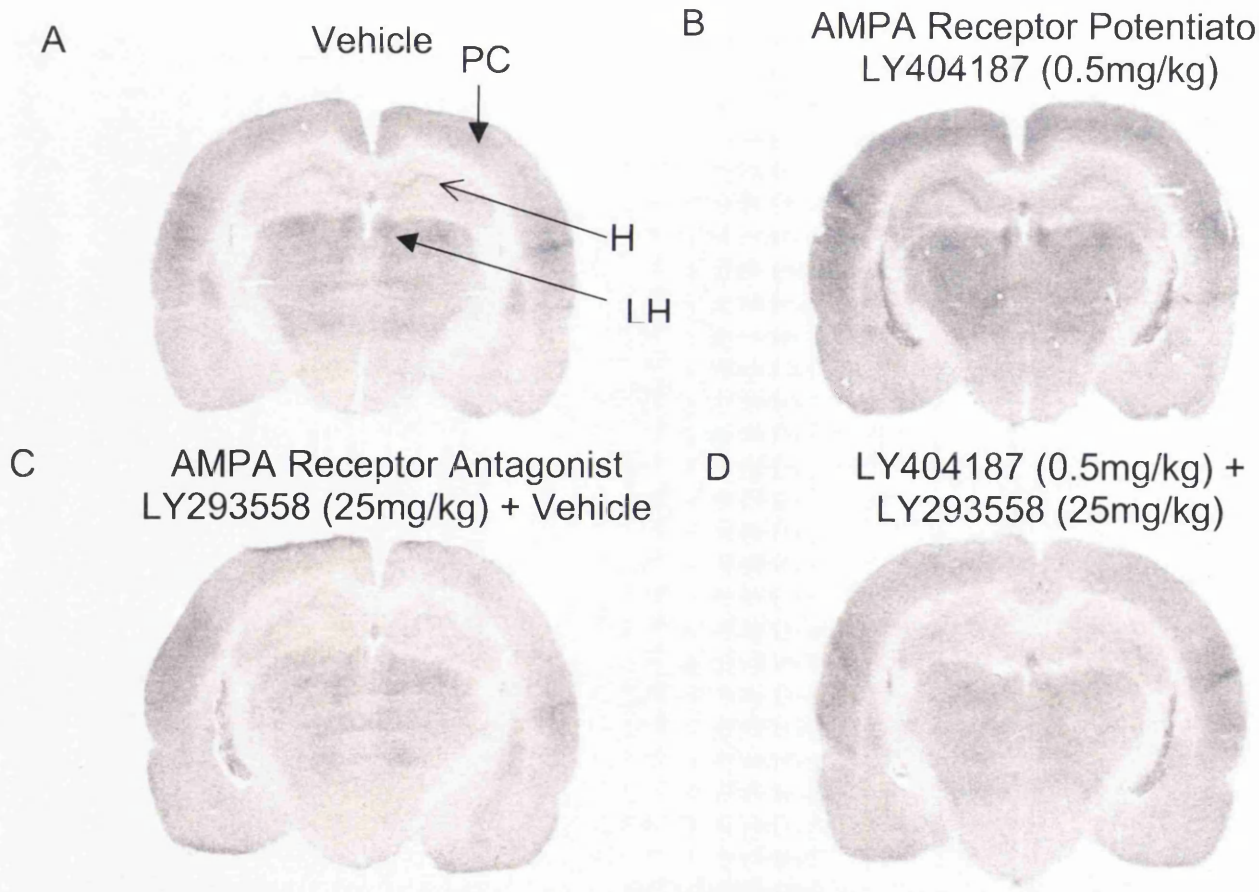

Figure 6.5 Representative autoradiograms illustrating changes in local cerebral glucose utilisation in the hippocampus, parietal cortex and lateral habenulae

Increases in glucose utilisation were evident in the parietal cortex (PC), hippocampus (H) and lateral habenula (LH) following administration of the AMPA receptor potentiator, LY404187 (0.5mg/kg) (B) compared to administration of the vehicle (A). In contrast, administration of the AMPA receptor antagonist, LY293558 (25mg/kg) caused decreases in glucose utilisation in these areas (C). Administration of the AMPA receptor antagonist LY293558 (25mg/kg), prior to administration of the AMPA receptor potentiator, LY404187 (0.5mg/kg) attenuated the effects of this drug on glucose utilisation (D).

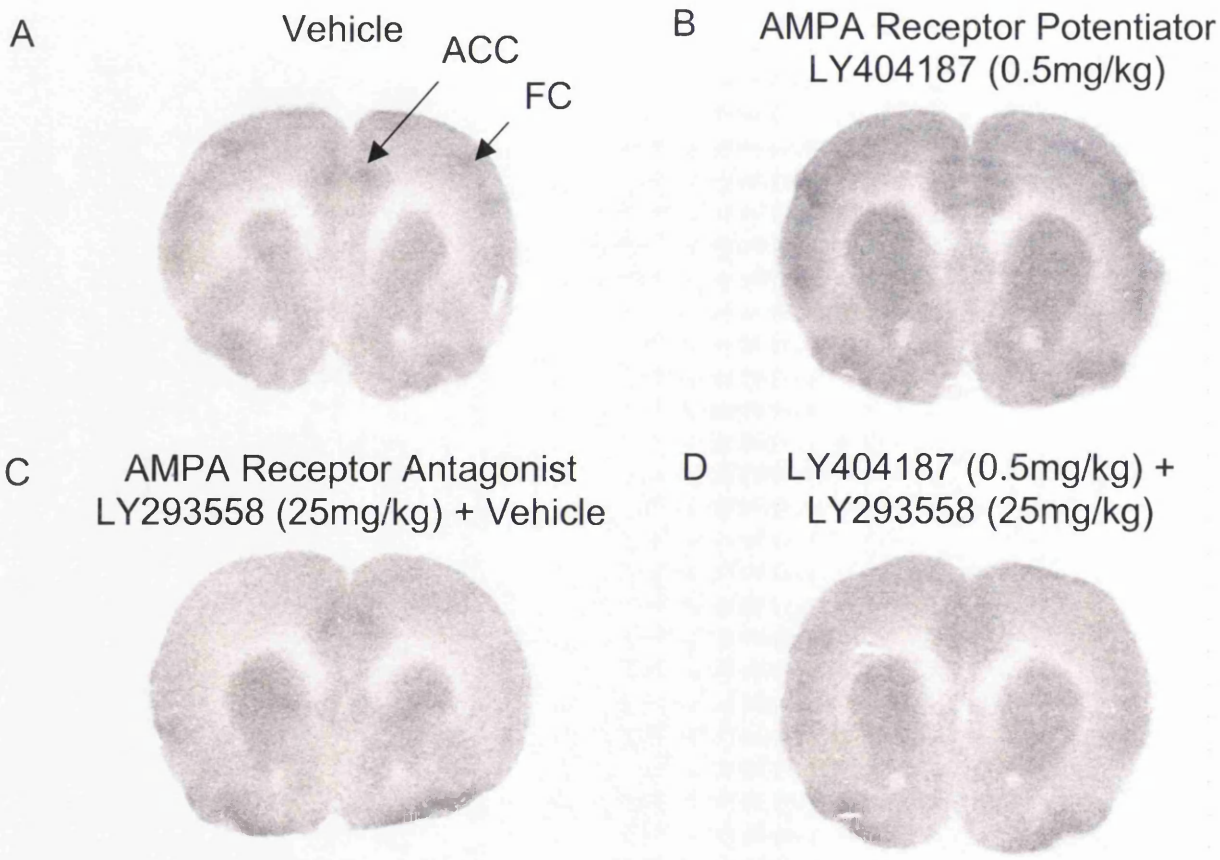

Figure 6.6 Representative autoradiograms illustrating changes in local cerebral glucose utilisation in the anterior cingulate and frontal cortex

Increases in glucose utilisation were evident in the anterior cingulate cortex (ACC) and frontal cortex (FC) following administration of the AMPA receptor potentiator, LY404187 (0.5mg/kg; B) compared to administration of the vehicle (A). In contrast, administration of the AMPA receptor antagonist, LY293558, caused decreases in glucose utilisation in these brain areas (C). Administration of the AMPA receptor antagonist LY293558 (25mg/kg), prior to administration of the AMPA receptor potentiator, LY404187 (0.5mg/kg) attenuated the effects of this drug on glucose utilisation (D).

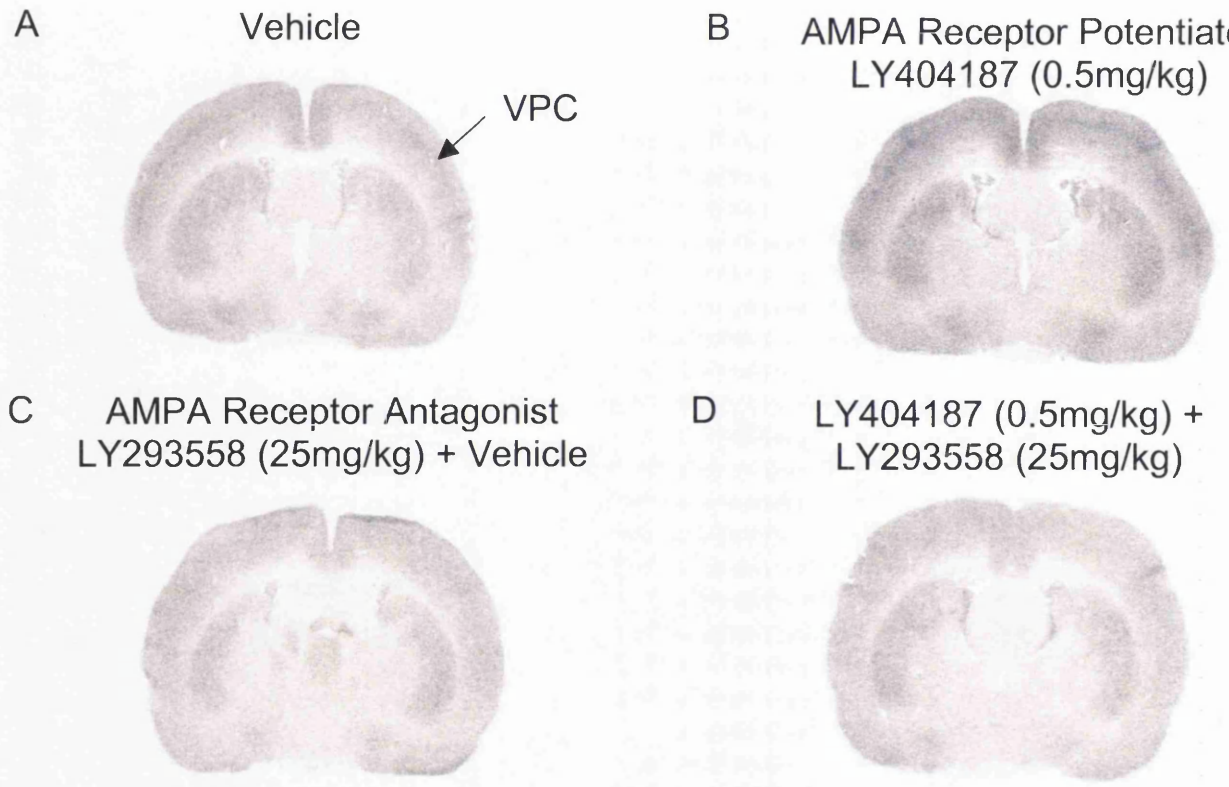

Figure 6.7 Representative autoradiograms illustrating changes in local cerebral glucose utilisation in the ventral parietal cortex (layer IV)

Increases in glucose utilisation were evident in the parietal cortex (VPC) following administration of the AMPA receptor potentiator, LY404187 (0.5mg/kg; B) compared to administration of the vehicle (A). In contrast, administration of the AMPA receptor antagonist, LY293558, caused decreases in glucose utilisation in this brain area (C). Administration of the AMPA receptor antagonist LY293558 (25mg/kg), prior to administration of the AMPA receptor potentiator, LY404187 (0.5mg/kg) attenuated the effects of this drug on glucose utilisation (D).

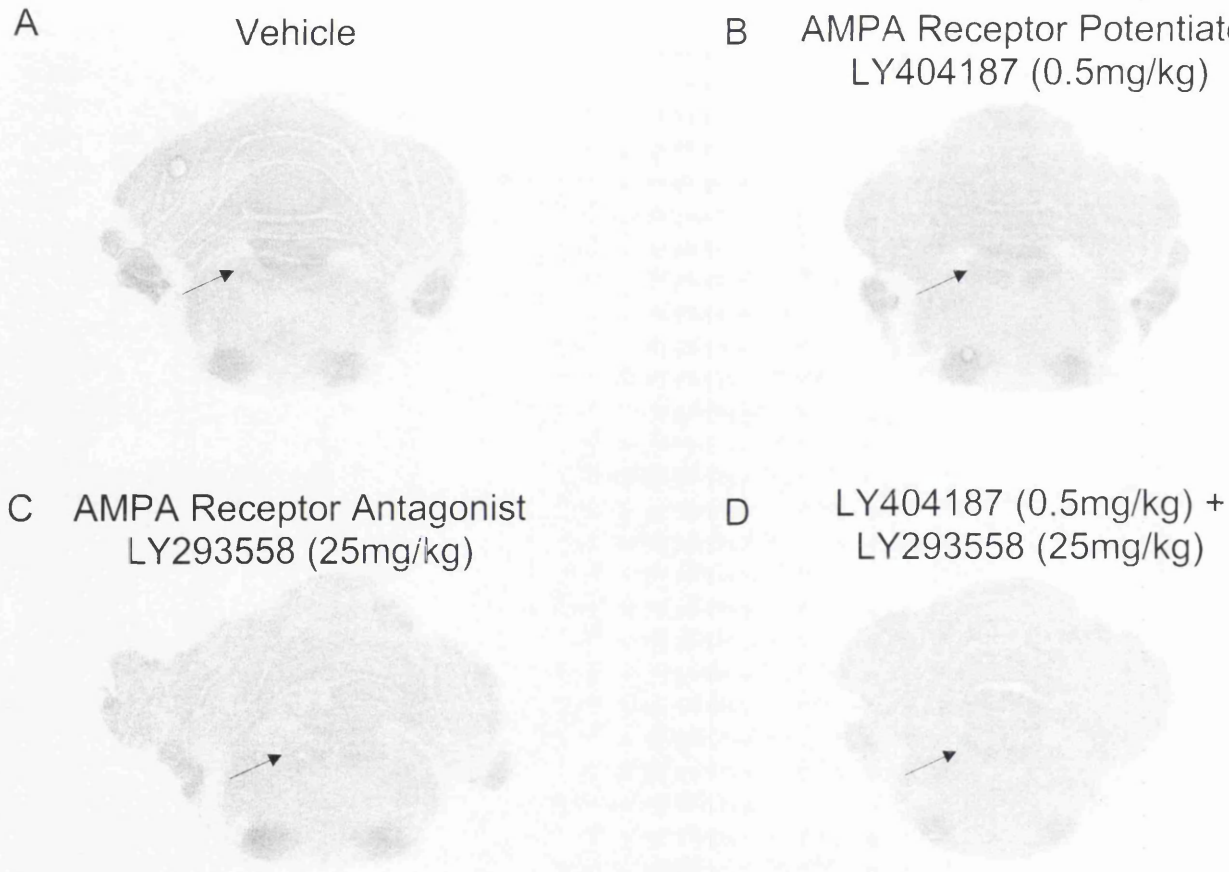

Figure 6.8 Representative autoradiograms illustrating changes in local cerebral glucose utilisation in the locus coeruieus

Increases in glucose utilisation were evident in the locus coeruleus following administration of the AMPA receptor potentiator, LY404187 (0.5mg/kg; B) compared to administration of the vehicle (A). In contrast, administration of the AMPA receptor antagonist, LY293558, caused decreases in glucose utilisation in this brain area (C). Administration of the AMPA receptor antagonist, LY293558 (25mg/kg), prior to administration of the AMPA receptor potentiator, LY404187 (0.5mg/kg) attenuated the effects of this drug on glucose utilisation in the locus coeruleus (D).

Extremely Sensitive	Very Sensitive	Sensitive	Insensitive
>25 % increase in G.U.	20-25 % increase in G.U.	15-19% increase in G.U.	<14% increase in G.U.
Locus Coeruleus ***	Superior Olives **	Hippocampus *	Red Nucleus
Ventral Parietal Cortex (IV) ***	Sensory Motor Cortex (IV) **	Dentate Gyrus	Nucleus Accumbens
Frontal Cortex (IV) **	Parietal Cortex (layer IV) **	Prefrontal Cortex	Cochlear Nucleus
Mediodorsal Thalamic Nuclei **	Cerebellar Cortex ***	Inferior Olives	Substantia Nigra (pars reticulata)
Anterior Cingulate Cortex ***	Ventolateral Thalamic Nuclei*	Auditory Cortex	Pons
Lateral Geniculates **	Globus Pallidus*	Amygdala	Hypothalamus
Superior Colliculi **	Dorsal Raphe **	Visual Cortex*	
	Medial Geniculates*	Laterodorsal Thalamic Nuclei	
	Lateral Habenulae *	Caudate Nucleus	
		Subthalamic Nucleus*	
		Cerebellar Nucleus	
		Inferior Colliculi	
		Posterior thalamic nuclei*	
		Substancia Nigra (pars compacta)	
		Septal Nuclei	
		Vestibular Nuclei **	

Table 6.7 Differential anatomical sensitivity to LY404187 (0.5mg/kg)

A hierarchy of responsiveness of different brain areas to LY404187 (0.5mg/kg) compared to vehicle treatment.. *P<0.05, ** P<0.01, ***P<0.001 (One way ANOVA followed by post hoc Student's *t* test and Bonferonni correction for comparison with vehicle treated group).

6.3.3 Effects of the AMPA receptor antagonist LY293558 prior to treatment with the AMPA receptor potentiator LY404187

Pre-treatment with the AMPA receptor antagonist LY293558 (25mg/kg) significantly reduced glucose utilisation in 42 out of the 52 anatomical areas examined, compared with administration of the vehicle (Tables 6.2 – 6.6; Fig. 6.9, 6.10). There were no significant differences in glucose utilisation in any of the anatomical areas in the animals treated with LY293558 (25mg/kg) and vehicle compared with administration of LY293558 (25mg/kg) and the AMPA receptor potentiator LY404187 (0.5mg/kg).

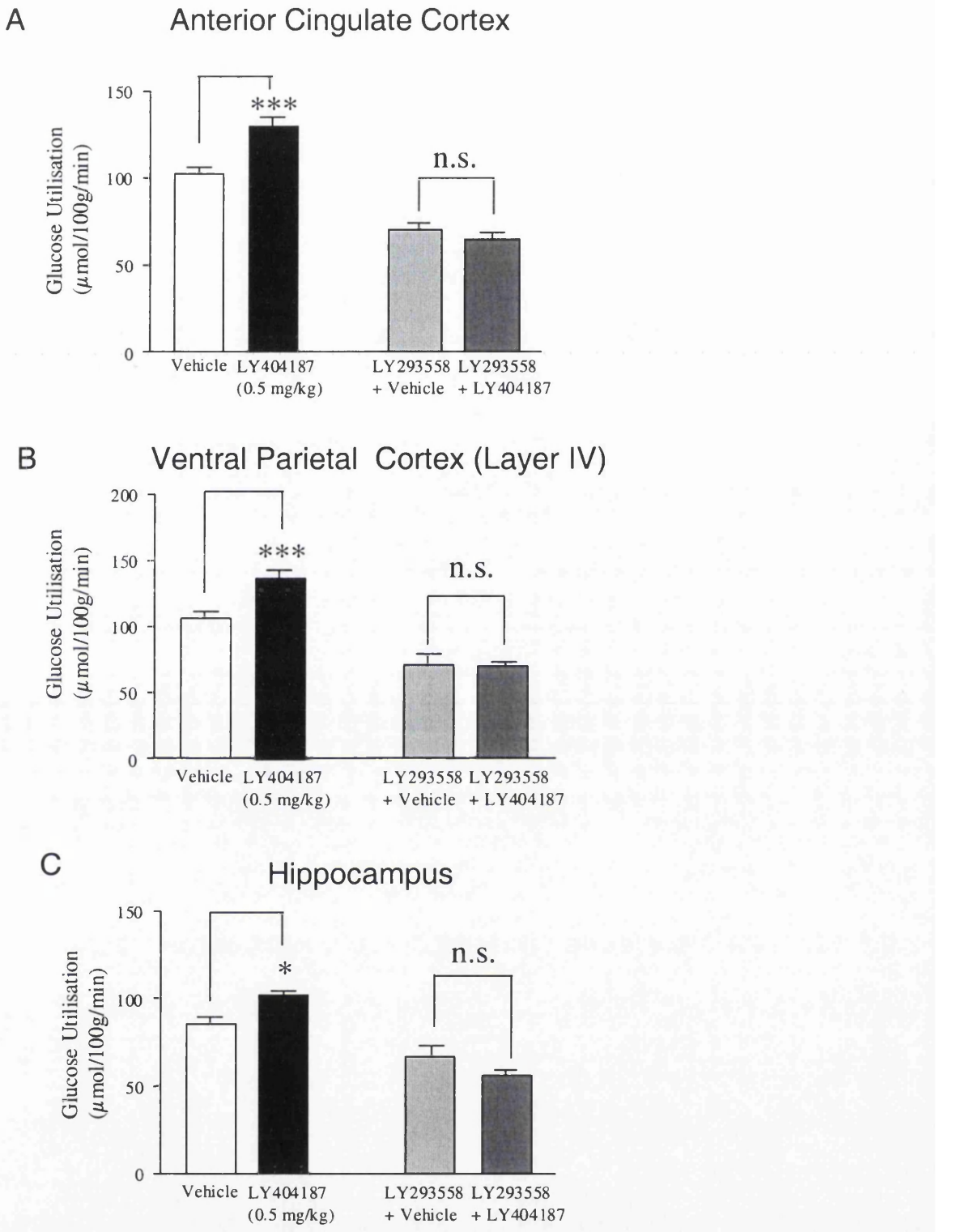

Figure 6.9 Effects of the AMPA receptor antagonist LY293558 on cerebral glucose utilisation in cortical areas and the hippocampus following LY404187 administration

A. Anterior Cingulate Cortex B. Ventral Parietal Cortex (Layer IV)

C. Hippocampus

Data are presented mean ± SEM. *P<0.05, ***P<0.001 for comparison between vehicle and the AMPA receptor potentiator LY404187 (0.5mg/kg). P>0.05 for comparison between AMPA receptor anatgonist LY293558 (25mg/kg) and vehicle administration with LY293558 (25mg/kg) and LY404187 administration (0.5mg/kg)

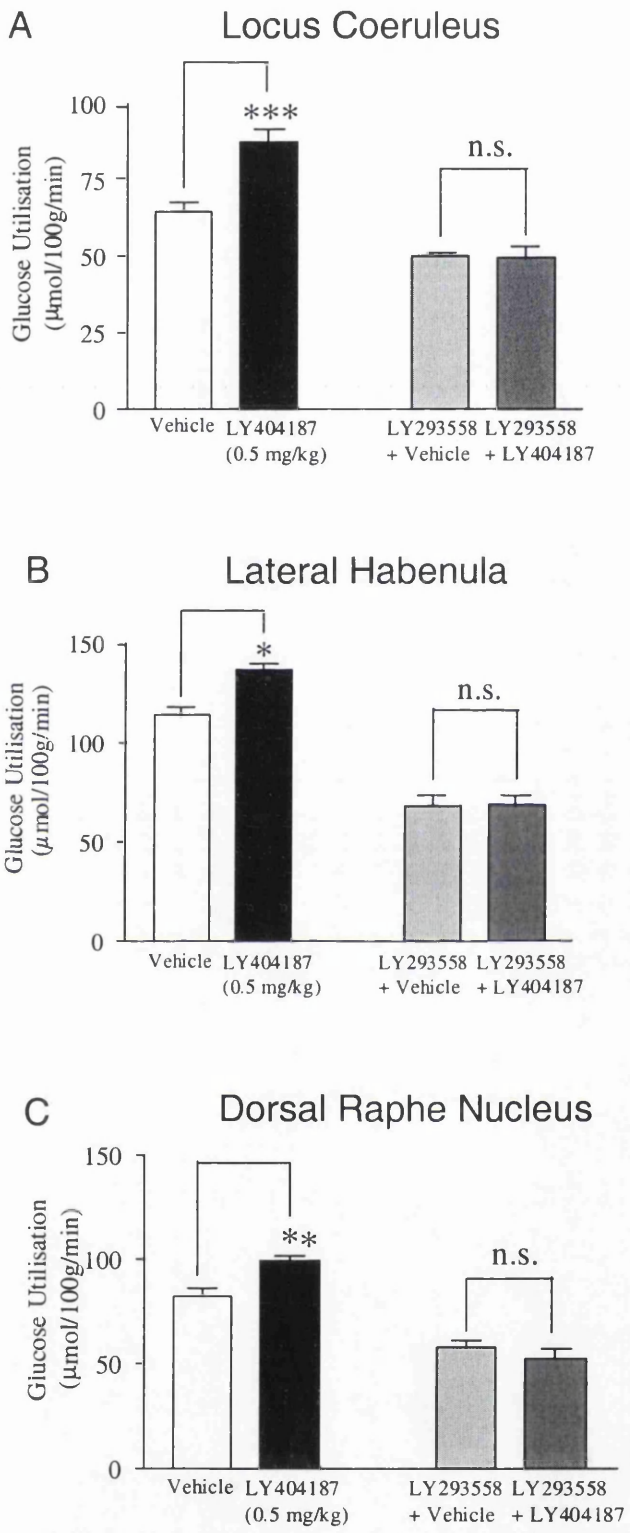

Figure 6.10 Effects of the AMPA receptor antagonist LY293558 on cerebral glucose utilisation in monoaminergic areas following LY404187 administration

A. Locus coeruleus B. Lateral Habenula C. Dorsal Raphe Nucleus

Data are presented mean ± SEM. *P<0.05, **P<0.01, ***P<0.001 for comparison between vehicle and the AMPA receptor potentiator LY404187 (0.5mg/kg). P>0.05 for comparison between AMPA receptor antagonist LY293558 (25mg/kg) and vehicle administration with LY293558 (25mg/kg) and LY404187 (0.5mg/kg)

6.4 Discussion

These results demonstrate that the AMPA receptor potentiator, LY404187 (0.5mg/kg) significantly increased glucose utilisation in 28 anatomically discrete areas of the brain such as the hippocampus, layer IV of the cerebral cortex, the raphe nucleus and the locus coeruleus; anatomical areas that are associated with learning and memory or depression. These increases were attenuated by pre-treatment with the AMPA receptor antagonist LY293558, suggesting that LY404187 acts through AMPA receptor mediated mechanisms. These data provide an anatomical basis for the behavioural effects of this compound in animal models of learning and memory and depression.

LY404187 enhances AMPA receptor-mediated transmission

LY404187 significantly increased glucose utilisation in 28 brain areas; no decreases in glucose utilisation were observed in any region. Under physiological normal conditions, glucose utilisation is closely related to energy consumption, which is thought to be predominately utilised for the maintenance of ionic gradients (Schwartz *et al.*, 1979). Therefore, the increase in glucose utilisation observed following LY404187 administration is probably due to its ability to enhance action potential discharge rate at AMPA receptors in response to endogenous glutamate. LY404187 has previously been shown to enhance ion influx in recombinant GLU_{A1-4} and to selectively enhance AMPA-mediated responses in native hippocampal neurons *in vitro* and *in vivo* (Gates *et al.*, 2001; Vandergriff *et al.*, 2001). In the present study, the AMPA receptor antagonist LY293558 attenuated the effects of the LY404187, confirming that the effects of the AMPA receptor poteniator are mediated via AMPA receptors. The anatomical distribution of altered glucose utilisation following administration of the AMPA receptor potentiator LY404187 is distinct from that observed with agents acting on other aspects of glutamatergic transmission, such as metabotropic glutamate agonists or NMDA receptor antagonists (Kurumaji *et al.*, 1989; Lam *et al.*, 1999). Even at the highest concentrations of LY404187, there was no evidence of the intense elevations in glucose utilisation observed with AMPA or kainate receptor agonists (Wooten & Collins, 1980; data in chapter 4).

Regional localisation of increased glucose utilisation in the rat brain

AMPA receptor antagonists produce widespread depression in glucose utilisation; for example NBQX (100mg/kg) and LY293558 (100mg/kg) produced significant reductions in glucose utilisation in 43 and 48 brain areas respectively (Browne and McCulloch, 1994). In contrast, the AMPA receptor potentiator LY404187 produced discrete increases in glucose utilisation in 28 out of the 52 brain areas analysed, even though AMPA receptors are widely distributed throughout the brain. NBQX and LY293558 are mixed AMPA/kainate antagonists, whereas recent developments in the molecular biology of glutamate receptors enabled the development LY404187, which selectively potentiates only AMPA receptors. Even so, there are some discrepancies when comparing the anatomical distribution of AMPA receptors revealed by [^{3}H]-AMPA binding studies with the areas that were activated by LY404187 (0.5mg/kg). Anatomical areas such as the superficial layers of the cortex and stratum lacunosum-moleculare of the hippocampus which contain the highest levels of AMPA receptors (Monaghan *et al.*, 1984; Rainbow *et al.*, 1984) did have significant elevations in glucose utilisation following LY404187 administration. In contrast, LY404187 had no significant influence on glucose utilisation in other areas with high levels of AMPA receptors, such as the caudate nucleus, nucleus accumbens and the amydala. In addition, LY404187 was found to activate areas such as the lateral habenula, and the lateral geniculate nucleus which were reported to contain lower levels of [^{3}H]AMPA binding sites (Monaghan *et al.*, 1984). In neuropharmacological investigations, the anatomical distribution of altered glucose utilisation after drug administration does not reflect the distribution of receptors at which the drug is targeted, but rather the polysynaptic circuits in which activity can be modulated by the drug. For instance, LY404187 may activate areas such as the superior colliculus, which contain lower levels of AMPA receptor subunits, as a consequence of activation of regions functionally associated with AMPA receptor-mediated activity.

This discrepancy may be further explained by the heterogeneity of AMPA receptor subunit composition in the brain. LY404187 and related biarylpropylsulfonamides have different profiles (potency and efficacy) at potentiating recombinant GLU_{A1-4}

(Miu *et al.*, 2001) and this effect is also observed on rat native neurons from various brain regions (M. J O'Neill, personal communication). The distribution of the individual AMPA receptor subunits, GLU_{A1-4} in the rat brain, also varies from the distribution pattern of [^{3}H]AMPA binding (Petralia and Wenthold, 1992). For example, high levels of the glutamate receptor subunits GluR2/3 have been reported in the lateral habenula and lateral geniculate nucleus (Petralia and Wenthold, 1992). LY404187 is most potent at recombinant receptors composed of the GLU_{A2} subunit (GLU_{A2}>GLU_{A4}>GLU_{A3}>GLU_{A1}; Miu *et al.*, 2001).

LY404187 caused increased c-fos protein expression

Using the same dosing regime as that deployed in the current chapter, the effects of the AMPA receptor potentiator LY404187 on Fos protein expression were also examined in a limited number of brain regions in a separate set of experiments carried out an Eli Lilly (M.J. O'Neill, personal communication, presented in Fowler *et al.*, 2003). Neurons transiently express the immediate early gene c-fos when stimulated (Sagar *et al.*, 1988). The protein expressed by the c-fos gene, Fos, can be detected using immunocytochemical techniques, enabling the detection of neuronal activation (Sharp *et al.*, 1993). The AMPA receptor potentiator, LY404187 (0.5mg/kg) caused increases in Fos expression 6 hours following administration, in the dorsal raphe nuclues, parietal cortex and locus coeruleus; whilst other brain regions such as the hypothalamus and substantia nigra were unaffected (Fig 6.12). A bell-shaped dose response curve for Fos expression was also evident following LY404187 administration (Fig. 6.12), which parallels the dose responses observed in the glucose utilisation studies. The changes in Fos expression occurred in areas that were most sensitive to the effects of LY404187 in the glucose utilisation studies, thus confirming that LY404187 causes neuronal activation in these anatomically discrete areas.

Effects of LY404187 on glucose utilisation in brain areas related to cognition

There are several theories on the anatomical basis of memory formation. Evidence suggests that there are many distinct classes of memory, such as declarative/episodic memory, which involves representations of facts and events that are subject to conscious recollection; and non-declarative/implicit memory, a heterogeneous

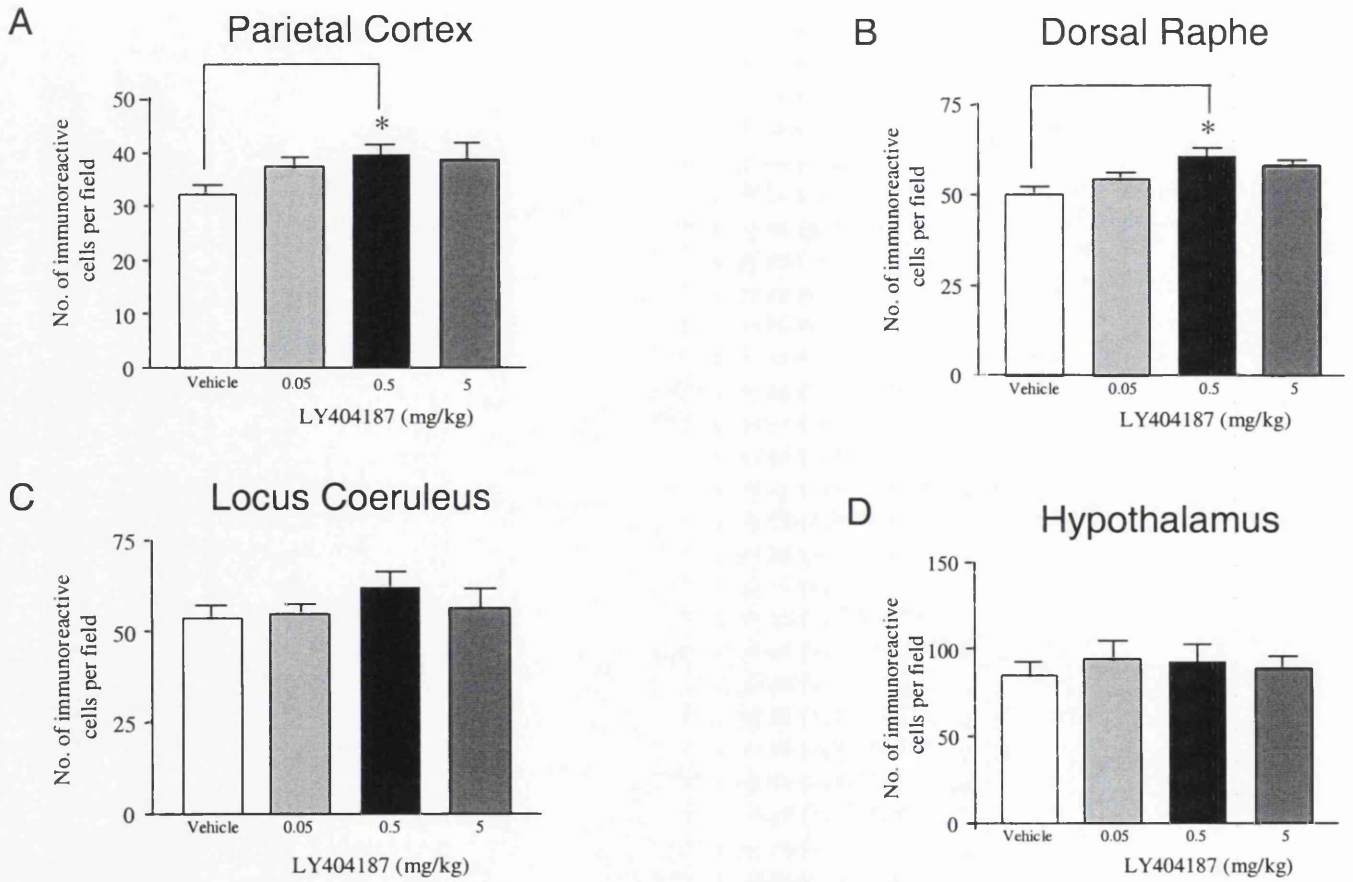

Figure 6.12 Expression of Fos protein 6 hours following subcutaneous administration of LY404187

Comparison of the effects of LY404187 (0.05, 0.5, 5mg/kg) on the number of c-fos positive cells in the parietal cortex (A), dorsal raphe nucleus (B), locus coeruleus (C) and hypothalamus (D). There were significant increases (*P<0.05) in Fos immunoreactivity in the parietal cortex and dorsal raphe nucleus following administration of 0.5mg/kg of LY404187 (One way ANOVA, *post-hoc* Student's *t* test with Bonferonni correction for multiple comparisons). Data are presented mean ± SEM, n=8 per group. Data presented in Fowler *et al.*, 2003.

collection of nonconscious learning capacities (Milner *et al.,* 1998). These distinct entities are likely to depend on different anatomical areas, and this is supported by evidence from amnesic patients, lesioning studies and a combination of physiological and functional MRI measures (Brewer *et al.,* 1998; Milner *et al.,* 1998; Wagner *et al.,* 1998; Deweer *et al.,* 2001). However, whilst multiple brain areas may contribute to the anatomical basis of memory, there is a general consensus that the cortex and hippocampus play a pivotal role in the formation, storage or retrieval of memories (Markowitsch, 1995; Fletcher *et al.,* 1997; Milner *et al.,* 1998; Bontempi *et al.,* 1999; Buckner *et al.,* 1999; Deweer *et al.,* 2001; Manns *et al.,* 2003). Molecular studies have indicated that LTP involves rapid increases in intracellular calcium and this then recruits a second slower LTP that involves secondary messengers and protein synthesis-dependant changes in synapses (Kandel, 2001). The effects can be observed using metabolic mapping of hippocampal and cortical activation with ^{14}C-2-deoxglucose autoradiography during a variety of cognitive tasks, aimed to test different memory entities in the non-human primate (Bontempi *et al.,* 1999; Sybirska *et al.,* 2000; Davachi and Goldman-Ravic, 2001). Intrahippocampal injection of AMPA receptor antagonists markedly and selectively reduce glucose use in this region and disrupt encoding, retrieval and storage of spatial memory (Riedel *et al.,*1999). Here, it has been demonstrated that the AMPA receptor potentiator LY404187, causes activation of the hippocampus and the frontal, anterior cingulate, sensory motor and parietal cortex in the rodent, suggesting that this compound activates brain areas that are associated with memory formation. It is not clear if these studies reflect increased glucose utilisation caused by the initial calcium influx, such as that observed with LTP produced by tetanic stimulation; or a secondary event. LY404187 also causes increases in BDNF expression in the hippocampus (Mackowiak *et al.,* 2002). BDNF and its receptor TrkB are highly localised in the hippocampus. BDNF secretion increases in an activity dependent manner and there is a substantial literature linking BDNF to learning and memory (Lu and Gottschalk, 2000; Poo, 2001).

Cognitive enhancing effects of LY404187

The cognitive enhancing effect of AMPA receptor potentiators has been demonstrated in a number of animal models of cognition. Cognitive enhancing effects of aniracetam and piracetam in delayed non-matching to sample and maze

exploration tasks (Pontecorvo *et al.,* 1985; Verloes, 1988) were demonstrated before the AMPA receptor mediated action of theses pyrrolidinones were discovered. Benzoylpiperidine compounds have since demonstrated positive effects in rodents in the radial arm maze, delayed-nonmatch-to-sample tests and the Morris water maze (Granger *et al.,* 1993, 1996; Staubli *et al.,* 1994a, b; Davis *et al.,* 1997; Hampson *et al.,* 1998). IDRA-21 also improves rodent performance in the water maze (Zivkovic *et al.,* 1995), and ablates pharamacologically induced cognitive impairments in non-human primates (Thompson *et al.,* 1995). In parallel studies, it has been demonstrated that the active isomer of LY404187, LY451646, enhances rodent performance in the radial arm maze, at equivalent doses that caused activation of the hippocampus and cortex in the 2-deoxglucose studies (Fowler *et al.,* 2003). Previous studies have indicated that LY404187 and related biarylpropylsulfonamide also improve performance in the water maze (Quirk and Nisenbaum, 2002) and passive avoidance tasks. The glucose utilisation studies described here therefore demonstrate that activation of the hippocampus and cerebral cortex may contribute to the anatomical circuitry involved in memory processes engaged during these tasks.

Effects of LY404187 on glucose utilisation in brain areas related to anti-depressant activity

The results described here demonstrate that administration of LY404187 produced activation of the locus coeruleus, the dorsal raphe nucleus and the lateral habenula, a key relay nucleus from the forebrain to the midbrain raphe. The locus coeruleus and raphe nucleus are the origin of noradrenergic and serotenergic projections, which may have a modulatory influence over memory processes (Meneses, 1999; Buhot *et al.,* 2000; Kobayashi And Yasoshima, 2001). Activation of the raphe nucleus and locus coeruleus with LY404187 may also contribute to the antidepressant effects of the drug. In recent years several new drug targets and animal models for development of antidepessants are emerging (Nestler *et al.,* 2002). As stated earlier, LY404187 has been reported to increase levels of BDNF (Legutko *et al.,* 2001, Mackowiak *et al.,* 2002). BDNF is up-regulated by both electroconvulsive shock treatment and by many conventional anti-depressants, and may exert a range of trophic and protective effects on monoaminergic neurons (Altar, 1999; Skolnick *et al.,* 2001). It has also been demonstrated that direct infusion of BDNF into the hippocampus produces effects in animal models of depression (Shirayama *et al.,*

2002). LY404187, related biarylpropylsulfonamides and other AMPA receptor potentiators are efficacious in the same rodent models (forced swim and tail suspension) of depression (Li *et al.,* 2001; Knapp *et al.,* 2002; Quirk and Nisenbaum, 2002). The present findings suggest that in addition to modulating BDNF, LY404187 also has actions on the biogenic amine neurotransmitter systems. Taken together, these data may provide a neurochemical basis for the antidepressant-like action of LY404187 and suggest that AMPA receptor potentiators may be effective in treating depression.

Based on the ability of AMPA receptor potentiators to enhance BDNF levels, the potential of the AMPA receptor potentiator, LY404187, to enhance regeneration following brain injury was examined next.

CHAPTER 7

THE EFFECTS OF THE AMPA RECEPTOR POTENTIATOR LY404187 ON REGENERATION IN THE DENTATE GYRUS FOLLOWING ENTORHINAL CORTEX LESION

7.1 Introduction

BDNF can enhance regeneration following brain injury (Mamounas *et al.,* 2000; Coumans *et al.,* 2001; Klocker *et al.,* 2001; Takano *et al.,* 2002). Based on the ability of AMPA receptor potentiators to enhance BDNF levels *in vitro* and *in vivo* (Lauterborn *et al.,* 2000; Legutko *et al.,* 2001; Mackowiak *et al.*, 2002), it can be hypothesised that they may enhance regenerative processes following brain injury. Trophic factors are thought to be involved in the regeneration and reorganisation in the dentate gyrus following entorhinal cortex lesioning (Deller and Frotscher, 1997). Adenovirus-mediated BDNF gene administration to rodents with entorhinal cortex lesions enhances LTP and performance in certain cognitive tests, suggesting that BDNF may enhance plasticity in this model (Ando *et al.,* 2002).

Increased rates of neurogenesis occur following brain injury such as entorhinal cortex lesion (Gould and Tanapat, 1997). BDNF has been shown to promote endogenous stem cell proliferation, survival and differentiation *in vivo* (Pencea *et al.,* 2001). The AMPA receptor potentiator LY451646 (the active isomer of LY404187) increases the rate of endogenous stem cell proliferation in the adult rat hippocampus (Bai *et al.,* 2003), however the fate of these cells is unknown.

7.1.1 Aim of Study

The aim of the current study was to determine if the AMPA receptor potentiator LY404187 could increase fibre sprouting and synaptogenesis in the molecular layer of the dentate gyrus 14 or 21 days following entorhinal cortex lesion with the excitotoxin, ibotenic acid. Drug or vehicle treatment commenced 7 days following the entorhinal cortex lesion, and GAP-43 and synaptophysin immunohistochemistry were deployed to examine degeneration and regeneration. In addition, the fate of proliferating stem cells in the dentate gyrus, labelled with BrdU one day before drug treatment commenced was compared for drug or vehicle treated animals.

7.2 Methods

7.2.1 Entorhinal Cortex Lesion

Thirty-three adult male Sprague Dawley rats (weight, Harlan Olac, Bicester, UK) received intracerebral injection of 0.5μl of ibotenic acid (10mg/ml) as outlined in section 2.4.1. Animals were housed individually post-operatively and returned to the animal unit the following day. After the appropriate survival time (see below), animals were re-anaesthetised, transcardially perfuse-fixed with saline (0.9%) then paraformaldehyde (4%); post-fixed, processed and paraffin embedded (section 2.4.3).

7.2.2 Drug Treatment

The experimental design is illustrated below. Animals were randomly assigned into either vehicle or drug treated groups. Six days following entorhinal cortex lesion, all animals were given an intraperitoneal injection of BrdU (100mg/kg in 0.007N NaOH/0.9% saline). Drug treatment commenced on day 7. Animals in group A received subcutaneous injections of either LY404187 (0.5mg/kg; n=10) or vehicle (10% ethanol, 3.75% hydroxypropyl-ß-cyclodextrin; n=9) for a further 7 days. Animals in group B received either LY404187 (n=7) or vehicle (n=7) treatment for 14 days.

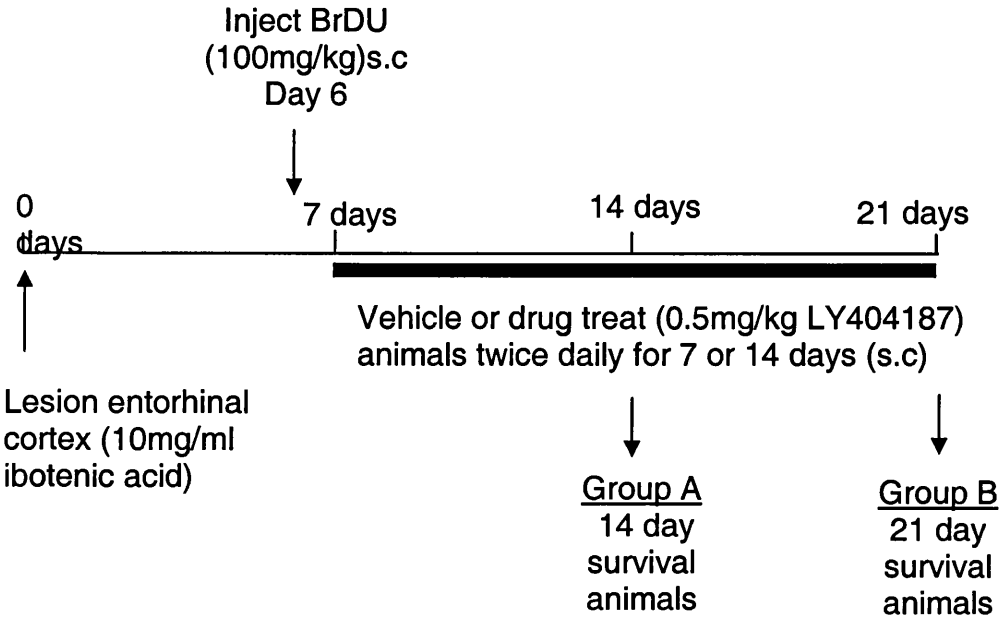

7.2.3 Histology and Immunocytochemistry

Sections (6μm) were taken from the entorhinal cortex area (2 sections were retained from every 20 cut) to confirm lesion placement, then sections (2 per slide) were retained from the hippocampus, at the level of the lateral habenula, for immunostaining. Sections from the anterior and posterior portion of the lateral habenula of each animal were processed for GAP-43 and synaptophysin immunostaining as described in section 2.5.5, however microwave pre-treatment was not undertaken for these antibodies. All GAP-43 or synaptophysin immunostaining was done simultaneously with reagents from the same batch, and DAB solution was applied to 6 sections at a time for precisely 3 minutes per section. Two sections from the anterior and posterior portion of the lateral habenula were also processed for BrdU immunostaining. These sections were pre-treated with pepsin (0.4% in 0.01 HCl) for 15 minutes, and washed for 15 minutes prior to microwave pre-treatment.

To quantify the GAP-43 and synaptophysin immunoreactivity, Tiff images were captured in grey scale from the molecular layer of the dentate gyrus at x10 magnification, using a Leica microscope and Image ProPlus software, as described in section 2.5.10. Images were also captured from a reference area, the optic tract and corpus callosum for GAP 43 and synaptophysin immunostaining, respectively. Relative optical densities of the inner, middle and outer molecular layer of the dentate gyrus ipsilateral and contralateral to the ECL, as well as the appropriate reference region from each section were measured using an MCID image analyser, as described in section 2.5.10. The optical density values from the inner, middle and outer molecular layer of the dentate gyrus of each animal were averaged and expressed as a percentage of the contralateral dentate gyrus.

Less than ten BrdU immunopositive cells were detected in the ipsilateral or granule cell layer of the dentate gyrus per section, therefore the total number of immunopositive cells in the ipsilateral and contralateral molecular layer was counted per section. Four sections were examined per animal, two from the anterior portion of the lateral habenula, and two from the posterior portion of the lateral habenula. The cell counts from the ipsilateral and contralateral molecular layer from these sections were then averaged for each animal.

7.2.4 Statistical Analysis

To determine if there was any significant difference in the synaptophysin or GAP-43 immunoreactivity (% change in optical density compared to the contralateral dentate gyrus) of vehicle or drug treated groups, two-tailed, unpaired Student's *t* test was used. To determine if there was any significant difference between the number of BrdU immunopositive cells in vehicle or drug treated groups, two-tailed, unpaired Student's *t* test was used.

7.3 Results

7.3.1 Assessment of lesion placement

All animals included in the study contained a lesion in the entorhinal cortex area, a representative example of the extent of the lesion in shown in figure 7.1. The lesions were confined to the entorhinal cortex and did not involve other cortical areas. The lesion spread approximately 1-2mm in a rostro-caudal extent but did not directly involve the hippocampus.

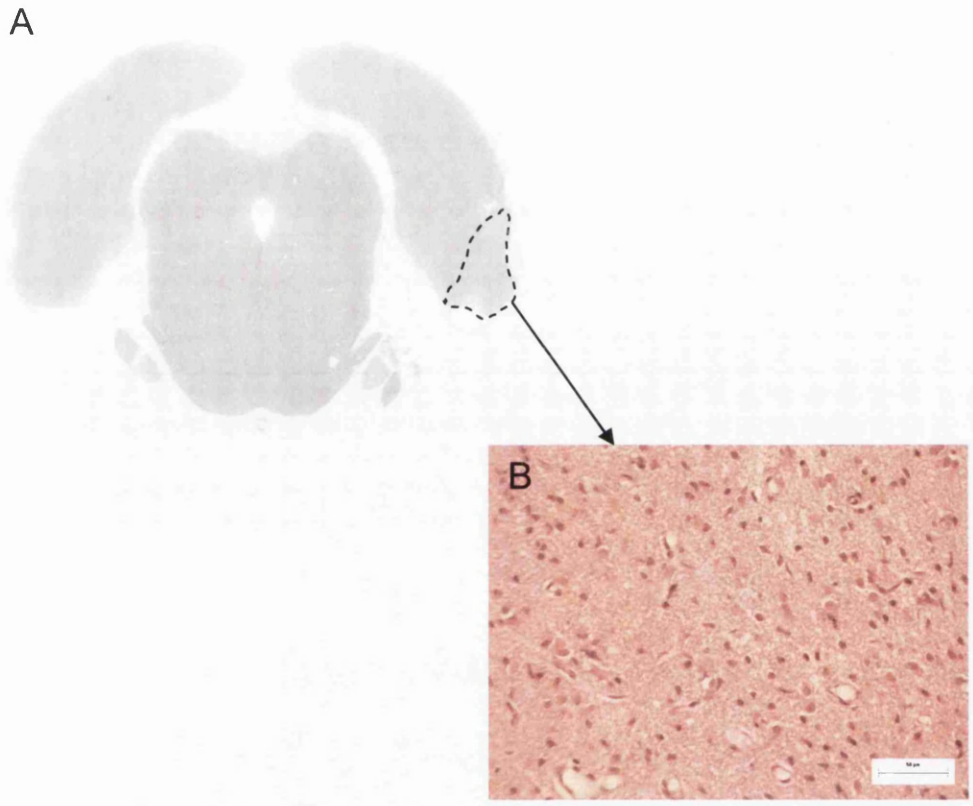

Figure 7.1 Entorhinal cortex lesion induced by stereotaxic injection of ibotenic acid

A. Digitised H & E stained section illustrating the extent of the lesion (within dashed black line)

B. Higher power image from the lesion site, illustrating the pallor and glial cell reaction.

Scale bar = 50μm.

7.3.2 GAP 43 immunostaining

In the dentate gyrus contralateral to the lesioned entorhinal cortex, the granule cell layer showed little staining, whilst the molecular layer displayed a granular pattern of immunostaining (Fig. 7.2A). The inner molecular layer was most intensely immunostained, whereas the outer two layers exhibited a lighter level of immunostaining. Quantification of GAP 43 immunoreactivity in the contralateral dentate gyrus revealed that there was no significant difference in the optical density values in the molecular layers of vehicle and LY404187 (0.5mg/kg) treated animals, thus validating this area as a control region (Fig 7.3A, B). In addition, there was no significant difference in the levels of immunostaining in the optic tract of vehicle or LY404187 (0.5mg/kg) treated animals (Fig 7.2B;7.3C, D).

In the dentate gyrus ipsilateral to the lesioned entorhinal cortex, changes in the intensity of immunostaining in the molecular layer were rarely observed when compared to the contralateral molecular layer, however a decrease in immunostaining in the outer molecular layer was observed in some animals (Fig. 7.4). Quantification of the immunoreactivity in the molecular layers of group A (14 days following entorhinal cortex lesion, 7 days of drug treatment) revealed that there were minimal changes in the levels of GAP-43 immunoreactivity in the MML and OML of vehicle treated animals compared to the contralateral dentate gyrus, and that there was no significant difference between vehicle and LY404187 treated animals (Figure 7.5A). There was a modest increase in the intensity of GAP 43 immunostaining in the IML compared to the contralateral IML of vehicle treated animals from Group A, however treatment with LY404187 (0.5mg/kg) significantly reduced the levels of GAP 43 immunostaining in the IML compared to the vehicle treated group (Figure 7.5A). In group B (21 days following entorhinal cortex lesion, 14 days of drug treatment), there were minimal changes in the levels of immunostaining in the 3 molecular layers of vehicle treated animals compared to the contralateral dentate gyrus; and no significant changes between vehicle and LY404187 treated animals was detected (Fig. 7.5B).

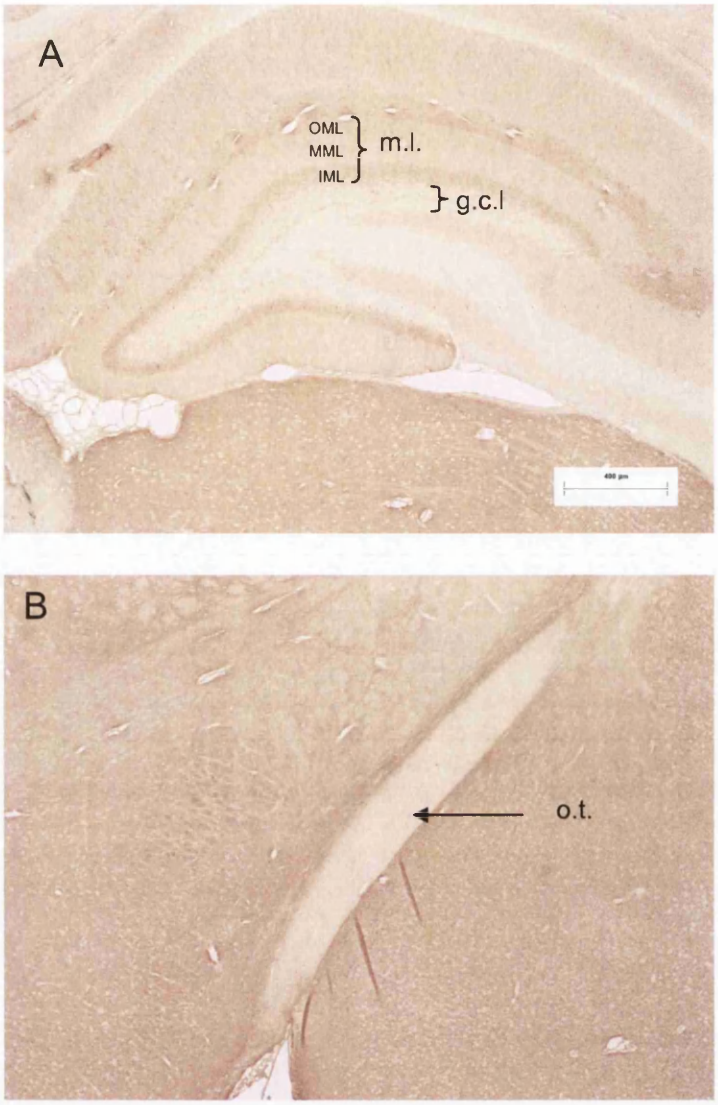

Figure 7.2 GAP 43 immunostaining in control regions

A. GAP 43 immunostaining in the dentate gyrus contralateral to the lesioned entorhinal cortex. In the molecular layer (m.l.) the inner molecular layer (IML) is most densely stained, whereas the middle (MML) and outer molecular layers (OML) are more lightly stained. The granule cell layer (g.c.l.) is relatively unstained.

B. The optic tract contains the lowest level of immunostaining at this coronal level in the brain.

Scale bar = 400μm.

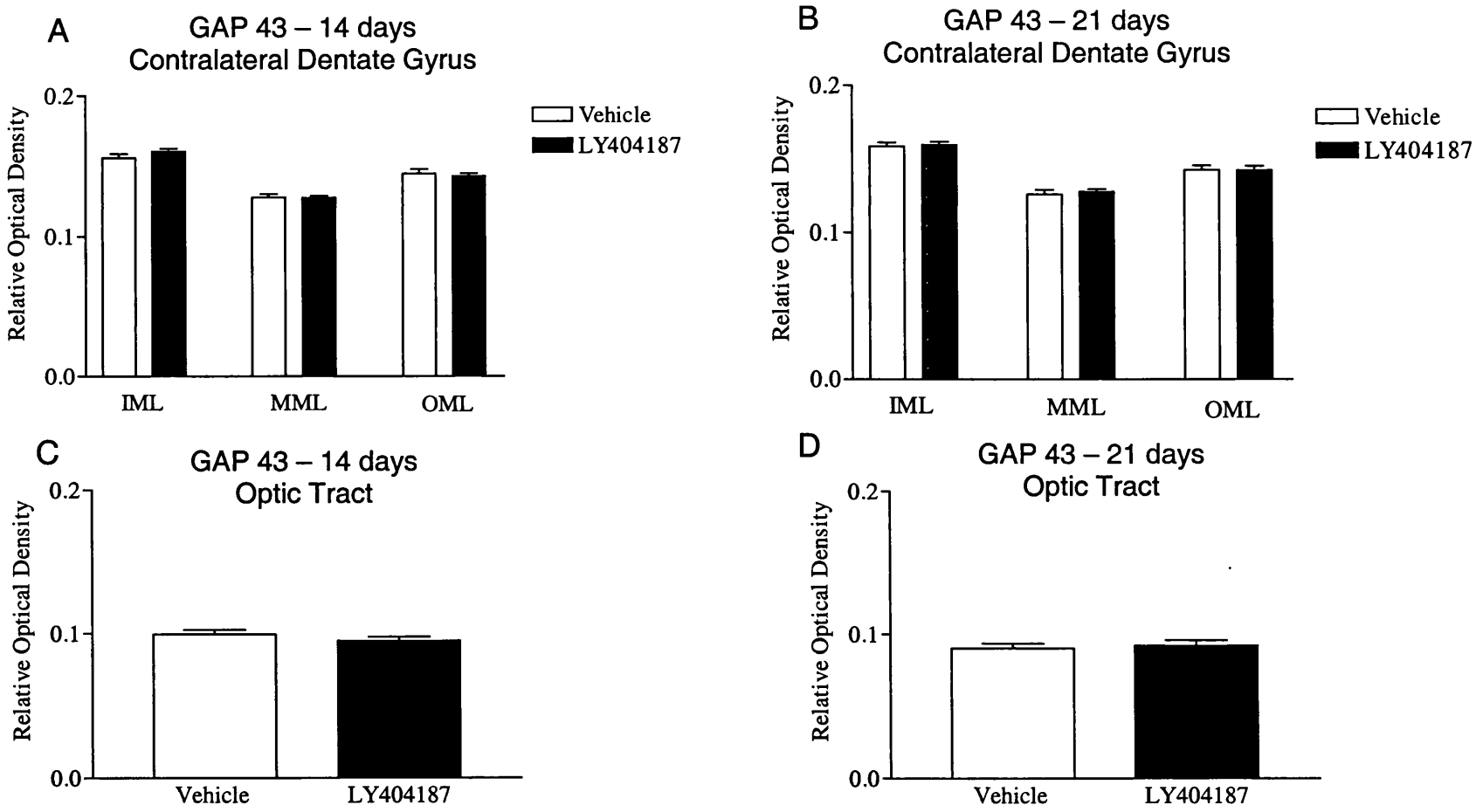

Figure 7.3 Relative optical density in control regions of GAP-43 immunostained sections

There was no significant difference in the relative optical density of the inner (IML), middle (MML) and outer (OML) molecular layers of the dentate gyrus contralateral to the lesion hemisphere between vehicle and drug (LY404187, 0.5mg/kg) treated animals at 14 (A) or 21 days (B). There was no significant difference in the relative optical density of the control region, the optic tract, between vehicle and drug treated animals at 14 (C) or 21 days (D). n=7-10 per group, unpaired Student's *t* test.

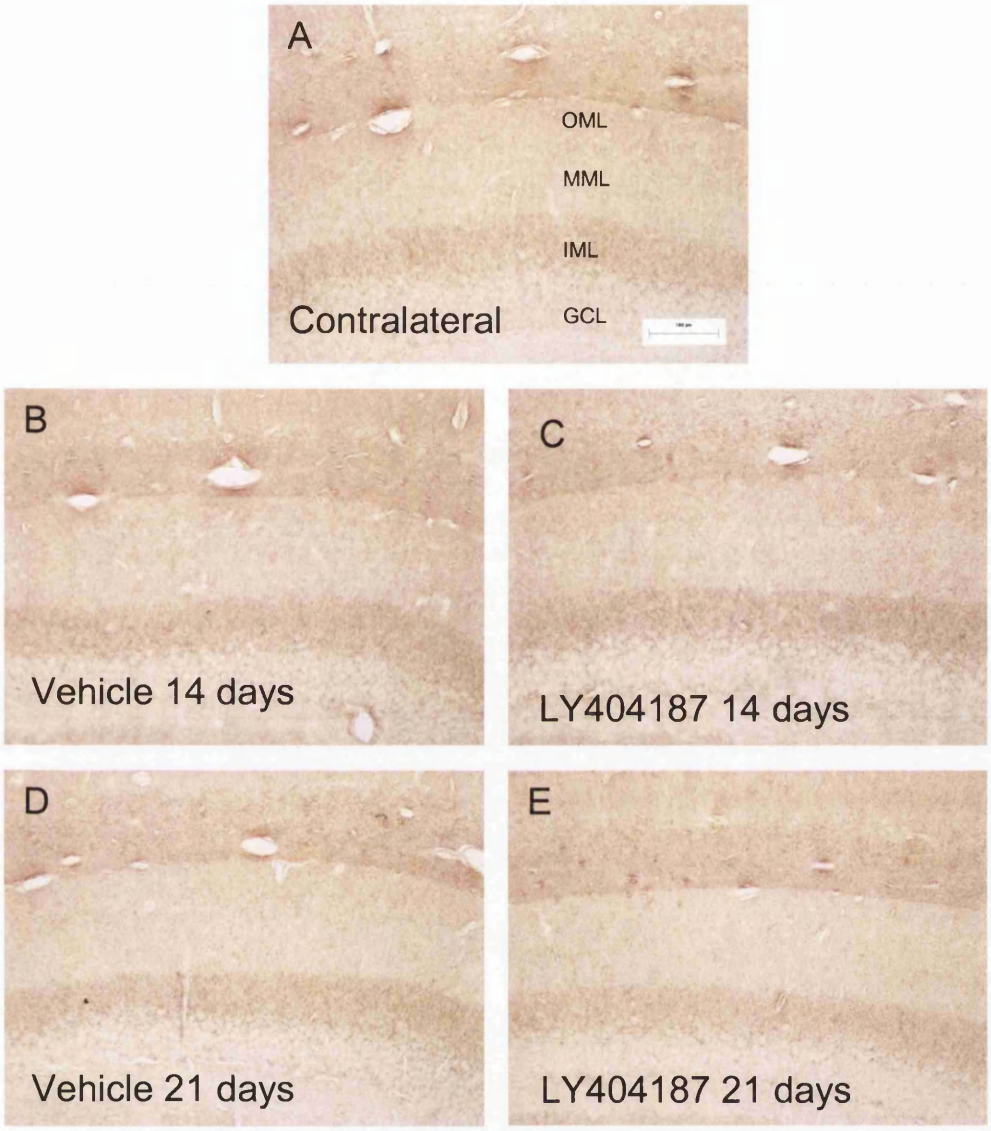

Figure 7.4 GAP 43 immunostaining in the dentate gyrus

A. GAP 43 immunostaining in the dentate gyrus contralateral to the lesioned entorhinal cortex. Immunostaining is evident in the outer (OML), middle (MML) and inner (IML) molecular layer of the dentate gyrus, however the granule cell layer is relatively unstained.

B. –E. GAP 43 immunostaining in the dentate gyrus ipsilateral to the entorhinal cortex lesion in representative animals that survived for 14 (B, C) or 28 days (D, E) following the lesion, that were treated with either vehicle (B, D), or LY404187 (0.5mg/kg; C, E) .

Scale bar = 100μm.

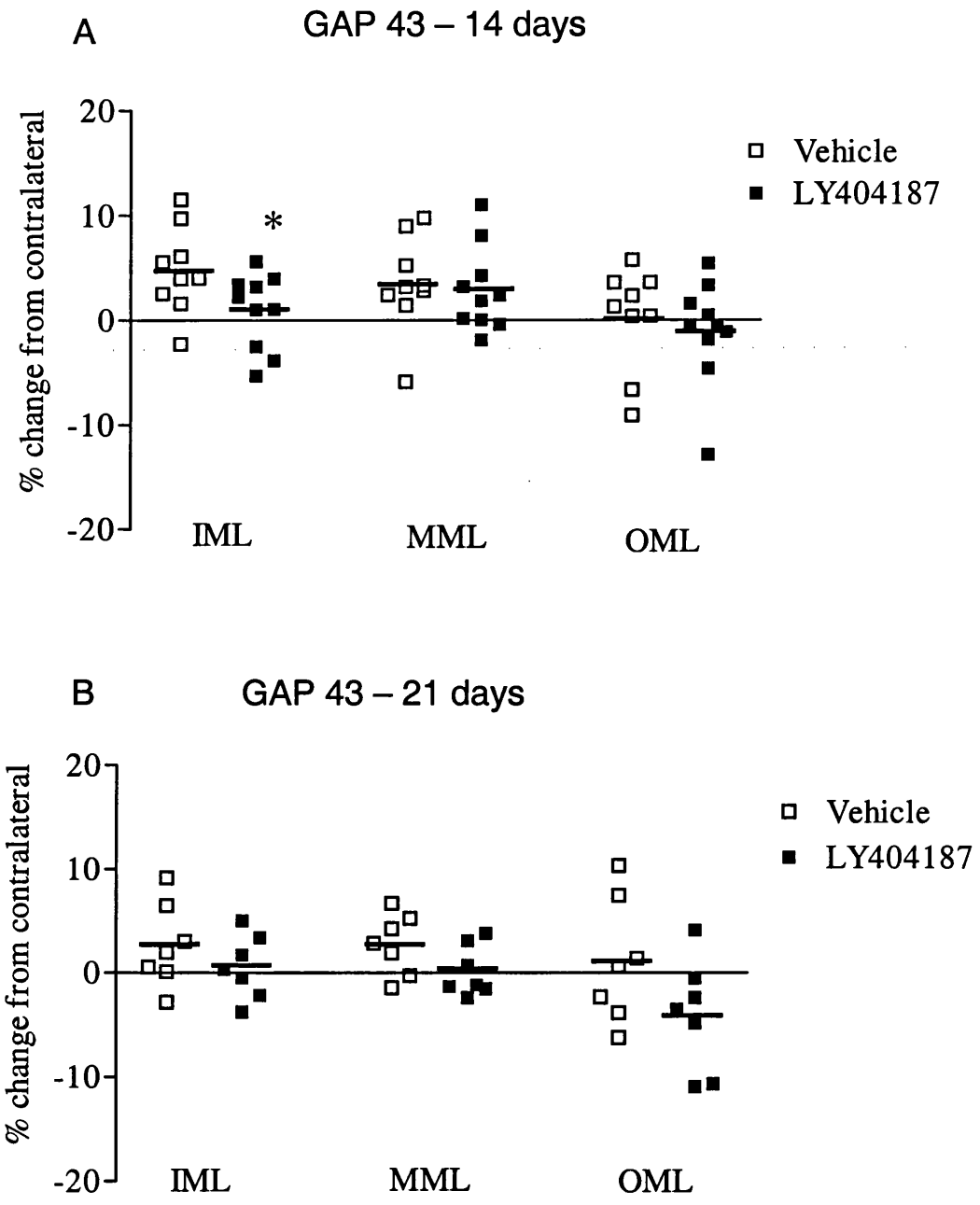

Figure 7.5 Quantification of GAP-43 immunoreactivity in the inner (IML), middle (MML) and outer molecular layers (OML) of the dentate gyrus

A. GAP 43 immunoreactivity was significantly reduced in the IML following treatment with the AMPA receptor poteniator LY404187 (0.5mg/kg) compared to vehicle treatment, but unchanged in the MML and OML, 14 days following entorhinal cortex lesion (Student's *t* test *P<0.05).

B. GAP 43 immunoreactivity was not significantly different in the IML, MML or OML after drug or vehicle treatment 21 days following entorhinal cortex lesion (Student's *t* test). Bar indicates means of groups.

7.3.3 Synaptophysin immunostaining

In the dentate gyrus contralateral to the lesioned entorhinal cortex, there was a granular, trilaminar synaptophysin immunostaining pattern in the molecular layer, whilst the granule cell layer was relatively unstained (Fig. 7.6A). The OML contained the densest level of synaptophysin immunostaining, whilst the IML and MML were more lightly immunostained. Comparison of the optical densities of the molecular layers in the contralateral dentate gyrus of vehicle or LY404187 (0.5mg/kg) treated animals revealed that there was no significant difference in the intensity of immunostaining; thus validating this anatomical area as the control region (Fig. 7.7A, B). There was minimal immunostaining of the corpus callosum, and this did not significantly differ between vehicle and drug treated animals (Fig. 7.6B; 7.7C, D).

In the dentate gyrus ipsilateral to the lesioned entorhinal cortex, there were minimal changes in the pattern of immunoreactivity in the IML and MML of vehicle treated animals compared to the contralateral molecular layer (Fig. 7.8). There was no significant difference in the density of synaptophysin immunostaining in vehicle or LY404187 (0.5mg/kg) treated groups in the IML or MML (Figure X.x) in either group A (14 days post ECL, 7 days of drug treatment) or group B (21 days post ECL, 14 days of drug treatment) (Fig. 7.9). In both group A and group B, there were modest reductions in the levels of immunostaining in the OML compared to the contralateral dentate gyrus (Fig7.8). However, there was no significant difference between the intensity of synaptophysin immunostaining in the OML of vehicle or LY404187 (0.5mg/kg) treated animals (Fig. 7.9).

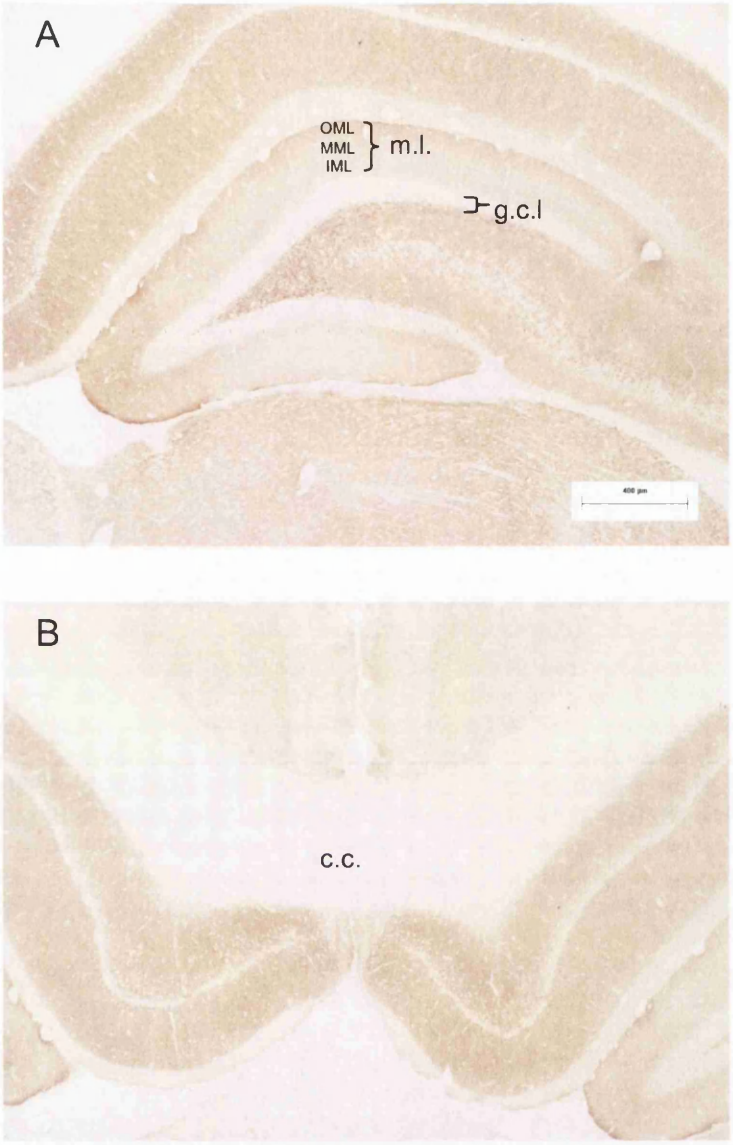

Figure 7.6 Synaptophysin immunostaining in control regions

A. Synaptophysin immunostaining in the dentate gyrus contralateral to the lesioned entorhinal cortex. In the molecular layer (m.l.) the outer molecular layer (OML) is most densely stained, whereas the middle (MML) and inner molecular layers (IML) are more lightly stained. The granule cell layer (g.c.l.) is relatively unstained.

B. The corpus callosum (c.c) contains the low levels of immunostaining. Scale bar = 400μm.

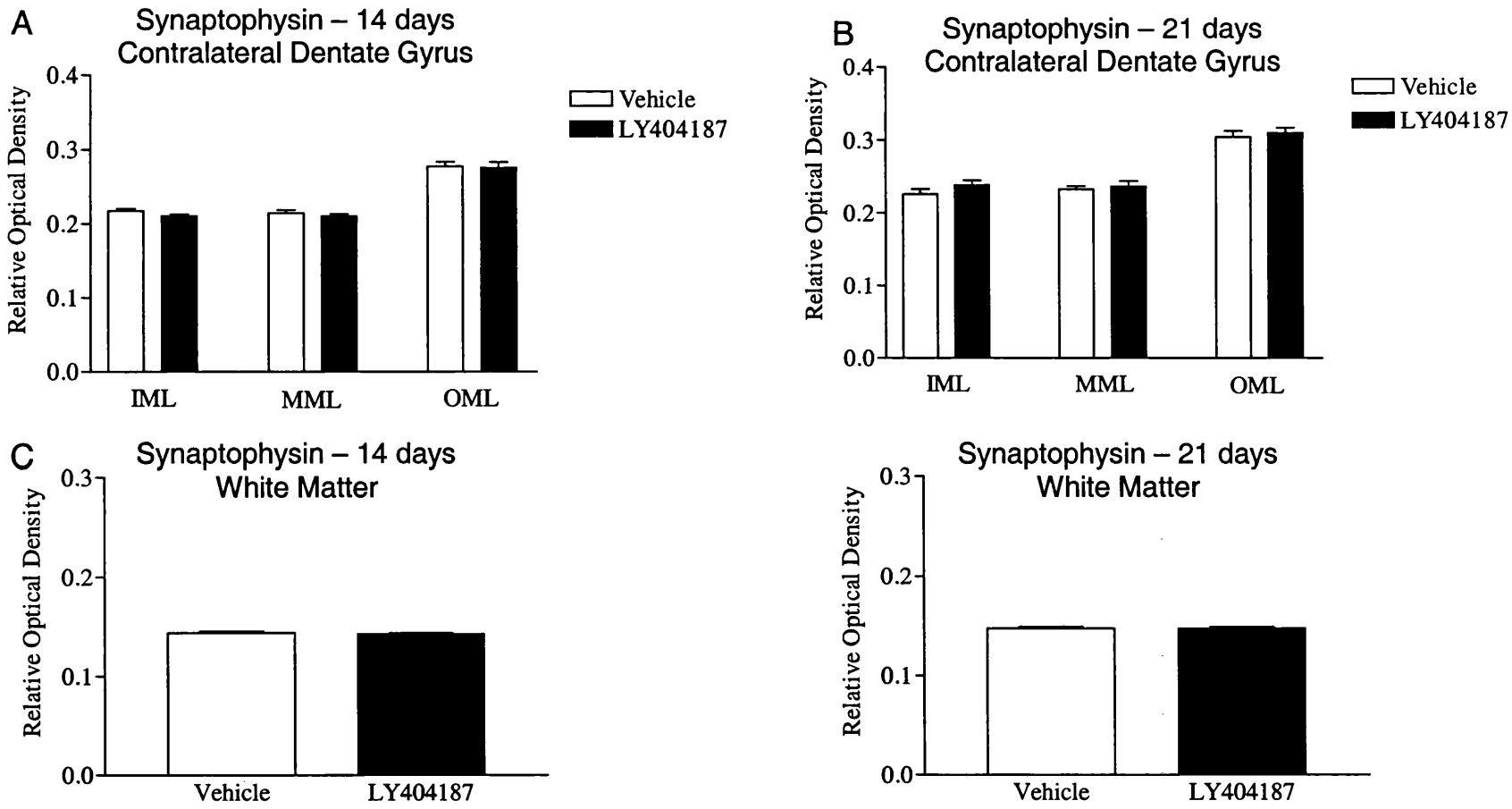

Figure 7.7 Relative optical density in control regions of synaptophysin immunostained sections

There was no significant difference in the relative optical density of the three molecular layers of the dentate gyrus contralateral to the lesion hemisphere between vehicle or drug (LY404187, 0.5mg/kg) treated animals at 14 (A) or 21 days (B). There was no significant difference in the relative optical density of the control region, the corpus callosum, between vehicle or drug treated animals at 14 (C) or 21 days (D). n=7-10 per group, unpaired Student's *t* test.

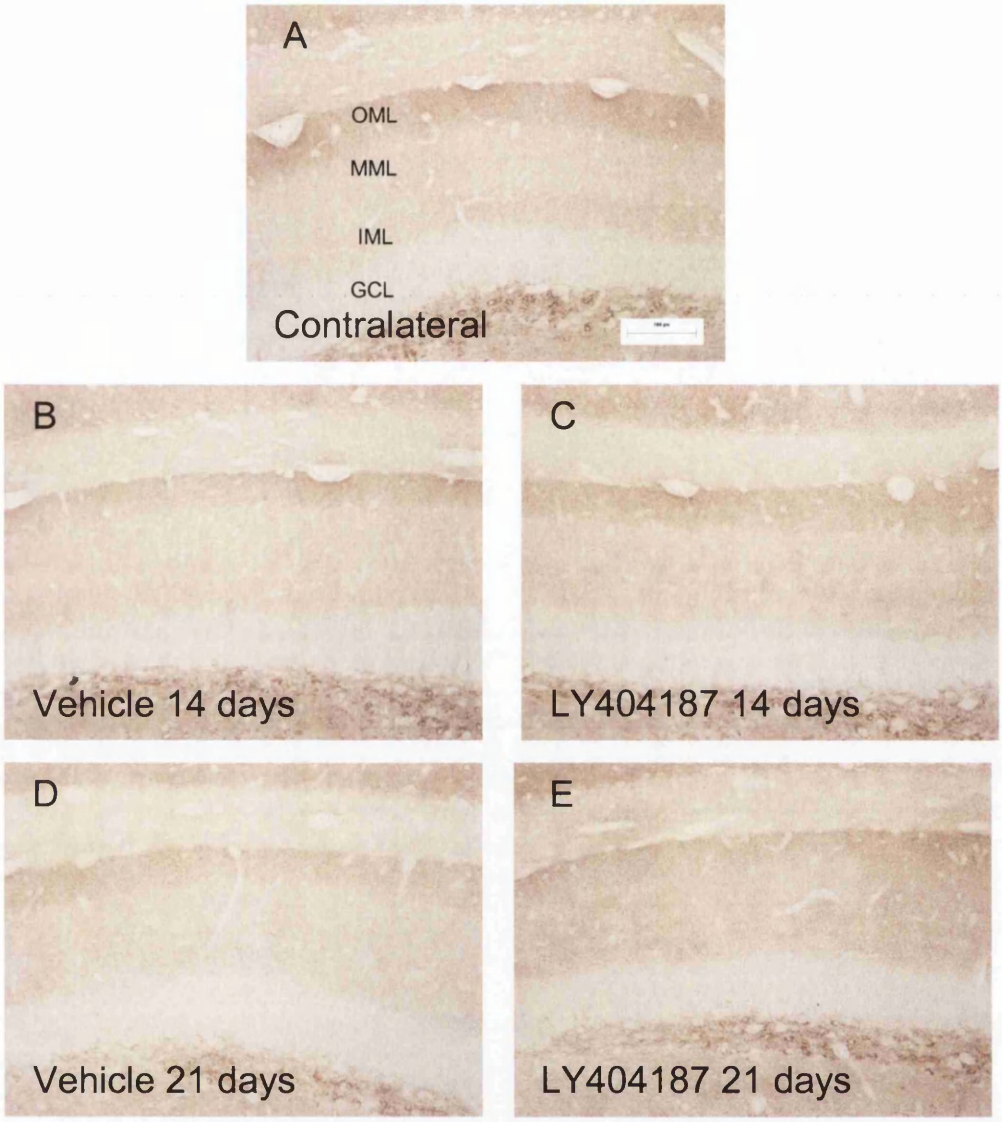

Figure 7.8 Synaptophysin immunostaining in the dentate gyrus

A. Synaptophysin immunostaining in the dentate gyrus contralateral to the lesioned entorhinal cortex. A trilaminar pattern of immunostaining is evident in the outer (OML), middle (MML) and inner (IML) molecular layer of the dentate gyrus, however the granule cell layer is relatively unstained.

B. –E. Synaptophysin immunostaining in the dentate gyrus ipsilateral to the entorhinal cortex lesion in representative animals that survived for 14 (B, C) or 28 days(D, E) following the lesion, that were treated with either vehicle (B, D), or LY404187 (0.5mg/kg; C, E) . Scale bar = 100μm.

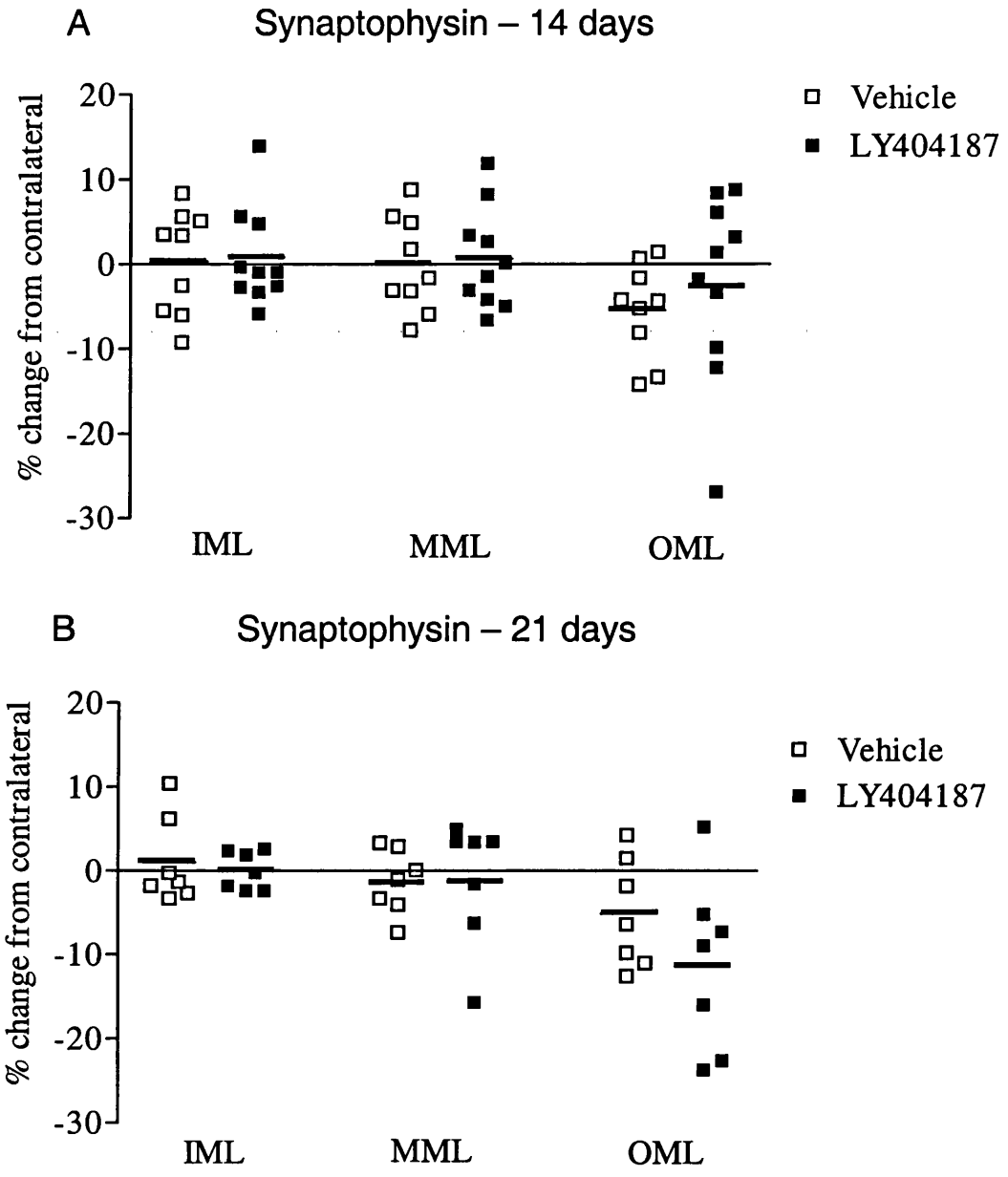

Figure 7.9 Quantification of synaptophysin immunoreactivity in the inner (IML), middle (MML) and outer molecular layers (OML) of the dentate gyrus

A. Synaptophysin immunoreactivity was not significantly altered in the IML, MML or OML after treatment with the AMPA receptor poteniator LY404187 (0.5mg/kg) compared to vehicle treatment, 14 days following entorhinal cortex lesion (Student's *t* test).

B. Synaptophysin immunoreactivity was not significantly different in the IML, MML or OML following LY404187 (0.5mg/kg) compared to vehicle treatment, 21 days after entorhinal cortex lesion (Student's *t* test).

Bars indicate means of groups.

7.3.4 Quantification of BrdU immunopositive cells

BrdU was administered on day 6 following ECL for all animals. Therefore, the number of 8 day old (Group A) and 15 day old (Group B) cells were compared following LY404187 or vehicle administration. BrdU immunopositive cells were present in the granule cell layer and hilus of the dentate gyrus, and in other areas of the hippocampus. Within the granule cell layer, cells were mainly present in the lower part of the cell layer, where the subgranular zone exists. BrdU immunostaining was present in the nuclei of BrdU immunopositive cells. In some cells, there was uniform, dark staining of the nuclei (Fig. 7.10A), whereas other cells were more lightly stained (Fig. 7.10B). Occasionally a punctate, spotted pattern of immunostaining was observed. No attempt was made to differentiate between these different patterns of immunostaining in the quantification. Quantification of the number of BrdU immunopositive cells in the granule cell layer revealed that there was no significant difference between the number of BrdU immunopositive cells in vehicle or LY404187 (0.5mg/kg) treated animals in group A (Fig. 7.11A). In group B, there was an increase in the mean number of BrdU cells in animals that had received 14 days of LY404187 (0.5mg/kg) treatment compared with vehicle treated animals, however, this increase did not reach accepted levels of statistical significance (Fig. 7.11B).

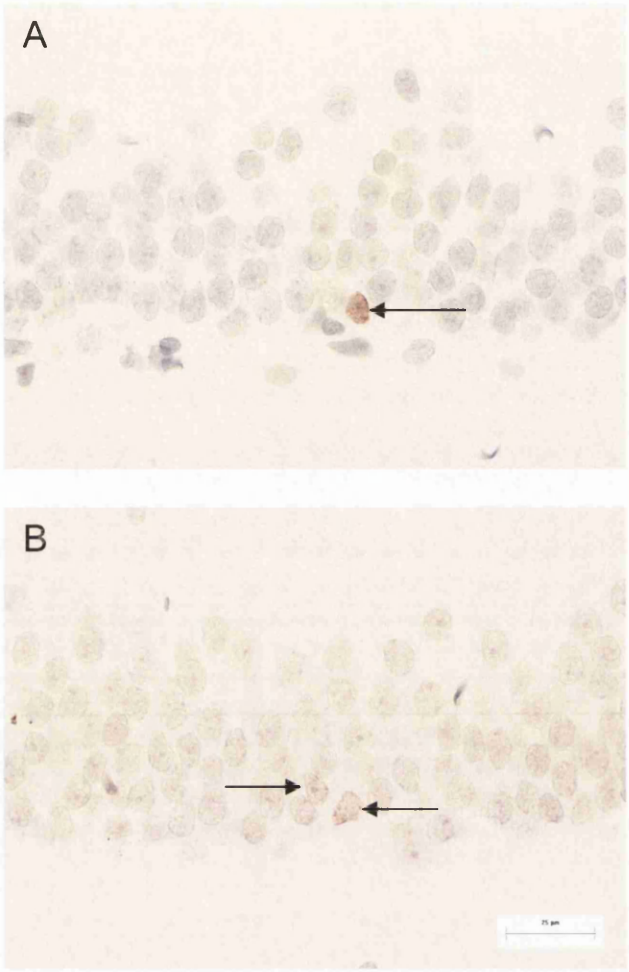

Figure 7.10 BrdU immunostaining in the dentate gyrus

A. A BrdU immunopositive cell in the granule cell layer of the dentate gyrus (arrow). The nucleus of this cell is uniformly, darkly stained. Nuclei of other cells have been stained with haematoxylin in these sections

B. Two BrdU immunopositive cells which are more lightly immunostained that the cell in A (arrow).

Scale bar = 25μm.

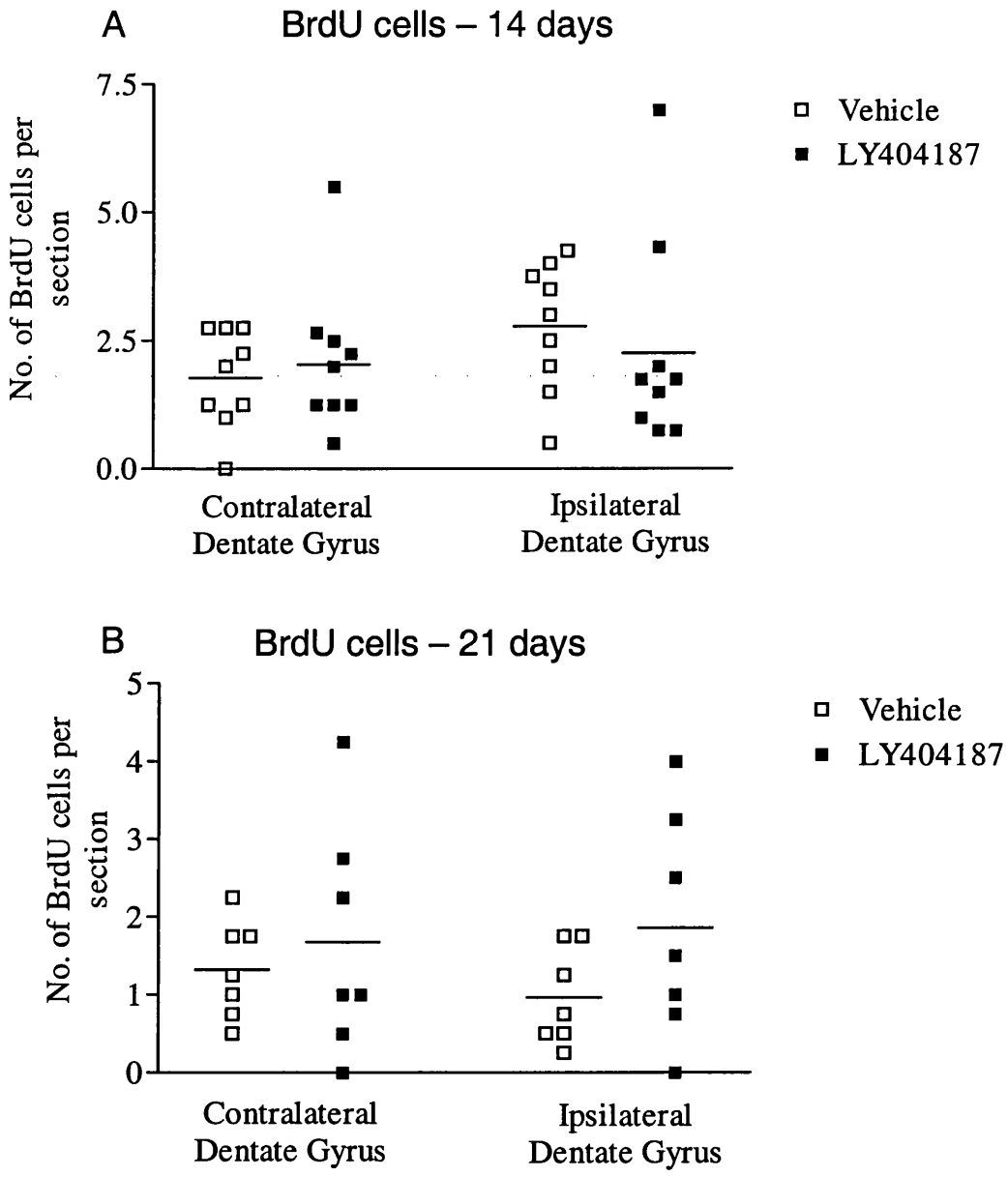

Figure 7.11 Quantification of BrdU immuoreactive cells in the granule cell layer of the dentate gyrus

A. There was no significant difference in the number of BrdU immunopositive cells in the dentate gyrus following 7 days of LY404187 (0.5mg/kg) compared to vehicle treatment, in animals which survived for 14 days following entorhinal cortex lesioning (Student's *t* test). BrdU was injected on day 6 following entorhinal cortex lesioning, 1 day before vehicle or LY404187 treatment commenced.

B. There was no significant difference in the number of BrdU immunopositive cells in the dentate gyrus following 14 days of LY404187 (0.5mg/kg) or vehicle treatment, in animals which survived for 21 days following entorhinal cortex lesioning (Student's *t* test). BrdU was injected on day 6 following entorhinal cortex lesioning, 24 hours prior to commencement of vehicle or LY404187 treatment.

7.4 Discussion

To summarise, the data presented in this chapter illustrates that lesioning the entorhinal cortex of adult rats resulted in very modest alterations in the pattern of GAP 43 and synaptophysin immunoreactivity in the dentate gyrus 14 and 21 days post lesion. Seven or 14 days of treatment with the AMPA receptor potentiator LY404187 did not enhance sprouting or synaptogenesis assessed with these markers. Treatment with the AMPA receptor potentiator LY404187 did not alter the number of BrdU cells in the granule cell layer 14 days following entorhinal cortex. However, by 21 days post ECL, there were increased numbers of BrdU cells in the LY404187 treated animals, although these did not reach significance levels.

Use of ibotenic acid to lesion the entorhinal cortex

A variety of techniques have been used to lesion the entorhinal cortex in studies that characterised the temporal evolution of degeneration and regeneration in the dentate gyrus. However, the most commonly used techniques are electrolytic and aspirational lesions and knife cuts of the perforant pathway. For instance, the laboratory of Dellar, Nitsch and Frotscher, who have extensively characterised the response of the hippocampus to ECL, deploy electrolytic lesions of the entorhinal cortex. This technique severs the area between entorhinal cortex and the hippocampus, resulting in the complete destruction of the entorhinal afferent input into dentate gyrus (eg Forster *et al.*, 1997). These electrolytic lesions result in an 80-90% loss of afferent synapses in the OML of the dentate gyrus (Matthews *et al.*, 1976). Masliah et al (1991) characterised degeneration and regeneration in the dentate gyrus of the rat using GAP 43 and synaptophysin following an aspirative lesion that removed the subiculum and parasubiculum, which is likely to have removed the majority of the afferent entorhinal input into the dentate gyrus. This resulted in a 50% loss of synapses in the OML at 7 days (Masliah *et al.*, 1991). The entorhinal cortex lesions induced by ibotenic acid in the current study resulted in small, discrete lesions confined to the caudal entorhinal cortex that generally did not involve the subiculum, parasubiculum or hippocampus. The entorhinal cortex is a large structure, extending approximately 4.5mm in a rostro-caudal direction in the brain. A large area of entorhinal cortex was undamaged in the current study, which presumably accounts for the minimal degeneration detected.

A similar protocol used in the current study with ibotenic acid has been used to lesion the caudal entorhinal cortex of the mouse, which resulted in a 40% loss of

synapses in the MML 28 days following lesion (White *et al.*, 2001). However, injecting a similar dose of ibotenic into the relatively smaller mouse brain will presumably result in a larger area of damaged entorhinal cortex, and more chance of involvement of the subiculum, parasubiculum and hippocampus. Inherent species differences may also exist in the degenerative and regenerative processes that occur following ibotenic acid ECL in rats and mice (Kadish and Van Groen, 2003). Few studies have examined the effects of ibotenic acid lesioning of the *rat* entorhinal cortex on plasticity in the hippocampus. Kurumaji and McCulloch (1990) injected the same concentration of ibotenic acid into the entorhinal cortex at similar stereotaxic co-ordinates to that deployed in the current study, and reported that there were no alterations in glucose utilisation in the dentate gyrus 14 days following the lesion. As alterations in glucose utilisation are thought to predominately reflect activity at synaptic terminals, this suggests there was a minimal loss of synapses in the dentate gyrus using this method (Kurumaji and McCulloch, 1991). However, removing the entire entorhinal cortex together with the pre- and parasubiculum resulted in significant reductions in glucose utilisation in the dentate gyrus, indicative of significant synapse loss (Jorgensen and Wright, 1988). Ibotenic acid lesions of the entorhinal cortex have also been shown to induce cognitive deficits in rats, assessed in the Morris water maze (Eijkenboom *et al.*, 2000). However, the rats in this study received 3 injections of ibotenic acid (0.5μl, 10mg/ml) over a 0.5mm area of each caudal entorhinal cortex, resulting in an extensive lesion that included the subiculum and a substantial portion of hippocampus. Collectively, these studies indicate that extensive damage to the entorhinal cortex and adjacent subiculum is required to induce substantial deafferation and degeneration in the dentate gyrus. The subtle levels of degeneration reported in the current study may reflect small, discrete lesions of the entorhinal cortex that contrast with the more extensive lesioning techniques used by other groups.

Alternatively, incorrect time points may have been chosen to examine degeneration in the current study. Sprouting of neighbouring afferent fibre systems has been reported to occur between 7-30 days following electrolytic entorhinal cortex lesioning (Matthews *et al.*, 1976; Lee *et al.*, 1977; Steward and Vinsant, 1983; Benowitz *et al.*, 1990; Masliah *et al.*, 1991). Fibre loss and sprouting may already have occurred prior to the time point chosen in the current study. The replacement of synapses is reported to occur over a slower time course than sprouting. For example

following electrolytic ECL, only 80% of synapses are recovered at 30 days, and synaptogenesis continues for months (Matthews *et al.,* 1976; Masliah *et al.,* 1991). However, the temporal evolution of synaptogenesis has not been characterised following ibotenic acid-induced ECL. Therefore it remains possible that a significant loss of synapses did occur in the current model, and that reactive synaptogenesis progressed over a quicker time course in the current paradigm. In addition to altering the density of GAP 43 and synaptophysin immunoreactivity following ECL, the width of the IML can expand, and outer molecular layer can shrink during the period of degeneration (Masliah *et al.,* 1991). The width of the molecular layers was not examined in the present study. However alterations in the width of these layers may have led to alterations in the optical density readings, which may not truly reflect the extent of sprouting or synaptogenesis.

Effect of the AMPA receptor potentiator LY404187 on regeneration in the dentate gyrus

Although there were only subtle alterations in GAP 43 and synaptophysin immunostaining in the current study, there were no indications that the AMPA receptor potentiator enhanced sprouting or synatogenesis. The adequacy of the dosing regime must firstly be addressed when discussing the observed ineffectiveness of LY404187 in this experimental paradigm. The ability of LY404187 to cross the blood brain barrier has been demonstrated in a number of studies where intravenous or subcutaneous administration of the compound has produced effects in the CNS (Vandergriff *et al.,* 2001; Mackowiak *et al.,* 2002; Bai *et al.,* 2003; results presented in chapter 6). In the current study, animals received twice-daily injections of LY404187 (0.5mg/kg) for seven or fourteen days. Administration of LY404187 (0.5mg/kg) was sufficient to induce significant increases in glucose utilisation, however these effects were not present following administration of the higher dose of LY404187 (5mg/kg; results in chapter 6). Bell shaped dose response curves have also been reported following administration of LY404187 or its active isomer LY451646, in the forced swim test and when examining stem cell proliferation in the dentate gyrus (Li *et al.,* 2001; Quirk and Nisenbaum, 2002; Bai *et al.,* 2003). Similarly, bell shaped dose response curves have been reported when examining axonal regeneration following administration of exogenous BDNF (Mamounas *et al.,* 2000); raising the possibility that higher doses of neurotrophins or AMPA receptor potentiators may be ineffective. It is therefore

possible that the cumulative effects of twice-daily injections of LY404187 (0.5mg/kg) have exceeded the dose range at which LY404187 is efficacious. However, twice daily injections of LY404187 (0.5mg/kg) for 28 days have been shown to enhance levels of GAP 43 and protect against 6-hydroxydopamine (6-OHDA) lesioning of the striatum (O'Neill *et al.*, 2003).

In the current study, animals were allowed to recover for 7 days following the entorhinal cortex lesion until drug treatment commenced. Studies have suggested that degenerative processes are at their peak 2 – 8 days following entorhinal cortex lesioning (Savaskan and Nitsch, 2001). As the lesion was caused by an excitotoxin and involves degeneration of glutamatergic fibres, it was decided not to administer the AMPA receptor potentiator LY404187 during the degenerative period so that excitotoxic mechanisms were not enhanced. However, the first week following the ECL may be a crucial time point when BDNF could enhance sprouting. In addition, recent studies have suggested, perhaps paradoxically, that AMPA receptor potentiators may be neuroprotective. For example, the AMPA receptor potentiator LY4503430 can reduce the loss of tyrosine hydroxylase immunopositive neurons following 6-OHDA administration in the substantia nigra or caudate nucleus (Murray *et al.*, 2003). Pre- or post-treatment with CX-516 can attenuate AMPA-induced pathology in hippocampal slice cultures, and co-injection of AMPA (50nmol) with CX-516 produces a dose-dependent reduction in lesion volume; conferring more than a 50% reduction at the highest dose (Bahr *et al.*, 2002). These studies suggest that AMPA receptor potentiators may protect rather than exacerbate excitotoxicity, and suggest that immediate treatment with LY04187 may have been efficacious in the current study.

Further experiments with different dosing protocols of LY404187 may reveal whether or not this AMPA receptor potentiator has the potential to enhance sprouting following an entorhinal cortex lesion. However, another possibility is that in this experimental paradigm, AMPA receptor potentiators may simply be ineffective in enhancing regeneration. A variety of neurotrophic factors, such as NGF, BDNF, CNTF, IL-1, FGF-2, TGF-ß1 and have been implicated in the regenerative reorganisation of the dentate gyrus following ECL based on reports of up regulation following entorhinal cortex lesion (reviewed in Deller and Frotcher, 1997). However, the temporal evolution, and relative importance of each of these growth

factors has not been examined or compared. BDNF mRNA is markedly upregulated following entorhinal cortex lesioning, however this generally occurs within 4 hours; between 24 hours and 10 days there is no evidence for further increases in BDNF (Lapchak *et al.,* 1993; Gwag *et al.,* 1994; Forster *et al.,* 1997). Furthermore, the initial large increase in BDNF mRNA can be mimicked with high frequency stimulation of the perforant pathway (Springer *et al.,* 1994), and can be blocked with the NMDA receptor antagonist MK-801; however this blockade did not attenuate the sprouting of cholinergic fibres 14 days post ECL (Forster *et al.,* 1997). These data suggest that the initial increase in BDNF mRNA following ECL may be related to glutamate release from the entorhinal terminals, and subsequent to this, there may be no role for BDNF in the mechanisms of sprouting. The ability of the structurally related AMPA receptor potentiator, LY503430, to enhance regeneration, assessed with GAP 43 immunohistochemistry, following 6-OHDA lesioning suggests that these group of compounds may be more effective in the striato-nigral system (Murray *et al.,* 2003). Whilst the lack of a concomitant increase in BDNF levels reported 6-OHDA study (Murray *et al.,* 2003) may simply reflect that BDNF was upregulated at an earlier timepoint, they also suggest that these compounds may act through a different mechanism to enhance plasticity. Finally, it is possible that LY404187 may have enhanced plasticity in the dentate gyrus without having an effect on fibre sprouting or synapse density. Phosporylation of AMPA receptor is a means of enhancing ion flux through the receptor (Wenthold and Roche, 1998), thereby enhancing glutamatergic transmission. Thus, it remains possible that the AMPA receptor potentiator LY404187 may have acted by this mechanism to enhance glutamatergic transmission. Electrophysiological studies could be used to examine this phenomenon.

Effect of the AMPA receptor potentiator LY404187 on the number of BrdU cells in the dentate gyrus

Several thousand new cells are generated in the dentate gyrus of mammals every day from proliferating neuronal and glial progenitor cells, yet between 1 - 2 weeks later; many of these cells die (Cameron *et al.,* 1993; Gould *et al.,* 1999). However, learning hippocampal dependent cognitive tasks can enhance the survival of these cells, the majority of which express neuronal markers (Gould *et al.,* 1999). This

study suggests that newly generated neurons that survive in the dentate gyrus may be involved in memory formation (Gould *et al.,* 1999; Shors *et al.,* 2001). In the current study, there was a reduction in the number of BrdU immunopositive cells between 1 and 2 weeks following BrdU administration. However, compared with vehicle treated animals, there were increased numbers of BrdU cells in the dentate gyrus ipsilateral to the ECL of animals treated with the AMPA receptor potentiator LY404187 (0.5mg/kg), although these were not statistically significant. At present, it is unclear if this signifies enhanced proliferation of the BrdU cells, or if these pilot studies suggest that LY404187 has the capacity to influence the survival of newly generated cells. Further experiments with different dosing regimes of LY404187, at later time points would determine if LY404187 could enhance the number of surviving, functional neurons in the dentate gyrus.

Clinical interventions that could enhance the proliferation of endogenous stem cells and the genesis and survival of new neurons would be beneficial in a number of clinical disorders. Arvidsson and colleagues (2002) recently demonstrated that focal cerebral ischaemia markedly increased the proliferation of endogenous stem cells in the subventricular zone of rats, which migrate into the core of the ischaemic lesion, where they develop the phenotype of striatal medium spiny neurons. However, between 2 and 8 weeks following ischaemia, approximately 80% of the new neurons died, presumably due to an unfavourable environment and lack of trophic support (Arvidsson *et al.,* 2002). The production of new dentate gyrus granule cells also decreases markedly in old age (Cameron and McKay, 1999); based on their proposed role in memory formation, this decline in neurogenesis may contribute to age-related memory deficits. Decreased serotenergic transmission, which is commonly associated with depression, attenuates the rate of neurogenesis (Brezun and Daszuta, 1999; 2000). These examples illustrate that altered levels of neurogenesis are associated with clinical disorders; however, whilst the brain has the capacity for self-repair, interventions which could augment this process would be highly desirable.

CHAPTER 8
GENERAL DISCUSSION

8.1 General Discussion

8.1.1 Role of AMPA-receptor mediated excitotoxicity in white matter damage

Considerable *in vitro* evidence has suggested a role for AMPA receptors in mediating white matter pathology; the data presented in this thesis has extended these observations *in vivo*. Thus, AMPA can induce white matter damage *in vivo,* in both the rat and the mouse, and AMPA receptor antagonism can attenuate white matter pathology following focal cerebral ischaemia *in vivo*. AMPA receptors therefore represent a pathogenic mediator of both grey *and* white matter damage, and may be an attractive focus for neuroprotective strategies. AMPA receptor antagonism also reduces axonal and oligodendrocyte damage following *in vivo* spinal cord ischaemia and trauma (Wrathall *et al.,* 1997; Kanellopoulous *et al.,* 2000; Li *et al.,* 1999; Rosenberg *et al.,* 1999b). Furthermore, the protection of axons and oligodendrocytes with AMPA antagonists has been shown to correlate with improved functional recovery, following spinal cord ischaemia (Kanellopoulos *et al.,* 2000; Wrathall *et al.,* 1994, 1997) and experimental autoimmune encephalomyelitis (Pitt *et al.,* 2000). However, more studies are required to establish if AMPA receptor antagonism has the potential to protect the cellular components of white and grey matter in the clinic.

A number of studies have demonstrated the presence of AMPA receptors in certain white matter tracts of rats and mice (see section 1.3.3). Yet relatively little information is known about the expression of AMPA receptors in the many other white matter tracts and glial cells in the rodent brain. As with grey matter AMPA receptors, a number of transcriptional and post-translational modifications of the AMPA receptor may give rise to vastly heterogeneous receptors with differing physiological properties. However little is known about such diversity in white matter AMPA receptors. A more anatomically widespread, systematic analysis of glutamate receptor subunit distribution in white matter would be valuable. A method that combines whole-cell patch clamp recording with RT-PCR (Lambolez *et al.,* 1992; Dixon *et al.,* 2000) would also be useful to correlate information about AMPA receptor subunit expression with the functional properties of AMPA receptors in white matter.

In comparison to the rodent brain, even less is known about the expression of AMPA/kainate receptors in white matter tracts of the human brain. Only a few studies have examined the expression of certain receptor subunits in limited human brain areas. For example, GluR4 has been localised to oligodendrocyte-precursor-like cells in the cerebral cortex, however, GluR1 is absent from cortical white matter (He *et al.,* 1996; Ong and Garey, 1996). Of interest however, it has been reported recently with PCR analysis of post mortem tissue that 7% of GluR2 in the prefrontal cortex (PFC) white matter of humans is unedited, which contrasts with <0.1% unedited GluR2 in human pre-frontal cortical grey matter (Akbarian *et al.,* 1995). As the unedited form of GluR2 is permeable to Ca^{2+}, this suggests that a higher proportion of glial cells in the PFC are Ca^{2+} permeable, which has implications for disease states (Pellegrini-Giampietro *et al.,* 1997; Weiss and Sensi, 2000). More studies like these, with post mortem brain tissue, are required to further elucidate the prevalence of white matter AMPA receptor expression in human brains, both in normal and diseased states. More sophisticated imaging techniques could also contribute to an increased understanding of AMPA receptor expression in human white matter. For instance, isotopically labelled MK 801 has been used to examine NMDA receptor activation during an ischaemic episode in living human patients with single photon emission tomography (SPET; Owens *et al.,* 1997). The development of isotopically labelled AMPA receptor ligands or subunit specific ligands for use with imaging techniques would contribute greatly to knowledge about AMPA receptor distribution in normal human brains, and possible pathophysiological processes occurring at these receptors in humans.

The concept of 'secondary' excitotoxicity as a pathogenic mediator of neuronal loss in chronic neurodegenerative diseases is frequently suggested by a number of groups. However, the experimental evidence for this is less compelling than for the role of excitotoxicity in acute neurological diseases. Thus, the role of 'secondary' excitotoxicity as a pathogenic mediator of *axonal* pathology in chronic neurological disorders remains purely hypothetical. However, there is evidence that excitotoxicity may contribute to the pathogenesis of ALS and multiple sclerosis, two disorders that are characterised by axonal swellings and degeneration (Ferguson *et al.,* 1997; Trapp *et al.,*1998). Chronic treatment with the AMPA receptor antagonist NBQX reduced

axonal damage in EAE mice, a demyelinating model of multiple sclerosis (Pitt *et al.*, 2000; Werner *et al.*, 2001). In post mortem MS tissue, increased levels of glutaminase, the enzyme that synthesises glutamate, and decreased levels of the glutamate transporter GLT-1 and the glutamate-metabolising enzymes glutamate dehydrogenase and glutamate synthetase were associated with oligodendrocyte loss and axonal damage (Werner *et al.*, 2001). This suggests that excitotoxicity may be induced by perturbations in normal glutamate homeostasis. Similar alterations have been reported in ALS. The glutamate transporter EAAT2 is decreased in the brain and spinal cord of ALS patients; furthermore, a decrease in the transport velocity of glutamate transporters has been localised to areas of the brain and spinal cord associated with ALS (Rothstein *et al.*, 1992; Rothstein *et al.*, 1995). It remains unclear if these perturbations in glutamate homeostasis are associated with, or are causative of axonal damage in ALS or MS. AMPA receptor activation may represent a common mechanism of neuronal, axonal, myelin and oligodendrocyte damage. AMPA receptor antagonists may have therapeutic potential in the treatment of a number of neurological conditions, where they offer superiority over drugs that protect only neuronal perikarya.

8.1.2. Other mechanisms of white matter damage

A number of other pathogenic mediators of cellular damage can affect white matter. Mitochondria contained within white matter to produce energy can also produce increased levels of oxygen radicals, such as superoxide, hydrogen peroxide and hydroxyl radicals in pathological situations. These have the potential to induce peroxidation injury of lipid membranes and proteins. Inhibiting mitochondria with 3-nitropropionic acid or malonate causes axonal damage (Dewar *et al.*, 2001; McCracken *et al.*, 2001; results in chapter 6) that is associated with increased oxidative stress (McCracken *et al.*, 2001). Intracerebral injection of 4-hydroxynoneal, a by-product of lipid peroxidation, induces axonal damage *in vivo* (McCracken *et al.*, 2000). The anti-oxidant compound ebselen and the spin trap agent PBN can protect axons (Imai *et al.*, 2001) and oligodendrocytes from focal cerebral ischaemia, (Irving *et al.*, 1997; Imai *et al.*, 2001). Nitric oxide, in submicromolar concentrations, can kill axons and oligodendroglia in white matter

(Smith *et al.,* 2001; Garthwaite *et al.,* 2002). Nitric oxide can react with free radicals to produce the highly toxic molecule, peroxynitrite, which can induce axonal damage (Touil *et al.,* 2001).

Studies from the laboratory of Stys and Waxman amongst others have highlighted the role of altered ionic homeostasis in causing axonal damage (reviewed in Waxman *et al.,* 1991; Stys, 1998). Thus, energy depletion and other pathogenic circumstances can induce influxes of Na^+ and Ca^{2+} into the axolemma, which can damage the axon. Intra-axonal Ca^{2+} influx can activate various Ca^{2+} enzymes, including proteases or caspases such as calpain, which can devastate the intra-axonal cytoskeleton and organelles (McCracken *et al.,* 1999; Buki *et al.,* 1999b, 2000; Jiang and Stys, 2000). Inhibitors of Na^+ influx can protect white matter from anoxic, traumatic or ischaemic insults (Teng and Wrathall, 1997; Garthwaite *et al.,* 1999; Rosenberg *et al.,* 1999a).

Inflammatory cells may invade white matter and produce cytotoxic factors that can cause axonal damage. For example, invading microglia and macrophages in post mortem MS lesions and EAE tissue containing damaged axons also contained high levels of the glutamate-producing enzyme, glutaminase, suggesting that these cells produce excitotoxic levels of glutamate. Treatment of EAE mice with NBQX did not alter lesion size or the amount of glutaminase producing cells, but it did attenuate axonal damage, further supporting this theory (Werner *et al.,* 2001). Inflammatory cells may also produce nitric oxide and oxygen radicals, which are implicated in axonal damage (see above). Inflammation can also result in uncontrolled expression of extracellular proteases known as matrix metalloproteinases (MMPs). Myelin basic protein is one of the substrates of MMP-9 (Chandler *et al.,* 1995). Intracerebral injection of MMP-9 and other MMPs induces axonal damage, whilst ischaemically-induced myelin damage is attenuated in MMP-9 gene knockout mice (Asahi *et al.,* 2001; Newman *et al.,* 2001).

The various pathogenic mediators of white matter damage described above are unlikely to act alone, but rather act in concert with each other to cause deleterious effects. As an examples of this, excitotoxic mechanisms can induce oxygen radicals (Underhill *et al.,* 2002b); nitric oxide mediated damage causes Na^+ and Ca^{2+} influx (Kapoor *et al.,* 2003); and inflammatory cells can produce glutamate (Werner *et al.,* 2001). Each of these mechanisms has been implicated in neuronal perikaryal

damage as well, thus representing appropriate targets for interventions which will protect components of grey and white matter.

The importance of white matter brain protection *in addition* to grey matter protection is becoming increasingly recognised (Stys, 1998; Bjartmar *et al.,* 1999; Dewar *et al.,* 1999; Petty and Wettstein, 1999; Coleman and Perry, 2002; Gladstone *et al.,* 2002; Medana and Esiri, 2003). The widespread use of sensitive immunocytochemical methods such as APP and NF immunohistochemistry has undoubtedly aided the increasing recognition of white matter damage. However, the discrepancies reported in the distribution of damaged axons in APP and NF immunostained sections in chapter 3-5 of this thesis, and in another study (Stone *et al.,* 2001) have highlighted the need for multiple markers for the evaluation of white matter damage. The use of sensitive imaging techniques in humans, such as MRS/MRI imaging of N-acetylaspartate (axonal marker) levels will also contribute to the understanding of white matter pathology and progression in human neurological conditions.

8.1.3 Clinical potential of AMPA receptor potentiators

The study described in chapter 6 suggests that the AMPA receptor potentiator LY404187 and related molecules may have therapeutic utility in the treatment of cognitive deficits arising in certain neurological conditions where glutamatergic hypofunction occurs. Administration of an AMPA receptor potentiator to healthy humans was well tolerated, and positive effects in certain memory tests were demonstrated. (Ingvar *et al.,* 1997). Deficits in glutamatergic transmission may contribute to cognitive decline in the elderly (Segovia *et al.,* 2001). CX-516 administration in elderly humans (65-76 years) improves delayed recall of nonsense syllables (Lynch *et al.,* 1997). Disruption in glutamatergic transmission may also contribute to the cognitive deficits observed in Alzheimer's disease and schizophrenia (Carlsson *et al.,* 1999; Tamminga *et al.,* 1999). Positive effects have been demonstrated in patients with Alzheimer's disease or schizophrenia following administration of AMPA receptor potentiator compounds (Lee and Benfield, 1994; Goff *et al.,* 2001). In this thesis, for the first time, an anatomical basis for the pre-clinical effects of LY404187 in models of depression and cognition has been determined. LY404187 is systemically active and far more potent that previous

AMPA potentiators. It has recently been shown that a related biarylpropylsulfonamide, LY451395 can be safely administered to humans; suggesting that these AMPA receptor potentiators may be useful in situations of cognitive decline. In addition to enhancing glutamatergic transmission, AMPA receptor potentiators may have neuroprotective and neurotrophic properties which augments their clinical potential. Whilst there was no evidence in this thesis that AMPA receptor potentiators can enhance regeneration following ECL, other studies have demonstrated the neurotrophic and neuroprotective potential of these compounds (Bahr *et al.,* 2002; Murray *et al.,* 2003).

8.1.4 Potential side effects of AMPA receptor antagonists and AMPA receptor potentiators?

Because excitotoxicity is mediated by over-activation of glutamate receptors, this raises the concern that enhancing glutamatergic transmission with AMPA receptor potentiators may have toxic effects. Conversely, the role of AMPA receptor potentiators in LTP and cognitive enhancement suggests that AMPA receptor antagonists may induce cognitive deficits. The latter has been demonstrated in a number of studies (Zivkovic *et al.,* 1995; Filliat *et al.,* 1998; Riedel *et al.,* 1999), although other studies have reported no effects (Miztal and Danysz, 1995). A temporary loss of cognitive function might be acceptable and justified to prevent permanent disability in conditions such as ischaemia and trauma. However, use of AMPA receptor antagonists as treatment for epilepsy, neuropathic pain or chronic neurodegenerative disorders may cause cognitive defects. More studies are required to establish if AMPA receptor antagonists are efficacious without inducing cognitive deficits. The reported involvement of specific AMPA receptor subunits or splice variants in neurological disorders (reviewed in Lees *et al.,* 2000; Sattler and Tymianski, 2001) suggests that the development of subunit- or splice-variant-specific ligands may be therapeutically beneficial in these disorders. Similarly, improved knowledge about the downstream, signal-transduction pathways involved in excitotoxicity may consequently lead to the identification of molecular targets for future therapy (Sattler and Tymianski, 2001).

Cyclothiazide is an AMPA receptor potentiator known to have toxic effects, causing seizures, cell death and lethality when administered to the brain (Yamada *et al.,*

1998a). However, other AMPA receptor potentiators do not seem to possess the same toxic effects as cyclothiazide. 1-BCP and IDRA-21 potentiate neuronal damage caused by glutamate exposure *in vitro* and global ischaemia *in vivo*, respectively (Yamada *et al.*, 1998a, b). However, the doses used in the latter studies are much higher than doses effective to enhance cognition (Staubli *et al.*, 1994; Zivkovic *et al.*, 1994). A number of other *in vivo* studies have reported no adverse side effects or toxicity. Indeed, administration of AMPA receptor potentiators is well tolerated in humans (Ingvar *et al.*, 1997; Lynch *et al.*, 1997). It has been hypothesised AMPA receptor potentiators are less likely to cause toxicity than AMPA receptor agonists, based on their mechanism of action. Thus, by enhancing only natural rates of glutamatergic transmission, rather than causing continued stimulation, they are less likely to induce toxicity. In addition, it is thought that drugs which affect only receptor deactivation have reduced toxic potential as desensitisation of receptors at high firing rates is not affected (Lees, 2000).

8.1.5 Concluding remarks

Based on their ubiquitous distribution in the CNS, and their involvement in both essential and damaging CNS functions, AMPA receptors are a therapeutic target in a number of CNS disorders. The data presented in the thesis have highlighted clinical usefulness of AMPA receptor ligands in a number of neurological disorders.

References

Adams, J.H., Graham, D.I., Murray, L.S., Scott, G. (1982) Diffuse axonal injury due to non-missile injury in humans: analysis of 45 cases. *Ann Neurol,* 12: 557-563.

Adams, J.H., Doyle, D., Ford, I., Gennarelli, T.A., Graham, D.I., McLellan, D.R. (1989) Diffuse axonal injury in head injury: definition, diagnosis and grading. *Histopathology,* 15: 49-59.

Agrawal, S.K. and Fehlings, M.G. (1997) Role of NMDA and Non-NMDA glutamate receptors in traumatic spinal cord injury. *J Neurosci,* 17(3): 1055-1063.

Aiello, G.L. and Bach-y-Rita, P. (2000) The cost of an action potential. *J Neurosci Methods,* 103: 145-149.

Akbarian, S., Smith, M.A., Jones, E.G. (1995) Editing for an AMPA receptor subunit RNA in prefrontal cortex and striatum in Alzheimer's disease, Huntington's disease and schizophrenia. *Brain Res,* 699(2): 297-304.

Alberdi, E., Sanchez Gomez, V., Marino, A., and Matute, C. (2002) Ca^{2+} influx through AMPA or kainate receptors alone is sufficient to initiate excitotoxicity in cultured oligodendrocytes. *Neurobiol of Disease,* 9: 234-243.

Alexianu, M.E., Ho, B.K., Mohamed, A.H., LaBella, V., Smith, R.G., Appel, S.H. (1994) The role of calcium-binding proteins in selective motoneuron vulnerability in amyotrophic lateral sclerosis. *Ann Neurol,* 36: 846-858.

Allan, S.M. and Rothwell, N.J. (2000) Coritcal death caused by striatal administration of AMPA and Interluekin-1 is mediated by activation of cortical NMDA receptors. *J Cereb Blood Flow and Metab,* 20(10): 1409-13.

Allan, S.M., Parker L.C., Collins B., Davies, R., Luheshi, G.N., Rothwell, N.J., (2000) Cortical death induced by IL-1 is mediated via actions in the hypothalamus of the rat. *Proc Nat Acad Sci, USA,* 97(10): 5580-5585.

Altar, C.A. (1999) Neurotrophins and depression. *TiPS,* 20: 59-61.

An, S.F., Giometto, B., Groves, M., Miller, R.F., Beckett, A.A., Gray, F., Tavolato, B., Scaravili, F. (1997) Axonal damage revealed by accumulation of beta-APP in HIV positive individuals without AIDS. *J Neuropath Exp Neurol,* 56: 1262-1268.

Ando, S., Kobayashi, S., Waki, H., Kon, K., Fukui, F., Tadenuma, T., Iwamoto, M., Takeda, Y., Izumiyama, N., Watanabe, K., Nakamura, H. (2002) Animal model of dementia induced by entorhinal synaptic damage and partial restoration of cognitive deficits by BDNF and carnitine. *J Neurosci Res,* 70:519-527.

Arai, A., Kessler, M., Xiao, P., Ambros-Ingerson, J., Rogers, G., Lynch, G. (1994) A centrally active drug that modulated AMPA receptor gated currents. *Brain Res,* 638: 343-346.

Arai, A., Kessler, M., Ambros-Ingerson, J., Quan, A., Yigiter, E., Rogers, S., Lynch, G. (1996) Effects of a centrally active benzopyrrolidine drug on AMPA receptor kinetics. *Neurosci,* 75(2): 573-585

Armstrong, N., Sun, Y., Chen, G.Q., Gouaux, E. (1998) Structure of a glutamate receptor ligand binding core in complex with kainate. *Nature,* 395: 913-917.

Arvidsson, A., Collin, T., Kirki, D., Kokaia, Z., Lindvall, O. (2002) Neuronal replacement from endogenous precursors in the adult brain after stroke. *Nature,* 8(9): 963-970.

Asahi, M., Wang, X., Mori, T., Sumii, T., Jung, J-C., Moskowitz, M.A., Fini, M.E., Lo, E.H. (2001) Effects of matrix metalloproteinase-9 gene knock-out on the proteolysis of blood-brain barrier and white matter components. *J Neurosci,* 21(19): 7724-7732.

Auer, R.N., Ingvar, M., Nevander, G. Olsson, Y., Siesjo, B.K. (1986) Early axonal lesion and preserved microvasculature in epilepsy-induced hypermetabolic necrosis of the substancia nigra. *Acta Neuropath,* 71: 207-215.

Bahr, B.A., Bendiske, J., Brown, A.B., Munirathinam, S., Caba, E., Rudin, M., Urwyler, S., Sauter, A., Rogers, G. (2002) Survival signalling and selective neuroprotection through glutamatergic transmission. *Exp Neurol,* 174: 34-47.

Bai, F., Bergeron, M., Nelson, D.L. (2003) Chronic AMPA receptor potentiator (LY451646) treatment increases cell proliferation in the adult rat hippocampus. *Neuropharmacol,* 44(8): 1013-1021.

Baltan Tekkok, S. and Goldberg, M.P. (2001) AMPA/Kainate receptor activation mediated hypoxic oligodendrocyte death and axonal injury in cerebral white matter. *J Neurosci,* 21(12): 4237-4248.

Barria, A., Muller, D., Derkach, V., Griffith, L.C., Soderling, T.R. (1997) Regulatory phosphorylation of AMPA-type glutamate receptors by CaM-KII during long term potentiation. *Science,* 276: 2042-2045.

Baumann, N. and Pham-Dinh, D. (2001) Biology of oligodendrocyte and myelin in the mammalian central nervous system. *Physiol Revs,* 81(2): 871-927.

Baumbarger, P.J., Muhlhauser, M., Zhai, J., Yang, C.R., Nisenbaum, E.S. (2001a) Positive modulation of α-Amino-3-hydroxy-4-isoxazole propionic acid (AMPA) receptors in prefrontal cortical pyramidal neurons by a novel allosteric potentiator. *J Pharm Exp Ther,* 298: 86-102.

Baumbarger, P.J., Muhlhauser, M., Yang, C.R., Nisenbaum, E.S. (2001b) LY392098, a novel AMPA receptor potentiator: electrophysiological studies in prefrontal cortical neurons. *Neuropharm,* 40: 992-1002.

Beal, M.F., Brouillet, E., Jenkins, B.G., Ferrante, R.J., Kowall, N.W., Miller, J.M., Storey, E., Srivastava, R., Rosen, B.R., Hyman, B.T. (1993a) Neurochemical and

histologic characterisation of striatal excitotoxic lesions produced by the mitochondrial toxin 3-nitropropionic acid. *J Neurosci,* 13(10): 4181-4192.

Beal, M.F., Brouillet, E., Jenkins, B., Henshaw, R., Rosen, B., Hyman, B.T. (1993b) Age-dependent striatal excitotoxic lesions produced by the endogenous mitochondrial inhibitor malonate. *J Neurochem,* 31(3): 1147-1150.

Beck, T.D., Lindholm, E., Castren, E., Wree, A. (1994) Brain derived neurotrophic factor protects against ischemic cell damage in rat hippocampus. *J Cereb Blood Flow & Metabolism,* 14: 689-692.

Ben-Ari, Y., Tremblay, O., Ottersen, O.P., Meldrum, B.S. (1980) The role of epileptic activity in hippocampal and 'remote' cerebral lesions induced by kainic acid. *Brain Res,* 191: 79-97.

Bennett, J.A. and Dingledine, R. (1995) Topology profile for a glutamate receptor: three transmembrane domains and a channel-lining re-entrant loop. *Neuron* 14: 373-384.

Benowitz, L.I., Rodroguez, W.R., Neve, R.L. (1990) The pattern of GAP-43 immunostaining changes in the rat hippocampal formation during reactive synaptogenesis. *Mol Brain Res,* 8: 17-23.

Benowitz, L.I. and Routtenberg, A. (1997) GAP-43: an intrinsic determinant of neuronal development and plasticity. *TiNS,* 20(2): 84-91.

Benowitz, L.I., Apostolides, P.J., Perrone-Bizzozero, N., Finklestein, S.P., Zwiers, H. (1988) Anatomical distribution of growth-associated protein GAP-43.B-50 in the adult rat brain. *J Neurosci,* 8(1): 339-352.

Benveniste, H., Drejer, J., Schousboe, A., Diemer, N.H. (1984) Elevation of extracellular concentrations of glutamate in rat hippocampus during transient cerebral ischaemia monitored by intracerebral microdialysis. *J Neurochem,* 43: 1369-1374.

Bergles, D.W., Roberts, D.B., Somogyi, P., Jahr, C.E. (2000) Glutamatergic synapses on oligodendrocyte precursor cells in the hippocampus. *Nature,* 405: 187-191.

Bertolino, M., Baraldi, M., Partenti, C., Braghiroli, D., diBella, M., Vicini, S., Costa, E. (1993) Modulation of AMPA/kainate receptors by analogues of diazoxide and cyclothiazide in thin slices of rat hippocampus. *Receptors Channels,* 1(4): 267-278.

Bessho, Y., Nakanishi, S., Nawa, H. (1993) Glutamate receptor agonists enhance the expression of BDNF mRNA in cultured cerebellar granule cells. *Mol Brain Res,* 18: 201-208.

Bettler, B., Boutler, J., Hermans-Borgmeyer, I., O'Shea-Greenfield, A., Deneris, E.S., Moll, C., Borgmeyer, U., Hollman, M., Heinemann, S. (1990) Cloning of a

novel glutamate receptor subunit, GluR5: expression in the nervous system during development, *Neuron,* 5: 583-595.

Bettler, B., Egebjerg, J., Sharma, G., Pecht, G., Hermans-Borgmeyer, I., Moll, C., Stevens, C.F., Heinemann, S. (1992) Cloning of a putative glutamate receptor: a low affininty kainate-binding subunit. *Neuron,* 8: 257-265.

Bettler, B. and Mulle, C. (1995) Review: Neurotransmitter Receptors II. AMPA and Kainate Receptors. *Neuropharmacology,* 34 (2) 123-139.

Bingham, D., Macrae, I.M., Carswell, H.V.O. (2002) Estrogen exacerbates brain damage after proximal diathery occlusion of the middle cerebral artery in the rat. *Society for Neuroscience Abstract* 392.4.

Birch, P.J., Grossman, C.J., Hayes, A.G. (1988) 6,7-dinitroquinoxaline-2,3-dione and 6-cyano-7-nitoquinoxaline-2,3-dione anatogonise responses to NMDA in the rat spinal cord via an action at the strychnine-insensitive glycine receptor (1988) *Eur J Pharamacol,* 156: 177-180.

Biscoe, T.J., Evans, R.H., Martin, M.R., Watkins, J.C. (1976) Structure-activity relations of excitatory amino acids of frog and rat spinal neurones. *Br J Pharmacol,* 58: 373-382.

Biziere, K. and Coyle, J.T. (1979) Effects of cortical ablation on the neurotoxicity and receptor binding of kainic acid in the striatum. *J Neurosci Res,* 4: 383-398

Bjartmar, C., Xinghua, Y., Trapp, B. (1999) Axonal pathology in myelin disorders. *J Neurocytol,* 28, 283-295.

Bjartmar, C., Battistuta, J, Terada, N, Dupree, E., Trapp, B.D. (2002) N-acetylaspartate is an axon-specific marker of mature white matter *in vivo*: a biochemical and immunohistochemical study on the rat optic nerve. *Ann Neurol,* 51: 51-58.

Bleakman D, Schoepp, DD., Ballyk, B., Bufton, H., Scharpe, E.F., Thomas, K., Ornstein, P.L., Kamboj, K. (1996) Pharmacological discrimination of GluR5 and GluR6 kainate receptor subtypes by (3*S*,4a*R*, 6*R*, 8a*R*)-6-[2-(1(2)*H*-tetrazole-5-yl)]decahydroisoquinoline-3-carboxylic acid. *Mol Pharmacol,* 49: 581-585.

Bleakman, D. and Lodge, D. (1998) Neuropharmacology of AMPA and kainate receptors. *Neuropharmacology,* 37: 1187-1204.

Bliss, T.V.P. and Lomo, T. (1973) Long-lasting potentiation of synaptic transmission in the dentate area of the unanesthetized rabbit following stimulation of the perforant path. *J Physiol (Lond),* 232: 331-356.

Bliss, T.V. and Collingridge, G.L. (1993) A synaptic model of memory: long-term potentiation in the hippocampus. *Nature,* 361: 31-39.

Blumbergs, P.C., Scott, G., Wainwright, H., Simpson, D.A., McLean, A.J. (1994) Staining of amyloid precursor protein to study axonal damage in mild head injury. *Lancet,* 344: 1055-1056.

Boison, D. and Stoffel, W. (1994) Disruption of the compacted myelin sheath of axons of the central nervous system in Proteolipid protein-deficient mice. *Proc Nat Acad Sci USA,* 91: 11709-11713.

Bongarazone, E.R., Campaganoni, C.W., Kampf, K., Jacobs, E.C., Handley, V.W., Schonmann, V., Campagnoni, A.T. (1999) Identification of a new exon in the myelin proteolipid protein gene encoding novel protein isoforms that are restricted to the somata of oligodendrocytes and neurons. *J Neurosci,* 19(19): 8349-8357.

Bontempi, B., Laurent-Demir, C., Destrade, C., Jaffard, R. (1999) Time-dependent reorganisation of brain circuitry underlying long-term memory storage. *Nature,* 400: 671-675.

Boucher, S.E.M., Cypher, M.A., Carlock, L.R., Skoff, R.P. (2002) Proteolipid protein gene modulates viability and phenotype of neurons. *J Neurosci,* 22(5): 1722-1783.

Brady, S.T. (1991) Molecular motors in the nervous system. *Neuron,* 7: 521-533.

Brady, S.T., Witt, A.S., Kirkpatrick, L.L., Waegh, S.M., Readhead, C., Tu, P-H., and Lee, V.M-Y. (1999) Formation of compact myelin is required for maturation of the axonal cytoskeleton. *J Neurosci,* 19(17) 7278-7228.

Bramlett, H.M., Kraydieh, S., Green, E.J., Dietrich, W.D. (1997) Temporal and regional patterns of axonal damage following traumatic brain injury: a beta-amyloid precursor protein immunocytochemical study in rats. *J Neuropath and Exp Neurol,* 56: 1132-1141.

Brand-Schieber, E. and Werner, P. (2003) AMPA/kainate receptors in mouse spinal cord cell-specific display of receptor subunits by oligodendrocytes and astrocytes and nodes of Ranvier. *Glia,* 42: 12-24.

Brewer, J.B., Zhao, Z., Desmond, J.E., Glover, G.H., Gabrieli, J.D.E. (1998) Making memories: Brain activity that predicts how well visual experience will be remembered. *Science,* 281: 1185-1187.

Brezun, J.M. and Daszuta, A. (1999) Depletion in serotonin decreases neurogenesis in the dentate gyrus and the subventricular zone of adult rats. *Neurosci,* 89: 99-1002.

Brezun, J.M. and Daszuta, A. (2000) Serotonin may stimulate granule cell proliferation in the adult hippocampus, as observed in rats grafted with foetal raphe neurosn. *Eur J Neurosci,* 12: 391-396.

Bridges, R.J., Stevens, D.R., Kahle, J.S., Nunn, P.B., Kadri, M., Cotman, C.W. (1989) Structure-function studies on *N*-oxalyl-diamino-dicarboxylyic acids and

excitatory amino acid receptors: evidence that β-L-ODAP is a selective non-NMDA antagonist. *J Neurosci,* 9: 2073-2079.

Browne, S.E. and McCulloch, J. (1994) AMPA receptor antagonists and local cerebral glucose utilisation in the rat. *Brain Res,* 641: 10-20.

Browne, S.E., Muir, J.L., Robbins, T.W., Page, K.J., Everitt, B.J., McCulloch, J. (1998) The cerebral metabolic effects of manipulating glutamatergic systems within the basal forebrain in conscious rats. *Eur J Neurosci.,* 10: 649-663.

Buchan, A. and Pulsinelli, W.A. (1990) Hypothermia but not the *N*-Methyl-D-Aspartate antagonist, MK-801, attenuates neuronal damage in gerbils subjected to transient global ischemia. *J Neurosci,* 10(1): 311-316.

Buchan, A.M., Lesiuk, H., Barnes, K.A., Li, H., Huang, Z., Smith, K.E., Xue, D. (1993) AMPA Antagonists: Do they hold more promise for clinical stroke trials than NMDA antagonists? *Stroke,* (suppl I) I-148-I-152.

Buckner, R.L., Kelley, W.M., Peterson, S.E. (1999) Frontal cortex contributes to human memory formation. *Nat Neurosci,* 2(4): 311-314.

Buhot, M.C., Martin, S., Sugu, L. (2000) Role of serotonin in memory impairment. *Ann Med,* 32:210-21.

Buki. A., Koizumi, H., Povlishock, J.T. (1999a) Moderate posttraumatic hypothermia decreases early calpain-mediated proteolysis and concomitant cytoskeletal compromise in traumatic axonal injury. *Exp Neurol,* 159: 319-328.

Buki A., Okonkwo, D.O., Povlishock, J.T. (1999b) Postinjury cyclosporin A administration limits axonal damage and disconnection in traumatic brain injury. *J Neurotrauma,* 16: 511-521.

Buki. A., Okokwo, D.O., Wang, K.K0, Povlishock, J.T. (2000) Cytochrome c release and caspase activation in traumatic axonal injury. *J Neurosci,* 20(8) 2825-2834.

Bullock, R., Graham, D.I., Chen, M.H., Lowe, I., McCulloch, J. (1990) Focal cerebral ischemia in the cat: pretreatement with a competitive NMDA receptor antagonist, D-CPPene. *J Cereb Blood Flow and Metab,* 10: 668-674.

Bullock, R., Graham, D.I., Swanson, S., McCulloch, J. (1994) Neuroprotective effect of the AMPA receptor antagonist LY-293558 in focal cerebral ischemia in the cat. *J Cereb Blood Flow and Metab,* 14: 466-471.

Burnashev, N., Khordova, A., Jonas, P., Helm, P.J., Wisden, W., Monyer, H., Seeburg, P.H., Sakmann, B. (1992) Calcium permeable AMPA-kainate receptors in fusiform cerebellar glial cells. *Science,* 256: 1566-1570.

Butcher, S.P., Bullock, R., Graham, D.I., McCulloch, J. (1990) Correlation between amino acid release and neuropathologic outcome following middle cerebral artery occlusion. *Stroke,* 21: 1727-1733.

Cameron, H.A., Wooley, C.S., McEwan, B.S., Gould, E. (1993) Differentiation of newly born neurons and glia in the dentate gyrus of the adult rat. *Neurosci,* 56: 337-344.

Cameron, H.A. and McKay, R.D.G. (1999) Restoring production of hippocampal neurons in old age. *Nature Neurosci,* 2(10): 894-897.

Cameron, H.A. and McKay, R.D.G. (2001) Adult neurogenesis produces a large pool of new granule cell in the dentate gyrus. *J Comp Neurol,* 435: 406-417.

Carlsson, A., Hansson, L.O., Waters, N., Carlsson, M.L. (1999) A glutamatergic deficiency model of schizophrenia *Br J Psychiatry Suppl,* 37: 2-6.

Castillo, J., Davalos, A., Noya, M. (1997) Progression of ischaemic stroke and excitotoxic amino acids. *Lancet,* 349: 79-83.

Cendes, F., Andermann, F., Carpenter, S., Zatorre, R.J., Cashman, N.R. (1995) Temporal lobe epilepsy caused by domoic acid intoxication: evidence for glutamate receptor-mediated excitotoxicity in humans. *Ann Neurol,* 37: 123-126.

Chandler, S., Coats, R., Gearing, A., Lury, J., Wells, G., Bone, E. (1995) Matrix metalloproteinases degrade myelin basic protein. *Neurosci Letts,* 201: 223-226.

Chapman, A.G. (1998) Glutamate receptors in epilepsy. *Prog in Brain Res,* 116: 371-383.

Choi, D.W. (1988) Calcium-mediated neurotoxicity: relationship to specific channel types and role in ischemic damage. *TiNS,* 11(10): 465-469.

Choi, D.W. (1987) Ionic dependence of neurotoxicity in cortical culture. *J Neurosci,* 7: 369-379.

Ciani, E., Guarnieri, T., Contestabile, A. (1994) Fos protein induction, neuropathology and pharmacological protection after excitotoxic brain insult. *Exp Brain Res,* 98: 421-430.

Coleman, M.P. and Perry, V.H. (2002) Axon pathology in neurological disease: a neglected therapeutic target. *TiNS* 25(10): 532-537.

Collingridge, G.L. and Lester, R.A.J. (1989) Excitatory amino acid receptors in the vertebrate nervous system. *Pharmacol Rev,* 40: 143-210.

Collins, R.C., McLean, M. and Olney, J. (1980) Cerebral metabolic responses to systemic kainic acid: 14-C-deoxyglucose studies. *Life Sci,* 27: 855-862.

Cotman, C.W. and Nadler, J.V. (1978) Reactive synaptogenesis in the hippocampus. In *Neuronal Plasticity,* pp 227-271. Ed. CW Cotman. Raven Press: New York.

Coumans, J.V., Lin, T.T-SL., Dai, H.N., MacAurthur, L., McAtee, M., Nash, C., Bregman, B.S. (2001) Axonal regeneration and functional recovery after complete spinal cord transection in rats by delayed treatment with transplants and neurotrophins. *J Neurosci,* 21(23): 9334-9344.

Coyle, J.T. and Schwarcz, R. (1976) Lesion of striatal neurones with kainic acid provides a model for Huntington's chorea. *Nature,* 263: 244-246.

Curtis, D.R., Phillis, J.W., Watkins, J.C. (1959) Chemical excitation of spinal neurons. *Nature,* 183: 611-612.

Curtis, D.R. and Watkins, J.C. (1963) Acidic amino acids with strong excitatory actions on mammalian neurones. *J Physiol (Lond),* 166: 1-14.

Davachi, L. and Goldman-Ravic, P.S. (2001) Primate rhinal cortex participates in both visual recognition and working memory tasks: Functional mapping with 2-DG. *J Neurophysiol,* 85: 2590-2601.

Davies, C.M., Moskovitz, B., Nguyen, M.A., Tran, B.B., Arai, A., Lynch, G., Granger, R. (1997) A profile of the behavioural changes produced by faciliation of AMPA-type glutamate receptors. *Psychopharmacol,* 133: 161-167.

De Cozar, M., Lucas, M., Monreal, J. (1987) Ionotrophic properties of the proteolipid apoprotein from bovine brain myelin. *Biochem Int* 14: 833-841.

Deller, T. and Frotscher, M. (1997) Lesion-induced plastiticy of central neurons: sprouting of single fibres in the rat hippocampus after unilateral entorhinal cortex lesion. *Prog Neurobiol,* 53: 687-727.

Devuyst, G. and Bogousslavsky, J. (1999) Clinical trial update: neuroprotection against acute ischaemic stoke. *Curr Opin Neurology,* 12: 73-79.

Dewar, D. and Dawson, D.A. (1995) Tau protein is altered by focal cerebral ischaemia in the rat: an immunohistochemical and immunoblotting study. *Brain Res,* 684: 70-78.

Dewar, D. and Dawson, D.A. (1997) Changes of cytoskeletal protein immunostaining in myelinated fibre tracts after focal cerebral ischaemia in the rat. *Acta Neuropathol,* 93: 71-77.

Dewar, D., Yam, P., McCulloch, J. (1999) Drug development for stroke: importance of protecting white matter. *Eur J Pharmacol,* 375: 41-50.

Dewar, D., McCracken, E., Grauert, M., Carter, A.J. (2001) Intrastriatal malonate induces axonal damage which is attenuated by sodium channel blockade with crobenetine (BIII890). *Soc for Neurosci Abst,* 27: 896.6.

deWaugh, S.M., Lee, V.M-Y., Brady, S.T. (1992) Local modulation of neurofilament phosphorylation, axon calibre, and slow axonal transport by myelinating Schwann cells. *Cell,* 68: 451-463.

Deweer, B., Pillon, B., Pochon, J.B., Dubois, B. (2001) Is the HM story only a 'remote memory'? Some facts about hippocampus and memory in humans. *Behav Brain Res*, 127: 209-224.

Dietrich, W.D., Kraydieh, S., Prado, R., Stagliano, N.E. (1998) White matter alterations following thromboemblolic stroke: a β-amyloid precursor protein immunocytochemical study in rats. *Acta Neuropath,* 95: 524-531.

Dingledine, R. and McBain, C.J. (1999) Glutamate and Aspartate. In:- (eds) Siegel GJ et al, Basic Neurochemistry. Luppincott-Raven Publishers, Philadelphia. pp315-333

Dingledine, R., Borges, K., Bowie, D., Traynelis, S.F. (1999) The Glutamate receptor ion channels. *Pharm Revs,* 51(1): 7-61.

Dixon, A.K., Richardson, P.J., Pinnock, R.D., Lee, K. (2000) Gene-expression analysis at the single-cell level. *TiPS*, 21: 65-70.

Donevan, S.D. and Rogawski, M.A. (1993) GYKI 52466, a 2,3 benzodiazepine, is a highly selective, non-competitive antagonist of AMPA/kainate receptor responses. *Neuron,* 10: 51-59.

Donevan, S.D., Yamaguchi, S., Rogawski, M.A. (1994) Non-*N*MDA receptor antagonism by 3-*N*-substituted 2,3-benzodiazepines: relationship to anticonvulsant activity. *J Pharmacol Exp Ther*, 271(11): 25-29.

Donevan, S.D., Rogawski, M.A. (1998) Allosteric regulation of alpha-amino-3-hydroxy-5-methyl-4-isoxazole-propionate receptors by thiocyanate and cyclothiazide at a common modulatory site distinct from that of 2,3-benzodiazepines. *Neuroscience,* 87(3): 615-29.

Dougherty, K.D., Dreyfus, C.F., Black, I.B. (2000) Brain-derived neurotrophic factor in astrocytes, oligodendrocytes, and microglia/macrophages after spinal cord injury. *Neurobiol of Dis,* 7: 574-585.

During, M.J. and Spencer, D.D. (1993) Extracellular hippocampal glutamate and spontaneous seizures in the conscious man. *Lancet,* 341: 1605-1610.

Dyck, P.J., Chance, P., Lebo, R., Carney, J.A. (1989) Longitudinal study of neuropathic deficits and nerve conduction abnormalities in hereditary motor and sensory neuropathy type 1. *Neurology,* 39: 1302-1308.

Dyker, A.G. and Lees, K.R. (1998) Duration of neuroprotective treatment for ischemic stroke. *Stroke,* 29:535-542.

Edgar, J.M., McLaughlin, M., McCulloch, M., Barrie, J., Nave, K-A., Griffiths, I.R. (2001) Proteolipid protein deficient myelin induces axonal swellings in shiverer mice. *Soc for Neurosci Abst*, 27: 103.11.

Egebjerg, J. and Jensen, H.S. (2002) Structure of ionotropic glutamate receptors. In (eds) Egebjerg, J., Schousboe, A. and Krogsgaard-Larsen, P., Glutamate and GABA receptors and transporters: Structure, function and pharmacology. Taylor and Francis Publishers, London, pp41-56.

Eijkenboom, M., Blokland, A., Van der Staay, F.J. (2000) Modelling cognitive dysfuctions with bilateral injections of ibotenic acid into the rat entorhinal cortex. *Neurosci,* 101(1): 27-39.

Farber, N.B., Newcomer, J.W., Olney, J.W. (2002) Glutamatergic transmission. Therapeutic prospects for schizophrenia and Alzheimer's disease. In (eds) Egebjerg J, Schousboe A and Krogsgaard-Larsen P, Glutamate and GABA receptors and transporters: Structure, function and pharmacology. Taylor and Francis Publishers, London, pp385-406.

Ferguson, B., Matysak, M.K., Esiri, M.M., Perry, V.H. (1997) Axonal damage in acute multiple sclerosis lesions. *Brain,* 120: 393-399.

Filliat, P., Pernot-Marino, I., Baubichon, D., Lallement, G. (1998) Behavioural effects of NBQX, a competitive antagonist of the AMPA receptors. *Pharm Biochem and Behav,* 59(4): 1087-1092.

Filippi, M., Bozzali, M., Rovaris, M., Gonen, O., Kesavadas, C., Ghezzi, A., Martinelli, V., Grossman, R.I., Scotti, G., Comi, G., Falini, A. (2003) Evidence for widespread axonal damage at the earliest clinical stage of multiple scelrosis. *Brain,* 126(2): 433-437.

Fiskum, G., Murphy, A.N., Beal, M.F. (1999) Mitochondria in neurodegeneration: acute ischemia and chronic neurodegenerative diseases. *J Cereb Blood Flow and Metab*, 19: 351-369.

Fletcher, E.J. and Lodge, D. (1996) New Developments in the molecular pharmacology of α-amino-3-hydroxy-5-methyl-4-isoxazole propionate and kainate receptors. *Pharmacol and Therapetuics,* 70(1) 65-89

Fletcher, P.C., Frith, C.D., Rugg, M.D. (1997) The functional neuroanatomy of episodic memory. *TiNS*, 20(5): 213-218.

Follet, P.L., Rosenberg, P.A., Volpe, J.J., Jensen, F.E. (2000) NBQX attenuates excitotoxic injury in developing white matter. *J Neurosci,* 20(24) 9235-9241.

Forster, E., Naumann, T., Deller, T., Straube, A., Nitsch, R., Frotscher, M. (1997) Cholinergic sprouting in the rat fascia dentate after entorhinal lesion is not linked to early changes in neurotrophin messenger RNA expression. *Neuroscience,* 80(3): 731-739.

Foster, A.C., Vezzani, A., French, E., Schwarz, R. (1984) Kynurenic acid blocks neurotoxicity and seizures induced in rats by the related brain metabolite quinolinic acid. *Neurosci Letts,* 48: 173-287.

Foster, A.C., Gill, R., Woodruff, G.N. (1988) Neuroprotective effects of MK-801 *in-vivo* : selectivity and evidence for delayed neurodegeneration mediated by NMDA receptor activation *J Neurosci,* 8: 4745-4754.

Fowler, J.H. O'Neill, M.J., Whalley, K., Murray, T.K., Crile, R., McKinzie, D., McCulloch, J. (2003) An anatomical basis for cognitive enhancing effects of the AMPA receptor potentiator LY404187: ^{14}C-2-deoxyglucose autoradiography and c-fos studies. *Submitted to J. Neurosci.*

Frahm, H.D., Stephan, M., Stephan, H. (1982) Comparison of brain structure volumes in *Insectivora* and Primates. I. Neocortex. *J Hirnforsch,* 23: 375-389.

Franklin, K.B.J. and Paxinos, G. (1997) The mouse brain in stereotaxic coordinates. Academic Press, San Diego, CA, USA.

Gahm, C., Holmin, S., Mathiesen, T. (2002) Nitric oxide synthase expression after human brain contusion. *Neurosurgery*, 50(6), 1319-1326.

Gallo, V. and Russell, J.T. (1995) Excitatory Amino Acid Receptors in Glia: Different subtypes for distinct functions? *J Neurosci Research,* 42: 1-8.

Gallo, V. and Ghiani, C.A. (2000) Glutamate receptors in glia: new cells, new inputs and new functions. *TiPs,* 21: 252-258.

Garbern, J.Y., Yool, D.A., Moore, G.J., Wilds, I.B., Faulk, M.W., Klugmann, M., Nave, K-A., Sistermans, E.A., van der Knaap, M.S., Bird, T.D., Shy, M.E., Kamholz, J.A. and Griffiths, I.R. (2002) Patients lacking the major CNS myelin protein, proteolipid protein 1, develope length-dependent axonal degeneration in the absence of demyelination and inflammation. *Brain,* 125, 551-561.

Garcia-Barcina, J.M. and Matute, C. (1998) AMPA-selective glutamate receptor subunits in glial cells of the adult bovine white matter. *Mol Brain Res,* 53, 270-276.

Garthwaite, G., Brown, G., Batchelor, A.M., Goodwin, D.A., Garthwaite, J. (1999) Mechanisms of ischaemic damage to central white matter axons: a quantitative histological analysis using rat optic nerve. *Neuroscience,* 94(4) 1219-1230.

Garthwaite, G., Goodwin, D.A., Batchelor, A.M., Leeming, K., Garthwaite, J. (2002) Nitric oxide toxicity in CNS white matter: an *in vitro* study using rat optic nerve. *Neurosci,* 109(1): 145-155.

Gates, M., Ogden, A., Bleakman, D. (2001) Pharmacological effects of AMPA receptor potentiators LY392098 and LY404187 on rat neuronal AMPA receptors *in vitro. Neuropharmacol.* 40: 984-991.

Geddes, J.F., Whitwell, H.L., Graham, D.I. (2000) Traumatic axonal injury: practical issues for diagnosis in medicolegal cases. *Neuropath & Applied Neurobiol,* 26: 105-116.

Gentleman, S.M., Roberts, G.W., Gennarelli, T.A., Maxwell, W.L., Adams, J.H., Kerr, S., Graham, D.I. (1993) β-Amyloid precusor protein (β-APP) as a marker for axonal injury after head injury. *Neurosci Lett,* 160: 139-144.

Gill, R., Foster, A.C., Woodruff, G.N. (1987) Systemic administration of MK-801 protects against ischaemia-induced hippocampal neurodegeneration in the gerbil. *J Neurosci,* 7: 3343-3349.

Gill, R., Nordholm, L., Lodge, D. (1992) The neuroprotective actions of NBQX in a rat focal ischaemia model. *Brain Res,* 580:35-43.

Gill, R. (1994) The Pharmacology of α-amino-3-hydroxy-5-methyl-4-isoxazole propionate (AMPA)/kainate antagonists and their role in cerebral ischaemia. *Cerebrovascular and Brain Metab Revs,* 6:225-256.

Ginsberg, M.D. (1990) Local cerebral metabolic responses to cerebral ischemia. *Cerebrovasc and Brain Metab Revs*, 2: 58-93.

Gladstone, D.J., Black, S.E., Hakim, A.M. (2002) Towards wisdom from failure. Lessons from neuroprotective stroke trials and new therapeutic directions. *Stroke,* 33: 2123-2136.

Goff, D.C., Leahy, L., Bermanm, I., Posever, T., Herz, L., Leon, A.C., Johnson, S.A., Lynch, G. (2001) A placebo-controlled pilot study of the AMPAkine CX516 added to clozapine in schizophrenia. *J Clin Psychopharm* 21(5): 484-487.

Gotti, B., Duverger, N., Bertin, J., Carter, C., Dupont, R., Frost, J., Gaudillier, B., McKenzie, E.T., Rosseau, J., Scatton, B., Wick, A. (1988) Ifenprodil and SL 82, 0715 as cerebral anti-ischaemic agents. I. Evidence for efficacy in models of focal cerebral ischaemia. *J Pharmacol Exp Ther,* 247: 1211-1221.

Gould, E. and Tanapat, P. (1997) Lesion-induced proliferation of neuronal progenitors in the dentate gyrus of the adult rat. *Neuroscience,* 80(2): 427-436.

Gould, E., Beylin, A., Tanapat, P., Reeves, A., Shors, T.J. (1999) Learning enhances adult neurogenesis in the hippocampal formation. *Nature Neurosci,* 2(3): 260-265.

Goutan, E., Marti, E., Ferrer, I. (1998) BDNF, and full length truncated TrkB expression in the hippocampus of the rat following kainic acid excitotoxic damage. Evidence of complex time-dependent and cell-specific responses. *Molec Brain Res,* 59: 154-164.

Grady, M.S., Mclaughlin, M.R., Christman, C.W., Valadka, A.B., Flinger, C.L., Povlishock, J.T. (1993) The use of antibodies targeted against neurofilament subunits for the detection of diffuse axonal injury in humans. *J Neuropath Exp Neurol,* 52, 143-152.

Graham, D.I. and Gennarelli, T.A. (1997) Trauma. In:- Greenfields Neuropathology, 6th ed. Arnold: London, pps 197-262

Graham, D.I., Gentleman, S.M., Nicoll, J.A.R., Royston, M.C., McKenzie, J.E., Roberts, G.W., Griffin, W.S.T. (1996) Altered β-APP metabolism after head injury and its relationship to the aetiology of Alzheimer's disease. *Acta Neurochir*, 66: 96-102.

Granger, R., Staubli, U., Davis, M., Perez, Y., Nilsson, L., Rogers, G.A., Lynch, G. (1993) A drug that facilitates glutamatergic transmission reduces exploratory activity and improves performance in a learning-dependent task. *Synapse,* 15(4): 326-329.

Granger, R., Deadwyler, S., Davis, M., Moskovitz, B., Kessler, M., Rogers, G., Lynch, G. (1996) Facilitation of glutamate receptors reverses an age-associated memory impairment in rats. *Synapse,* 22(4): 332-337.

Gray, F., Belec, L., Chretien, F., Dubreuil-Lemaire, M.L., Ricolfi, F., Wingertsmann, L., Poron, F., Gherardi, R. (1998) Acute, relapsing brain oedema with diffuse blood-brain barrier alteration and axonal damage in the acquired immunodeficiency syndrome. *Neuropath Appl Neurobiol,* 24(3): 209-216.

Greenberg, J.H., Hamar, J., Welsh, F.A., Harris, V., Reivich, M. (1992) Effect of ischemia and reperfusion of λ of the lumped constant of the [^{14}C]Deoxyglucose technique. *J Cereb Blood Flow and Metab.* 12: 70-77.

Greene, J.G., Porter, R.H., Eller, R.V., Greenamyre, T. (1993) Inhibition of succinate dehyrdogenase by malonic acid produces an "excitotoxic" lesion in rat striatum. *J Neurochem*, 61: 1151-1154.

Griffiths, I., Klugmann, M., Anderson, T., Yool, D., Thomson, C., Schwab, M.H., Schneider, A., Zimmerman, F., McCulloch, M., Nadon, N. and Nave, K-A. (1998) Axonal swellings and degeneration in mice lacking the major proteolipid of myelin. *Science,* 280, 1610-1613.

Gwag, B.J., Sessler, F., Kimmerer, K., Springer, J.E. (1994) Neurotrophic factor mRNA expression in dentate gyrus in increased following angular bundle transection. *Brain Res,* 647(1): 23-29.

Hampson, R.E., Rogers, G., Lynch, G., Deadwyler, S.A. (1998) Facilitative effects of the AMPAkine CX516 on short-term memory in rats: enhancement of delayed-nonmatch-to-sample performance. *J Neurosci,* 18(7): 2740-2747.

Hanemann, C.O., Gabreels-Festen, A.A.W.M., De Jonghe, O. (2001) Axon damage in CMT due to myelin protein P_0. *Neuromusc Disorders,* 11: 753-756.

Harris, E.W. (1995) Subtypes of Glutamate Receptors: Pharmacological Classification. In (ed) Stone T.: CNS Neurotransmitters And Neuromodulators: Glutamate. Publishers: Circa, London

Hayashi, T. (1952) A Physiological study of epileptic seizures following cortical stimulation in animals and its application to human clinics. *Japn J Physiol,* 3: 46-64.

Hayashi, T. (1954) Effects of sodium glutamate on the nervous system. *Keio J Med,* 3: 183-192.

Hayashi, T., Umemori, H., Mishina, M., Yamamoto, T. (1999) The AMPA receptor interacts with and signals through the protein tyrosine kinase Lyn. *Nature,* 397(7): 72-76.

He, Y., Ong, W.Y., Leong, S.K., Garey, L.J. (1996) Distribution of glutamate receptor subunit GluR1 and GABA in human cerebral cortex: a double Immunolabelling and electron microscope study. *Exp Brain Res,* 112(1): 147-157.

Henley, J.M. (2003) Proteins interactions implicated in AMPA receptor trafficking: a clear destination and an improving route map. *Neurosci Res,* 45: 243-254.

Henshaw, R., Jenkins, B.G., Schulz, J.B., Ferrant, R.J., Kowall, N.W., Rosen, B.R., Beal, M.F. (1994) Malonate produces striatal lesions by indirect NMDA receptor activation. *Brain Res,* 647 (1): 161-166.

Hicks, R.R., Martin, V.B., Zhang, L., Seroogy, K.B. (1999) Mild experimental brain injury differentially alters the expression of neurotrophin and neurotrophin receptor mRNAs in the hippocampus. *Exp Neurol,* 160: 469-478.

Higuchi, M., Single, F.N., Kohler, M., Sommer, B., Sprengel, R., Seeberg, P.H. (1993) RNA editing of AMPA receptor subunit-B: a base paired intron-exon structure determines position and efficiency. *Cell,* 75: 1361-1370.

Hollmann, M., O`Shea-Greenfield, A., Rogers, S.W. and Heinemann, S. (1989) Cloning by functional expression of a member of the glutamate receptor family. *Nature,* 342: 643-648.

Hollmann, M., Hartley, M., Heinemann, S. (1991) Ca^{2+} permeability of KA-AMPA gated-glutamate receptor channels depends on subunit compostion. *Science*, 252: 851-853.

Hollmann, M. and Heinmann, S. (1994) Cloned glutmate receptors. *Ann Rev Neurosci,* 17:31-108.

Honore, T., Davies, S.N., Drejer, J., Fletcher, E.J., Jacobsen, P., Lodge, D., Nielson, F.E. (1988) Quinoxalinediones: potent competitive non-NMDA glutamate antagonists. *Science,* 241: 701-703.

Hopkins, K.J., Wang, G-J., Schmued, L.C. (2000) Temporal progression of kainic acid induced neuronal and myelin degeneration in the rat forebrain. *Brain Res*, 864, 69-80.

Huettner, J.E. (1990) Glutamate receptor channels in rat dorsal root ganglion neurons: activation by kainate and quisqualate and blockade of desensitisation by concanavalin A. *Neuron,* 5: 255-266.

Hume, R.I., Dingledine, R., Heinemann, S.F. (1991) Identification of a site in glutamate receptor subunits that controls calcium permeability. *Science,* 253: 1028-1031.

Icaason, J.S. and Nicoll, R.A. (1991) Aniracetam reduces glutamate receptors desensitisation and slows decay of fast excitatory synaptic currents in the hippocampus. *Proc Natl Acad Sci USA,* 88: 10963-10940.

Ikononkidou, C. and Turski, L. (1997) Pharmacology of the AMPA Antagonist 2,3-Dihdroxy-6-nitro-7-sulfamoylbenzo-(*F*)-Quinoxaline. *Annals of the NY Acad of Sci,* 825: 394-402.

Imai, H., Masayasu, H., Dewar, D., Graham, D.I., Macrae, I.M. (2001) Ebselen protects both grey and white matter in a rodent model of focal cerebral ischemia. *Stroke,* 32: 2149-2154.

Imai, H., McCulloch, J., Graham, D.I., Masayasu, H., Macrae, I.M. (2002) New method for the quantitative assessment of axonal damage in focal cerebral ischemia. *J Cereb Blood Flow and Metab,* 22: 1080-1089.

Impagnatiello, F., Oberto, A., Longone, P., Costa, E., Guidotti, A. (1997) 7-Chloro-3-methly-3,4-dihydro-2*H*-1,2,4-benzothiadiazine *S,S*-dioxide: a partial modulator of AMPA receptor desensitisation devoid of neurotoxicity. *Proc Nat Acad Sci USA,* 94: 7053-7058.

Ingvar, M. and Siesjo, B.K. (1983) Local blood flow and glucose consumption in the rat brain during sustained bicuculline-induced seizures. *Acta Neurol Scand,* 68: 129-144.

Ingvar, M., Folbegrova, J., Siesjo, B.K. (1987) Metabolic alterations underlying the development of hypermetabolic necrosis in the substantia nigra in status epilepticus. *J Cereb Blood Flow and Metab* 7: 103-108.

Ingvar, M., Ambros-Ingerson, J., Davis, M., Granger, R., Kessler, M., Rogers, G.A., Schehr, R.S., Lynch, G. (1997) Enhancement by an AMPAkine of memory encoding in humans. *Exp Neurol,* 146: 553-559.

Insel, T.R., Miller, L.P., Gelhard, R.E. (1990) The ontogeny of excitatory amino acid receptors in rat forebrain –I. *N*-methyl-D-aspartate and quisqualate receptors. *Neurosci,* 35(1): 31-43.

Irving, E.A., McCulloch, J., Dewar, D. (1996a) Intracortical perfusion of glutamate in vivo induces alterations of tau and microtubule-associated protein 2 immunoreactivity in the rat. *Acta Neuropathol,* 92:186-196.

Irving, E.A., Nicholl, J., Graham, D.I. and Dewar, D. (1996b) Increased tau immunoreactivity following human stroke and head injury. *Neurosci Letts,* 213: 189-192.

Irving, E.A., Yatsushiro, K., McCulloch, J. and Dewar, D. (1997) Rapid alteration of tau in oligodendrocytes after focal ischaemic injury in the rat: Involvement of free radicals. *J Cereb Blood Flow and Metab,* 17:612-622.

Irving, E.A., Bentley, D.L., Parsons, A.A. (2001) Assessment of white matter injury following prolonged focal cerebral ischaemia in the rat. *Acta Neuropathol,* 102: 627-635.

Ito, I., Tanabe, S., Kohda, A., Sugiyama, H. (1990) Allosteric potentiation of quisqualate receptors by a nootropic drug aniracetam. *J Physiol,* 424: 533-543.

Jamin, N., Junier, M-P., Grannec, G. and Cadusseau, J. (2001) Two temporal stages of oligodendroglial response to excitotoxic lesion in the gray matter of the adult rat brain. *Exp Neurol,* 172: 17-28.

Jendroska, K., Hoffman, O.M., Patt, S. (1997) Amyloid β peptide and precursor protein (APP) in mild and severe brain ischemia. *Annals N Y Acad Sci,* 26: 401-405.

Jensen, A.M., and Chiu, S.Y. (1993) Expression of glutamate receptor genes in white matter: developing and adult rat optic nerve. *J Neurosci*, 13(4), 1664-1675.

Jiang, Q. and Stys, P.K. (2000) Calpain inhibitors confer biochemical, but not electrophysiological protection against anoxia in rat optic nerves. *J Neurochem,* 74: 2101-2107.

Johnston, G.A.R., Curtis, D.R., Davies, J., McCulloch, R.M. (1974) Spinal interneurone excitation by conformationally restricted analogues of L-glutamic acid. *Nature,* 248: 804-805.

Jonas, P. and Burnashev, N. (1995) Molecular mechanisms controlling calcium entry through AMPA-type glutamate receptor ion channels. *Neuron,* 15: 987-990.

Jorgensen, M.B. and Wright, D.C. (1998) The effect of unilateral and bilateral removal of the entorhinal cortex on the glucose utilisation in various hippocampal regions in the rat. *Neurosci Letts*, 87(3): 227-232.

Kadish, I. and Van Groen, G. (2003) Differences in lesion-induced hippocampal plasticity between mice and rats. *Neurosci,* 116: 499-509.

Kalaria, R.N., Bhatti, S.U., Palatinsky, E.E.E.A., Pennington, D.H., Shelton, E.R., Chan, H.W., Perry, G., Lust, W.D. (1993) Accumulation of the β amyloid precursor protein at sites of ischemic injury in the rat brain. *Neuroreport,* 4: 211-214.

Kandel, E.R. (2001) The molecular biology of memory storage: a dialogue between genes and synapses. Science 294: 1030-1038.

Kanellopoulos, G.K., Xu, X.M., Hsu, C.Y., Lu, X., Sundt, T.M., Kouchoukos, N.T. (2000) White matter injury in spinal cord ischemia: Protection by AMPA/kainate glutamate receptor antagonism. *Stroke,* 31: 1945-1952.

Kapoor, R., Davies, M., Blaker, P.A., Hall, S.M., Smith, K.J. (2003) Blockers of sodium and calcium entry protect axons from nitric oxide-mediated degeneration. *Ann Neurol.*, 53(2): 174-180.

Keinanen, K., Wisden, W., Sommer, B., Werner, P., Herb, A., Verdoon, T.A., Sakmann, B., Seeburg, P.H. (1990) A family of AMPA selective glutamate receptors. *Science,* 249: 556-560.

Kirkpatrick, L.L. and Brady, S.T. (1999) Cytoskeleton of neurons and glia. In (eds) Siegel, G.L. et al, Basic Neurochemistry: Molecular, cellular and medical aspects. 6th ed, Lippincott-Raven Publishers, Philadelphia, USA.

Kirkpatrick, L.L., Witt, A.S., Payne, R., Shine, H.D. and Brady, S.T. (2001) Changes in microtubule stability and density in myelin-deficient shiverer mouse CNS axons. *J Neurosci,* 21(7): 2288-2297.

Kitagawa, K., Sinoway, M.P., Yang, C., Gould, R.M., Colman, D.R. (1993) A proteolipid protein gene family: expression in sharks and rays and possible evolution from an ancestral gene encoding a pore-forming polypeptide. *Neuron* 11: 433-438.

Klocker, N., Jung, M., Stuermer, C.A.O., Bahr, M. (2001) BDNF increases the number of axotomized rat retinal ganglion cells expressing GAP-43, L1, and TAG-1 mRNA – a supportive role for nitric oxide? *Neurobiol of Disease,* 8: 103-113.

Klugmann, M., Scwab, M.H., Puklhofer, A., Schneider, A., Zimmerman, F., Griffiths, I.R., Nave, K-A. (1997) Assembly of CNS myelin in the absence of Proteolipid protein. *Neuron,* 18: 59-70.

Knapp, R.J., Goldenberg, R., Shuck, C., Cecil, A., Watkins, J., Miller, C., Crites, G., Malatynska, E. (2002) Antidepressant activity of memory-enhancing drugs in the reduction of submissive behaviour model. *Eur J Pharmacol*, 440: 27-35.

Kobayashi, K. and Yasoshima, Y. (2001) The central noradrenaline system and memory consolidation. *Neuroscientist,* 7(5): 371-376.

Kohler, M., Burnashev, N., Sakmann, B., Seeberg, P.H. (1993) Determinants of calcium permeability in both TM1 and TM11 of high affinity kainate receptor channels: diversity by RNA editing. *Neuron,* 10: 491-500.

Kokaia, Z., Zhao, Q., Kokaia, M., Elmer, E., Metsis, M., Smith, M-L., Siesjo, B.K., Lindvall, O. (1995) Regulation of brain-derived neurotrophic factor gene expression after transient middle cerebral artery occlusion with and without brain damage. *Exp Neurol,* 136: 73-88.

Kokaia, Z., Andsberg, G., Yan, Q., Lindvall, O. (1998) Rapid alterations of BDNF protein levels in the rat brain after focal ischemia: evidence for increased synthesis and anterograde axonal transport. *Exp Neurol,* 154: 289-301.

Kokaia, Z. and Lindvall, O. (2003) Neurogenesis after ischaemic brain insults. *Curr Opin in Neurobiol,* 13: 127-132.

Komjati, K., Valeriani, V., Imai, H., Dewar, D., McCulloch, J. (2000) White matter blood flow after rat middle cerebral artery occlusion is highly model dependent. *J Cereb Blood Flow and Metab,* 21 (suppl 1): S14.

Koo, E.H., Sisoodia, S.S., Archer, D.R., Martin, L.J., Weidemann, A., Beyreuther, K., Fischer, P., Masters, C.L., Price, D.L. (1990) Precursor of amyloid protein in Alzheimer disease undergoes fast anterograde axonal tranport. *Proc Natl Acad Sci USA,* 87: 1561-1565.

Kornek, B., Storch, M.K., Weissert, R., Wallstroem, E., Stefferl, A., Olsson, T., Linington, C., Schmidbauer, M. Lassmann, H. (2000) Multiple sclerosis and chronic autoimmune encephalomyelitis. A comparitive study of axonal injury in active, inactive and remyelinated lesions. *Am J Pathol,* 157(1) 267-276.

Kristian, T. and Siesjo, B.K. (1997) Calcium in ischemic cell death. *Stroke,* 29: 705-718.

Krogsgaard-Larsen, P., Honore, T., Hansen, J.J., Curtis, D.R., Lodge, D. (1980) New class of glutamate agonist structurally related to ibotenic acid. *Nature,* 284: 64-66.

Kurumaji, A., Nehls, D.G., Park, C.K., McCulloch, J. (1989) Effects of NMDA receptor antagonists, MK-801 and CPP, upon local cerebral glucose use. *Brain Res,* 496: 268-284.

Kurumaji, A. and McCulloch, J. (1990) Effects of MK-801 upon local cerebral glucose utilisation in conscious rats following unilateral lesion of caudal entorhinal cortex. *Brain Res,* 531: 72-82.

Laezza, C., Wolff, J., Bifulco, M. (1997) Identification of a 48-kDa prenylated protein that associates with microtubules as 2',3'-cyclic nucleotide 3'-phosphdiesterase in FRTL-5 Zellan. *FEBS Lett,* 413: 260-264.

Lam, A.G.M., Monn, J.A., Schoepp, D.D., Lodge, D. and McCulloch, J. (1999) Group II selective metabotropic glutamate receptor agonists and local cerebral use in the rat. *J Cereb Blood Flow and Metab,* 19: 1083-1091.

Lambolez, B., Audinat, E., Bochet, P., Crepel, F., Rossier, J. (1992) AMPA receptor subunits expressed by single Purkinje cells. *Neuron,* 9: 247-258.

Lapchak, P.A., Araujo, D.M., Hefti, F. (1993) BDNF and TrkB mRNA expression in the rat hippocampus following entorhinal cortex lesions. *Neuroreport,* 4(2): 191-194.

Lappe-Siefke, C., Goebbels, S., Gravel, M., Nicksch, E., Lee, J., Braun, P.E., Griffiths, I.R., Nave, K-A. (2003) Disruption of *Cnp1* uncouples oligodendroglial fuctions in axonal support and myelination. *Nature Genetics,* 33: 366-374.

Lauterborn, J.C., Lynch, G., Vanderklish, P., Arai, A., Gall, C.M. (2000) Postive modulation of AMPA receptors increases neurotrophin expression by hippocampal an cortical neurons. *J Neurosci,* 20(1): 8-21.

Lawrence, C.B., Allan, S.M., Rothwell, N.J. (1998) Interluekin-1β and the interluekin-1 receptor antagonist act in the striatum to modify excitotoxic brain damage in the rat. *Eur J Neurosci,* 10: 1188-1195.

Lazzaro, J.T., Paternain, A.V., Lerma, J., Chenard, B.L., Ewing, F.E., Huang, J-H., Welch, W.M., Ganong, A.H., Menniti, F.S. (2002) CP-465,022 is a potent and selective non-competitive AMPA receptor antagonist. *Neuropharmacol,* 42: 143-153.

Lee, C.R. and Benfield, P. (1994) Aniracetam. An overview of its pharmacodynamic and pharmacokinetic properties, and a review of its therapeutic potential in senile cognitive disorders. *Drugs & Aging,* 4(3): 257-273.

Lee, K.S., Stanford, E.J., Cotman, C.W., Lynch, G.S. (1977) Ultrastructural evidence for bouton proliferation in the partially deafferated dentate gyrus of the adult rat. *Exp Brain Res,* 29: 475-485.

Lees, G.J. (2000) Pharmacology of AMPA/kainate receptor ligands and their therapeutic potential in neurological and psychiatric disorders. *Drugs,* 59(1): 33-78.

Lees, K.R., Lavelle, J.F., Cunha, L., Diener, H.C., Sanders, E.A., Tack, P., Wester, P. (2001) Glycine antagonist (GV150526) in acute stroke: a multicentre, double-blind placebo-controlled phase II trial. *Cerebrovasc Dis,* 11:20-29.

Legutko, B., Li, X., Skolnick, P. (2001) Regulation of BDNF expression in primary neuron culture by LY392098, a novel AMPA receptor potentiator. *Neuropharm,* 40: 1019-1027.

Levy, L. (2002) Strucutre, function and regulation of glutamate transporters. In (eds) Egebjerg J, Schousboe A and Krogsgaard-Larsen P; Glutamate and GABA receptors and transporters. Taylor and Francis (pubs) London; pp307-336.

Leys, D., Englund, E., Del Ser, T., Inzitair, D., Fazekas, F., Borstein, N., Erkinjuntti, T., Bowler, J.V., Pantoni, L., Parnetti, L., De Reuck, J., Ferro, J., Bogousslavsky, J. (1999) White Matter Changes in stroke patients. Relationship with stroke subtype and outcome. *Eur Neurol,* 42:67-75.

Li, S., Mealing, G.A.R., Morley, P. and Stys, P.K. (1999) Novel Injury Mechanism in Anoxia and Trauma of Spinal Cord White Matter: Glutamate release via reverse Na^+ -dependent glutamate transport. *J Neurosci,* 19 RC16: 1-9.

Li, S. and Stys, P.K. (2000) Mechanisms of Ionotropic Glutamate receptor-mediated excitotoxicity in isolated spinal cord white matter. *J Neurosi,* 20(3) 1190-1196.

Li, X., Tizzano, J.P., Griffey, K., Clay, M., Lindstrom, T., Skolnick, P. (2001) Antidepressant-like actions of an AMPA receptor potentiator (LY392098). *Neuropharmacology* 40: 1028-1033.

Linden, A-M., Yu, H., Zarrinmayeh, H., Wheeler, W.J., Skolnick, P. (2001) Binding of an AMPA receptor potentiator ([^{3}H]LY395153) to native and recombinant AMPA receptors. *Neuropharm,* 40: 1010-1018.

Lipton, S.A. and Rosenberg, P.A. (1998) Excitatory amino acids as a final common pathway for neurological disorders. *N Eng J Med,* 330, 613-622.

Liu, H., Giasson, B.I., Mushynski, W.E., Almazon, G. (2002) AMPA receptor-mediated toxicity in oligodendrocyte progenitors involves free radical generation and activation of JNK, calpain and caspase 3. *J Neurochem,* 82, 398-409.

Liu, J., Solway, K., Messing, R.O., Sharp, F.R. (1998) Increased neurogenesis in the dentate gyrus after transient global ischemia in gerbils. *J Neurosci,* 18(19): 7768-7778.

Lodge, D. and Collingridge, G. (1990) Les agents provocateurs: a series on the pharmacology of excitatory amino acids. *TiPS,* 11: 22-24.

Lomeli, H., Mosbacher, J., Melcher, T., Hoger, T., Geiger, J.R.P., Kuner, T., Monyer, H., Higuchi, M., Bach, A., Seeberg, P.H. (1994) Control of kinetic properties of AMPA receptor channels by nuclear RNA editing. *Science,* 266: 1709-1713.

Longa, E.Z., Weinstein, P.R., Carlsson, B.S., Cummins, R. (1989) Reversible middle cerebral artery occlusion without craniectomy in rats. *Stroke*, 20: 84-91.

Lothman, E.W. and Collins, R.C. (1981) Kainic acid induced limbic seizures: metabolic, behavioral, electroencephalographic and neuropathological correlates. *Brain Res*, 218(1-2): 299-318.

Lu, B., Gottschalk, W. (2000) Modulation of hippocampal synaptic transmission and plasticity by neurotrophins. *Prog Brain Res,* 128: 231-241.

Lucas, D.R. and Newhouse, J.P. (1957) The toxic effect of sodium L-glutamate on the inner layers of the retina. *A.M.A. Arch Opthalmol,* 58: 193-201.

Ludolph, A.C., He, F., Spencer, P.S., Hammerstad, M., Sabri, M. (1991) 3-Nitropropionic acid: exogenous neurotoxin and possible striatal toxin. *Can J Neurosci Sci*, 18: 492-498.

Ludwin, S.M. (1997) The Pathobiology of the oligodendrocyte. *J Neuropath and Exp Neurobiol,* 56(2) 111-124.

Luscher, C. and Frerking, M. (2001) Restless AMPA receptors: implications for synaptic transmission and plasticity. *TiNS*, 24(11): 665-670.

Lynch, G. and Baudry, M. (1984) The biochemistry of memory: A new and specific hypothesis. *Science,* 224: 1057-1063.

Lynch, G., Granger, R., Ambros-Ingerson, J., Davis, M.C., Kessler, M., Schehr, R. (1997) Evidence that a positive modulator of AMPA-type glutamate receptors improves delayed recall in aged humans. *Exp Neurol,* 145: 89-92.

Lyons, S.A. and Kettenmann, H. (1998) Oligodendrocytes and microglia are selectively vulnerable to combined hypoxia and hypoglycemia injury *in vivo. J Cereb Blood Flow and Metab,* 18: 521-530.

Mackler, S.A. and Eberwine, J.H. (1993) Diversity of glutamate receptor subunit mRNA expression within live hippocampal CA1 neurons. *Molec Pharmacol,* 44: 308-315.

Mackowiak, M., O'Neill, M.J., Hicks, C.A., Bleakman, D., Skolnick, P. (2002) An AMPA receptor potentiator modulates hippocampal expression of BDNF: and *in vivo* study. *Neuropharmacol,* 43: 1-10.

Mallon, B.S., Shick, H.E., Kidd, G.J., Macklin, W.B. (2002) Proteolipid promoter activity distinguishes two populations of NG2-positive cells throughout neonatal cortical development. *J Neurosci,* 22(3): 876-885.

Mamounas, L.A., Altar, A., Blue, M.E., Kaplan, D.R., Tessarollo, L., Lyons, W.E. (2000) BDNF promotes the regenerative sprouting, but not survival, of injured serotonergic axons in the adult rat brain. *J Neurosci,* 20(2): 771-782.

Manns, J.R., Hopkins, R.O., Reed, J.M., Kitchener, E.G., Squire, L.R. (2003) Recognition memory and the human hippocampus. *Neuron,* 37:171-180.

Marcoux, F.W., Morawetz, R.B., Crowell, R.M., DeGirolami, U., Hasley, J.R. (1982) Differential regional vulnerability in transient focal cerebral ischemia. *Stroke,* 13: 339-346.

Markowitsch, H.J. (1995) Which brain regions are critically involved in the retrieval of old episodic memory? *Brain Res Revs,* 21: 117-127.

Martin, I., Blackstone, C.D., Levey, A.I., Huganir, R.L., Price, D. (1993) AMPA glutamate receptor subunits are differentially distributed in the rat brain. *Neuroscience,* 53: 327-358.

Masliah, E., Fagan, A.M., Terry, R.D., DeTeresa, R., Mallory, M., Gage, F.H. (1991) Reactive synaptogenesis assessed in synaptophysin immunoreactivity is associated with GAP-43 in the dentate gyrus of adult rats. *Exp Neurol,* 113: 131-142.

Matthews, D.A., Cotman C., Lynch, G. (1976) An electron microscopic study of lesion-induced synaptogenesis in the dentate gyrus of the adult rat. II Reapperance of morphologically normal synaptic contacts. *Brain Res,* 115: 23-41.

Matute, C., Sanchez-Gomez, M.V., Martinez-Millan, L., Miledi, R. (1997) Glutamate receptor-mediated toxicity in optic nerve oligodendrocytes. *Proc Natl Acad Sci USA,* Aug 5 94(16): 8830-5.

Matute, C. (1998) Characteristics of acute and chronic excitotoxic damage to the optic nerve. *Proc. Natl Acad Sci USA,* 95:10229-10234.

Maxwell, W.L., Povlishock, J.T. and Graham, D.I. (1997) A mechanistic analysis of non-disruptive axonal injury: a review. *J Neurotrauma,* 14: 419-439.

Mayer, M.L. and Vyklicky, L. Jnr. (1989) Concavalin A selectively reduces desensitisation of mammalian neuronal quisqualate receptors. *Proc Nat Acad Sci USA,* 86: 1411-1415.

McAllister, A.K., Katz, L.C., Lo, D.C. (1999) Neurotrophins and synaptic plasticity. *Ann Rev Neurosci,* 22: 295-318.

McCracken, E., Hunter, A.J., Patel, S., Graham, D.I., Dewar, D. (1999) Calpain activation and cytoskeletal protein breakdown in the corpus callosum of head-injured patients. *J Neurotrauma*, 16: 749-761.

McCracken, E., Jover, T., McCulloch, J. and Dewar, D. (2000) The lipid peroxidation by-product 4-hydroxynonenal in toxic to axons and oligodendrocytes. *J Cereb Blood Flow and Metab*, 20: 152-1536.

McCracken, E., Dewar, D. and Hunter, A.J. (2001) White matter damage following systemic injection of the mitochondrial inhibitor 3-nitropropionic acid in rat. *Brain Res*, 892, 329-335.

McCracken, E., Fowler, J.H., Dewar, D., Morrison, S., McCulloch, J. (2002) Grey matter and white matter ischemic damage is reduced by the competitive AMPA receptor antagonist, SPD 502. *J Cereb Blood Flow and Metab,* 22, 1090-1097.

McCulloch, J. (1992) Excitatory amino acid antagonists and their potential for the treatment of ischaemic brain damage in man. *Br J Clin Pharmacol,* 34: 106-114

McDonald, J.W., Althomsons, S.P., Hyrc, K.L., Choi, D.W., Goldberg, M.P. (1998a) Oligodendrocytes from forebrain are highly vulnerable to AMPA/kainate receptor-mediated excitotoxicity. *Nature Med,* Mar 4(3) 291-297.

McDonald, J.W, Levine, J.M., Qu, Y. (1998b) Multiple classes of the oligodendrocyte lineage are highly vulnerable to excitotoxicity. *Neuroreport,* 9: 2757-2762.

McGeer, E.G., McGeer, P.L., Singh, K. (1978) Kainate-induced degeneration of neostriatal neurons: dependency on cortico-striatal tract. *Brain Res,* 139: 381-383.

McKenzie, K.J., McLellan, D.R., Gentleman, S.M., Maxwell, W.L., Gennarelli, T.A., Graham, D.I. (1996) Is β-APP a marker of axonal damage in short-surviving head injury? *Acta Neuropath,* 92: 608-613.

Medana, I.M., Day, N.P., Hien, T.T., Mai, N.T.H., Bethell, D., Phu, N.H., Farrar, J., Esiri, M.M., White, N.J., Turner, G.D. (2002) Axonal injury in cerebral malaria. *Am J Pathol,* 160 (2): 655-666

Medana, I.M. and Esiri, M.M (2003) Axonal damage: a key predictor of outcome in human CNS diseases. *Brain,* 126: 515-530.

Meldrum, B. and Garthwaite, J. (1990) Excitatory amino acid neurotoxicity and neurodegenerative disease. *TiPS,* 11: 379-387.

Meller, D., Bellander, B.M., Schmidt-Kastner, R., Ingvar, M. (1993) Immunohistochemical studies with antibodies to neurofilament proteins on axonal damage in experimental focal lesions in rat. *J Neurol Sci* 117: 164-174.

Meneses, A. (1999) 5-HT system and cognition. *Neurosci and Biobehav Rev,* 23: 1111-1125.

Menniti, F.S., Buchan, A.M., Chenard, B.L., Critchett, D.J., Ganong, A.H., Guanowsky, V., Seymour, P.A., Welch, W.M. (2003) CP-465,022, a selective non-competitive AMPA receptor antagonist, blocks AMPA receptors but is not neuroprotective *in vivo. Stroke,* 34 171-176.

Merrill, J.E., Murphy, S.P., Mitrovic, B., Mackenzie-Graham, A., Dopp, J.C., Ding, M., Griscavage, J., Ignarro, L.J., Lowenstein, C.J. (1997) Inducible nitric oxide synthase and nitric oxide production by oligodendrocytes. *J Neurosci Res*, 48(4), 372-384.

Miller, M.J., Haxhiu, M.A., Georgiadis, P., Gudz, T.I., Kangas, C.D., Macklin, W. (2003) Proteolipid protein gene mutation induces altered ventilatory response to hypoxia in the myelin-deficient rat. *J Neurosci*, 23(6): 2265-2273.

Miller, M.W., Nowakowski, R.S. (1988) Use of bromodeoxyuridine-immunohistochemistry to examine the proliferation, migration and time of origin of cells in the central nervous system. *Brain Res,* 457: 44-52.

Milner, B., Squire, L.R., Kandel, E.R. (1998) Cognitive neuroscience and the study of memory. *Neuron,* 20: 445-468.

Mistal, M. and Danysz, W. (1995) Comparison of glutamate antagonists in continuous multiple trial and single trial dark avoidance. *Beh Pharmacol* 6: 550-561.

Miu, P., Jarvie, K.R., Radhakrishnan, V., Gates, M.R., Ogden, A., Ornstein, P.L., Zarrinmayeh, H., Ho, K., Peters, D., Grabell, J., Gupta, A., Zimmerman, D.M., Bleakman, D. (2001) Novel AMPA receptor potentiators LY392098 and LY404187: effects on recombinant human AMPA receptors in vitro. *Neuropharmacol,* 40: 976-983.

Monaghan, D.T., Yao, D., Cotman, C.W. (1984) Distribution of [^{3}H]AMPA binding sites in rat brain as determined by quantitative autoradiography. *Brain Res,* 324:160-164.

Monuki, E.S. and Lemke, G. (1995) Molecular biology of myelination. In (eds) Waxman, S.G., Kocsis, J.D., Stys, P.K. The axon: structure, function and pathophysiology. Oxford University Press, New York, USA. pp144-163.

Monyer, H., Seeberg, P.H., Wisden, W. (1991) Glutamate-operated channels: Developmentally early and mature forms arise by alternative splicing. *Neuron,* 6: 779-810.

Morris, R.G.M., Davies, S., Butcher, S.P. (1990) Hippocampal synaptic plasticity and NMDA receptors: a role in information storage? *Philos Trans R Soc Lond B Biol Sci,* 29; 329(1253): 187-204.

Murray T.K., Whalley K., Robinson C.S., Ward M.A., Hicks C.A., Lodge D., Vandergriff J.L., Baumbarger P., Siuda E., Gates M., Ogden A.M., Skolnick P., Zimmerman D.M., Nisenbaum E.S., Bleakman D., O'Neill M.J. (2003) LY503430, a novel alpha-amino-3-hydroxy-5-methylisoxazole-4-propionic acid receptor potentiator with functional, neuroprotective and neurotrophic effects in rodent models of Parkinson's disease. *J Pharmacol Exp Ther*; 306(2): 752-762.

Nestler, E.J., Gould, E., Manji, H., Bucan, M., Duman, R.S., Gershenfeld, H.K., Hen, R., Koester, S., Lederhendler, I., Meaney, M.J., Robbins, T., Winsky, L., Zalcman, S. (2002) Preclinical models: Status of basic research in depression. *Biological Psychiatry*, 52:503-528.

Newman, T.A., Woolley, S.T., Hughes, P.M., Sibson, N.R., Anthony, D.C., Perry, V.H. (2001) T-cell and macrophage-mediated axon damage in the absence of a CNS-specific immune response: involvement of metalloproteinases. *Brain* 124: 2203-2214.

Nicholls, D.G. (1998) Presynaptic modulation of glutamate release. *Prog in Brain Res,* 116: 15-22.

Nicoletti, F., Meek, J.L., Iadarola, M.J., Chuagnge, D.M., Roth, B.L., Costa, E. (1986) Coupling of inositol phospholipid metabolism with excitatory amino acid recognition sites in the rat hippocampus. *J Neurochem,* 46: 40-46.

Nielsen, E.O., Varming, T., Mathiesen, C., Jensen, L.F., Moller, A., Gouliaev, A.H., Watjen, F., Drejer, J. (1999) SPD 502: A water soluble and *in-vivo* long-lasting AMPA antagonist with neuroprotective activity. *J Pharm Exp Ther,* 289(3): 1492-1501.

Noda, M., Nakanishi, H., Nabekura, J., Akaike, N. (2000) AMPA-kainate subtypes of glutamate receptor in rat cerebral microglia. *J Neurosci,* 20 (1) 251-258.

Norton, W.T. and Poduslo, S.E. (1973) Myelination in rat brain: method of myelin isolation. *J Neurochem,* 21(4): 749-757.

Novelli, A., Relly, J.A., Lysko, P.G., Henneberry, R.C. (1988) Glutamate becomes neurotoxic via the NMDA receptor when intracellular energy levels are reduced. *Brain Res,* 451: 205-212.

Ohmori, J., Pandit, J., Kang, C-H., Nikaido, K., Gokcen, S., Ames, G.F-L., Kim, S-H. (1994) 6-(1J-imidazol-1-yl)-7-nitro-2,3(1H,4H)-quinoxalinedione hydrochloride (YM90K) and related compounds: structure-activity relationships for the AMPA-typenon-NMDA receptor. *J Med Chem,* 37: 467-475.

Ohno, K., Tsutsumi, R., Matsumoto, N., Yamashita, H., Amada, Y., Shishikura, J-I., Inami, H., Yatsugi, S-I., Okada, M., Sakamoto, S., Yamaguchi, T. (2003) Functitonal characterisation of YM928, a novel non-competitive AMPA receptor antagonist. *J Pharmacol Exp Ther,* March 26.

Oka, A., Belliveau, M.J., Rosenberg, P.A. and Vople, J.J. (1993) Vulnerability of Oligodendroglia to glutamate: pharmacology, mechanisms and prevention. *J Neurosci,* 13 (4): 1441-1453.

Olney, J.W. (1969) Brain lesions, obesity and other disturbances in mice treated with monosodium glutamate. *Science,* 164: 719-21.

Olney, J.W. and Sharpe, L.G. (1969) Brain lesions in an infant rhesus monkey treated with monosodium glutamate. *Science,* 166, 386-388.

Olney, J.W. (1971) Glutamate induced neuronal necrosis in the infant mouse hyothalamus. *J Neuropathol & Exp Neurol,* 30: 75-90.

Olney, J.W., Misra, C.H., deGubareff, T. (1975) Cysteine-S-sulphate brain damaging metabolite in sulfite oxidase deficiency. *J Neuropath & Exp Neurol*, 34: 167-177.

Olney, J.W., deGubareff, T., Labruyere, J. (1979) α-aminoadipate blocks the neurotoxic action of *N*-methylaspartate neurotoxicity. *Life Sci*, 25(6): 537-540.

Olney, J.W., Labruyere, J., Collins, J., Curry, K. (1981) D-Aminophospho-novalerate is 100-fold more powerful than D-alpha-aminoadipate in blocking *N*methlyaspartate neurotoxicity. *Brain Res,* 221: 207-210.

Olney, J.W., Price, M.T., Samson, L., Labruyere, J. (1986) The role of specific ions in glutamate neurotoxicity. *Neurosci Letts,* 65: 65-71.

Olney, J.W. (1990) Excitotoxic amino acids and neuropsychiatric disorders. *Ann Rev Pharmacol Toxicol*, 30: 47-71.

Olsen, R.W., Szamraj, O., Houser, C.R. (1987) [^{3}H]AMPA binding to glutamate receptor subpopulations in rat brain. *Brain Res*, 402: 243-254.

O'Neill, M.J., Bond, A., Ornstein, P.L., Ward, M.A., Hicks, C.A., Hoo, K., Bleakman, D., Lodge, D. (1998) Decahydroisoquinolines: novel competitive

APMA/kainate antagonists with neuroprotective affects in global cerebral ischaemia. *Neuropharmacology,* 37: 1211-1222.

Ornstein, P.L., Zimmerman, D.M., Arnold, M.B., Bleisch, T.J., Cantrell, B., Simon, R., Zarrinmayeh, H., Baker, S.R., Gates, M., Tizzano, J.P., Bleakman, D. (2000) Biarylpropylsulfonamides as novel, potent potentiators of 2-amino-3-(5-methyl-3-hydroxyisoxazol-4-yl)-propanoic acid (AMPA) receptors. *J Med Chem,* 43: 4354-4358.

Osborne, K.A., Shinego, T., Balarsky, A.M., Ford, I., McCulooch, J., Teasdale, G.M., Graham, D.I. (1987) Quantitative assessment of early brain damage in a rat model of focal cerebral ischaemia. *J Neurol, Neurosurg & Psych,* 50: 402-410.

Owens, J., Wyper, D.J., Patterson, J., Brown, D.R., Elliot, A.T., Teasdale, G.M., McCulloch, J. (1997) First SPET images of glutamate (NMDA) receptor activation *in vivo* in cerebral ischaemia. *Nucl Med Commun,* 18(2): 149-158.

Ozyurt, E., Graham, D.I., Woodruff, G.N., McCulloch, J. (1988) Protective effect of the glutamate antagonist MK-801 in focal cerebral ischemia. *J Cereb Blood Flow and Metab,* 8:138-143.

Palmer, A.J. and Lodge, D. (1993) Cyclothiazide reverses AMPA receptor antagonism of the 2,3 benzodiazepine, GYKI 53655. *Eur J Pharmacol,* 244: 193-194.

Pantoni, L., Garcia, J.H., Gutierrez, J.A. (1996) Cerebral White matter is highly vulnerable to ischemia. *Stroke,* 27:1641-1647.

Parent, J.M., Yu, T.W., Leibowitz, R.T., Geschwind, D.H., Sloviter, R.S., Lowenstein, D.H. (1997) Dentate granule cell neurogenesis is increased in seizures and contributes to aberrant network reorganisation in the adult rat hippocampus. *J Neurosci,* 17: 3727-3728.

Park, C.K., Nehls, D.G., Graham, D.I., Teasdale, G.M., McCulloch, J. (1988a) The glutamate antagonist MK-801 reduces focal cerebral ischaemic brain damage in the rat. *Annals of Neurol,* 24: 543-551.

Park, C.K., Nehls, D.G., Graham, D.I., Teasdale, G.M., McCulloch, J. (1988b) Focal cerebral ischemia in the cat: treatement with the glutamate antagonist MK-801 after induction of cerebral ischemia. *J Cereb Blood Flow and Metab,* 8: 757-762.

Partin, K.M., Patneau, D.K., Winters, C.A., Mayer, M.L., Buonanno, A. (1993) Selective modulation of desensitisation at AMPA vs kainate receptors by cyclothiazide and concanavalin A. *Neuron,* 11: 1069-1082.

Partin, K.M., Patneau, D.K., Mayer, M.L. (1994) Cyclothiazide differentially modulates desensitization of AMPA receptor splice variants. *Mol Pharmacol,* 46: 129-138.

Partin, K.M., Bowie, D., Mayer, M.L. (1995) Structural determinants of allosteric regulation in alternatively spliced AMPA receptors. *Neuron,* 14: 833-843.

Partin, K.M. and Mayer, M.L. (1996) Negative allosteric modulation of wild-type and mutant AMPA receptors by GYKI 53655. *Mol Pharmacol,* 49: 142-148.

Partin, K.M., Fleck, M.W., Mayer, M.L. (1996) AMPA receptor flip/flop mutants affecting deactivation, desensitization, and modulation by cyclothiazide, aniracetam and thiocyanate. *J Neurosci,* 16(21): 6634-6647.

Patel, H., Heenan, L., Davies, R., Rothwell, N., Allan, S. (2002) IL-1beta exacerbates excitotoxin induced neuronal cell death by potentiating seizure activity. *Eur J Neurosci Abst,* 3: 148.3.

Patneau, D.K., Wright, P.W., Winters, C., Mayer, M.L., Gallo, V. (1994) Glial cells of the oligodendrocyte lineage express both kainate- and AMPA-preferring subtypes of glutamate receptor. *Neuron,* 12: 357-371.

Paxinos, G. and Watson, C. (1986) The rat brain in stereotaxic co-ordinates. 3rd Ed. Academic Press Sydney, Australia.

Paxinos, G. and Watson, C. (1998) The rat brain in stereotaxic coordinates. 4th Ed. Academic Press, San Diego, USA.

Pellegrini-Giampietro, D.E., Gorter, J.A., Bennett, M.V.L., Zukin, R.S. (1997) The Glur2 (GluR-B) hypothesis: Ca^{2+}- permeable AMPA receptors in neurological disorders. *TiNS,* 20: 464-470.

Pencea, V., Bingaman, K.D., Wiegand, S.J., Luskin, M.B. (2001) Infusion of brain derived neurotrophic factor into the lateral ventricle of the adult rat leads to new neurons in the parenchyma of the striatum, septum, thalamus and hypothalamus. *J Neurosci,* 21: 6706-6717.

Perkinton, M.S., Sihra, T.S., Williams, R.J. (1999) Ca^{2+} permeable AMPA receptors induce phosphorylation of cAMP response element-binding protein through a phosphatidylinositol 3-kinase dependent stimulation of mitogen-activated protein kinase signalling cascade in neurons. *J Neurosci,* 19: 5861-5874.

Perl, T.M., Debdard, L., Kosatsky, T., Hockin, J.C., Todd, E.C.D., Remis, R.S. (1990) An outbreak of toxic encephalopathy caused by eating mussels contaminated with domoic acid. *N Engl J Med,* 322: 1775-1780.

Perry, V.H. and Anthony, D.C. (1999) Axonal damage and repair in multiple sclerosis. *Phil Trans R Soc Lond,* 354: 1641-1647.

Persson, L., Hillered, L. (1992) Chemical monitoring of neurosurgical intensive care patients using intracerebral microdialysis. *J Neurosurg,* 76: 72-80.

Peters, A., Palay, S.L., and Webster, H.DeF. (1991) The fine structure of the nervous system: The neurons and supporting cells, 3rd ed. Oxford University Press, New York, USA.

Petito, C.K. (1986) Transformation of post-ischemic perineuronal glial cells. I. Electron Microscope studies. *J Cereb Blood Flow and Metab* 6: 616-624.

Petito, C.K., Olarte, J-P., Roberts, B., Nowak, T.S., Pulsinelli, W.A. (1998). Selective glial vulnerability following transient global ischemia in the rat brain. *J Neuropath Exp Neurol,* 57: 231-238.

Petralia, R.S. and Wenthold, R.J. (1992) Light and electron immunocytochemical localization of AMPA-selective glutamate receptors in the rat brain. *J Comp Neurol,* 318: 329-354.

Petty, M.A. and Wettstein, J.G. (1999) White matter ischaemia. *Brain Res,* 31: 58-64.

Pitt, D., Werner, P., Raine, C.S. (2000) Glutamate excitotoxicity in a model of multiple sclerosis. *Nature Med,* 6(1) 67-70.

Pontecorvo, M.J., Evans, H.L. (1985) Effects on aniracetam on delayed non-matching-to-sample performance of monkeys and pigeons. *Pharmacol Biochem,* Behav 22: 745-752.

Poo, M. (2001) Neurotrophins as synaptic modulators. *Nat Revs Neurosci,* 2: 24-32.

Povlishock, J.T., Marmarou, A., McIntosh, T.K., Trojanowski, J.Q., Moroi, J. (1997) Impact acceleration in the rat: evidence for focal axolemmal change and related neurofilament sidearm alteration. *J Neuropath and Exp Neurol*, 56(4): 347-359.

Pulsinelli, W.A. and Duffy, T.E. (1979) Local cerebral glucose utilisation during controlled hypoxemia in rats. *Science*, 204: 626-629.

Quirk, J.C. and Nisenbaum, E.S. (2002) LY404187: A novel positive allosteric modulator of AMPA receptors. CNS Drug Revs 8(3): 255-282.

Quirk, J.C., Linden, A-M., Strakhova, M., Yu, H., Skolnick, P., Nisenbaum, E.S. (2002) A single residue contributes sensitivity to allosteric modulation of AMPA receptors by LY395153. *E J Pharmacol*, 454: 125-129.

Rainbow, T.C., Wieczorek, C.M., Haplain, S. (1984) Quantitative autoradiography of binding sites for [^{3}H]AMPA, a structural analogue of glutamic acid. *Brain Res,* 309: 173-177.

Raja, F., Sherriff, F.E., Morris, C.S., Bridges, L.R., Esiri, M.M. (1997) Cerebral white matter damage in HIV infection demonstrated using beta-amyloid precursor protein immunoreactivity. *Acta Neuropathol,* 93(2): 184-189.

Ramirez, J.J. (2001) The role of axonal sprouting in functional reorganization after CNS injury: lessons from the hippocampal formation. *Restorative Neurol and Neurosci,* 19: 237-262.

Ransom, B.R., Brown, A.M., Baltan Tekkok, S. (2002) Why CNS white matter is relatively resistant to anoxia. *Soc for Neurosci Abst,* 299.2.

Raymond, L.A., Blackstone, C.D., Huganir, R.L. (1993) Phoshporylation and modulation of recombinant GluR6 glutamate receptors by cAMP-dependent protein kinase. *Nature,* 361: 637-641.

Readhead, C., Popko, B., Takahashi, N., Shine, H.D., Saavedra, R.A., Sidman, R.L., Hood, L. (1987) Expression of myelin basic protein gene in transgenic shiverer mice: correction of the dysmyelinating phenotype. *Cell,* 48: 703-712.

Riedel, G., Micheau, J., Lam, A.G., Roloff, E., Martin, S.J., Bridge, H., Hoz, L., Poeschel, B., McCulloch, J., Morris, R.G. (1999) Reversible neural inactivation reveals hippocampal participation in several memory processes. *Nat Neurosci,* 2(10):898-905.

Ritchie, J.M. and Rogart, R.B. (1977) The density of sodium channels in the mammalian myelinated nerve fibres and the nature of the axonal membrane under the myelin sheath. *Proc Nat Acad Sci USA,* 74: 211-215.

Roach, A., Boylan, K., Horvath, S., Prusiner, S.B., Hood, L.E. (1983) Characterisation of cloned cDNA representing rat myelin basic protein: Absence of expression in brain of shiverer mutant mice. *Cell,* 34: 799-806.

Rosenberg, L.J., Teng, Y.D. and Wrathall, J. (1999a) Effects of the sodium channel blocker tetrodotoxin on acute white matter pathology after experimental contusive spinal cord injury. *J Neurosci,* 19(14): 6122-6133.

Rosenberg, L.J., Teng, Y.D. and Wrathall, J.R. (1999b) 2,3-Dihydroxy-6-Nitro-7 Sulfamoyl-Benzo(f) Quinoxaline reduces glial loss and acute white matter pathology after experimental spinal cord contusion. *J Neurosci,* 19(1): 464-475.

Rothman, S.M. (1984) Synaptic release of excitatory amino acid neurotransmitter mediates anoxic neuronal cell death. *J Neurosci,* 4(7) 1884-1891.

Rothman, S.M. (1985) The neurotoxicity of excitatory amino acids is produced by passive chloride influx. *J Neurosci,* 5: 1483-1489.

Rothstein, J.D., Martin, L.J., Kuncl, R.W. (1992) Decreased glutamate transport by the brain and spinal cord in amyotrophic lateral scelrosis. *N Engl J Med* 326: 1464-1468.

Rothstein, J.D., Van Kammen, M., Levey, A.I., Martin, L.J., Kuncl, R.W. (1995) Selective loss of glial glutamate transporter GLT-1 in amyotrohpic lateral sclerosis. *Ann Neurol,* 38: 73-84.

Saatman, K.E., Graham, D.I., McIntosh, T.K. (1998) The neuronal cytoskeleton is at risk after mild and moderate brain injury. *J Neurotrauma,* 15(12), 1047-1057.

Sagar, S.M., Sharp, F.R., Curran, T. (1988) Expression of c-fos protein in brain: metabolic mapping at the cellular level. *Science*, 240(4857): 1328-1331.

Saji, M. and Reis, D.J. (1987) Delayed transneuronal death of substancia nigra neurons prevented by γ-aminobutyric acid agonist. *Science* 235: 66-9.

Sanchez-Gomez, M.A. and Matute, C. (1999) APMA and kainate receptors mediate excitotoxicity in oligodendroglial cultures. *Neurobiol of disease,* 6 (6): 475-85.

Sasaki, S. and Iwata, M. (1999) Immunoreactivity of ß-amyoid precursor protein in amyotrophic lateral sclerosis. *Acta Neuropath* 97: 463-468.

Sato-Yoshitake, R., Shiomura, Y., Miyasaka, H., Hirokawa, N. (1989) Microtubule-associated protein 1B: Molecular structure, localisation and phosphorylation dependent expression in developing neurons. *Neuron,* 3: 229-238.

Sattler, R. and Tymianski, M. (2001) Molecular mechanisms of glutamate receptor-mediated excitotoxic neuronal cell death. *Mol Neurobiol,* 24: 107-129.

Savaskan, N.E. and Nitsch, R. (2001) Molecules involved in reactive sprouting in the hippocampus. *Revs in the Neurosciences,* 12: 195-215.

Sawamura, A., Hashizume, K., Yoshioda, K., Tanaka, T. (2001) Kainic acid-induced substantia nigra seizure in rats: behavior, EEG and metabolism. *Brain Res,* 911: 89-95.

Schabitz, W-R., Schwab, S., Spranger, M., Hacke, W. (1997) Intraventricular brain-derived neurotrophic factor reduces infarct size after focal cerebral ischemia in rats. *J Cereb Blood Flow & Metab,* 17: 500-506.

Scherer-Singler, U. and McGeer, E.G. (1979) Distribution and persistence of kainic acid in brain. *Life Sci,* 24: 1015-1022.

Schwartz, W.J., Smith, C.B., Davidsen, L., Savaki, H., Sokoloff, L., Mata, M, Fink, D.J., Gainer, H. (1979) Metabolic mapping of functional activity in the hypothalamo-neurohypophysial system of the rat. *Science,* 205: 723-725.

Segovia, G., Porras, A., Del Arco, A., Mora, F. (2001) Glutamatergic neurotransmission in aging: a critical perspective. *Mechs Aging and Dev,* 122: 1-29.

Sekiguchi, M., Fleck, M.W., Mayer, M.L., Takeo, J., Chiba, Y., Yamashita, S., Wada, K. (1997) A novel allosteric potentiator of AMPA receptors: 4-[2-(Phenylsulfonylamino)ethylthio]-2,6-Difluoro-Phenoxyacetamide. *J Neurosci,* 17(15): 5790-5771.

Seifert, G. and Steinhauser, C. (2001) Ionotropic glutamate receptors in astrocytes. *Prog in Brain Res,* 132: 287-299.

Sharp, F.R., Sagar, S.M., Swanson, R.A. (1993) Metabolic mapping with cellular resolution: c-fos vs. 2-deoxyglucose. *Crit Revs in Neurobiol*, 7(3/4): 205-228.

Sheller, R.A., Tytell, M., Smyers, M., Bittner, G.D. (1995) Glia-to-axon communication: enrichment of glial proteins transferred to the squid giant axon. *J Neurosci Res,* 41(3): 324-334.

Sheardown, M.J. (1993) AMPA, but not NMDA, receptor antagonism is neuroprotective in gerbil global ischaemia, even when delayed 24 h. *Eur J Pharmacol,* 347-353.

Sheardown, M.J., Nielsen, E.O., Hansen, A.J., Jacobsen, P. and Honore, T. (1990) 2,3-Dihydroxy-6-nitro-7-sulfamoyl- benzo(F)quinoxaline: A Neuroprotectant for cerebral ischemia. *Science,* 24: 571-574.

Sherriff, F.E., Bridges, L.R., Gentleman, S.M., Sivaloganathan, S., Wilson, S. (1994a) Markers of axonal pathology in post mortem human brain. *Acta Neuropath,* 88: 433-439.

Sheriff, F.E., Bridges, L.R., Sivaloganathan, S. (1994b) Early detection of axonal injury after human head injury using immunocytochemistry for β-amyloid precursor protein. *Acta Neuropath,* 87: 55-62.

Shinozaki, H. and Shibuya, I. (1974) A new, potent excitant, quisqualic acid: effects on crayfish neuromuscular junction. *Neuropharmacol,* 13: 665-672.

Shirayama, Y., Chen, A.C.H., Nakagawa, S., Russell, D.S., Duman, R.S. (2002) Brain-derived neurotrophic factor produces antidepressant effects in behavioral models of depression. *J Neurosci,* 22:3251-3261.

Shors, T.J., Miesegaes, G., Beylin, A., Zhao, M., Rydel, T., Gould, E. (2001) Neurogenesis in the adult is involved in the formation of trace memories. *Nature,* 410: 372-376.

Simson, E.L., Gold, R.M., Standish, L.J., Pellet, P.L. (1977) Axon-sparing brain lesioning technique: the use of monosodium-L-glutamate and other amino acids. *Science*, 198, 515-517.

Skene, J.H.P., Jacobson, R.D., Snipes, G.J., McGuire, C.B., Norden, J.J., Freeman, J.A. (1986) A protein induced during nerve regeneration (GAP-43) is a major component of growth cone membranes. *Science,* 233: 783-786.

Skolnick, P., Legutko, B, Bymaster, F.P. (2001) Current perspectives on the development of non-biogenic amine-based antidepressants. *Pharmacol Res*, 43: 411-422.

Sladeczek, F., Pin, J-P., Recasens, M., Bockaert, J., Weiss, S. (1985) Glutamate stimulates inositol phosphate formation in striatal neurons. *Nature,* 317: 717-719.

Smith, D.H., Chen, X.H., Nonaka, M., Trojanowski, J.Q., Lee, VM-Y., Saatman, K.E., Leoni, M.J., Wolf, J.A., Meany, D.F. (1999) Accumulation of amyloid β and tau and the formation of neurofilament inclusions following diffuse brain injury in the pig. *J Neuropath and Exp Neurol*, 58: 982-992.

Smith, K.J., Kapoor, R., Hall, S.M., Davie, M. (2001) Electrically active axons degenerate when exposed to nitric oxide. *Ann Neurol,* 49(4), 470-476.

Smith, S.E. and Meldrum, B.S. (1992) Receptor site specificity for the acute effects of β-*N*-methylaminoalanine in mice. *Eur J Pharmacol,* 187: 131-134.

Smith, T., Groom, A., Zhu, B., Turski, L. (2000) Autoimmune encephalomyelitis ameliorated by AMPA antagonists. *Nature Med,* 6 (1): 62-66.

Sokoloff, L., Reivich, M., Kennedy, C., Des Rosiers, M.H., Patlak, C.S., Pettigrew, K.D., Sakurada, O., Shinohara, M. (1977) The [^{14}C]deoxyglucose method for the measurement of local cerebral glucose utilisation: theory, procedure, and normal values in the conscious and anesthetised albino rat. *J Neurochem*, 28: 897-916.

Sokoloff, L. (1981) Localization of functional activity in the central nervous system by measurement of glucose utilization with radioactive deoxyglucose. *J Cereb Blood Flow and Metab,* 1: 7-36

Sommer, B., Keinanen, K., Verdoorn, T.A., Wisden, W., Burnashev, N., Herb, A., Kohler, M., Takagi, T., Sakmann, B., Seeburg, P.H. (1990) Flip and flop: a cell-specific functional switch in glutamate operated channels of the CNS. *Science,* 249: 1580-1585.

Sommer, B., Kohler, M., Sprengel, R. and Seeburg, P.H. (1991) RNA editing in brain controls a determinant of ion flow in glutamate-gated channels. *Cell,* 67: 11-19.

Spencer, P.S., Nunn, P.B., Hugon, J., Ludolph, A.C., Ross, S.M., Roy, D.N., Robertson, R.C. (1987) Guam amyotrophic lateral sclerosis-parkinsonism-dementia linked to a plant excitant neurotoxin. *Science,* 237: 517-522.

Spencer, P.S., Roy, D.N., Ludolph, A., Hugon, J., Dwivedi, M.P., Schaumburg, H.H. (1986) Lathyrism: evidence for the role of neuroexcitatory aminoacid BOAA. *Lancet,* 2: 1066-1067.

Springer, J.E., Gwag, B.J., Sessler, F.M. (1994) Neurotrophic factor mRNA expression in the dentate gyrus is increased following *in vivo* stimulation of the angular bundle. *Brain Res Mol Brain Res,* 23 (1-2): 135-143.

Staubli, U., Rogers, G., Lynch, G. (1994a) Facilitation of glutamate receptors enhances memory. *Proc Nat Acad Sci, USA* 91: 777-781.

Stuabli, U., Perez, Y., Xu, F., Rogers, G., Ingvar, M., Stone-Elander, S., Lynch, G. (1994b) Centrally active modulators of glutamate receptors facilitate the induction of long-term potentiation *in vivo*. *Proc Nat Acad Sci, USA*, 91: 11158-11162.

Stamer, K., Vogel, R., Thies, E., Mandelkow, E., Mandelkow, E.M. (2002) Tau blocks traffic of organelles, neurofilaments, and APP vesicles in neurons and enhances oxidative stress. *J Cell Biol*, 156(6): 1051-1063.

Stefano, N., Narayanan, S., Francis, G.S., Arnaoutelis, R., Tartaglia, M.C., Antel, J.P., Matthews, P.M., Arnold, D.L. (2001) Evidence of axonal damage in the early stages of multiple sclerosis and its relevance to disability. *Arch Neurol,* 58: 65-70.

Stegmuller, J., Werner, H., Nave, K-A., Trotter, J. (2003) The proteoglycan NG2 is complexed with α-amino-3-hydroxy-5-methyl-isoxazolepropionic acid (AMPA) receptors by the PDZ glutamate receptor interaction protein (GRIP) in glial progenitor cells. *J Biol Chem,* 287(6): 3590-3598.

Steinhäuser, C. and Gallo, V. (1996) News on glutamate receptors in glial cells. *TiNS,* 19(8): 339-345.

Stenoien, D.L. and Brady, S.T. (1999) Axonal transport. In (eds) Siegel, G.J. et al., Basic Neurochemistry: Molecular, cellular and medical aspects. 6th ed. Lippincott-Raven Publishers, Philadelphia, USA.

Stephenson, D.T., Rash, K., Clemens, J.A. (1992) Amyloid precursor protein accumulates in regions of neurodegeneration following focal cerebral ischemia in the rat. *Brain Res,* 393: 128-135.

Sternberger, L.A. and Sternberger, N.H. (1983) Monoclonal antibodies distinguish phosphorylated and nonphosphorylated forms on neurofilaments *in situ. Proc Nat Acad Sci USA*, 80: 6126-6130.

Steward, O. and Vinsant, S.L. (1983) The process of reinnervation in the dentate gyrus of adult rats: a quantitative electron microscope analysis of terminal proliferation and reactive synaptogenesis. *J Comp Neurol,* 214: 370-386.

Stone, J.R., Walker, S.A., Povlishock, J.T. (1999) The visualisation of a new class of traumatically injured axons through the use of a modified method of microwave antigen retrieval. *Acta Neuropath* 97: 335-354.

Stone, J.R., Singleton, R.H., Povlishock, J.T. (2001) Intra-axonal neurofilament compaction does not evoke local axonal swelling in all traumatically injured axons. *Exp Neurol,* 172: 320-331.

Stone, J.R., Okonkwo, D.O., Singleton, R.H., Mutlu, L.K., Helm, G.A., Povlishock, J.T. (2002) Caspase-3-mediated cleavage of amyloid precursor protein. *J Neurotrauma*, 19(5): 601-614.

Stys, P.K., Ransom, B.R., Waxman, S.G., Davies, P.K. (1990) Role of extracellular calcium in anoxic injury of mammalian central white matter. *Proc Natl Acad Sci USA,* 87: 4212-4216.

Stys, P.K., Waxman, S.G. and Ransom, B.R. (1992) Ionic mechanisms of axonic injury in mammalian CNS white matter: role of Na^+ channels and Na^+-Ca^{2+} exchanger. *J Neurosci,* 12: 430-439.

Stys, P.K. (1998) Anoxic and Ischaemic injury of myelinated axons in the central nervous system white matter. *J Cereb Blood Flow and Metab,* 18:2-25.

Suzdak, P.D. and Sheardown, M.J. (1993) Effect of the non-NMDA receptor antagonist 2,3-Dihydro-6-Nitro-7-Sulfamoyl benzo (f) quinoxaline on local cerebral glucose uptake in the limbic forebrain. *J Neurochem,* 61: 1577-1580.

Sybirska, E., Davachi, L., Goldman-Ravic, P.S. (2000) Prominance of direct entorhinal-CA1 pathway activation in sensorimotor and cognitive tasks revealed by 2-DG functional mapping in nonhuman primate. *J Neurosci,* 20(15): 5827-5834.

Takahashi, M., Kohara, A., Shishikura, J., Kawasaki-Yatsugi, S., Ni, J.W., Yatsugi, S., Sakamoto, S., Okada, M., Shimizu-Sasamata, M., Yamaguchi, T. (2002) YM872: a selective, potent and highly water-soluble alpha-amino-3-hydroxy-5-methylisoxazole-4-propionic acid receptor antagonist. *CNS Drug Rev,* 8(4): 337-352.

Takano, M., Horie, H., Iijima, Y., Dezawa, M., Sawada, H., Ishikawa, Y. (2002) Brain derived neurotrophic factor enhances neurite regeneration from retinal ganglion cells in aged human retina *in vitro. Exp Eye Res,* 74: 319-323.

Tamminga, C. (1998) Glutamatergic aspects of schizophrenia. *Crit Rev Neurobiol,* 12: 21-36.

Tang, C-M., Sji, Q-Y., Katchamn, A., Lynch, G. (1991) Modulation and time course of fast EPSCs and glutmate channel kinetics by aniracetam. *Science,* 254: 288-290.

Teitelbaum, J.S., Zatorre, R.J., Carpenter, S., Gendron, D., Evans, A.C., Gjedde, A., Cashman, N.R. (1990) Neurotoxic sequelae of domoic acid intoxication due to the ingestion of contaminated mussels. *N Eng J Med,* 322: 1781-1787.

Teng, Y.D. and Wrathall, J.R. (1997) Local blockade of sodium channels by Tetrodotoxin ameliorates tissue loss and long-term functional deficits resulting from experimental spinal cord injury. *J Neurosci,* 17(11) 4359-436.

Thompson, D.M., Guidotti, A., DiBella, M., Costa, E. (1995) 7-chloro-3-methyl-3,4-dihydro-2*H*-1,2,4-banzothiadiazine *S,S*-dioxide (IDRA-21), a congener of aniracetam, potently ablates pharmacologically induced cognitive impairments in patas monkeys. *Proc Nat Acad Sci,* 92: 7667-7671.

Thomson, C.E., Anderson, T.J., McCulloch, M.C., Dickinson, P.J., Vouyiouklis, D.A., Griffiths, I.R. (1999) The early phenotype associated with the *jimpy* mutation of the proteolipid protein gene. *J Neurocytol,* 28: 207-221.

Touil, T., Deloire-Grassin, M.S., Vital, C., Petry, K.G., Brochet, B. (2001) *In vivo* damage of CNS myelin and axons induced by peroxynitrite. *Neuroreport*, 12(16), 3637-3644.

Trapp, B.D. (1990) Myelin-associated glycoprotein. Location and potential functions. *Ann N Y Acad Sci,* 605: 29-43.

Trapp, B.D., Peterson, J., Ransohoff, R.M., Rudick, R., Mork, S., Bo, L. (1998) Axonal transection in the lesion of multiple sclerosis. *N Engl J Med,* 338: 278-285.

Trussell, L. (1998) Control and time course of glutamatergic synaptic currents. *Prog in Brain Res,* 116: 59-69.

Turski, L., Huth, A., Sheardown, M., McDonald, F., Neuhaus, R., Schneider, H.H., Dirnagl, U., Wiegand, F., Jacobbsen, P., Ottow, E. (1998) ZK200775: A phosphonate quinoxalinedione AMPA antagonist for neuroprotection in stroke and trauma. *Proc Natl Acad Sci USA,* 95: 10960-10965.

Tymianski, M., Wallace, M.C., Spiegelamn, I., Uno, M., Carlen, P.L., Tator, C.H., Charlton, M.P. (1993) Cell permanent Ca^{2+} chelators reduce early exctitotoxic and ishcemic neuronal injury *in vitro* and *in vivo*. *Neuron,* 11: 221-235.

Underhill, S.M. and Goldberg, M.P. (2001) Glutamate-independent hypoxic injury of isolated axons from cultured cortical neurons. *Soc Neurosci Abst*, 27, 869.2.

Underhill, S.M. and Goldberg, M.P. (2002a) Cell culture models of white matter vulnerability to excitotoxicity. *Glia, Suppl 1,* 247.

Underhill, S.M. and Goldberg, M.P. (2002b) Axons potentiate oligodendrocyte vulnerability to excitotoxicity. *Soc for Neurosci Abst,* 28: 299.7.

Uschkureit, T., Sporkel, O., Stracke, J., Bussow, H., Stoffel, W. (2000) Early onset of axonal degeneration in double (plp-/-mag-/-) and hypomyelinosis in triple (plp-/-mbp-/-mag-/-) mutant mice. *J Neurosci,* 20(14): 5225-5233.

Valeriani, V., Dewar, D., McCulloch, J. (2000) Quantitative Assessment of ischaemic pathology in axons, oligodendrocytes, and neurons: attenuation of damage after transient ischemia. *J Cereb Blood Flow Metab,* 20:765-771.

Vandergriff, J., Huff, K., Bond, A., Lodge, D. (2001) Potentiation of responses to AMPA on central neurons by LY392098 and LY404287 *in vivo*. *Neuropharmacol,* 40: 1003-1009.

van Praag, H., Schinder, A.F., Christie, B.R., Toni, N., Palmer, T.D., Gage, F.H. (2002) Functional neurogenesis in the adult hippocampus. *Nature,* 415: 1030-1034.

Verkhratsky, A. and Steinhauser, C. (2000) Ion channels in glial cells. *Brain Res Rev,* 32: 380-412.

Verloes, R., Scotto, A.M., Gobert, J., Wulfert, E. (1988) Effects of nootropic drugs in scopolamine-induced amnesia model in mice. *Psychopharmacol,* 95(32) 226-230.

Verndoorn, T.A., Burnashev, N., Moyner, H., Seeberg, P.H., Sakmann, B. (1991) Structural determinants of ion flow through recombinant glutamate receptor channels. *Science,* 252: 1715-1718.

Vizi, E.S., Mike, A., Tarnawa, I. (1996) 2,3-Benzodiazepines (GYKI 52466 and analogs): Negative allosteric modulators of AMPA receptors. *CNS Drug Rev,* 2(1): 91-126.

Wagner, A.D., Scachter, D.L., Rotte, M., Koutstaal, W., Maril, A., Dale, A.M., Rosen, B.R., Buckner, R.L. (1998) Building memories: Remembering and forgetting of verbal experiences as predicted by brain activity. *Science,* 281: 1188-1191.

Wahl, P., Madsen, U., Banke, T., Krogsgaard-Larsen, P., Schousboe, A. (1996) Different characteristics of AMPA receptor agonists acting at AMPA receptors expressed in *Xenopus* oocytes. *Eur J Pharmacol,* 308: 211-218.

Wang, H., Allen, M.L., Grigg. J.J., Noebels, J.L., Tempel, B.L. (1995) Hypomyelination alters K^+ channel expression in mouse mutant *shiverer* and *trembler. Neuron,* 15: 1337-1347.

Wang, Y. and Durkin, J.P. (1995) AMPA, but not NMDA, activates mitogen-activated protein kinase though G-protein subunits in rat cortical neurons. *J Biol Chem,* 270: 22783-22787.

Wang, Y., Small, D.B., Stanimirovic, P., Morley, P., Durkin, J.P. (1997) AMPA receptor-mediated regulation of the G_i-protein in neurons. *Nature,* 389: 502-504.

Wang, Y.T., Yu, X.M., Salter, M.W. (1996) Ca^{2+}-independent reduction of *N*-methyl-D-aspartate channel activity by protein tyrosine phosphatases. *Proc Nat Acad Sci USA,* 93: 1721-1725.

Watkins, J.C. and Evans, R.H. (1981) Excititory amino acid transmitters. *Ann Rev Pharmacol Toxicol* 21: 165-204.

Waxman, S.G., Ransom, B.R. and Stys, P.K. (1991) Non-synaptic mechanisms of Ca^{2+} mediated injury in CNS white matter. *TiNS,* 14(10): 461-468.

Waxman, S.G., Black, J.A., Stys, P.K., Ransom, B.R. (1992) Ultrastructural concomitants of anoxic injury and early post-anoxic recovery in rat optic nerve. *Brain Res,* 574: 105-119.

Waxman, S.G. and Ritchie, J.M. (1993) Molecular dissection of the myelinated axon. *Ann Neurol,* 33: 121-136.

Weber, B., Fouad, K., Burger, C., Buck, A. (2002) White matter glucose metabolism during intracortical electrostimulation: a quantitative [^{18}F]Fluorodeoxyglucose autoradiography study in the rat. *NeuroImage* 16: 993-998.

Weiss, J.H. and Sensi, S.L. (2000) Ca^{2+} and Zn^{2+} permeable AMPA or kainate receptors: possible key factors in selective neurodegeneration. *TiNS,* 23: 365-371.

Wenthold, R.J., Petralia, R.S., Blahos, J., Niedzielski, A.S. (1996) Evidence for multiple AMPA receptor complexes on hippocampal CA1/CA2 neurons. *J Neurosci,* 16: 1982-1989.

Wenthold, R.J. and Roche, K.W. (1998) The organisation and regulation of non-NMDA receptors in neurons. *Prog Brain Res,* 116: 133-152.

Werner, P., Pitt, D., Raine, C.S. (2001) Multiple sclerosis: altered glutamate homeostasis in lesions correlates with oligodendrocyte and axonal damage. *Ann Neurol,* 50: 169-180.

Wetmore, C., Olson, L., Bean, A.J. (1994) Regulation of brain-derived neurotrophic factor (BDNF) expression and release from hippocampal neurons is mediated by non-NMDA type glutamate receptors. *J Neurosci,* 13(3): 1688-1700.

White, F., Nicoll, J.A.R., Horsburgh, K. (2001) Alterations in ApoE and ApoJ in relation to degeneration and regeneration in a mouse model of entorhinal cortex lesion. *Exp Neurol,* 169: 307-318.

Wiedenmann, B. and Franke, W.W. (1985) Identification and localisation of synaptophysin, an integral membrane glycoprotein of Mr 38,000 characterisitic of presynaptic vesicles. *Cell* 41(3): 1017-1028.

Wilding, T.J. and Huettner, J.E. (1995) Differential antagonism of α-amino-3-hydroxy-5-methyl-4-isoxazolepropionic acid-preferring and kainate-preferring receptors by 2,3-benzodiazepines. *Mol Pharmacol,* 47: 528-587.

Wilding, T.J. and Huettner, J.E. (1997) Activation and desensitisation of hippocampal kainate receptors. *J Neurosci,* 17: 2713-2721.

Wilkinson, A.E., Bridges, L.R., Sivaloganathan, S. (1999) Correlation of survival time with size of axonal swellings in diffuse axonal injury. *Acta Neuropath,* 98: 197-202.

Willis, C.L., Meldrum, B.S., Nunn, P.B., Anderton, B.H. (1993) Neuronal damage induced by β-*N*-oxalylamino-L-alanine in the rat hippocampus can be prevented by a non-NMDA antagonist, 2,3-dihydro-6-nitro-7-sulfamoyl(*F*)quinoxaline. *Brain Res,* 627: 55-62.

Wooten, G.F. and Collins, R.C. (1980) Regional brain glucose utilisation following intrastriatal injections of kainic acid. *Brain Res,* 201: 173-187.

Wrathall, J.R., Choinire, D. and Teng, Y.D. (1994) Dose-dependent reduction of tissue loss and functional impairment after spinal cord trauma with the AMPA/ Kainate Antagonist NBQX. *J Neurosci,* 14(11) 6598-6607.

Wrathall, J.R., Teng, Y.D., Marriot, R. (1997) Delayed antagonism of AMPA/kainate receptors reduces long-term functional deficits resulting from spinal cord trauma. *Exp Neurol,* 145: 565-573.

Wuerthele, S.M., Lovell, K.L., Jones, M.Z., Moore, K.E. (1978) A histological study of kainic-acid induced leisons in the rat brain. *Brain Res,* 149: 489-497.

Xue, D., Huang, Z.G., Barnes, K., Lesiuk, H.J., Smith, K.E., Buchan, A.M. (1994) Delayed treatement with AMPA, but not NMDA, antagonists reduces neocortical infarction. *J Cereb Blood Flow and Metab,* 14 (2): 251-61.

Yaghmai, A and Povlishock, J. (1992) Traumatically induced reactive change as visualized through the use of monoclonal antibodies targeted to neurofilament subunits. *J Neuropathol Exp Neurol*, 51(2), 158-76.

Yam, P.S., Takasago, T., Dewar, D., Graham, D.I. and McCulloch, J. (1997) Amyloid precursor protein accumulates in white matter at the margin of a focal ischaemic lesion. *Brain Res,* 760: 150-157.

Yam, P.S., Dewar, D, and McCulloch, J. (1998) Axonal injury caused by focal cerebral ischemia in the rat. *J Neurotrauma,* 15(6) 441-450.

Yam, P.S., Dunn, L.T., Graham, D.I., Dewar, D.D., McCulloch, J. (2000) NMDA receptor blockade fails to alter axonal injury in focal cerebral ischemia. *J Cereb Blood Flow Metab,* 20:772-779.

Yamada, K.A. and Rothman, S.M. (1992) Diazoxide blocks glutamate desensitization and prolongs excitatory postsynaptic currents in rat hippocampal neurons. *J Physiol,* 458: 409-423.

Yamada, K.A. and Tang, C.M. (1993) Benzothiazides inhibit rapid glutamate receptor desensitisation and enhance glutamergic synaptic currents. *J Neurosci,* 13: 3904-3915.

Yamada, K.A. (1998a) Modulating excitatory synaptic neurotransmission: potential treatment for neurological disease. *Neurobiol of Disease*, 5: 67-80.

Yamada, K.A., Covey, D.F., Hsu, C.Y., Hu, R., Hu, Y., He, Y.Y. (1998b) The diazoxide derivative IDRA 21 enhances ischemic hippocampal neuron injury. *Ann Neurol*, 43: 664-669.

Yamaguchi, S., Donevan, S.D., Rogawaki, M.A. (1993) Anticonvulsant activity of AMPA/kainate antagonists: comparison of GYKI 52466 and NBQX in maximal electroshock and chemoconvulsant seizure models. *Epilepsy Res,* 15: 179-184.

Yang, X. and Skoff, R.P. (1997) Preteolipid protein regulates the survival and differentiation of oligodendrocytes. *J Neurosci,* 17(6): 2056-2070.

Yin, X., Crawford, T.O., Griffin, J.W., Tu, P., Lee, V.M-Y., Li, C., Roder, J., Trapp, B.D. (1998) Myelin-associated glycoprotein is a myelin signal that modulates the calibre of myelinated axons. *J Neurosci* 18: 1953-1963.

Yoshoika, A, Hardy, M., Younkin, D.P., Grinspan, J.B., Stern, J.L., Pleasure, D. (1995) α-Amino-3-Hydroxy-5-Methyl-4-Isoxazoleproprionate (AMPA) Receptors mediate excitotoxicity in the oligodendroglial lineage. *J Neurochem,* 64: 2442-2448.

Yoshoika, A., Bacskai, B. and Pleasure, D. (1996) Pathophysiology of Oligodendroglial Excitotoxicity. *J Neurosci Res,* 46: 427-437.

Yoshioka, A., Yamaya, Y., Saiki, S., Kanemoto, M., Hirose, G., Beesley, J. and Pleasure, D. (2000) Non-*N*-methyl-D-aspartate glutamate receptors mediate oxygen-glucose deprivation-induced oligodendroglial injury. *Brain Res,* 854 207-215.

Young, A.B. and Fagg, G.E. (1990) Excitatory amino acid receptors in the brain: membrane binding and receptor autoradiographic approaches. *TiPs,* 11: 126-133.

Zaczek, R., Nelso, M.F., Coyle, J.T. (1978) Effects of anaesthetics and anticonvulsants on the action of kainic acid in the rat hippoocampus. *Eur J Pharm,* 52: 323-327.

Zafra, F., Henergerer, B., Leibrock, J., Thoenen, H., Lindholm, D. (1990) Activity dependent regulation of BDNF and NGF mRNAs in the rat hippocampus is mediated by non-NMDA receptors. *EMBO J,* 9: 3545-3550.

Zeevalk, G.D. and Nicklas, W.J. (1990) Chemically-induced hypoxia and anoxia: relationship to glutamate receptor-mediated toxicity in the retina. *J Pharmacol Exp Ther* 257: 870-878.

Zhang, K. and Sejnowski, T.J. (2000) A universal scaling law between gray matter and white matter of cerebral cortex. *Proc Nat Acad Sci USA,* 5621-5626.

Zivkovic, I., Thompson, D.M., Bertolino, M., Uzunov, D., DiBella, M., Costa, E., Guidotti, A. (1995) 7-Chloro-3-methyl-3-4-dihydro-2H-1,2,4 benzothiadiazine S,S-dioxide (IDRA 21): a benzothiadiazine derivative that enhances cognition by attenuating DL-alpha-amino-2,3-dihydro-5-methyl-3-oxo-4-isoxazolepropanoic acid (AMPA) receptor desensitization. *J Pharmacol Exp Ther,* 272: 300-309.

Publications

Papers

Polgar, E., **Fowler, J.H.**, McGill, M.M., Todd, A.J. (1999) The types of neuron which contain protein kinase C gamma in rat spinal cord. *Brain Research,* 833(1): 71-80.

Fowler, J., MacKinnon, M-A., Ragupathi, R., Saatman, K.E., McIntosh, T.K., Graham, D.I. (2002). Age does not influence DNA Fragmentation in the hippocampus after fatal traumatic brain injury in young and aged humans compared with controls. *Clinical Neuropathology,* 21 (4): 156-162.

McCraken, E., **Fowler, J.H.,** Dewar, D., Morrison, S., McCulloch, J. (2002) Grey matter and white matter ischemic damage is reduced by the competitive AMPA receptor antagonist, SPD 502. *J Cereb Blood Flow and Metab,*

Fowler, J.H., McCracken, E., Dewar, D., McCulloch, J. (2003) Intracerebral injection of AMPA causes axonal damage *in vivo. Provisionally accepted to Brain Res.*

Fowler, J.H. O'Neill, M.J., Whalley, K., Murray, T.K., Crile, R., McKinzie, D., McCulloch, J. (2003) An anatomical basis for cognitive enhancing effects of the AMPA receptor potentiator LY404187: ^{14}C-2-deoxyglucose autoradiography and c-fos studies. *Submitted to J. Neurosci.*

Cuthill, D.J., **Fowler, J.H.,** McCulloch, J., Dewar, D. (2003) Mechanisms of axonal damage *in vivo. In preparation.*

Fowler, J.H., Dewar, D., McCulloch, J., McLaughlin, M., Griffiths, I.R., Nave, K-A., Garbern, J.Y., Edgar, J.M. (2003) AMPA-induced axonal damage is reduced in proteolipid protein deficient mice. *In preparation.*

Abstracts

Fowler, J.H., McCracken, E., McCulloch, J., Dewar, D. (2001) Intracerebral injection of AMPA caused axonal damage. *British Neuroscience Association Abstracts* 16, 57.02.

Fowler, J.H., McCracken, E., Dewar, D., McCulloch, J. (2001) Intracerebral injection of AMPA causes axonal damage. *Journal of Cerebral Blood Flow and Metabolism* 21;S54.

Dewar, D., **Fowler, J.H.**, McCracken, E., McCulloch, J. (2002) Mechanisms of white matter damage in ischaemia. *Glia Suppl* 1; W 9.4.

Fowler, J.H., O'Neill, M.J., McCulloch, J. (2002) Effects of the AMPA potentiator LY404187 on cerebral glucose utilisation in the rat. *European Journal of Neuroscience Abstract* 176.7.

Fowler J.H., O'Neill M.J., McCulloch J. (2002) Mapping the functional effects of the AMPA receptor potentiator LY404187 with 2-deoxyglucose autoradiography. *Society for Neuroscience Abstract*

Cuthill D.J., McCulloch J., **Fowler J.H.,** Dewar, D.(2002) Axonal pathology differs following intrastriatal injection of Malonate or AMPA in the mouse. *Society for Neurosciece Abstract.*

Fowler, J.H., Dewar, D., McCulloch, J., McLaughlin, M., Griffiths, I.R., Nave, K-A., Garbern, J.Y., Edgar, J.M. (2003) AMPA-induced axonal damage is reduced in proteolipid protein deficient mice. *British Neuroscience Association Abstracts,* 17: 57.09.

Cuthill, D.J., McCulloch, J., **Fowler, J.H.,** Dewar, D. (2003) Energy failure or excitotoxicity lead to distinct axonal pathologies in the mouse. *British Neuroscience Association Abstracts,* 17: 57.07.

Appendix 1: Rat and Mouse Tissue Processing

Whole rat and mouse brains were processed using a Tissue-Tek® automated processor (VIP).

Station	Solution	Temp	Time	
			Rat	Mouse
1	70% Alcohol	35°C	2 hours	2 hours
2	80% Alcohol	35°C	3 hours	2 hours
3	96% Alcohol	35°C	4 hours	2 hours
4	Absolute Alcohol	35°C	4 hours	2 hours
5	Absolute Alcohol	35°C	5 hours	2 hours
6	Absolute Alcohol	35°C	5 hours	2 hours
7	Absolute Alcohol	35°C	6 hours	2 hours
8	Xylene/Abs Al	35°C	4 hours	2 hours
9	Xylene 1	35°C	5 hours	2 hours
10	Xylene 2	35°C	5 hours	2 hours
11	Paraffin wax 1	60°C	5 hours	2 hours
12	Paraffin wax 2	60°C	5 hours	2 hours
13	Paraffin wax 3	60°C	6 hours	2 hours

Appendix 2: Details of solutions used

Perfusion fixation, processing and immunohistochemistry

- **50mM phosphate buffer**

  Solution A 31.2g/L of NaH_2PO_4 (0.2M)
  Solution B 28.4g/L of Na_2HPO_4 (0.2M)

  Take 95ml of stock solution A and 405mls of stock solution B; make up to 2L with distilled H_2O

- **4% Paraformaldehyde Fixative**

  40g/L of paraformaldehyde (Sigma) was dissolved into 50mM phosphate buffer heated to 65°C, which was then allowed to cool before being filtered.

- **Phosphate buffered Saline (PBS, 10mM, pH 7.2)**

  Made from 1:20 dilution of following stock:-

NaCl	174g/L
KH_2PO_4	10.2g/L
Na_2HPO_4	31.6g/L

- **Poly-L-lysine slides**

  Slides were racked, then placed in a 1:10 dilution of Poly-L-lysine (0.1%, Sigma) solution for 5 minutes, then dried in an oven at 65°C for 1 hour

- **Cryoprotectant**

  30% glycerol/30% ethylene glycol in 10 mM sodium phosphate buffer, store at -20°C

Western Blotting

- **For preparation of membrane enriched brain homogenates**

  Solution A 0.85M sucrose, 10mM hepes pH 7.4, 2mM DTT, 1mM TLCK (Nα-p-Tosyl-L-lysine chicromethyl ketone hydrochloride)

  Solution B 0.25M sucrose, 10mMH hepes pH 7.4

- **Acrylamide Gels**

  To make 2 gels for mini gel system:-

	Resolving Gel (10%)	Stacking Gel (4%)
Acrylamide	6.6mls	880µl
1.5M Tris pH 8.8	5mls	
0.5M Tris pH 6.8		1.64mls
10% SDS	200µl	30µl
10% APS	100µl	50µl
Distilled H_2O	8.1mls	4mls
Temed	10µl	8µl

- **1X T-TBS Tris buffered saline**

  Made from 1:10 dilution of stock

Tris	24.2g
NaCl	175.4g
Tween	20ml
H_2O	2L pH7.4

- **10X PAGE buffer**

  Made from 1:10 dilution of stock:-

Glycine	144g/L	Dissolve glycine, then add Tris, add SDS last
Tris	30.3g/L	
SDS	10g/L	

- **Anode I buffer**

Tris	36g/L
Methanol	74ml/L

- **Anode II buffer**

Tris	3g/L
Methanol	74ml/L

- **Cathode buffer**

Tris	3g/L
Glycine	3g/L
Methanol	74ml/L

Appendix 3: Reproducibility of MAP 5 scoring system

To quantify axonal damage following intracerebral injection of AMPA into the subcortical white matter of rats, a grid scoring system was used. Firstly, MAP 5 immunostained sections were captured and digitised with a video camera connected to an MCID-M4 image analyser (Imaging Research, Canada). The image of each coronal section was printed, at a fixed magnification, onto A4 paper using a laser printer, and areas containing axonal damage were plotted onto the images with the aid of a light microscope. A 2mm spaced transparent grid was then placed over each digitised MAP 5 image, and the number of grid intersections that fell within the area containing damaged axons was counted. To determine the reproducibility of the grid scoring technique, it was repeated the following day for the animals described in section 3.2.1. The results, presented in the graph below, demonstrate that the grid system is a highly reproducible technique.

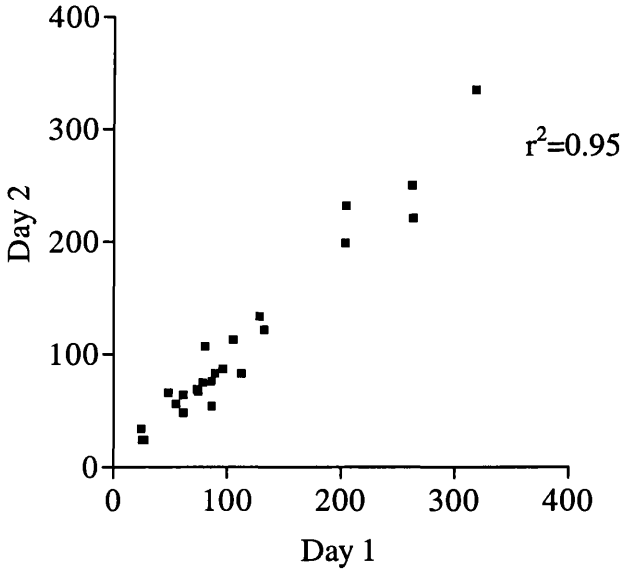

Figure A.1 Reproducibility of the grid scoring method

Next, the reproducibility of the entire technique (plotting axonal damage onto digitised sections and the grid scoring system) was tested by repeating the quantification two days after the original analysis, for the animals described in section 3.2.1. The results are presented in figure A.2. overleaf. As would be expected, there is slightly more variability in this trial. However, the strong correlation between the analyses done on the two days confirms the reproducibility of this technique.

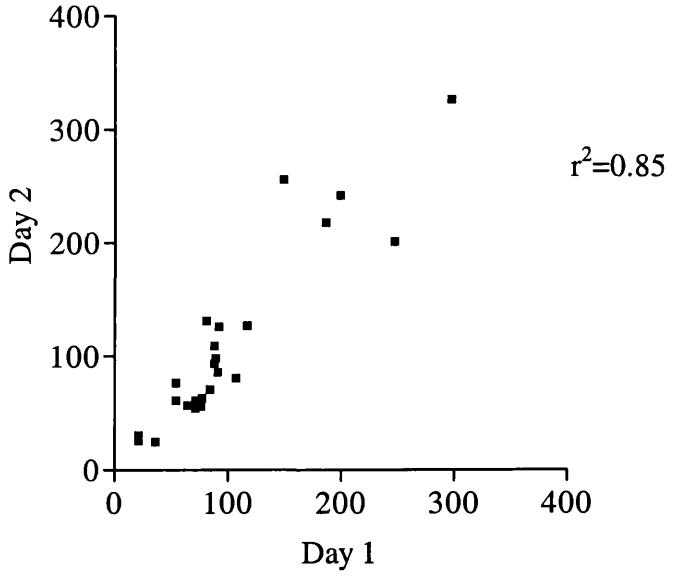

Figure A.2 Reproducibility of the MAP 5 scoring system for quantifying axonal damage

Appendix 4: Quantification of axonal and neuronal damage following intrastriatal injection of AMPA or malonate – Reproducibility of technique

I performed the quantification of all neuronal and axonal damage in the AMPA-induced lesions, whilst Mr Daniel Cuthill performed all quantification of the malonate-induced lesions. However, the ability of Mr Daniel Cuthill to quantify AMPA-induced lesions, and my ability to quantify malonate-induced lesions was also assessed in eight animals from each group (2 per dose), to determine inter-rater variability. The results are presented in figure A.3 and A.4. Slight discrepancies were detected from animal to animal (Fig A.3.A, C, E; Fig. A.4.A, C, E) when comparing the results of individual animals. However, correlation analysis revealed that our results were highly reproducible (Fig A.3.B, D, F – Fig. A.4.B, D, F). The only exception was the quantification of APP immunostaining following intracerebral injection of AMPA (Fig A.4.E and A.4.F). However, this is because the actual volume of damaged axons assessed in APP immunostained sections is very low, therefore slight variations can appear exaggerated.

Fig A.3 **(Overleaf) Quantification of malonate-induced neuronal and axonal damage – reproducibility studies.**

Comparison of my results (Clear bars) with Dan's results (Black bars) for individual animals following intracerebral injection of vehicle or malonate (0.34-1.35μmol) (A, C, F). Correlating these data (B, D, F) revealed that our results were highly reproducible.

Fig A.4 **(On page A8) Quantification of AMPA-induced neuronal and axonal damage – reproducibility studies.**

Comparison of my results (Clear bars) with Dan's results (Black bars) for individual animals following intracerebral injection of vehicle or AMPA (1.5-6nmol) (A, C, F). Correlating these data (B, D, F) revealed that our results were highly reproducible, with the exception of APP immunostaining (see above).

A3 - malonate

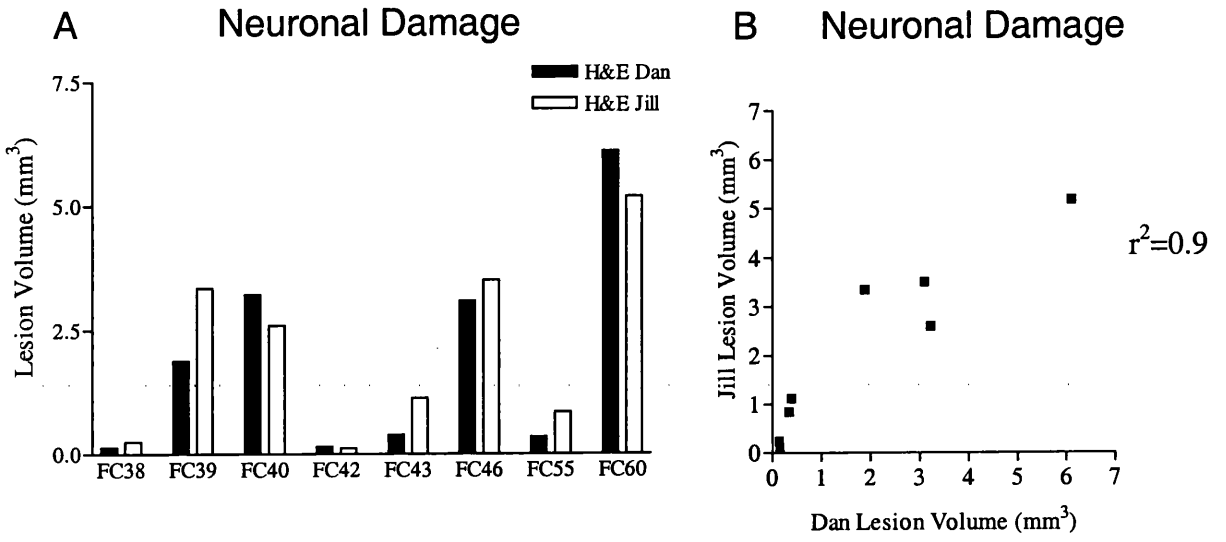
A
Neuronal Damage
H&E Dan
H&E Jill
Lesion Volume (mm3)
7.5
5.0
2.5
0.0
FC38
FC39
FC40
FC42
FC43
FC46
FC55
FC60
B
Neuronal Damage
Jill Lesion Volume (mm3)
Dan Lesion Volume (mm3)
r2=0.9

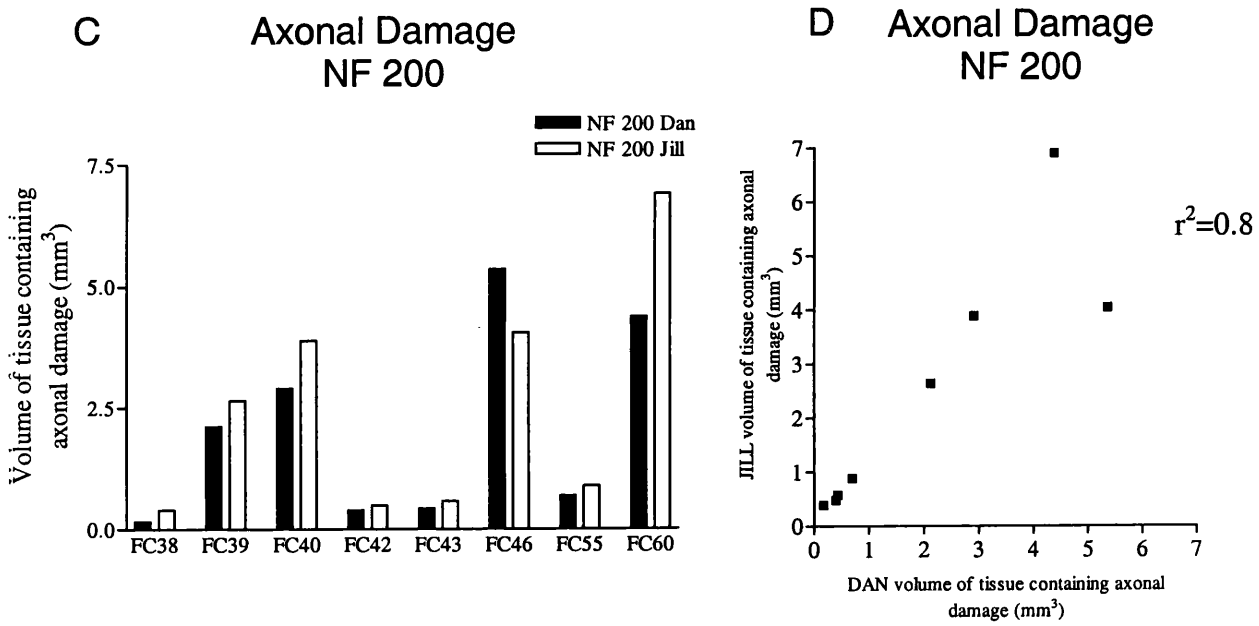
C
Axonal Damage
NF 200
NF 200 Dan
NF 200 Jill
Volume of tissue containing axonal damage (mm3)
7.5
5.0
2.5
0.0
FC38
FC39
FC40
FC42
FC43
FC46
FC55
FC60
D
Axonal Damage
NF 200
JILL volume of tissue containing axonal damage (mm3)
DAN volume of tissue containing axonal damage (mm3)
r2=0.8

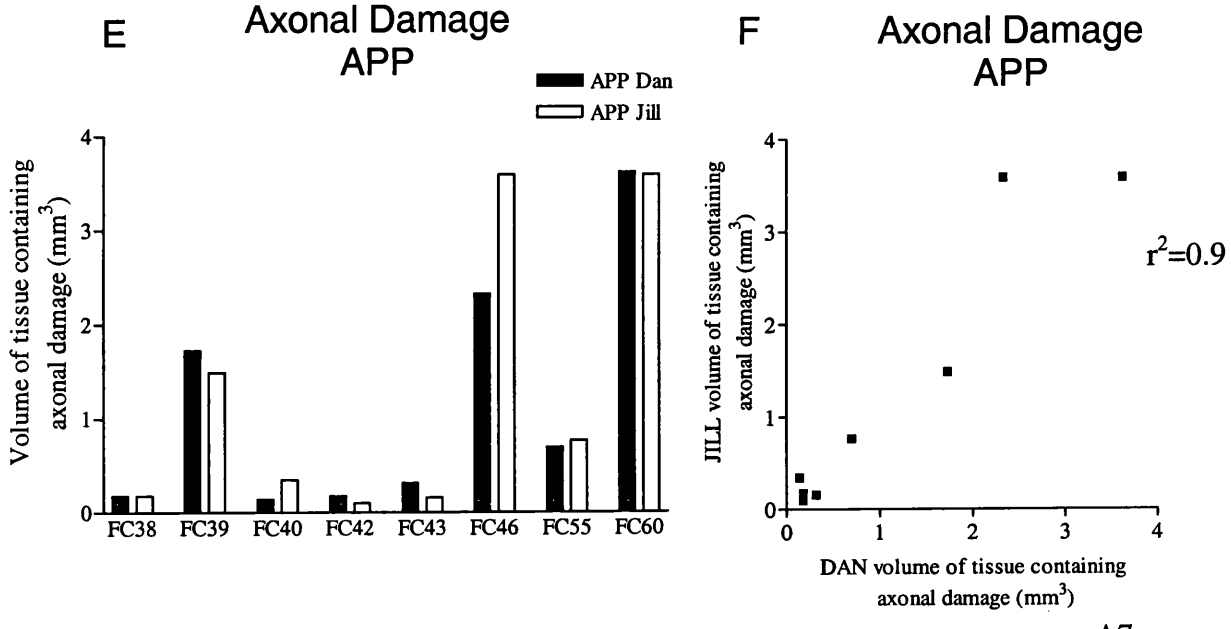
E
Axonal Damage
APP
APP Dan
APP Jill
Volume of tissue containing axonal damage (mm3)
4
3
2
1
0
FC38
FC39
FC40
FC42
FC43
FC46
FC55
FC60
F
Axonal Damage
APP
JILL volume of tissue containing axonal damage (mm3)
DAN volume of tissue containing axonal damage (mm3)
r2=0.9

A4 - AMPA

A Neuronal Damage

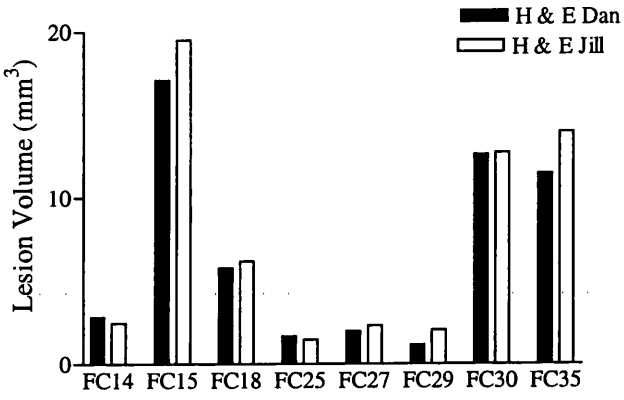

B Neuronal Damage

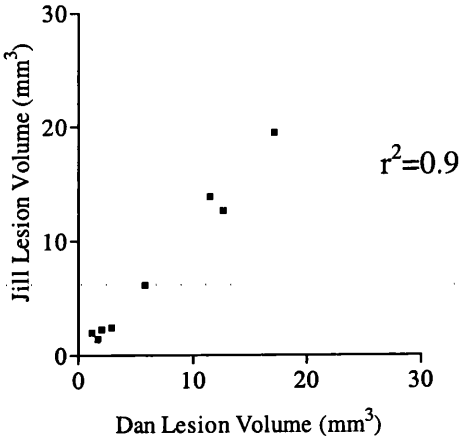

C Axonal Damage NF 200

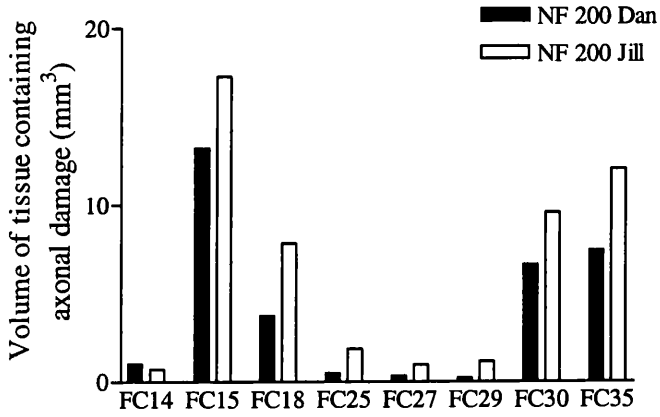

D Axonal Damage NF 200

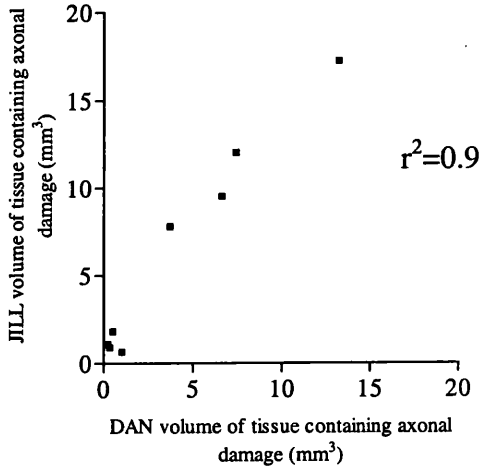

E Axonal Damage APP

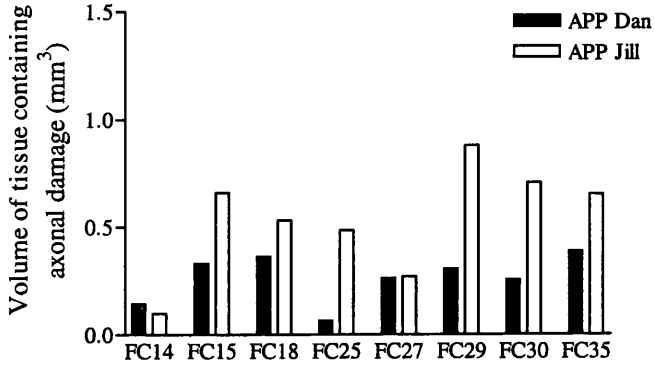

F Axonal Damage APP